Methane reforming by carbon dioxide over metal supported on nanocrystalline mixed oxides : mechanism and transient kinetics for relating catalysts structure and performance

Alexey Bobin

N° d'ordre : Année 2014

THESE

présentée devant

L'UNIVERSITE CLAUDE BERNARD LYON 1

École Doctorale de Chimie de Lyon

et le

BORESKOV INSTITUTE OF CATALYSIS,

NOVOSSIBIRSK STATE UNIVERSITY

pour l'obtention du
DIPLOME DE DOCTORAT EN CO-TUTELLE
(Arrêté du 01 Octobre 2008)

Présentée et soutenue publiquement le 09 Septembre 2014 par

Alexey BOBIN

Methane reforming by carbon dioxide over metal supported on nanocrystalline mixed oxides: mechanism and transient kinetics for relating catalysts structure and performance

Directeurs de thèse: Claude MIRODATOS et V.A. SADYKOV

Co-directeur de thèse: Yves SCHUURMAN

Jury:

Claude MIRODATOS
Anne-Cécile ROGER (rapporteur)
Vladislav A. SADYKOV
Yves SCHUURMAN
Mikhail Yu. SINEV (rapporteur)
Andrey ZAGORUIKO

UNIVERSITE CLAUDE BERNARD - LYON 1

Président de l'Université	**M. François-Noël GILLY**
Vice-président du Conseil d'Administration	M. le Professeur Hamda BEN HADID
Vice-président du Conseil des Etudes et de la Vie Universitaire	M. le Professeur Philippe LALLE
Vice-président du Conseil Scientifique	M. le Professeur Germain GILLET
Directeur Général des Services	M. Alain HELLEU

COMPOSANTES SANTE

Faculté de Médecine Lyon Est – Claude Bernard	Directeur : M. le Professeur J. ETIENNE
Faculté de Médecine et de Maïeutique Lyon Sud – Charles Mérieux	Directeur : Mme la Professeure C. BURILLON
Faculté d'Odontologie	Directeur : M. le Professeur D. BOURGEOIS
Institut des Sciences Pharmaceutiques et Biologiques	Directeur : Mme la Professeure C. VINCIGUERRA
Institut des Sciences et Techniques de la Réadaptation	Directeur : M. le Professeur Y. MATILLON
Département de formation et Centre de Recherche en Biolog Humaine	Directeur : Mme. la Professeure A-M. SCHOTT

COMPOSANTES ET DEPARTEMENTS DE SCIENCES ET TECHNOLOGIE

Faculté des Sciences et Technologies	Directeur : M. F. DE MARCHI
Département Biologie	Directeur : M. le Professeur F. FLEURY
Département Chimie Biochimie	Directeur : Mme Caroline FELIX
Département GEP	Directeur : M. Hassan HAMMOURI
Département Informatique	Directeur : M. le Professeur S. AKKOUCHE
Département Mathématiques	Directeur : M. Georges TOMANOV

Département Mécanique	Directeur : M. le Professeur H. BEN HADID
Département Physique	Directeur : M. Jean-Claude PLENET
UFR Sciences et Techniques des Activités Physiques et Sportives	Directeur : M. Y.VANPOULLE
Observatoire des Sciences de l'Univers de Lyon	Directeur : M. B. GUIDERDONI
Polytech Lyon	Directeur : M. P. FOURNIER
Ecole Supérieure de Chimie Physique Electronique	Directeur : M. G. PIGNAULT
Institut Universitaire de Technologie de Lyon 1	Directeur : M. C. VITON
Ecole Supérieure du Professorat et de l'Education	Directeur : M. A. MOUGNIOTTE
Institut de Science Financière et d'Assurances	Directeur : M. N. LEBOISNE

TITRE DE LA THESE:
Reformage du méthane par le dioxyde de carbone sur métaux supportés sur oxydes mixtes nanocristallins: approche mécanistique et cinétiques transitoires pour relier structures et performances catalytiques.

RESUME :

L'énergie de liaison, la mobilité et la réactivité de l'oxygène dans des matériaux nanocristallins de type cérine-zircone dopée aux terres rares (La, Gd, Pr, Sm) supportant des métaux (Pt, Ni, Ru) ont été étudiées par échange isotopique en réacteurs statiques et traversés ($^{18}O_2$ and $C^{18}O_2$), DTP d'O_2, RTP d'H_2 et CH_4, microcalorimétrie pulsée et réacteur TAP. La mobilité d'oxygène de cœur apparait comme contrôlée par le réarrangement des sphères de coordination des cations Ce et Zr et par des chemins préférentiels le long de chaines Pr^{3+}/Pr^{4+}. En surface et sub-surface, ce contrôle se ferait par des interactions fortes métal/support avec l'incorporation de cations métalliques. Cette mobilité de l'oxygène limiterait le vieillissement et le frittage en conditions réalistes de reformage par le gaz carbonique.

Des études cinétiques non stationnaires et par marquage isotopique ont permis de proposer un mécanisme bi-fonctionnel fondé sur des étapes rédox indépendantes pour l'activation du méthane et du dioxyde de carbone. L'étape limitante serait l'activation du méthane tandis que l'activation du gaz carbonique s'opérerait plus rapidement sur des sites réduits du support, générant de l'oxygène diffusant aisément vers l'interface métal/support (enthalpie de désorption ≈600-650 kJ/mol) pour oxyder les fragments du méthane en CO et H_2. Dans les meilleures formulations catalytiques, des agrégats Ni-Ru faciliteraient l'activation du CO_2 dans son état de transition, en marge de carbonates stables qui restent "spectateurs" de la réaction. Pour le Pt/PrCeZrO, il existerait une autre voie d'activation de carbonates faiblement adsorbés sur des ions $Pt^{\delta+}$ stabilisés par des cations Pr^{4+}. Cette spécificité confère à cette formulation des perspectives très intéressantes en reformage à sec, notamment sur des supports structurés de type alumine corindon, bien adaptés à des réacteurs compacts à temps courts pour des ressources en gaz dispersées et de capacité limitée.

TITRE en anglais

Methane reforming by carbon dioxide over metal supported on nanocrystalline mixed oxides: mechanism and transient kinetics for relating catalysts structure and performance.

RESUME en anglais

Oxygen bonding strength, mobility and reactivity in nanocrystalline Ln-doped ceria-zirconia (Ln=La, Gd, Pr, Sm) with supported Pt, Ni, Ru were studied by state-of-the-art techniques such as isotopic exchange in static and flow reactors with $^{18}O_2$ and $C^{18}O_2$, O_2 TPD, H_2 and CH_4 TPR, pulse microcalorimetry and TAP reactor. Bulk oxygen mobility is found controlled by a rearrangement of

Ce and Zr cations coordination sphere with doping as well as by fast oxygen migration along Pr^{3+}/Pr^{4+} cationic chains. Surface and near-surface oxygen mobility appears controlled by a strong metal-support interaction with incorporation of metallic ions into surface layers and domain boundaries. In realistic feeds, the catalytic activity in dry reforming of methane correlates with oxygen mobility, required to prevent coking and metal sintering.

Transient kinetic studies (non steady-state and SSITKA) allowed us to propose a bi-functional reaction mechanism corresponding to independent redox steps of CH_4 and CO_2 activation. The rate-limiting step is shown to be the irreversible activation of CH_4 on metal sites, while CO_2 dissociation on reduced sites of oxide supports proceeds much faster (being reversible for the steady-state surface) followed by a fast oxygen transfer along the surface/domain boundaries to metal sites where CH_4 molecules are transformed to CO and H_2. The CH_4 selective conversion into syngas would involve strongly bound bridging oxygen species with heat of desorption ≈600-650 kJ/mol O_2. For optimized formulations, Ni+Ru clusters could be involved in CO_2 activation via facilitating C-O bond breaking in the transition state, thus increasing the rate constant of the surface reoxidation by CO_2, while strongly bound carbonates behave as spectators. For Pt/PrCeZrO, an additional fast route to syngas would occur on Pt ions with participation of weakly bound carbonates stabilized by neighboring Pr^{4+} ions. Such specificity makes this system highly promising for methane oxi-dry reforming, especially on structured corundum supports for short contact time compact reactors, well adapted to stranded and limited gas resources.

DISCIPLINE
Chimie-Catalyse

MOTS-CLES
Reformage du méthane par le dioxyde de carbone, mécanisme, cinétiques non stationnaires, réacteurs structurés, oxydes mixtes nanocristallins

Key-words
Methane reforming by carbon dioxide, mechanism, transient kinetics, structured reactors, nanocristalline oxides

INTITULE ET ADRESSE DE L'U.F.R. OU DU LABORATOIRE :

Institut de Recherches sur la Catalyse et l'Environnement de Lyon, Université Lyon 1, CNRS. 2, Av. Albert Einstein F-69626 Villeurbanne

Boreskov Institute of Catalysis, Novossibirsk State University

Outline

Chapter one

Objectives and state-of-the-art analysis

1 Objectives of the thesis

Generation of synthesis gas via routes alternative to traditional processes such as steam reforming of methane has recently attracted considerable attention due to both environmental and commercial reasons. Transformation of natural gas using carbon dioxide is among the most promising processes for the following reasons: Dry reforming transforms cheap undesirable greenhouse gases and is particularly important in the case of biogas or gas fields containing a significant amount of methane and carbon dioxide. The synthesis gas produced in this reaction having the H_2/CO ratio close to unity is a favorable feedstock for further chemical processes such as the Fischer–Tropsch synthesis and production of oxygenates followed by the liquid fuel synthesis[1,2,3,4].

The active catalysts for methane dry reforming are usually based on supported Ni or noble metals[1,2,3,4,5,6,7,8,9,10,11,12,13,14,15,16]. The major problem of this process hindering its industrial application is the coking of catalysts and, as a result, their deactivation especially in the case of Ni catalysts on traditional supports[1,2,3,4,9,10,11,12,13,14,15,16]. Among different approaches to minimize the coke deposition on catalysts, the most attractive option is to use complex oxides supports (perovskites, fluorites) with a high lattice oxygen mobility and reactivity[11,12,13,14,15,16,17,18]. Indeed, catalysts based on doped ceria-zirconia oxides with supported precious metals and/or Ni-based alloys demonstrate a high activity and coking stability in carbon dioxide reforming of methane[11,12,13,14,15,16]. However, up to date, the factors controlling the performance of these catalysts have not been studied in details due to rather limited screening in the composition of support and supported metals. In addition, their implementation in micro-structured reactors was proposed as a unique opportunity to combine such an endothermic process with an exothermic one like the oxidative coupling, as targeted by the European project OCMOL which granted part of the research carried out in this PhD. In this manuscript, the study will be restricted to the composition and the structural effects of the dry reforming catalysts on their performances with an in-depth study of the reaction mechanism.

To that end, it was required to establish relevant relationships between the kinetic parameters of the reaction, characteristics of the oxygen bonding strength, mobility (bulk and surface diffusion) and

reactivity in these systems and the structural parameters of the catalysts like their nano dispersion and composition, the oxygen stoichiometry and the state of the metal phase/supports interface.

This work was carried out under the agreement for a shared PhD thesis between the BORESKOV INSTITUTE OF CATALYSIS and IRCELYON-CNRS-UCBL laboratories.

2 Strategy to reach these objectives

The strategy to reach these objectives is illustrated in Figure 1, showing also the way that the work was shared between the two laboratories.

As basic oxide system with a high lattice oxygen mobility and phase stability in strongly reducing conditions of methane dry reforming, ceria-zirconia solid solution (Ce:Zr =1) doped with rate-earth cations (La, Pr, Gd) was selected, and Pt (Pt+Ni, Ru+Ni) were used as components for activating methane. The catalytic performance of these selected systems in methane (oxy)dry reforming was estimated both for fractions of active components as well as thin layers supported on corundum channels, selected as a suitable material for designing short contact time microstructured reactors.

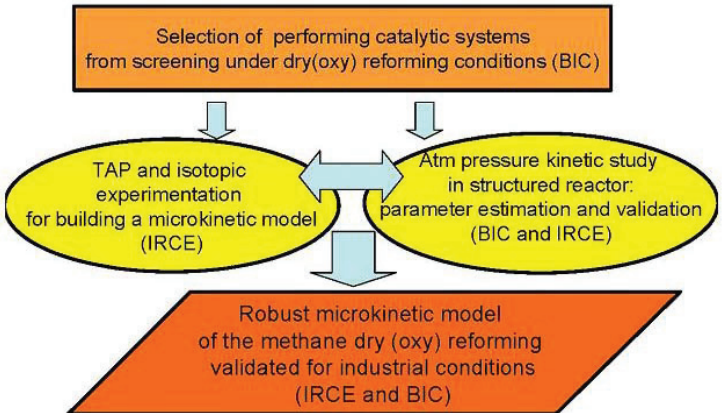

Figure 1. Structure of research and dispatching of the main tasks between the two guest laboratories.

A detailed characterization of the kinetic parameters related to oxygen mobility in these systems being dependent upon their composition (including oxygen stoichiometry) was carried out using a unique combination of experimental techniques (oxygen exchange in both static and flow reactors with $^{18}O_2$ and $C^{18}O_2$, including experimental procedures and approaches to the analysis developed within this work). These data were combined with detailed characteristics of the oxygen bonding strength and reactivity (by O_2 TPD, H_2 and CH_4 TPR, pulse microcalorimetry, TAP) as well as with information on the real structure and surface properties of these systems obtained by combination of methods such as XRD, neutron diffraction, high resolution TEM, FTIRS of

adsorbed CO to elucidate atomic-scale factors controlling catalytic activity/reactivity of these catalysts. Transient studies of the reaction mechanism (including pulse studies, chemical and isotope transients) allowed us to formulate a scheme of the reaction mechanism and estimate basic constants of the main reaction steps

3 State-of-the-art analysis.

3.1 Materials

While a lot of research in methane dry reforming has been carried out for catalysts on traditional supports such as alumina, lanthana, silica, zirconia, ceria etc or even ceria-zirconia solid solutions or perovskite-like precursor[1,2,3,4,5,6,7,8,9,10,11,12,13,14,15,16,17,18,19], for ceria-zirconia solid solutions doped by rare-earth cations (La, Gd, Pr) with supported Pt, only methane partial oxidation and steam reforming were studied[20,21]. The demonstrated advantage of these doped systems is a higher specific surface area as compared with ceria, much higher oxygen mobility and reactivity as compared with zirconia, and a higher phase stability in real operation conditions since doping suppresses segregation of ceria-zirconia solid solution into two phases enriched by Ce and Zr, respectively leading to performance degradation[22,23]. However, the key parameters characterizing oxygen bonding strength, mobility and reactivity for these catalysts based upon doped ceria-zirconia solid solutions required to select the best systems for further development on new generation of short contact time reactors. These studies which are the basis of this thesis have never been reported in the literature to our knowledge.

3.2 Main mechanistic features of the methane dry reforming reaction

The main factors controlling catalytic activity in MDR reaction are usually related to the activation of the reactants. The dissociative adsorption and activation of both CH_4 and CO_2 is sensitive to the composition and structure of nanocatalysts based on fluorite-like/perovskite-like oxides precursors, as far as it depends on both electronic and geometric factors[24,25].

It is generally accepted that methane is dissociatively adsorbed on the metal species to form H_2 and CH_x fragment on the catalyst surface, whereas CO_2 activation pathway can be different, depending on the type of support[26].

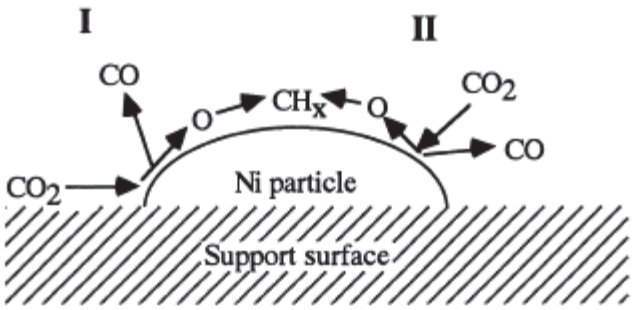

Figure 2. Scheme of the MDR reaction by Tomishige et al[26].

Thus, at the activation of CO_2 adsorbed on support surface at interface between metal particle and support (path I), rapid oxidation of CH_x on metal surface occurred. The other path is activation of CO_2 on the metal surface (path II). It was suggested that path I is more effective for the inhibition of carbon formation than path II.

Similarly, the following steps are proposed by Slagtern et al.[27] for the MDR on Ni/La_2O_3, where the carbonate lanthana phase in tight contact with Ni particles acts as the oxidizing phase for the surface Ni carbide species.

$$CH_4 + Ni \rightarrow NiC + 2H_2 \quad (1)$$

$$La_2O_2CO_3 + Ni \rightarrow O + NiO + La_2O_3 \quad (2)$$

$$NiC + NiO \rightarrow CO + 2Ni \quad (3)$$

$$CO_2 + La_2O_3 \rightarrow La_2O_2CO_3 \quad (4)$$

For nanocatalysts, oxygen vacancies formed at the oxide surface in reducing reaction conditions can act as active sites for dissociative adsorption of CO_2 with subsequent migration of mobile surface oxygen species to the metal-support interface. Apparently, the catalyst stability to coking is determined by the balance between the rate of methane dissociation on metal particle producing CH_x species (CO and coke precursors) and rate of CO_2 dissociation and surface oxygen diffusion. For the irreducible oxides supports, CO_2 dissociation is supposed to be promoted by the H (ads) originating from the CH_4 dissociation, which can be assisted by oxygen atoms on the support. Also, the reactive intermediates are mostly support-related species[28,29,30,31,32,33.34,35,36,37,38,39,40,41]. Thus, Bradford and Vannice [29] have suggested for nickel supported catalysts, that CO_2 participates in the reaction mechanism through the reverse water-gas shift to produce surface OH groups. The surface OH groups react with adsorbed CH_x intermediates being formed through CH_4 decomposition, yielding a formate-type intermediate, CH_xO. Decomposition of CH_xO leads to the principal products of reforming - H_2 and CO. Decomposition

of both CH_4 and CH_xO are the slow kinetic steps. According to the observations of O'Connor et al.[7] over both Pt/Al_2O_3 and Pt/ZrO_2 catalysts, methane decomposition takes place over clean platinum. The main difference between the two catalysts concerns the carbon dioxide dissociation: for zirconia support it occurs on oxygen vacancies at Pt/zirconia interface. On the other hand, Bychkov et al.[42,43] demonstrated by using microcalorimetric measurements that for Pt/Al_2O_3, CO_2 is activated via direct interaction with surface carbon atoms on Pt which is deemed to be determining for MDR. For Ni/SiO_2 catalyst, transient studies reported by Schuurman and Mirodatos[44] revealed that CO_2 is activated by direct dissociation on Ni particles, while the rate-limiting step is related to the surface reaction between C and O adspecies on Ni. For Ni/lanthana catalyst, a "bi-functional" mechanism was proposed by Slagtern et al.[27] to account for the observed kinetic behaviour: methane is activated on the Ni particles, and carbon dioxide interacts with the basic sites of La_2O_3 to form carbonates which will decompose at the Ni–La_2O_3 interface into CO and surface oxygen able to react with the CH_X intermediates formed from methane cracking.

Hence, depending upon the support and the metal, different routes of reactants activation and rate-determining steps seem to control the catalysts performance, unless the thermodynamic equilibrium is achieved, which preclude determining the effective mechanism that operates. However, it should be mentioned that according to Wei and Iglesia[25], for all traditional supports without noticeable oxygen mobility and reactivity and supported metals, only CH_4 activation by C-H bond rupture is of any kinetic significance, all other stages proceeding much faster. Since this conclusion was based only on steady-state kinetic experiments (isotopic effects), apparently for nanocomposite/nanocrystalline systems studied in this thesis, a tight check of the main features of the MDR reaction mechanism is required by applying advanced combination of transient techniques. It cannot be excluded that key features of CH_4 dry reforming mechanism depend not only on support and supported metal, but on operation conditions (concentration of reactants and temperature) and oxygen mobility in support as well. This requires carrying out transient kinetic experiments under realistic conditions, characteristic of a real MDR catalysis. Similarly, the oxygen mobility in complex oxide supports has to be characterized not only in the standard oxidized state but after achieving the steady state in realistic feeds as well when relatively weakly bound and, hence, mobile oxygen species are to be absent. In this respect, oxygen isotope heteroexchange between catalyst and $C^{18}O_2$ is very useful to characterize the oxygen mobility in the catalysts reduced by reaction feed.

Chapter two

Techniques and methodologies

4 Main implemented techniques

4.1 Samples preparation

Complex fluorite-like $Ln_x (Ce_{0.5}Zr_{0.5})_{1-x}O_2$ (Ln = Pr, Sm, Pr+Sm; x = 0.3) oxides were prepared by polymerized complex precursor (Pechini) route followed by drying and calcination in air at 700-900°C for 2 h[20,21]. Nanocomposite 80%$Sm_{0.3}Ce_{0.35}Zr_{0.35}O_2$+10% $Y_{0.08}Zr_{0.92}O_2$ (YSZ) +10%NiO was prepared by one-pot Pechini route[21]. Pt (~1 wt.%), Ru (~1 wt.%), Ni (5-7 wt.%), $LaNiO_3$ (7 wt.%) and their combinations were supported from solutions of respective salts (H_2PtCl_6, $RuCl_3$, Ni and La nitrates) or their mixtures by incipient wetness impregnation followed by drying and calcination at 700-800^{o}C.

Structured catalytic elements were prepared by using substrates of separate triangular channels cut from an α-Al_2O_3 monolith. The wall thickness was 0.2 mm, the side width of the inside triangle amounted to 2.33 mm and the channel length was cut to 10 mm. After annealing at 1300°C the specific surface area of the corundum support was estimated to be 3 m^2/g. Layers of $Ln_{0.3}$-Ce-Zr-O complex mixed oxides were supported on these substrates by washcoating with water based suspensions[45]. Pt (1.6 wt.%) was supported by the wet impregnation followed by drying and calcination under air at 900°C.

The specific surface area of samples was determined from Ar thermal desorption data by using BET method. XRD patterns were obtained with an ARL XTRA diffractometer using Cu Kα monochromatic radiation (λ=1.5418 Å); the 2θ-scanning region was 20-85°. The TEM micrographs were obtained with a JEM-2010 instrument (lattice resolution 1.4 Å, acceleration voltage 200 kV). Local elemental analysis was performed with EDX method (a Phoenix Spectrometer)[8,21,22,23,24,25].

4.2 Isotope exchange experiments.

The theoretical bases of isotope heteroexchange analysis are given in the next section.

The first set of oxygen isotope heteroexchange (**IE**) experiments were carried out in a static installation with on-line control of the gas phase isotope composition by mass-spectrometer in two modes:

1. Temperature-programmed isotope exchange (**TPIE**) with the temperature linear increase (5K/min) from 100 to 750°C.

2. Isothermal isotope exchange (**IIE**) at 360–650°C.

Before experiments, samples were pretreated for 2 h under air at 650°C followed by pretreatment in vacuum (p ~ 10^{-6} – 10^{-7} Torr) at 400°C for 90 min.

Oxygen pressure in closed reaction volume (680 cm^3) was equal to 1.5–4.5 Torr, weight of powdered sample — 0.1–0.3 g (for catalysts supported on the walls of corundum channels ~ 0.01 g). The initial ^{18}O content in the gas phase was ~ 100%. Details of experimental procedure are described in [46].

The second set of oxygen isotope heteroexchange experiments were carried out in a flow reactor (SSITKA mode) following earlier described procedures[47],[48]. After achieving dynamic oxygen adsorption-desorption equilibrium at 500-700°C, a flow of 1% $^{16}O_2$ in He was switched to the same flow of 1% $^{18}O_2$ in He, and concentrations of $^{16}O_2$, $^{16}O^{18}O$ and $^{18}O_2$ were monitored by the mass-spectrometer UGA 200 (Stanford Research Systems, USA). In a similar mode oxygen isotope heteroexchange was carried out using a flow of 1% $C^{18}O_2$ in He (^{18}O fraction 75%) for samples after different pretreatments (either in O_2 or after achieving the steady state in CH_4 DR).

Both steady state and transient experiments in CH_4 dry reforming were carried out at atmospheric pressure using quartz reactors and flow installation equipped with GC and on-line IR absorbance, electrochemical and polarographic gas sensors for different components as described elsewhere[49],[50],[51]. To compare specific catalytic activities of samples, effective first-order rate constants satisfactorily describing methane conversion data in plug-flow reactors were calculated. Transient kinetic experiments were carried out by switching the stream of reaction mixture to that containing CO_2, CH_4, $^{13}CH_4$+CO_2 or CH_4+$^{13}CO_2$ in He. Analysis of ^{13}C SSITKA experiments was carried out by solving the system of differential equations for the plug-flow reactor[48,52].

TAP experiments were performed in quartz microreactor placed in vacuum (10^{-4} – 10^{-5} Pa). The weight of the catalyst sample was 20 mg. A narrow pulse of gas molecules (~10^{14} molecules) was injected into the reactor by means of two high speed pulse valves. The products and remaining reactants were monitored at the exit of the reactor by a UTI 100C quadrupole mass spectrometer at fixed atomic mass units (AMU): 40 for Ar, 44 for CO_2, 16 for CH_4, 2 for H_2, 28 for CO, 18 for H_2O, and 32 for O_2[52].

Pulse microcalorimetric studies were carried out using a Setaram Sensys DSC TG calorimeter and a pulse kinetic installation. The reactants and products concentrations were determined by a gas chromatograph “Chromos GH -1000”. Samples were pretreated in a flow of 5% O_2 in He at 700°C for 0.5 h and then in He for 0.5 h at the same temperature with subsequent cooling down in the He

flow (flow rate 40 mL/min) to the temperature of experiments. Steady-state of catalysts in CH_4 dry reforming was usually achieved by flowing reaction feed 7% CH_4 + 7% CO_2 in He at 700°C for 2 h. Pulses of different compositions (7% CH_4 in He, 7% CH_4 + 7% CO_2 in He, 7% CO_2 in He, 5% O_2 in He) with volume 1-5 mL and time interval between pulses 15 min were fed in different sequences onto the stream of He flowing through the reactor (vide infra). Due to rather small weights of catalysts (~ 30 mg + 60 mg quartz fraction) and rather big reactor volume (≈5 cm^3), these pulse experiments were carried out in the batch-flow mode[53].

4.3 Theory of oxygen heteroexchange

The redistribution of the isotope molecules during heteroexchange $^{18}O_i{}^{16}O_{2-i}$ (i = 0, 1, 2) characterized by their molar fractions $\boldsymbol{x}_i$ ($x_0 + x_1 + x_2 = 1$) is described by isotope-kinetic equations[54,55,56,57,58]

$$\frac{N}{S}\frac{d\alpha}{dt} = -R(\alpha - \alpha_s) \tag{5}$$

$$\begin{aligned}\frac{N}{S}\frac{dx_1}{dt} &= K_1[2\alpha(1-\alpha) - x_1] + K_2[\alpha(1-\alpha_s) + \alpha_s(1-\alpha) - x_1] + \\ &+ K_3[2\alpha_s(1-\alpha_s) - x_1]\end{aligned} \tag{6}$$

Here N is the number of O_2 molecules, S – the surface area of oxide, t – time, $\alpha = 0.5\, x_1 + x_2$-isotope fraction, $R = 0.5K_2 + K_3$ – the rate of heteroexchange, K_1, K_2 and K_3 – the rates of exchange of the 1st, 2nd and 3rd type (with participation of 0, 1 and 2 surface oxygen atoms, respectively[54,55,56,57,58]), their sum giving the total rate of exchange R.

For a complete description of the isotope redistribution, differential equations reflecting the isotope transfer in the solid phase must be added to this system

$$\frac{N_s}{S}\frac{\partial\alpha_s}{\partial t} = R(\alpha - \alpha_s) - r_D\frac{N_e}{S}\frac{\partial\alpha_v}{\partial\eta}\bigg|_{\eta=0} \tag{7}$$

$$\frac{\partial\alpha_v}{\partial t} = r_D\frac{\partial^2\alpha_v}{\partial\eta^2} \tag{8}$$

with the initial and boundary conditions:

$$\begin{aligned}&t=0:\ \alpha = \alpha^0,\ \alpha_s = \alpha_v = \alpha_s{}^0; \\ &\eta = 0:\ \alpha_v = \alpha_s\end{aligned} \tag{9}$$

where α_v is the fraction of ^{18}O in the oxide bulk, N_S and N_e are the number of oxygen atoms in the surface layer of oxide and the number of exchangeable atoms in the bulk of the oxide, respectively; η is the reduced depth (z) of the oxide layer η=z/h, where h is the characteristic size of oxide particles; $r_D = \frac{D}{h^2}$ is the effective diffusion coefficient (diffusion relaxation constant), D is the oxygen self-diffusion coefficient.

By transformation of isotope equations (5) and (6), so called isotope-mechanistic equation (10) without time was derived

$$\ln\frac{v+b}{v^0+b} = -a\ln\frac{s}{s^0} \tag{10}$$

Here $\mathbf{v = z/s^2}$, $\mathbf{s = \alpha - \alpha_s}$, $\mathbf{z} = x_2 - \boldsymbol{\alpha}^2\, x_2$, x_2 –fraction of $^{18}O_2$ molecules, and parameters **a** and **b** are determined by the type of mechanism:

$$a = 2\frac{k}{r} = \frac{\kappa_2 + 2\kappa_3 - 1}{0.5\kappa_2 + \kappa_3} \tag{11}$$

$$b = \frac{k_3}{2r - k} = \frac{\kappa_3}{\kappa_2 + 2\kappa_3 - 1} \tag{12}$$

The depth of isotope penetration from the gas phase into the oxide in the course of TPIE can be characterized by the value N_X determined from the relation

$$2N\alpha^0 + N_X\alpha_S^0 = \alpha(2N + N_X) \tag{13}$$

The value $\mathbf{N_X}$ is related to the average depth of isotope incorporation into the solid phase (l_α) by relation $\mathbf{N_X = n_O \cdot S \cdot l_\alpha}$, (here $\mathbf{n_O}$ is the number of oxygen atoms in the unit volume of oxide). This quantity termed as "dynamic degree of isotope exchange" is expressed in relative units $X_S = \frac{N_X}{N_S}$ and $X_V = \frac{N_X}{N_V}$, corresponding, respectively, to the number of exchanged oxygen monolayers X_s, (1 monolayer = $1.4\cdot10^{19}$ atoms/m^2) and the exchanged fraction of the bulk oxygen, X_v.

Cheselske, Hall et al.[59, 60] derived equation to estimate apparent activation energy of heteroexchange in experiments with a linear temperature ramp and uniform by reactivity species:

$$E = -\left[\frac{RT^2\frac{d\alpha}{dT}}{\alpha-\gamma}\right]_I \qquad (14)$$

Here, -dα/dT is taken at the inflection point where it achieves a maximum value, α — respective isotope fraction at this point, γ — equilibrium isotope fraction.

4.4 SSITKA data analysis

Fitting of experimental responses $\alpha(t)$ and $x_1 t)$ was carried out in frames of diffusion model with a due regard for three types of the surface exchange (K_1, K_2 and K_3 as well as diffusion of isotope atoms into the bulk of oxide particles[48]:

$$\begin{aligned}
&C_{O_2}\left(\frac{\partial\alpha}{\partial t}+\frac{1}{\tau}\frac{\partial\alpha}{\partial\xi}\right) = -b(0.5K_2+K_3)(\alpha-\alpha_s)\\
&C_{O_2}\left(\frac{\partial x_1}{\partial t}+\frac{1}{\tau}\frac{\partial x_1}{\partial\xi}\right) = bK_1(2\alpha(1-\alpha)-x_1)+\\
&\quad +bK_2(\alpha(1-\alpha_s)+\alpha_s(1-\alpha)-x_1)+bK_3(2\alpha_s(1-\alpha_s)-x_1)\\
&\frac{\partial\alpha_s}{\partial t} = (0.5K_3+K_3)(\alpha-\alpha_s)-\frac{N_{bulk}}{N_S}\frac{D}{h^2}\left.\frac{\partial\alpha_{bulk}}{\partial\eta}\right|_{\eta=0}\\
&\frac{\partial\alpha_{bulk}}{\partial t} = \frac{D}{h^2}\frac{\partial^2\alpha_{bulk}}{\partial\eta^2}
\end{aligned} \qquad (15)$$

Initial and boundary conditions:

$$\begin{aligned}
&t=0:\ \alpha=0,\ x_1=0,\ \alpha_s=0,\ \alpha_{bulk}=0\\
&\xi=0:\ \alpha_g=\alpha_g^{input},\ x_1=x_1^{input}\\
&\eta=0:\ \alpha_{bulk}=\alpha_s
\end{aligned} \qquad (16)$$

Here α_S and α_{bulk} - fractions of ^{18}O on the surface and in the bulk of oxide, respectively; τ - contact time (s); b – number of the surface centers (mole) related to the number of gas phase moles; K_1, K_2 and K_3 – rates of respective exchange types (s^{-1}); D - coefficient of ^{18}O diffusion in the bulk of oxide (m^2s^{-1}); h - typical size of particles (m), N_S and N_{bulk} - number of oxygen atoms on the surface and in the bulk of particles; ξ - normalized reactor length; η - normalized depth of oxide particle layer.

Chapter three

Main results and discussion

5 Results and discussion

5.1 Characteristics of the studied catalysts

The compositions of the studied catalysts with various active components supported on doped ceria-zirconia oxides are presented in Table 1.

Composition	**Abbreviation**	**Specific surface area, m^2/g**
1.4%Pt/$La_{0.3}Ce_{0.35}Zr_{0.35}O_2$	Pt/LCZ	-
1.4%Pt/$Gd_{.3}Ce_{0.35}Zr_{0.35}O_2$	Pt/GCZ	12
1.4%Pt/$Gd_{.3}Ce_{0.35}Zr_{0.35}O_2$ / Al_2O_3 channel	Pt/GCZ	15
1.4%Pt/$Pr_{0.3}Ce_{0.35}Zr_{0.35}O_2$	Pt/PCZ	29
1.4%Pt/$Pr_{0.3}Ce_{0.35}Zr_{0.35}O_2$ / Al_2O_3 channel	Pt/PCZ	21
6%$LaNiO_3$/$Sm_{0.15}Pr_{0.15}Ce_{0.35}Zr_{0.35}O_2$	LaNi/SPCZ	28
1.4%Ru/$Sm_{0.15}Pr_{0.15}Ce_{0.35}Zr_{0.35}O_2$	Ru/SPCZ	20
1%Ru/80%$Sm_{0.3}Ce_{0.35}Zr_{0.35}O_2$+10%NiO+10%YSZ	Ru/SCZ+NiO+YSZ	24
(0.57%Ru+6.6%NiO)/ $Sm_{0.15}Pr_{0.15}Ce_{0.35}Zr_{0.35}O_2$	Ru,Ni/SPCZ	21

Table 1: Composition, abbreviations and surface area of the main prepared catalysts.

Structural, microstructural and surface characteristics of samples elucidated by X-ray diffraction, neutron diffraction, EXAFS, transmission electron microscopy with elemental analysis are given in [45,46,47,51,52,53,61,62].

Doped ceria-zirconia fluorite-like oxides prepared by Pechini route are single-phase materials with a specific surface area increasing with the dopant content up to 100- 150 m^2/g. (calcined at 700°C) or 30-40 m^2/g (calcined at 900°C). In as-prepared samples, metals (Pt, Ru, Ru+Ni) supported on fluorite-like oxides or nanocomposites are mainly in the form of oxidic species strongly interacting with oxide particles and partially incorporated into their surface layers. For nanocomposites prepared via one-pot Pechini route, NiO particles decorated by fluorite-like oxidic fragments are present as well. In reduced steady-state of CH_4 DR catalysts, metal or metal alloy nanoparticles/clusters (including Ni (Ru, Pt) alloy clusters segregated from supported $LaNi(Pt,Ru)O_3$), are epitaxially bound with supports and partially decorated by support oxidic species.

5.2 Oxygen mobility for nanocomposite catalysts characterized by oxygen heteroexchange

5.2.1 Temperature-programmed isotope exchange (TPIE) in a static reactor

For all samples of $Ln_x(Ce_{0.5}Zr_{0.5})_{1-x}O_{2-\delta}$ fluorite-like oxides including those promoted by Pt, linearization of results in coordinates of isotope-mechanistic Equation 5 revealed that the 3rd type of mechanism (a share in the range of 0.7-0.9) was dominant, without any impact of the 1st type of exchange.

Estimation of the dynamic degree of exchange revealed that at temperatures below 600°C, the oxygen exchange is limited to the surface layers (X_S below 1 monolayer) due to much faster surface reaction and surface diffusion as compared to the bulk diffusion. At higher temperatures incorporation of isotope into the bulk of oxide particles occurs rather fast, so, for some samples, i.e., for $Pt/Ce_{0.5}Zr_{0.5}O_{2-x}$ sample, X_S achieves 4-5 monolayers at 700-750 °C.

To characterize mainly the surface/near surface oxygen mobility, 650°C was selected as the temperature of comparison. Indeed, at this temperature for majority of samples considered here X_S is below a monolayer (Figure 3), thus mainly reflecting the oxygen migration within the surface/near-surface layers.

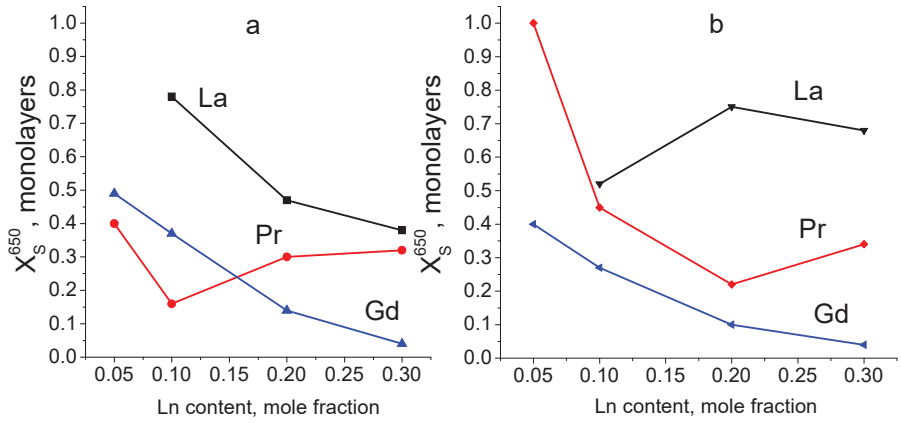

Figure 3. Dependence of dynamic degree of exchange X_S on the dopant content for samples of $Ln_x(Ce_{0.5}Zr_{0.5})_{1-x}O_{2-\delta}$ (a) and $Pt/ Ln_x(Ce_{0.5}Zr_{0.5})_{1-x}O_{2-\delta}$ (b). PO_2 = 2.5 Torr.

As integral parameter, X_s depends upon all factors controlling dynamics of the surface reaction and diffusion in solid, namely, the sample pretreatment, gas phase oxygen concentration, temperature ramp, etc.

For the undoped samples $Ce_{0.5}Zr_{0.5}O_{2-x}$ and $Pt/Ce_{0.5}Zr_{0.5}O_{2-x}$, X_S values at 650°C and 2.5 Torr O_2 are equal to 0.5 and 1.7, respectively, i. e. being in general higher than for doped samples. This

feature is explained by the well-documented structural microheterogeneity of nanocrystalline ceria-zirconia solid solutions, consisting of domains enriched by Zr and Ce cations, respectively[51,61,62]. This microheterogeneity generates Frenkel-type defects (pairs anion vacancy-oxygen interstitial). Such defects decrease the activation barriers for the oxygen diffusion and provide surface sites with a low oxygen bonding strength more active in the oxygen exchange. Extended defects present at domain boundaries in $Ce_{0.5}Zr_{0.5}O_{2-x}$ sample and detected also as microstrains by neutron diffraction data analysis[51,61,62] can also provide pathways for facile oxygen migration due to strongly distorted coordination polyhedra in their vicinity.

As seen in Figure 3a, doping by smaller Pr and Gd cations provides more uniform distribution of Ce and Zr cations, thus decreasing the density of Frenkel-type defects and microstrains and, as the result, decreasing the oxygen mobility. On the other hand, for largest La cations, X_S increases from 0.5 for undoped sample to 0.8 for moderate (xLa = 0.1) doping level. In this case, the increase of the lattice parameter accompanied by the decrease of the surface Ce-O bond strength as revealed by SIMS[20,61] appears to be responsible for the increase of X_S for this moderately doped sample.

According to EXAFS data SIMS[20,61,62], for samples doped by Gd or La, symmetry and average coordination numbers (CN) for Zr-O and Ce-O spheres increase with the dopant content, while Ce-O sphere contracts, which suggests strengthening of Ce-O bond and disappearance of "free" anion vacancies near Ce cations caused by a complex rearrangement of coordination polyhedra. Usually, for ceria-zirconia solid solutions distortion of Zr-O and Ce-O spheres and lattice expansion leading to the appearance of longer (and, hence, weaker) metal-oxygen bonds are considered as the most important factors controlling oxygen mobility. Hence, clear trends in declining of X_S with the doping level for Gd- or La-containing samples can be explained by such complex rearrangement of coordination spheres and disappearance of "free" oxygen vacancies.

For Pr-doped samples some increase of XS at a high Pr content can be explained by increasing the Pr^{4+} share which favors mixed ionic-electronic conductivity via chains of Pr^{3+}-Pr^{4+} cations, and, hence, enhanced oxygen mobility, perhaps, along domain boundaries enriched by Pr cations[20,61,62].

As can be seen in Figure 3b, adding Pt to these doped oxides will change X_S values, depending upon the type and content of doping cation. This suggests a specific interaction of Pt with the surface sites/dopants, including, possibly a rearrangement of the surface layer caused by leaching of basic-type Ln^{3+} cations during incipient wetness impregnation by acid H_2PtCl_6 solutions and incorporation of Pt^{n+} cations into the surface vacant sites.

For undoped sample, high values of X_S (~ 1.7 at 650 ^oC[20,61,62]) was explained by a high density of microstrains and Frenkel-type defects taking parts in stabilization of ionic Pt forms. For

doped samples, a minor (if any) effect of Pt supporting for Gd-doped samples appears to correlate with mainly subsurface location of small Gd cations, while the strongest effect is observed for samples doped with the biggest La cations segregated in the surface layer. The most positive effect of Pt on X_S, especially at low doping content, is observed for Pr-doped samples. This seems to correlate with the highest ability of $Pr^{3+/4+}$ cations to stabilize Pt as 2+/4+ cations[20,45,61,62]. Incorporation of these Pt cations into the subsurface/near surface positions as well as into domain boundaries is expected to generate oxygen vacancies as well as to enhance mixed ionic-electronic conductivity along Pr^{3+}/Pr^{4+} chains thus facilitating oxygen diffusion.

Estimation of E_a of heteroexchange by Eq. (14) (vide supra) helps to elucidate the effect of doping cations on the reactivity of surface sites.

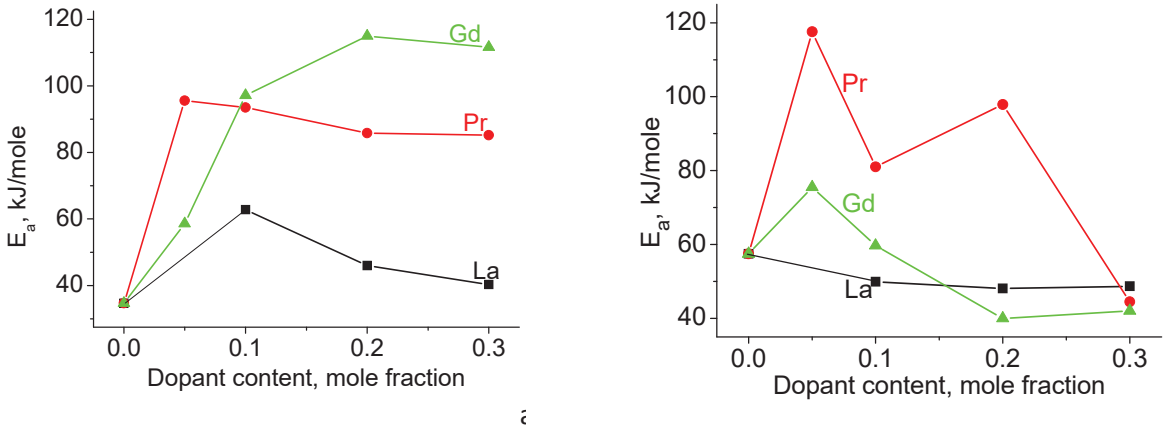

Figure 4. Effect of dopant content in $Ln_x(Ce_{0.5}Zr_{0.5})_{1-x}O_{2-y}$ (a) and $Pt/Ln_x(Ce_{0.5}Zr_{0.5})_{1-x}O_{2-y}$ (b) samples on E_a, estimated from Hall et al [61]

In typical experiments inflection point is situated at temperatures ~ 600-700°C, thus being close to the temperature range of X_S estimation. Hence, the activation energy estimated in such a way can be considered as characteristic of the surface reaction steps. For samples without Pt, E_a of isotope exchange is higher for doped samples reflecting variation of the real structure (disappearance of extended defects at domain boundaries, more symmetric and dense coordination sphere of Ce cations in the surface layer) increasing the Ce-O bond strength and decreasing the density of oxygen vacancies in the surface layer. Decrease of E_a with increasing the size of doping cation Gd<Pr<La (and, hence, increasing the lattice parameter[20,61] agrees with this suggestion, since a longer (and, hence, weaker) Ce-O bond strength suggests a lower activation barrier for its rupture as well as a higher density of anion vacancies at chemical equilibrium with the gas phase oxygen.

As seen in Figure 4b, the effect of adding Pt on E_a clearly depends upon the type and content of doping cation. Pt added to undoped Ce-Zr-O sample increases apparent activation energy. Since

Pt sites are known to be much more active in oxygen isotope exchange than ceria-zirconia surface centers[48], this suggests that the estimated E_a is mainly determined by steps like oxygen spillover from the Pt to support and/or surface /near surface diffusion. The estimation by fitting SSITKA data for Pt/La-Ce-Zr-O sample revealed that at 650^{o}C specific rates of exchange on Pt and Pt-support spillover are 1-2 orders of magnitude higher than the rates of surface diffusion and exchange on support, the latter being comparable[48]. Hence, the temperature dependence of the exchange rate on Pt-supported samples should be determined mainly by the isotope surface diffusion from Pt clusters to surrounding oxide regions.

For the largest (and, hence, the most basic) La cation, E_a only decreases with the doping level (Figure 4b). Since the fraction of oxidic Pt forms (oxidic clusters, isolated Pt^{2+} species, including those incorporated into the surface/subsurface layers and domain boundaries) increases with La content[21,61], this implies that the barriers for O_2 dissociation and surface/near-surface diffusion are decreased due to such action of Pt oxidic forms. This can be explained by the generation of oxygen vacancies due to Pt^{2+} incorporation into the surface layer.

For Gd-doped samples, the addition of Pt decreases E_a for all doping levels (Figure 4b). This can be explained by the same mechanism of oxygen vacancies generation due to Pt^{2+} incorporation into the surface layer. The decrease of activation energy does not increase X_S (Figure 3). Hence, the concentration factor – the density of "free" oxygen vacancies is more important than the energetic one.

For Pr-doped sample the effect of Pt supporting on E_a is the most complex, since increasing it for some compositions and decreasing for others. At the highest doping level, E_a is identical for samples with all dopants, agreeing with the suggestion about changing the rate-limiting stage determined by the oxygen surface diffusion. A non-uniform distribution of Pt and Pr cations in/on the surface layer and domain boundaries might also affect pathways of fast surface diffusion.

Activation energies of exchange were also estimated from the initial low-temperature parts of temperature-programmed exchange curves where the degree of exchange is small. In general, there is a reasonable correlation between the values of activation energy estimated by these two procedures as shown for Pr-doped samples in Figure 5.

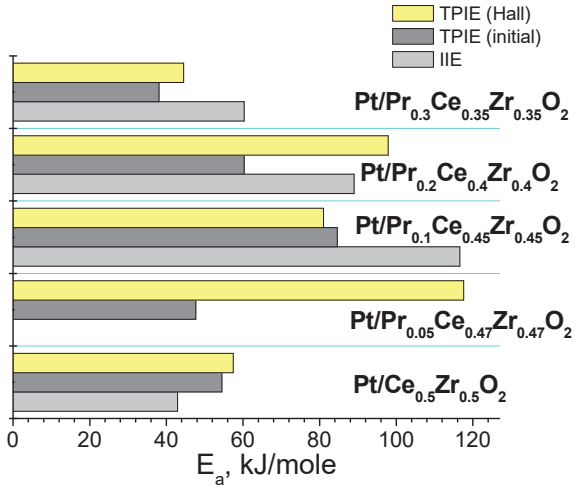

Figure 5. Comparison of E_a estimated by different procedures for Pt/Pr-Ce-Zr-O samples

The values of E_a estimated from the initial parts of exchange curves tend to be lower than those obtained by the Hall approach. This may be due to both a higher impact of steps occurring on Pt sites as well as the participation of defect sites with a lower oxygen bonding strength at lower temperatures.

5.2.2 Isothermal isotope exchange in a static reactor.

For all samples, the α(t) was close to vary exponentially, which might indicate an identical reactivity of exchangeable oxygen forms[54,55,56,57,58]. This allowed us to estimate specific rates of exchange R by using a simple integral form of Eq. (5). As follows from Figure 6, the dependence of these rates on the dopant content is similar to that of X_S. This agrees with the fact that for Pt-supported samples, dynamics of the oxygen heteroexchange is controlled by the surface diffusion step.

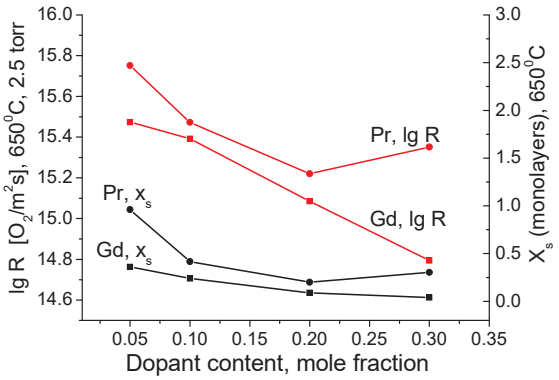

Figure 6. The rate of oxygen heteroexchange and dynamic degree of exchange for Pr or Gd – doped Pt-supported Ce-Zr-O systems at 650 °C and 2.5 Torr O_2

The values of the activation energies, estimated from the temperature dependence of specific rates of heteroexchange obtained in isothermal experiments, were found to correlate in general with values derived from results of TPIE experiments (Figure 5).

To figure out the constants corresponding to the surface process and bulk diffusion, respectively, the IIE data were fit by solving the system of differential rate equations (5), (6), (7), (8). Typical results of fitting are shown in Figure 7.

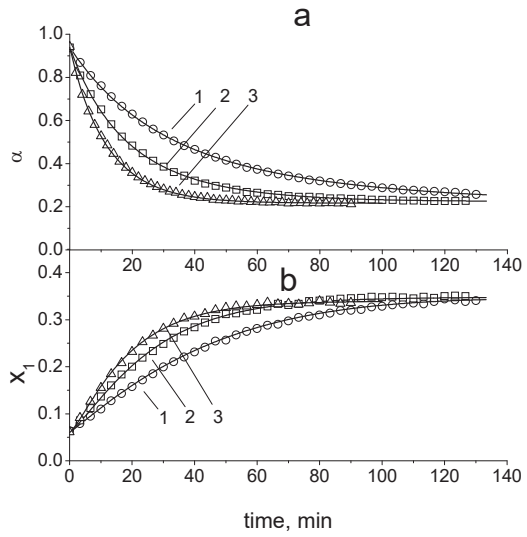

Figure 7. . Results of $\alpha(t)$ (a) $x_1(t)$ (b) fitting in isothermal isotope exchange at 1) 550 ^{0}C; 2) 600 ^{0}C; 3)650 ^{0}C for Pt/$Pr_{0.3}Ce_{0.35}Zr_{0.35}$ sample

The rates of heteroexchange estimated from the integral equations and by fitting were found to be quite close. The share of the 3rd type of exchange varies from 0.85 to 0.93, i.e. close to the values estimated by isotope-mechanistic equation (vide supra). The value of the activation energy related to heteroexchange (~ 70 kJ/mole) was found close to the value estimated from IIE data by using an integral equation (~ 60 kJ/mole).

The values of oxygen self-diffusion coefficients D (10^{-15}-10^{-16} m^2/s in studied temperature range) found by fitting are by 1-2 order of magnitude higher than the maximum values of D estimated for the near-surface layer for Pt/supported La-Ce-Zr-O sample (~ 10^{-17} m^2/s) from results of SSITKA experiments[48]. As expected, the activation energy of bulk diffusion (~ 150 kJ/mol) is higher than that of the surface processes (vide supra).

TPIE experiments for layers of catalysts supported on walls of corundum channels (Fig. 8) agree in general with results obtained for powders. Pt supporting clearly increases oxygen mobility in the middle-temperature range (500-600^{o}C). After testing in reducing reaction feed (partial oxidation/dry reforming of methane) the oxygen mobility is somewhat decreased due to the removal of part of weakly bound oxygen located within domain boundaries (vide infra).

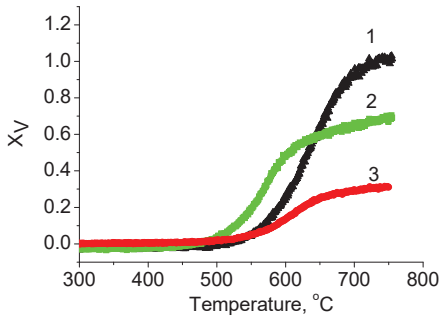

Figure 8. Temperature dependence of the dynamic degree of exchange X_V for layers of $Pr_{0.3}Ce_{0.35}Zr_{0.35}O_x$ (1), $Pt/Pr_{0.3}Ce_{0.35}Zr_{0.35}O_x$ (2, 3) supported on the walls of corundum channels. 1, 2 –fresh samples, 3- after testing in methane reforming. PO_2 1.7-1.8 Torr

5.2.3 Oxygen isotope heteroexchange in a flow reactor (SSITKA)

Isotope transients carried out by isothermal oxygen isotope exchange with $^{18}O_2$

Typical dynamics of these SSITKA experiments are shown in Figure 9, and results of such curves fitting are presented in Table 2.

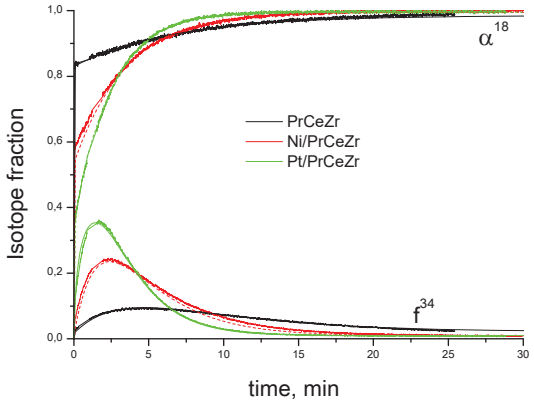

Figure 9. Effect of supported active component (Pt , Ni) on dynamics of isotope response: points –experimental data, lines –calculated time dependence of the atomic fraction of ^{18}O (α^{18}) and $^{16}O^{18}O$ (f^{34}) in the gas phase. 600 ^{o}C, flow rate 300 ml/min, weight 0.05 g.

As expected, the rate of exchange is higher for Pt than for Ni, much exceeding the rate of exchange for the oxide sites. Note also a high rate of Pt-oxide spillover which supports the conclusions made on the basis of experiments in a static reactor. Similarly, the value of the coefficient of oxygen diffusion along domain boundaries (Table 2) is very close to the values obtained by fitting isothermal exchange curves in a static reactor (Figure 7).

Table 2. Parameters of oxygen exchange for CeZrPr with supported Ni or Pt.

Temperature, [°C]	600	700	800
Rate of exchange on the oxide sites [s^{-1}]*	0.02	0.1	0.3
Rate of exchange on Ni sites [s^{-1}]**	0.4		0.9
Rate of exchange on Pt sites [s^{-1}]**	15	30	
Rate of Ni – oxide spillover [s^{-1}]**	>1		>2
Rate of Pt – oxide spillover [s^{-1}]**	$>4\times10^{1}$	$>1\times10^{2}$	
Coefficient of oxygen diffusion along domain boundaries [m^2s^{-1}]		3×10^{-15}	
Coefficient of oxygen diffusion in oxide domains [m^2s^{-1}]		4×10^{-18}	

*rate of exchange per one center of oxide, ** - rate of exchange per one atom of metal (Ni or Pt).

Oxygen diffusion characteristics of catalysts in the steady state of CH_4 dry reforming by $^{18}CO_2$ SSITKA.

These experiments allow us to estimate the effect of catalyst reduction by the reaction feed on the oxygen mobility in fluorite-like oxide support. As follows from Figure 10, for LaNiPt/PrSmCeZr catalyst isotope transients are practically identical for the case of pretreatment in oxygen and after achieving the steady-state in the reaction feed.

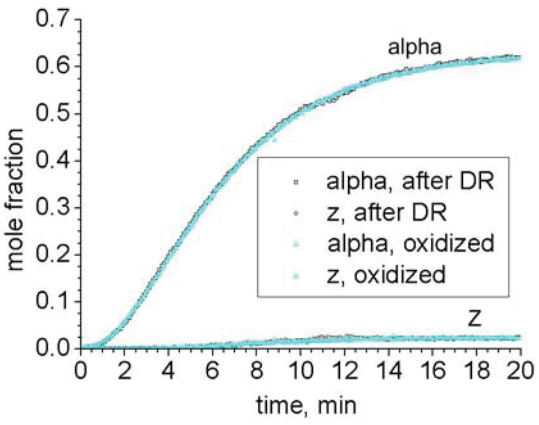

Figure 10. Effect of pretreatment on isotope transients in the course of $C^{18}O_2$ exchange with LaNiPt/PrSmCeZr sample at 700 °C; $\alpha = 0.5$ X_1+X_2, where α - fraction of ^{18}O in the gas phase, X_2 – fraction of $C^{18}O_2$, X_1 = fraction of $C^{16}O^{18}O$; $z = X_2 - \alpha^2$ - deviation from the binomial distribution for $C^{18}O_2$ molecules with fraction X_2.

Similar to the case of oxygen heteroexchange with $^{18}O_2$, all oxygen atoms of the catalyst were equilibrated with the oxygen in the gas phase. The estimation of oxygen diffusion coefficients in the bulk of oxide domains (D_{bulk}) and along domain boundaries ($D_{interfaces}$) (Table 3) revealed that they are somewhat decreased as compared with values found for completely oxidized states but remained at a high level. According to O_2 TPD data (vide infra), this decrease is explained by a removal of weakly bound mobile oxygen atoms located within or along the domain boundaries.

Table 3. Coefficients of oxygen diffusion in Pt/PrCeZr and LaNiPt/PrSmCeZr catalysts by $^{18}O_2$ and $C^{18}O_2$ SSITKA

Sample	$*D_{eff}$, s^{-1}	D_{bulk}, 10^{-18} m^2/s	$D_{interfaces}$, 10^{-16} m^2/s
Pt/PrCeZr			
$^{18}O_2$	0.04	4	>33
$C^{18}O_2$	0.003	-	>2
LaNiPt/PrSmCeZr			
$^{18}O_2$	>0.03	3	>25
$C^{18}O_2$	0.008	-	>5

According to the analysis of dynamics of CH_4 dry reforming on Pt/PrCeZr[45], the values of oxygen diffusion coefficients along the interfaces (surface and domain boundaries) ~ 10^{-12}-10^{-13} cm^2/s are sufficient to provide an effective supply of oxygen species to the metal/oxide interface required for maintaining a high catalytic activity

5.3 Temperature-programmed O_2 desorption

Typical O_2 TPD spectra for samples pretreated in oxygen at 500°C are shown in Figure 11. The total amount of oxygen desorbed in TPD run varies from 14% monolayer (Pr) to 5-6% monolayer (Gd, La), thus corresponding only to a very small part of the total oxygen content in the samples. Oxygen desorption from doped ceria-zirconia oxides without supported Pt starts in the same temperature range[23], hence, easily desorbed surface oxygen forms are bound not only with Pt cations but with some surface defects on the surface of oxide particles as well. Moreover, oxygen desorption is accompanied by oxygen diffusion along domain boundaries to the surface. With a due regard for SSITKA data (vide supra), nearly all oxygen desorbed in TPD run can originate from domain boundaries. Indeed, a higher rate of oxygen desorption at ~ 400°C from Pt/PrCeZr sample as compared with that for Pt/LaCeZr (Figure 11) correlates with a higher coefficient of oxygen diffusion along domain boundaries for the former catalyst.

5.4 Temperature-programmed reduction by CH_4

In these experiments, all reducible Me^{4+} cations (Ce^{4+}, Pr^{4+}) are reduced to Me^{3+} state after keeping under contact with CH_4 stream at 880°C[23], which corresponds to the removal of ca. 10 monolayers of oxygen. Hence, the reduction process is clearly associated with a rapid oxygen

diffusion from the bulk of oxide support particles to their surface where it is consumed by interaction with CH_x species generated by the dissociation of CH_4 molecules on Pt sites. Such a dissociation continues at high temperatures even after nearly complete samples reduction when CO_x release is practically no more observed (Figure 12).

The parallel release of CO, CO_2 and H_2 at ~ 400°C (Figure 12) for all oxidized samples demonstrates the ability of these systems to selectively transform CH_4 into syngas. The intensity of these low-temperature peaks clearly correlates with the surface/near-surface oxygen mobility characterized by X_S (La>Pr>Gd) (vide supra).

For Pr-doped sample the second peak of syngas release is situated at the lowest temperature (~550°C) among the studied samples, indicating it is apparently controlled by the lattice oxygen diffusion and reactivity of strongly bound surface oxygen forms. This would correlate with the highest catalytic activity of Pt/PrCeZrO in the high-temperature region in concentrated feeds (Figure 1).

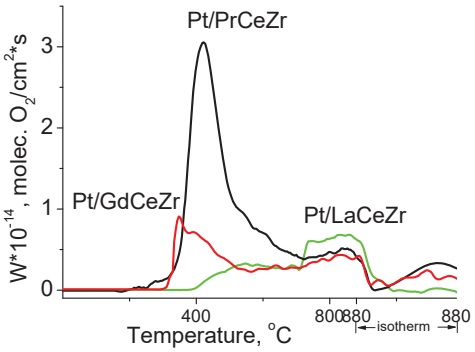

Figure 11. O_2 TPD spectra for Pt/$Ln_{0.3}$Ce-Zr-O samples calcined at 900°C. Pretreatment in O_2 at 700°C for 1 h.

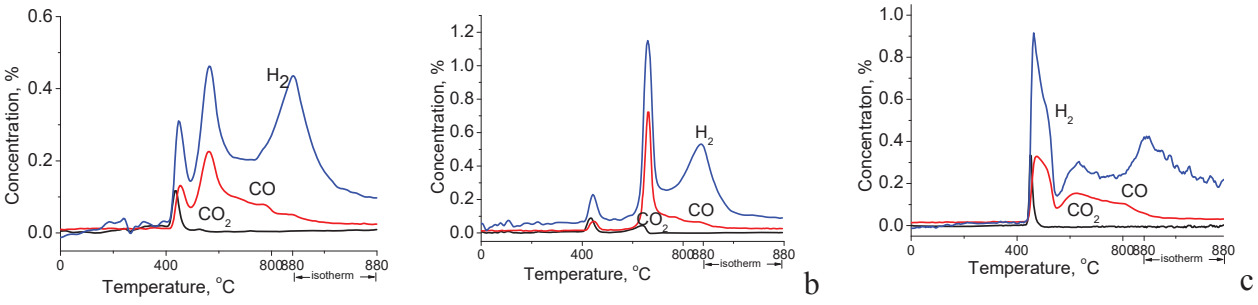

Figure 12. CH_4 TPR spectra for Pt-supported ceria-zirconia oxides doped by 30 at.% of Pr (a), Gd (b) or La (c).

5.5 Comparison of oxygen mobility and reactivity with catalytic activity in dry reforming on catalysts supported on structured corundum channels.

The search for relationship between oxygen mobility and catalytic performances was achieved on corundum structured channels at short contact time to avoid any heat and mass-transfer effect[49,50]. Results obtained with supported layers of Pt-promoted ceria-zirconia oxides doped by 30 at.% of Pr, Gd or La, are reported in Figure 13.

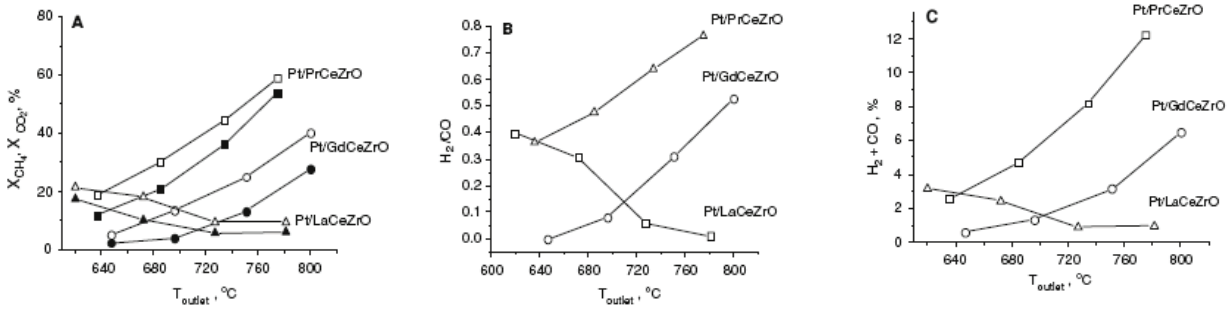

Figure 13. Temperature dependence of the reactants conversion (a, XCH4—filled symbols, $X CO_2$—open symbols), molar H_2/CO ratio (b) and syngas content (c) in DR. Feed composition: 7 %CH_4 + 7% CO_2 in N_2, contact time 15 ms

As can be seen, at ~ 600°C the highest activity is obtained with the La-doped sample which possesses the highest surface oxygen mobility in the oxidized state in this temperature range. This feature was assigned to a stabilization effect of Pt cationic forms (vide supra). However, at higher temperatures, this catalyst is deactivating due to a progressive reduction of these Pt ions leading to Pt sintering and segregation from the La hydroxocarbonates covering the surface of ceria-zirconia oxide. Such a catalyst restructuring is deemed to prevent CO_2 molecules activation on redox sites. Thus, the deactivation process would be caused by the loss of interface sites responsible for both reactants activation : i) methane due to Pt sintering and ii) CO_2 due to less efficient activation via La hydroxocarbonates.

For catalysts doped with less basic cations – Gd, Pr - the catalytic performance was found to remain stable even at high temperature. Again, the Pr-doped catalyst displaying the highest oxygen mobility was found to present the highest activity. Also worthy to note is that the H_2/CO ratio was also higher for this Pr –doped sample. It might be speculated that the reverse water gas shift reaction is hindered for catalysts characterized by a high oxygen mobility, which would keep Pt in a more oxidized state, probably less active for this reaction (vide infra).

For catalysts based upon Pr-doped ceria-zirconia tested as particles of 0.25-0.5 mm size mixed with quartz sand in a fixed-bed layer, comparison of specific first-order rate constants

revealed that supported Ru+Ni systems provide even better steady-state performance as compared with supported Pt, though the range of activity remains narrow (Table 4).

Table 4. Chemical composition, abbreviation, specific surface area and specific catalytic activity of Me-supported fluorite-like catalysts

Chemical composition	**Abbreviation**	**S_{BET}, m^2/g**	**K, $s^{-1}m^{-2}$ at 700°C**
8%$LaNiO_3$ / $Pr_{0.15}Sm_{0.15}Ce_{0.35}Zr_{0.35}O_2$	LaNi/ PrSmCeZr	21	1.7
8%$LaNiO_3$ +1%Pt/ $Pr_{0.15}Sm_{0.15}Ce_{0.35}Zr_{0.35}O_2$	LaNiPt/ PrSmCeZr	21	1.7
1.4%Pt/ $Pr_{0.15}Sm_{0.15}Ce_{0.35}Zr_{0.35}O_2$	Pt/ PrSmCeZr	30	0.7
1.4%Pt/$Pr_{0.3}Ce_{0.35}Zr_{0.35}O_2$	Pt/ PrCeZr	16	1.5
1%Ru+10%NiO/ $Pr_{0.15}Sm_{0.15}Ce_{0.35}Zr_{0.35}O_2$/YSZ	Ru+Ni/PrSmCeZr/YSZ	30	4
1.4%Ru/ $Pr_{0.15}Sm_{0.15}Ce_{0.35}Zr_{0.35}O_2$	Ru/PrSmCeZr	20	2.4
1.4%Ru+6.6%Ni/ $Pr_{0.15}Sm_{0.15}Ce_{0.35}Zr_{0.35}O_2$	Ru+Ni/PrSmCeZr	18	7.5

Since in this case a stable performance is likely to come from a high oxygen mobility in doped ceria-zirconia support, not suppressed after Ni or Ru addition, the level of activity will depend essentially from the reactants activation, which was studied by transient techniques.

5.6 Main features of the mechanism of methane dry reforming by transient studies

5.6.1 Chemical non steady-state transients

Figure 14 and Figure 15 present the transient behaviour of catalytic systems obtained by switching the stream at the reactor inlet from one reacting or pre-treatment mixture to another one. In Figure 14, a He stream was switched at 700°C to a similar stream containing 0.5% CH_4 in He. CO appears at the reactor outlet simultaneously with CH_4, which might correspond to the kinetic behaviour of a non adsorbing primary product, while CO_2 curve is delayed, which might correspond to the kinetic behaviour of a secondary product, or of a strongly adsorbing primary product. Hydrogen is delayed even more suggesting that it produced from methane cracking, but

immediately oxidized by the reactive oxygen species available from the support. A primary route of CH_4 activation on oxidized Pt sites producing CO and hydroxyls (or water) cannot be excluded. In any case, a high activity of oxidized Pt cationic species in CH_4 activation is apparent, which is unique feature of Pt among all studied metals[47].

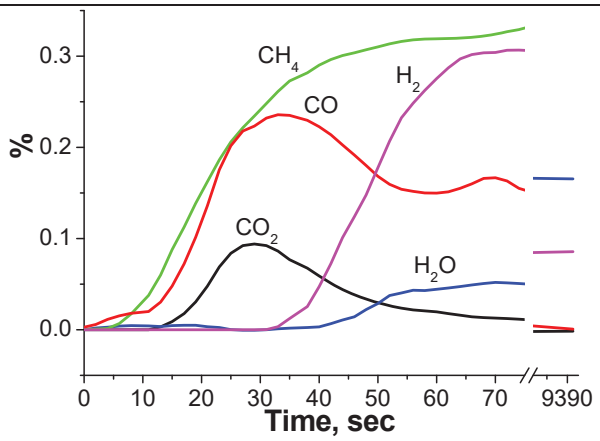

Figure 14. Transient responses to a switch He to 0.5% CH_4 in He at 700°C over $Pt/Pr_{0.3}CeZrO_x$ supported on a corundum channel after a pretreatment in O_2. Contact time 5 ms

Figure 15 presents typical kinetic transients obtained for a RuNi/SmPrCeZrO sample after switching the reacting feed CH_4+CO_2 to feeds containing only one component - CO_2 or CH_4 - and back. As can be seen from these experiments, in the initial period after the switch, the exit concentrations of products (and, hence, the initial rates of their formation) – H_2 in the case of a switch to CH_4 and CO in the case of a switch to CO_2- coincide with those for the steady-state catalytic reaction. This tends to indicate that (i) the catalytic reaction proceeds through independent stages of CH_4 and CO_2 transformation, apparently on different active sites, and (ii) the oxygen diffusion in the surface/near-surface layers is really fast to provide rather slow variation of the products concentrations with time-on-stream after switch. Hence, it is to be even higher in the reaction conditions, thus providing required conjugation between stages of CH_4 and CO_2 transformation occurring on different active sites.

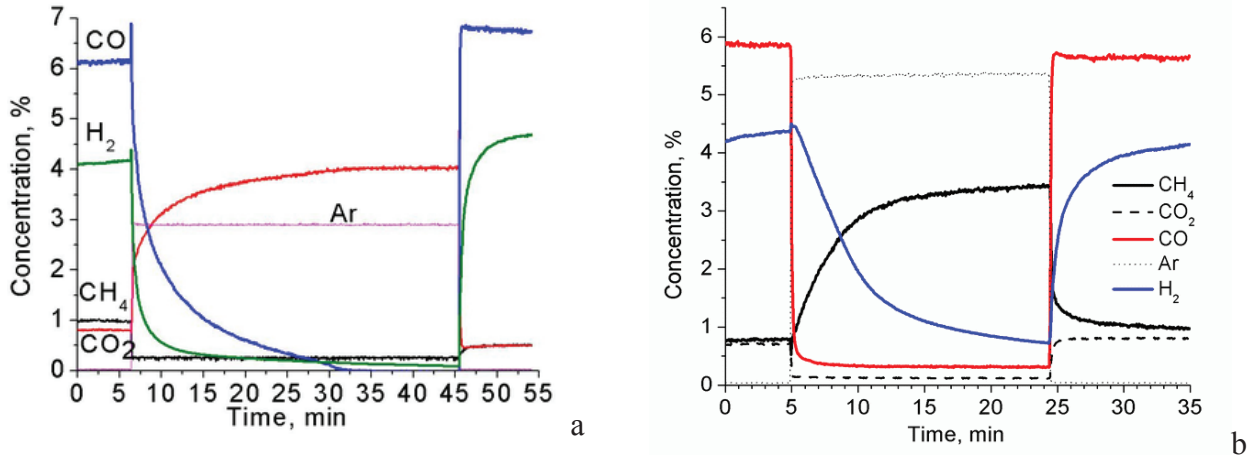

Figure 15. Typical transient responses for RuNi/SmPr catalysts to the feed switches $CH_4+CO_2 \rightarrow CO_2 \rightarrow CH_4+ CO_2$ (a) and $CH_4+CO_2 \rightarrow CH_4 \rightarrow CH_4+CO_2$ (b) at 650°C. Feed composition 3.8% CH_4 + 3.8%CO_2 in He, contact time 15 ms.

Hence, along with metal-support interaction, the oxygen mobility in the catalysts is deemed to be required for ensuring a high activity and a resistance to coke deposition for metal-supported catalysts on fluorite-like oxide supports.

5.6.2 SSITKA experiments

Figure 16 illustrates typical SSITKA responses corresponding to the feed switches with ^{12}C normal isotope composition to that containing labelled $^{13}CH_4$. As can be seen, the transients are fast, so the steady-state surface coverage by carbon-containing species is quite low not exceeding 10% of a monolayer (calculated on the basis of the metallic surface). After switching the feed stream from $^{12}CH_4+^{12}CO_2$+He to $^{12}CH_4+^{13}CO_2$+He+1%Ar for Ru+Ni/PrSmCeZr catalyst at 650°C, the fractions of ^{13}C in CO and CO_2 in the exit stream increased without any delay relative to the Ar tracer concentration, and at each moment the total number of ^{13}C atoms in CO and CO_2 was equal to that in the inlet $^{13}CO_2$, so there was no carbon isotope accumulation, in addition to the amount of carbon adsorbed on the catalyst surface under steady-state conditions. This demonstrates that the concentration of C-containing intermediates (carbonates, carbides etc) on the steady-state surface remains small but stable. That statement also suggests that the fraction of ^{13}C in CO should be equal to a half a sum of ^{13}C fractions in CO_2 and CH_4:

$$\alpha_{CO} = \frac{\alpha_{CO_2} + \alpha_{CH_4}}{2} \qquad (17)$$

In the present experiments, the ^{13}C fractions in the reactants were equal to $\alpha_{CO_2} = 0.7$, $\alpha_{CH_4} = 0$, respectively. In this case, the estimated ^{13}C fraction in CO should be equal to 0.35, while the experimental value was found equal to 0.4. At the same time, the ^{13}C fraction of CO_2 in the exit stream is much lower than that in the inlet feed being equal to 0.46. This means that in the course of reaction the exchange of carbon atoms between CO and CO_2 proceeds, while there is no transfer of ^{13}C into CH_4. This proves that stages of catalyst interaction with CH_4 and CO_2 are independent, the first one being irreversible, and the second one reversible.

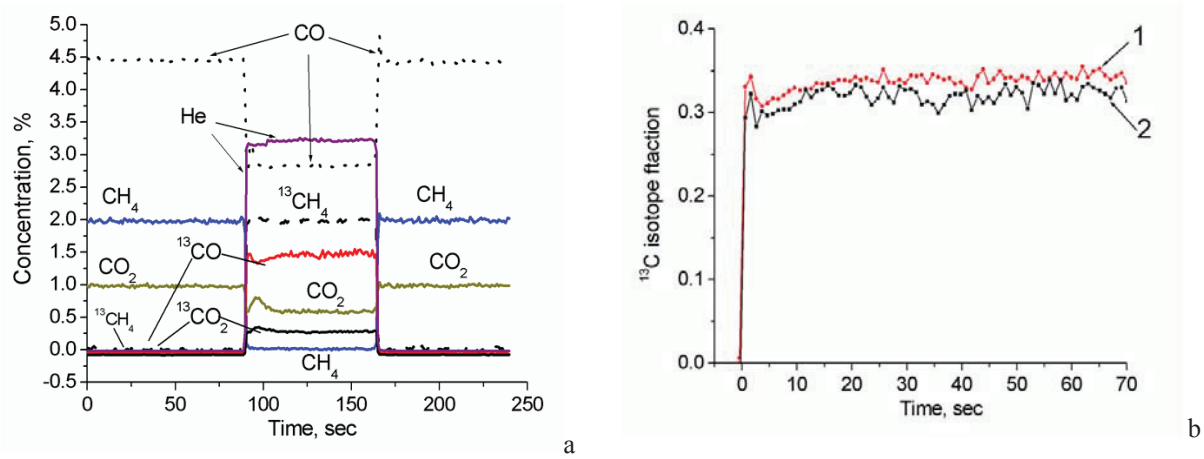

Figure 16. a) Steady State Isotopic Transients after the feed switches CH_4+CO_2 +He → $^{13}CH_4+CO_2$+He → CH_4+CO_2 +He for Pt/PrCeZr sample at 830°C, 15 ms contact time and inlet concentration of CH_4 and CO_2 4%
b) Time dependence of ^{13}C isotope fraction in CO (1) and CO_2 (2) after switching CH_4+CO_2 +He → $^{13}CH_4+CO_2$+He for Pt/PrCeZr sample at 830°C, 15 ms contact time and inlet concentration of CH_4 and CO_2 4%.

The simplest mechanism corresponding to this statement can be presented as follows:

$$\text{I. } [ZO] + CH_4 \rightarrow [Z] + CO + 2H_2 \qquad (18)$$

$$\text{II. } [Z] + CO_2 \leftrightarrow [ZO] + CO \qquad (19)$$

Here methane irreversibly interacts with oxidized centers of the catalyst with CO and H_2 formation (most likely being metallic centers), which is followed by a reversible reoxidation of reduced centers by carbon dioxide..

The total rate of CO formation in frames of this scheme is equal to:

$$w_{\Sigma_{CO}} = w_1 + w_2 - w_{-2}. \qquad (20)$$

In the case of labeled CH_4, the redistribution of ^{13}C among all C-containing feed compounds is observed. The kinetic parameters characterizing the rate of exchange and specific rates of CH_4

and CO_2 consumption are shown in Table 5. The rate constants of CO_2 transformation estimated by SSITKA data analysis exceed those of CH_4 consumption by ca. an order of magnitude. As already mentioned, these results are in line with the resistance to coking of the studied catalysts.

Hence, under steady-state conditions, the rate of methane dry reforming is limited by the step of methane interaction with catalyst. Note that both w_1 (rate of CH_4 transformation) and w_2 (rate of catalyst reoxidation by CO_2) at a lower (550^{o}C) temperature are apparently higher for catalysts containing Ru+Ni as compared with those for Pt/PrCeZr at a higher (735^{o}C) temperature. Since specific activity of Pt/PrSmCeZr catalyst is even lower than that of Pt/PrCeZr catalyst (Table 5), this difference could not be explained by the effect of support composition. Hence this result suggests that Ru+Ni alloy nanoparticles are not only involved in CH_4 activation but help to activate carbon dioxide as well. This confirms the key role of interface sites for this bi-functional reaction mechanism.

Table 5. Estimation of the rates of basic stages of CH_4 dry reforming by SSITKA

T,^{o}C	α_{CO_2}	α_{CO}	w_2/w_1	w_1 **mkmol/g*min**	w_2 **mkmol/g*min**	w_{-2} **mkmol/g*min**
Pt/PrCeZr						
735	0.12	0.14	42	0.6	25	24
785	0.21	0.23	34	1.0	34	33
830	0.32	0.34	30	1.6	48	46
Ru+Ni/PrSmCeZr						
550	0.52	0.46	7.7	4.2	32	28
600	0.49	0.42	6.0	6.2	36	30
650	0.46	0.39	5.5	7.6	42	34
Ru+Ni/PrSmCeZr/YSZ						
550	0.49	0.46	11.5	1.5	17	15
600	0.44	0.42	24	2.0	47	45
650	0.40	0.39	43	2.5	106	103

5.6.3 TAP experiments

Typical results of TAP studies are shown in Figure 17, Figure 18, Figure 19 for the case of Ni+Ru-supported catalysts. In oxidized state, these catalysts possess rather low activity providing only complete oxidation (combustion) of methane, which is a well-known feature of Ni/Ru containing catalysts (not shown for brevity). After reduction by hydrogen, successive pulses of CO_2 and CH_4 are efficiently transformed into CO and CO+ H_2, respectively (Figure 17). As follows from this figure, the amounts of CO produced after a pulse of CO_2 and after a subsequent pulse of CH_4 are very close, which agrees with our previous conclusion about independent activation of reactants based on SSITKA results. The comparison of CO responses for mixed CH_4 +CO_2 pulses and

separate pulses of the reactants (Fig. 18) shows that the amount of CO produced in the mixed pulse corresponds to the sum of CO produced in separate pulses. This demonstrates again that activation and transformation of CO_2 and CH_4 indeed proceed independently.

The results of $^{13}CO_2$ and $^{12}CH_4$ pump-probe experiments (sequential pulsing) confirm this conclusion (Figure 19). Indeed, pulse of $^{13}CO_2$ produces only ^{13}CO while a subsequent pulse of $^{12}CH_4$ gives only ^{12}CO. This clearly excludes any exchange of carbon atoms between reactants, and, hence, the existence of any common intermediate.

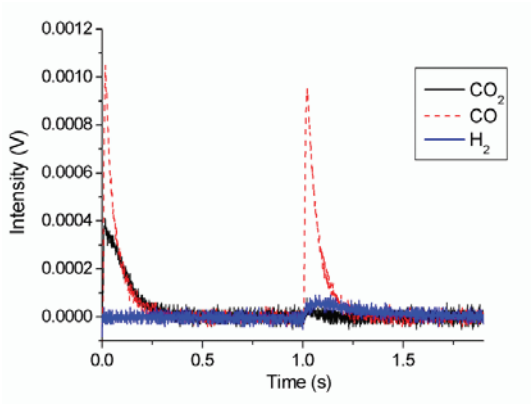

Figure 17. CO_2, CO, CH_4, and H_2 responses corresponding to CO_2 and CH_4 pump-probe experiment over reduced Ru+Ni/PrSmCeZr at 754°C. Injection times were 0 s for CO_2 and 1.0 s for CH_4

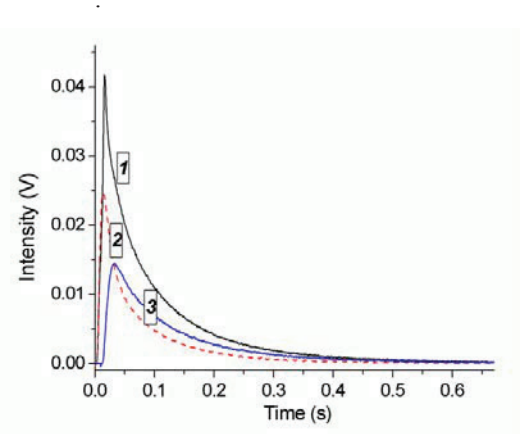

Figure 18. CO responses obtained over reduced Ru+Ni /PrSmCeZr catalyst at 754°C in: 1) CO_2 and CH_4 pump-probe experiment (time delay between CO_2 and CH_4 pulses was 0.01 s); 2) CO_2 single-pulse experiment; 3) CH_4 single-pulse experiment

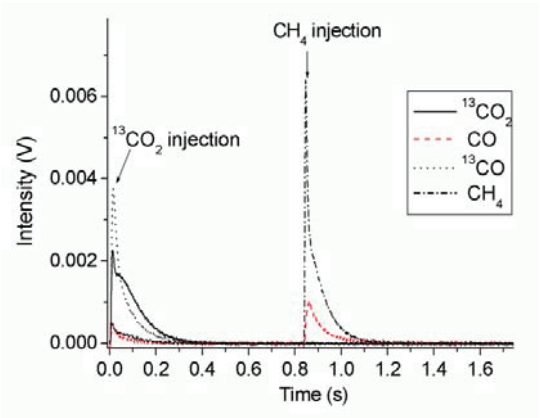

Figure 19. $^{13}CO_2$, ^{12}CO, ^{13}CO, and CH_4 responses corresponding to $^{13}CO_2$ and $^{12}CH_4$ pump-probe experiment over reduced Ru+Ni/PrSmCeZr at 750°C. Injection times were 0 s for $^{13}CO_2$ and 0.8 s for CH_4.

5.6.4 Pulse experiments at realistic CH_4 concentrations followed by microcalorimetry

In general, the changes in CH_4 conversion and CO/CO_2 selectivity with the CH_4 pulse number (degree of sample reduction) (Figure 20) reasonably agrees with the trends observed for unsteady state chemical transients and TAP data (vide supra). The CO formation even for the first pulse of CH_4 admitted onto the oxidized sample surface supports the hypothesis about a primary route of syngas formation via a CH_4 pyrolysis-partial oxidation route. The observation of rather high degrees of CH_4 conversion after removal from the sample of about one monolayer of oxygen again underlines a high rate of oxygen diffusion from the bulk of oxide particle to the surface, in order to compensate the used surface oxygen during the preceding pulses. The average heat of oxygen adsorption on partially reduced surface (~ 600 kJ/mol O_2, Fig. 21) is close to values corresponding to bonding strength of bridging (M_2O) oxygen forms located at Ce cations[53].

The enthalpy of CH_4 interaction with the catalyst (Figure 21, endothermic process) increases with the reduction degree corresponding to the enthalpy of its transformation into deep and partial oxidation products with a due regard for syngas selectivity and variation of the average oxygen bonding strength. Some decline of the heat of reduction at a reduction degree exceeding 1.5 monolayer can be explained by the increasing contribution of CH_4 cracking in agreement with results of CH_4 TPR data (vide supra). Nearly linear (i.e., rather weak) dependence of CH_4 conversion on the reduction degree agrees with this weak variation of the heat of CH_4 transformation.. Since the rate of the surface diffusion (reverse oxygen spillover from the support to Pt) is high, this provides some coverage of Pt by adsorbed oxygen thus favoring the activation of CH_4 molecules.

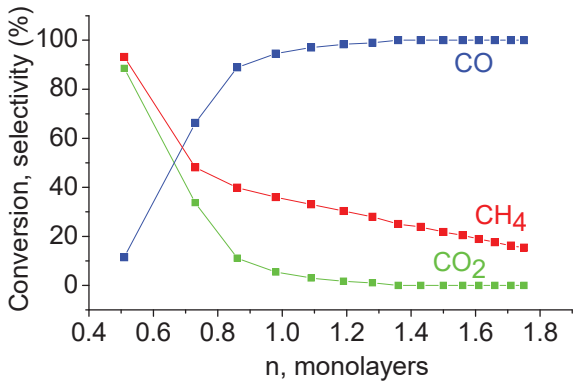

Figure 20. Dependence of CH_4 conversion, CO and CO_2 selectivity on the degree of Pt/PrCeZrO sample reduction (n) by pulses of 7% CH_4 in He at 600°C.

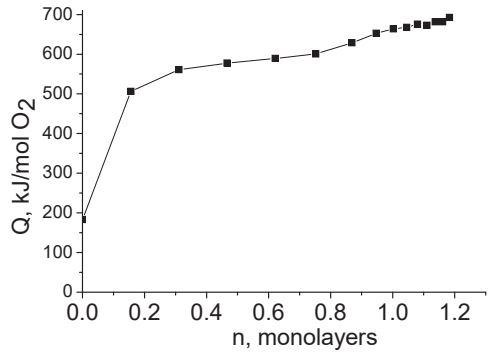

Figure 21. Enthalpy of oxygen adsorption (Q) versus reduction degree (n) estimated from the heats of 1.4% $Pt/Pr_{0.3}Ce_{0..35}Zr_{0.35}O_2$ sample reduction by CO pulses at 600°C.

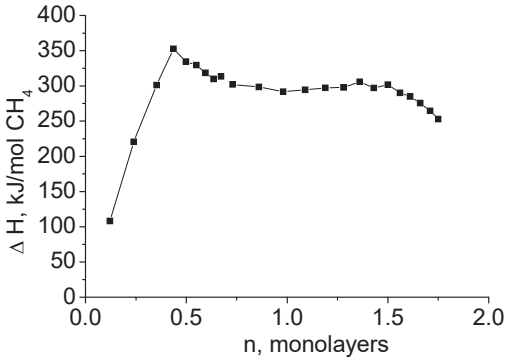

Figure 22. Enthalpy of CH_4 interaction with 1.4% $Pt/Pr_{0.3}Ce_{0.35}Zr_{0.35}O_2$ sample as a function of reduction degree (n) at 600 °C.

For all the studied catalysts in the steady-state of methane dry reforming, conversions of reactants in mixed pulses and in pulses containing only separate components were practically identical (Figure 23, Figure 24). Moreover, the products selectivity was the same –methane producing $CO+H_2$, CO_2-CO in several pulses until ~ 30% of oxygen is not removed/replenished. In agreement with the isotope transient studies and TAP, this underlines the independent activation of the two reactants on different active sites with rapid oxygen migration between them.

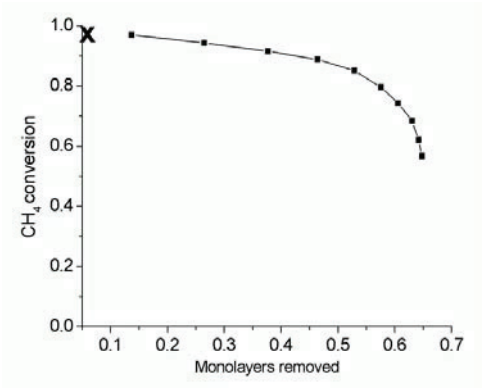

a

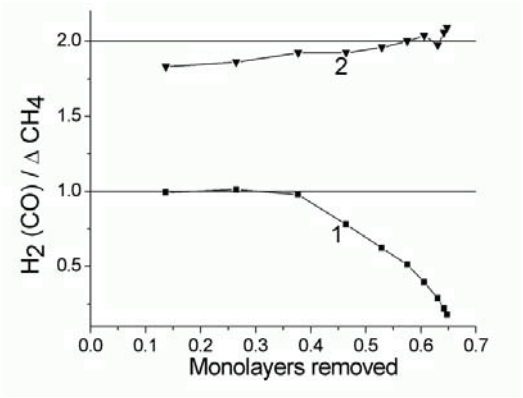

b

Figure 23. Variation of CH_4 conversion (a, **x** on the ordinate axes marks CH_4 conversion in the mixed CH_4 +CO_2 pulse) and products selectivity (b, 1-$CO/\Delta CH_4$; 2- $H_2/\Delta CH_4$) in the course of steady-state Ru+Ni/PrSmCeZr catalyst reduction by pulses of 7% CH_4 in He at 700°C.

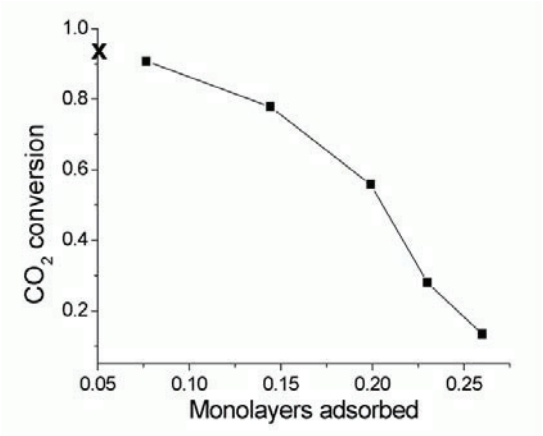

Figure 24. Variation of CO_2 conversion in the course of steady-state Ru+Ni/PrSmCeZr catalyst oxidation by pulses of 7% CO_2 in He at 700°C; **x** on the ordinate axes marks CO_2 conversion in the mixed CH_4 +CO_2 pulse

The measured heat values correspond to removal/replenishing of the interface surface oxygen forms with a desorption heat ≈600-650 kJ/mol O_2 (Table 7).

Note that CO_2 conversion rapidly declines with the pulse number as the catalyst is reoxidized (Figure 24). In agreement with calorimetric data demonstrating that the heat of surface reoxidation by CO_2 is constant, such kinetics reasonably fitted by the first-order equation for the batch-flow reactor suggests that the surface sites are occupied following a uniform adsorption energy. The rate constants of CO_2 consumption are very close for Pt or $LaNiO_3$-supported samples (~10^2 s^{-1}) while being an order of magnitude higher for Ni+Ru-supported sample (~10^3 s^{-1}). In agreement with SSITKA results (vide supra), this suggests that Ni-Ru alloy nanoparticles participate in CO_2 activation, perhaps, by favouring the C-O bond rupture in CO_2 molecules adsorbed at metal-support interface.

Table 6. Characteristics of bonding strength of reactive bridging oxygen forms for catalysts in the steady-state by reduction of CH_4 or CO pulses and reoxidation by CO_2 or O_2 pulses at 700°C.

Catalyst composition	**Heat of oxygen desorption, kJ/mol O_2**			
	CO_2*	**CH_4***	**CO***	**O_2***
Pt/PrCeZr	640	650	640	640
LaNi/PrSmCeZr	660	630	650	560
Ru + Ni/PrSmCeZr	630	670	635	550
Ru+Ni/PrSmCeZr/YSZ	640	740	645	550

* estimated by using pulses of respective component

5.7 Basic kinetic models for methane dry reforming

The analysis of kinetic transients obtained by contacting various reaction feeds with active oxidized Pt/PrCeZrO catalyst supported on walls of corundum channel (Figure 25) allowed to formulate kinetic scheme which takes into account the specificity of cationic Pt species[45].

A kinetic scheme consisting of 6 catalytic stages has been considered. The scheme reflects the methane transformation on the active cationic Pt-centers, the stabilization of Pt centers by the lattice oxygen, the interaction of carbon dioxide with oxidized Pt centers and surface oxygen vacancies of the catalyst layer, and a step accounting for RWGS:

$$CO_2 + [PtO] \leftrightarrow [PtCO_3] \quad (21)$$

$$CH_4 + [PtCO_3] \rightarrow 2\,CO + 2\,H_2 + [PtO] \quad (22)$$

$$CH_4 + [PtO] \rightarrow CO + 2\,H_2 + [Pt] \quad (23)$$

$$[Pt] + [O_s] \leftrightarrow [PtO] + [V_s] \quad (24)$$

$$CO_2 + [V_s] \rightarrow CO + [O_s] \quad (25)$$

$$H_2 + [PtO] \rightarrow H_2O + [Pt] \quad (26)$$

Here [PtO] and [Pt] denote the oxidized and vacant Pt-centers, $[PtCO_3]$ is a weakly bound carbonate complex, $[O_s]$ and $[V_s]$ are the oxidized and vacant sites inside the lattice layer. From the surface science point of view, stabilization of carbonate complexes in coordination sphere of Pt cations is possible only due to participation of neighbouring Pr^{4+} cations. Pr^{4+}-O oxygen bond involved in stabilization of this carbonate complex appears to be of an optimum strength providing by one hand a substantial concentration of these complexes at reaction temperatures, while on the other hand not making them too strongly bound to suppress their reactivity. Indeed, as was directly demonstrated by FTIRS *in situ* studies[52], strongly bound carbonates located apparently at $Ce^{3+/4+}$ cations with a higher Ce-O bond strength are of a much lower reactivity not being able to provide any substantial increment in the total rate of reagents transformation along the dry reforming route.

All the above elementary steps lead to the following overal stoichiometric equations:

$$\text{I. } CH_4 + CO_2 \leftrightarrow 2\,CO + H_2 \quad (27)$$

$$\text{II. } CO_2 + H_2 \leftrightarrow CO + H_2O \quad (28)$$

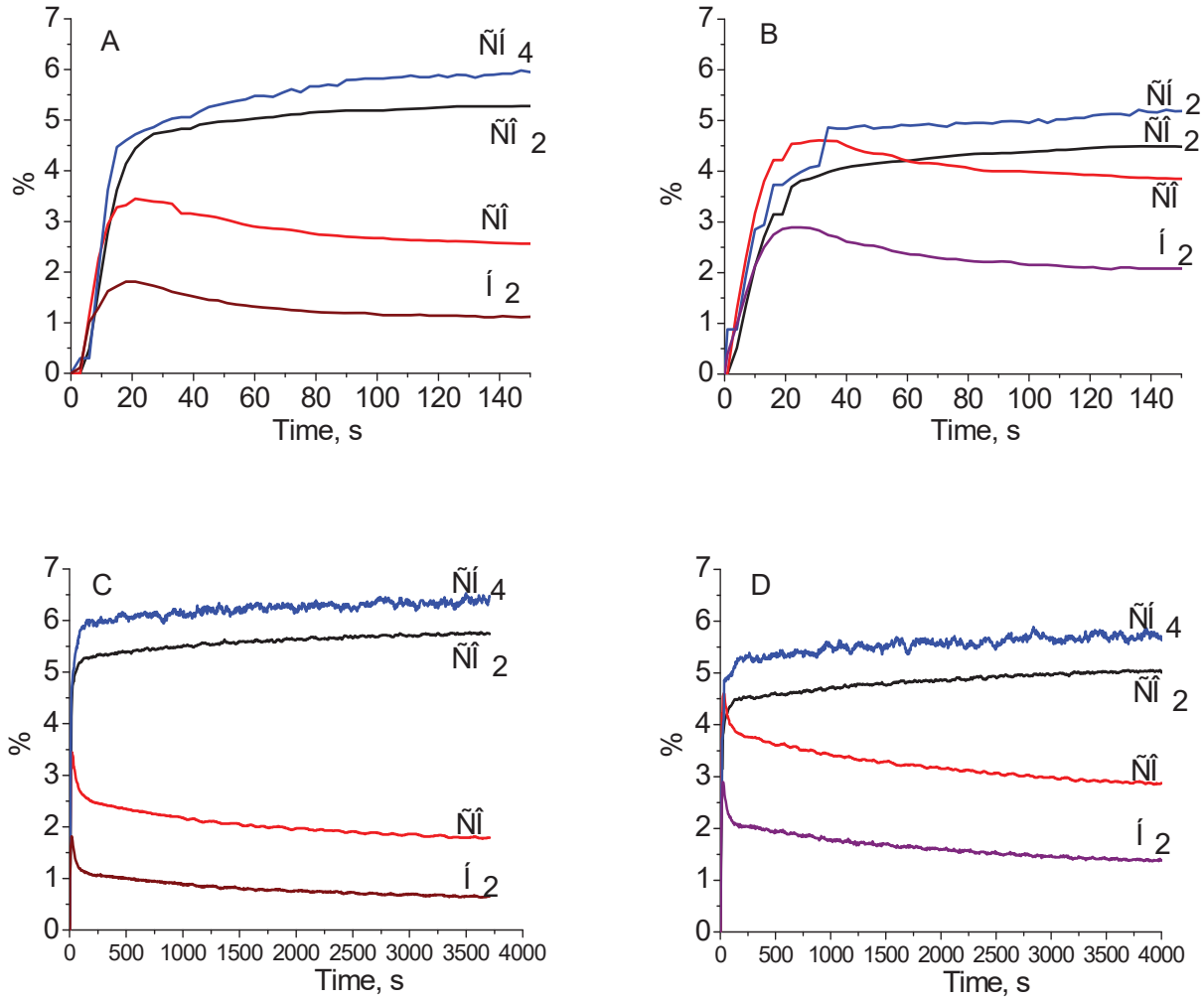

Figure 25. Fast (A,B) and slow (C,D) parts of transients for the corundum channel coated with the oxidized 1.6 wt.% Pt/ $Pr_{0.3}Ce_{0.3}Zr_{0.35}O_{2-x}$ catalyst at contact with feed 7% CH_4 +7% CO_2 in He at 750 ^oC. Contact time 4.72 ms (A,C) and 8ms (B,D).

According to the mass conservation law the rates of catalytic steps can be written as follows:

$$r_1 = k_1 C_{CO2} \theta_1 \quad (29)$$

$$r_{-1} = k_{-1} \theta_2 \quad (30)$$

$$r_2 = k_2 C_{CH4} \theta_2 \quad (31)$$

$$r_3 = k_3 C_{CH4} \theta_1 \quad (32)$$

$$r_4 = k_4 (1 - \theta_1 - \theta_2) \theta_3, \quad (33)$$

$$r_{-4} = k_{-4} \theta_1 (1 - \theta_3) \quad (34)$$

$$r_5 = k_5 C_{CO2} (1 - \theta_3) \quad (35)$$

$$r_6 = k_6 C_{H2} \theta_1 \quad (36)$$

where r_i is the rate of the ith catalytic stage (i = 1, 2, .., 6); c_{CH4}, c_{CO2}, and c_{H2} are the concentrations of H_4, CO_2 and H_2 in the gas mixture correspondingly; θ_1, θ_2, and θ_3 are the relative surface concentrations of oxidized Pt-centers [PtO], carbonate complexes [$PtCO_3$], and oxidized lattice layer sites [O_s] respectively; k_i is the rate constant of the ith catalytic stage (i = 1, 2, .., 6).

It is assumed that the total number of active Pt-centers is equal to

$$[ZO] + [ZCO_3] + [Z] = \alpha N_\theta \quad (37)$$

and the number of active lattice layer sites available for spillover is equal to

$$[ZO^*] + [Z^*] = \beta N_\theta \quad (38)$$

where N_θ is the total number of active centers on the catalyst surface, α is the relative surface concentration of Pt-centers, β is the ratio of the number of active lattice layer sites under the surface to the total number of active surface centers.

Data processing has allowed us to evaluate the kinetic parameters and characteristics of the catalyst structure. Some examples of modeling and experimental results comparison are given in Figure 26 for the following values of parameters: τ = 4.7 s, k_1 = 200 s^{-1}, k_{-1} = 0.6 s^{-1}, k_2 = 600 s^{-1}, k_3 = 60 s^{-1}, k_4 = 300 s^{-1}, k_{-4} = 5 s^{-1}, k_5 = 55 s^{-1}, k_6 = 1100 s^{-1}, α = 0.04, β = 0.2, $S_b = 20 \cdot 10^4$ cm^{-1}, $D = 2.5 \cdot 10^{-13}$ cm^2/s, $H = 5 \cdot 10^{-6}$ cm.

The satisfactory fit observed in Figure 26 (except for H_2 concentration) suggests that the tested kinetic scheme reflects rather well the main peculiarities of the catalyst behavior. The experimental values of gas concentrations and the modeling data are in a good agreement. This does not exclude indeed that other kinetic models might reasonably fit the experimental data as well.

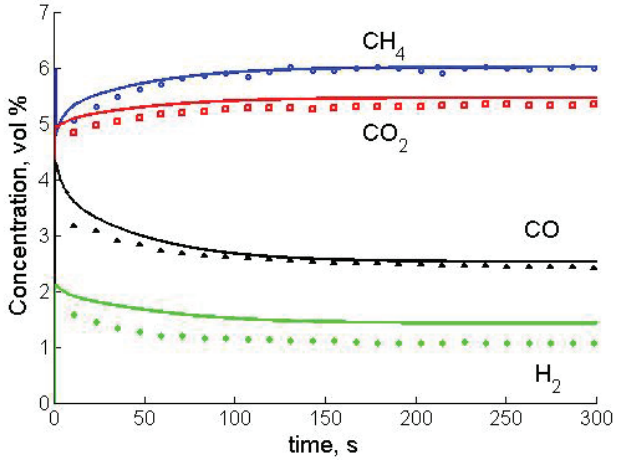

Figure 26. Comparison of the experimental (points) and computed (lines) time dependences of concentrations in transient experiments. 750°C, gas feed rate 18 l/h, feed 7%CH_4 + 7%CO_2 in He, contact time 4.7 ms.

Hence, under unsteady-state conditions of dry-reforming or mixed oxi-dry reforming for Pt supported on Pr-doped ceria-zirconia, weakly bound carbonates could assist the activation of methane molecule.

Chapter four

Conclusion and perspectives

6 Conclusion and perspectives

The main features demonstrated during this study can be summarized as follows:

A. New methods and data treatment of oxygen isotope heteroexchange for characterizing oxygen mobility were developed and successfully applied for catalysts based on doped ceria-zirconia oxides promoted by Pt and Ru+Ni.

B. For catalysts based on doped ceria-zirconia oxides with a high oxygen mobility and reactivity with supported Pt, Ru, Ni and their combinations, the occurrence of a bi-functional red-ox type mechanism of methane dry reforming under steady-state conditions was proposed. The rate determining step would be related to the dissociation of methane C-H bond on metal sites, while CO_2 activation would proceed more easily on basic sites of the ceria doped surface, possibly involving highly dispersed metal ions, near the metal support boundaries.

C. Under methane oxi-dry reforming conditions, the most promising system was found to be Pt supported on Pr-doped ceria-zirconia due to stabilization of cationic Pt species by this doped support, acting as a permanent and efficient active oxygen provider. These Pt cations would be highly active for methane C-H bonds activation and the further selective oxidation the CHx fragments into syngas. In this permanently oxidized state of the catalyst, weakly bound carbonate species stabilized by neighboring Pr cations would be directly involved in this transformation of activated CHx species into syngas.

In the dry reforming reaction, Ni+Ru alloy nanoparticles are actively involved in CO_2 activation which helps to provide a high rate of active oxygen species regeneration thus preventing coking.

D. For practical application in dry reforming of methane and other fuels in real concentrated feeds and using short contact time reactors able to handle large flows of reacting feedstocks, promising systems based on Pr(Sm)-doped ceria-zirconia with supported Pt or Ru+Ni are proposed, to be coated on structured supports stable at high temperature and avoiding significant mass transfer limitations and pressure drops.

E. In line with the previous objective, kinetic and mechanistic studies were carried out on corundum channels with supported active components. They demonstrated the absence of any heat-

and mass-transfer effects as well as any possible negative effects which would be caused by interaction of the active components with corundum substrate.

F. As perspectives for industrial application of natural gas dry/oxy-dry reforming at short contact times, promising engineering designs could be based on microchannel stainless steel plates used for their high thermal conductivity, but protected against catalyst corrosion and fast ageing by a thin and dense corundum layer as substrates for these nanocrystalline active type components. Such plates could be efficiently used for combining in the same reactor exo and endothermic reactions. Such engineering solutions have been partly tested within the frame of the OCMOL EU project where the endothermic dry reforming of methane is compensated by the exothermic methane coupling to ethylene, aiming at a self sufficient autothermal system [63].

G. Another perspective linked to the compulsory diversification of methane sources in a near future will be to use the knowledge acquired in the present study for reforming biogas (which contains large concentrations of methane and carbon dioxide) into bio-syngas for sustainable processes. Designing efficient catalysts able to accommodate the pollutants of biogas in small units adapted to stranded sources of biogas via structured micro-reactors is certainly a new challenge for continuing the present work.

References

[1] T. Inui, Reforming of CH_4 by CO_2, O_2 and/or H_2O, Catalysis, V.16, The Royal Society of Chemistry, 2002, pp. 133-154

[2] Y.H. Hu and E. Ruckenstein, Catalytic conversion of methane to synthesis gas by partial oxidation and CO_2 reforming, *Adv. Catal.* 48 (2004) 297

[3] Y.H. Hu and E. Ruckenstein, Binary MgO-based solid solution catalysts for methane conversion to syngas, *Catal. Rev.* 44 (2002) 423

[4] X.E. Verykios, Catalytic dry reforming of natural gas for the production of chemicals and hydrogen, *Int. J. Hydrogen Energy* 28 (2003) 1045

[5] M.C.J. Bradford, M.A. Vannice, CO_2 reforming of CH_4 over supported Pt catalysts, *J. Catal.* 173 (1998) 157

[6] J.M. Wei, B.Q. Xu, J.L. Li, Z.X. Cheng and Q.M. Zhu, Highly active and stable Ni/ZrO_2 catalyst for syngas production by CO_2 reforming of methane, *Appl. Catal., A: Gen.*196 (2000) 167

[7] M. O'Connor, Y. Schuurman, J.R.H. Ross, C. Mirodatos, Transient studies of carbon dioxide reforming of methane over Pt/ZrO_2 and Pt/Al_2O_3, *Catal. Today* 115 (2006) 191

[8] H. Li, J. Wang, Study on CO_2 reforming of methane to syngas over Al_2O_3-ZrO_2 supported Ni catalysts prepared via a direct sol-gel process. *Chem. Eng. Sci.* 59 (2004) 4861

[9] Zh. Zhang, X. Verykios, Performance of Ni/La_2O_3 catalyst in carbon dioxide reforming of methane to synthesis gas, *Stud. Surf. Sci. Catal.* 107 (1997) 511

[10] H.M. Swaan, V.C. H. Kroll, G.A. Martin, C. Mirodatos, Deactivation of supported nickel catalysts during the reforming of methane by carbon dioxide, *Catal. Today* 21 (1994) 571

[11] S. Damyanova, B. Pawelec, K. Arishtirova, M.V. Martinez Huerta, J.L.G. Fierro, The effect of CeO_2 on the surface and catalytic properties of Pt/CeO_2–ZrO_2 catalysts for methane dry reforming, *Appl. Catal. B: Envir.* 89 (2009) 149

[12] F.B. Noronha, E.C. Fendley, R.R. Soares, W.E. Alvarez, D.E. Resasco, Correlation between catalytic activity and support reducibility in the CO_2 reforming of methane over Pt/$Ce_xZr_{1-x}O_2$ catalysts, *Chem. Eng. J.* 82 (2001) 21

[13] S.M. Stagg-Williams, F.B. Noronha, G. Fendley, and D.E. Resasco, CO_2 Reforming of CH_4 over Pt/ZrO_2 Catalysts Promoted with La and Ce Oxides, *J. Catal.* 194 (2000) 240

[14] J.A. Montoya, E. Romero-Pascual, C. Gimon, P. Del Angel, A. Monzon, Methane reforming with CO_2 over Ni/ZrO_2–CeO_2 catalysts prepared by sol–gel, *Catal. Today* 63 (2000) 71

[15] H.-S. Roh, H.S. Potdar, K.-W. Jun, J.-W. Kim, Y.-S. Oh, Carbon dioxide reforming of methane over Ni incorporated into Ce–ZrO_2 catalysts, *Appl. Catal. A: General* 276 (2004) 231

[16] B. Koubaissy, A. Pietraszek, A.C. Roger, A. Kiennemann, CO_2 reforming of methane over Ce–Zr– Ni–Me mixed catalysts, *Catal. Today* 157 (2010) 436

[17] A. Horvath, G. Stefler, O. Geszti, A. Kienneman, A. Pietraszek, L. Guczi, Methane dry reforming with CO_2 on CeZr-oxide supported Ni, NiRh and NiCo catalysts prepared by sol–gel technique: Relationship between activity and coke formation, *Catal. Today* 169 (2011) 102

[18] G.C. Gallego, F. Mondragon, J. Barrault, J.-M. Tatibouët, C. Batiot-Dupeyrat, CO_2 reforming of CH_4 over La-Ni based perovskite precursors, *Appl. Catal. A: Gen. A* 311 (2006) 164

[19] G.S. Gallego, F. Mondragon, J.-M. Tatibouët, J. Barrault, C. Batiot-Dupeyrat, Carbon dioxide reforming of methane over La_2NiO_4 as catalyst precursor — Characterization of carbon deposition, *Catal. Today* 133–135 (2008) 200

[20] V.A. Sadykov, N.V. Mezentseva, G.M. Alikina, A.I. Lukashevich, Yu.V. Borchert, T.G. Kuznetsova, V.P. Ivanov, S.N. Trukhan, E.A. Paukshtis, V.S. Muzykantov, V.L. Kuznetsov, V.A. Rogov, J. Ross, E. Kemnitz, C. Mirodatos, Pt-supported nanocrystalline ceria-zirconia doped with La, Pr or Gd: factors controlling syngas generation in partial oxidation/autothermal reforming of methane or oxygenates, *Solid State Phenom.* 128 (2007) 239

[21] V. Sadykov, N. Mezentseva, G. Alikina, R. Bunina, V. Pelipenko, A. Lukashevich , S.Tikhov, V. Usoltsev, Z. Vostrikov, O. Bobrenok, A. Smirnova, J. Ross, O. Smorygo, B. Rietveld, Nanocomposite catalysts for internal steam reforming of methane and biofuels in solid oxide fuel cells: design and performance, *Catal. Today* 146 (2009) 132

[22] V. Sadykov, N. Mezentseva, G. Alikina, R. Bunina, V. Pelipenko, A. Lukashevich, Z. Vostrikov, V. Rogov, T. Krieger, A. Ishchenko, V. Zaikovsky, L. Bobrova, J. Ross, O. Smorygo, A. Smirnova, B. Rietveld, F. van Berkel, Nanocomposite catalysts for steam reforming of methane and biofuels: design and performance, *in: Nanocomposite Materials, Theory and Applications*, INTECH, Austria, Vienna, 2011, pp. 909–946

[23] V.A. Sadykov, T.G. Kuznetsova, G.M. Alikina, Yu.V. Frolova, A.I. Lukashevich, V.S. Muzykantov, V.A. Rogov, L.G. Ivanov, S. Pinaeva, E. Neophytides, K. Kemnitz, C. Scheurel, C. Mirodatos, *in: D.K. McReynolds (Ed.), Book: New Topics in Catalysis Research, Ch. 5*, Nova Science Publishers, NY, USA, 2007, pp. 97–196

[24] M.C.J. Bradford, M.A. Vannice, CO_2 Reforming of CH_4. *Catal. Rev.-Sci. Eng.* 41 (1999) 1

[25] J. Wei and E. Iglesia, Structural requirements and reaction pathways in methane activation and chemical conversion catalyzed by rhodium, *J. Catal.* 225 (2004) 116

[26] K. Tomishige, O. Yamazaki, Y. Chen, K. Yokoyama, X. Li, and K. Fujimoto, Development of ultra-stable Ni catalysts for CO_2 reforming of methane, *Catal. Today* 45 (1998) 35

[27] A. Slagtern, Y. Schuurman, C. Leclercq, X. Verykios, C. Mirodatos, Specific Features Concerning the Mechanism of Methane Reforming by Carbon Dioxide over Ni/La_2O_3 Catalyst, *J. Catal.* 172 (1997) 118.

[28] Y. Schuurman, V.C.H. Kroll, P. Ferreira-Aparicio, C. Mirodatos, Use of transient kinetics techniques for studying the methane reforming by carbon dioxide, *Catal. Today* 38 (1997) 129

[29] R.W. Stevens, S.S.C. Chuang, In situ IR study of transient CO_2 reforming of CH_4 over Rh/Al_2O_3, *J. Phys. Chem. B* 108 (2004) 696

[30] M.C.J. Bradford, M.A. Vannice, Catalytic reforming of methane with carbon dioxide over nickel catalysts II. Reaction kinetics, *Appl. Catal. A: Gen.*142 (1996) 97

[31] Y. Schuurman, C. Marquez-Alvarez, V.C.H. Kroll, C. Mirodatos, Unraveling mechanistic features for the methane reforming by carbon dioxide over different metals and supports by TAP experiments, *Catal. Today* 46 (1998) 185

[32] P. Ferreira-Aparicio, Y. Schuurman, C. Mirodatos, et al A transiet kinetic study of the carbon dioxide reforming of methane over supported Ru catalysts, *J. Catal.* 184 (1999) 202

[33] V.C.H. Kroll, H.M. Swaan, S. Lacombe, C. Mirodatos, Methane reforming reaction with carbon dioxide over Ni/SiO_2 catalyst. II. A mechanistic study, *J. Catal.* 164 (1997) 387

[34] T. Osaki, T. Mori, Kinetic studies of CO_2 dissociation on supported Ni catalysts, React. Kinet. Catal. Lett., 87 (2006) 149

[35] A.M. Efstathiou, A. Kladi, V.A. Tsipouriari, X.E. Verykios, Reforming of methane with carbon dioxide to synthesis gas over supported rhodium catalysts. II. A steady-state tracing analysis: mechanistic aspects of the carbon and oxygen reaction pathways to form CO, *J. Catal.* 158 (1996) 64

[36] Y. Hang Hu and E. Ruckenstein, Transient Response Analysis via a Broadened Pulse Combined with a Step Change or an Isotopic Pulse. Application to CO_2 Reforming of Methane over NiO/SiO_2, *J. Phys. Chem. B* 101 (1997) 7563

[37] X.E. Verykios, Mechanistic aspects of the reaction of CO_2 reforming of methane over Rh/Al_2O_3 catalyst, *Applied Catalysis A: General* 255 (2003) 101

[38] J.H. Bitter, K. Seshan, J.A. Lercher, Mono and bifunctional pathways of CO_2/CH_4 reforming over Pt and Rh based catalysts, *J. Catal.* 176 (1998) 93

[39] A.M. O' Connor, F.C. Meunier, and J.R.H. Ross, An in-situ DRIFT study of the mechanism of the CO_2 reforming of CH_4 over a Pt/ZrO_2 catalyst, *Stud. Surf. Sci. Catal.* 119 (1998) 819

[40] V.A. Tsipouriari, X.E. Verykios, Kinetic study of the catalytic reforming of methane with carbon dioxide to synthesis gas over Ni/La_2O_3 catalyst, *Catal. Today* 64 (2001) 83

[41] J.F. Múnera, S. Irusta, L.M. Cornaglia, E.A. Lombardo; D.V. Cesar; M. Schmal, Kinetics and reaction pathway of the CO_2 reforming of methane on Rh supported on lanthanum-based solid, *J. Catal*. 245 (2007) 25

[42] V. Bychkov, Yu. Tyulenin, O. Krylov and V. Korchak, Methane reforming with carbon dioxide on the $Co/\alpha\text{-}Al_2O_3$ catalyst: The formation, state, and transformations of surface carbon, *Kinetika i Kataliz* 43 (2002) 775

[43] V. Bychkov, Yu. Tyulenin, O. Krylov and V. Korchak, The mechanism of carbon dioxide reforming of methane: Comparison of supported Pt and Ni (Co) catalysts, *Kinetika i Kataliz* 44 (2003) 384

[44] Y. Schuurman and C. Mirodatos, Uses of transient kinetics for methane activation studies, *Appl. Catal. A: Gen.* 151 (1997) 305

[45] V.A. Sadykov, E.L. Gubanova, N.N. Sazonova, S.A. Pokrovskaya, N.A. Chumakova, N.V. Mezentseva, A.S. Bobin, R.V. Gulyaev, A. V. Ishchenko, T. A. Krieger, C. Mirodatos, Dry reforming of methane over Pt/PrCeZrO catalyst: kinetic and mechanistic features by transient studies and their modelling, *Catal. Today* 171 (2011) 140

[46] V. Sadykov, V. Muzykantov, A. Bobin, N. Mezentseva, G. Alikina, N. Sazonova, E. Sadovskaya, L. Gubanova, A. Lukashevich, C. Mirodatos, Oxygen mobility of Pt-promoted doped CeO_2–ZrO_2 solid solutions: Characterization and effect on catalytic performance in syngas generation by fuels oxidation/reforming, *Catal. Today* 157 (2010) 55

[47] V.A. Sadykov, N.N. Sazonova, A.S. Bobin, V. S. Muzykantov, E.L. Gubanova, G.M. Alikina, A.I. Lukashevich, V.A. Rogov, E.N. Ermakova, E.M. Sadovskaya, N.V. Mezentseva, E.G. Zevak, S. A. Veniaminov, M. Muhler, C. Mirodatos, Y. Schuurman, A. C. van Veen, Partial oxidation of methane on Pt-supported lanthanide doped ceria-zirconia oxides: effect of the surface/lattice oxygen mobility on catalytic performance, *Catal. Today* 169 (2011) 125

[48] E.M. Sadovskaya, Y.A. Ivanova, L.G. Pinaeva, G. Grasso, T.G. Kuznetsova, A. van Veen, V.A. Sadykov and C. Mirodatos, Kinetics of Oxygen Exchange over CeO_2-ZrO_2 Fluorite-Based Catalysts, *J. Phys. Chem. A* 111 (2007) 4498

[49] N.N. Sazonova, V.A. Sadykov, A.S. Bobin S.A. Pokrovskaya, E.L. Gubanova, C. Mirodatos, Partial oxidation of methane into syngas on Pt-supported mixed oxides: effect of surface/lattice oxygen mobility in complex oxides on the kinetic features of the reaction and performance stability, *React. Kinet. Catal. Lett.* 98 (2009) 27

[50] N.N. Sazonova, V.A. Sadykov, A.S. Bobin, S.A. Pokrovskaya, E.L. Gubanova, C. Mirodatos, Dry reforming of methane over fluorite-like mixed oxides promoted by Pt, *React Kinet Catal Lett* 98 (2009) 35

[51] V. Sadykov, N. Mezentseva, V. Muzykantov, D. Efremov, E. Gubanova, N. Sazonova, A. Bobin, E. Paukshtis, A. Ishchenko, V. Voronin, J. Ross, C. Mirodatos, A. van Veen, Real Structure — Oxygen Mobility Relationship in Nanocrystalline Doped Ceria-Zirconia Fluorite-Like Solid Solutions Promoted by Pt, *Mater. Res. Soc. Symp. Proc.* 1122 (2009) 1122-O05-03

[52] A.S. Bobin, V.A. Sadykov, V.A. Rogov , N.V. Mezentseva, G.M. Alikina, E.M. Sadovskaya, T.S. Glazneva, N.N. Sazonova, M.Yu Smirnova, S.A. Veniaminov, C. Mirodatos, V. Galvita, G.B. Marin, Mechanism of CH_4 Dry Reforming on Nanocrystalline Doped Ceria-Zirconia with Supported Pt, Ru, Ni, and Ni–Ru, *Topics in Catalysis* 56 (2013) 958

[53] V. Sadykov, V. Rogov, E. Ermakova, D. Arendarsky, N. Mezentseva, G. Alikina, N. Sazonova, A. Bobin, S. Pavlova, Y. Schuurman and C. Mirodatos, Mechanism of CH_4 Dry Reforming by Pulse Microcalorimetry: metal nanoparticles on perovskite/fluorite supports with high oxygen mobility, *Thermochimica Acta* 567 (2013) 27

[54] G.K. Boreskov, V.S. Muzykantov, Investigation of oxide type oxidation catalysts by reactions of oxygen isotopic exchange *Ann. N. Y. Acad. Sci.* 213 (1973) 137

[55] V.S. Muzykantov, Isotopic studies of dioxygen activation: problems, results and perspectives *React. Kinet. Catal. Lett.* 35 (1987) 437

[56] V.S. Muzykantov, A.A. Shestov, Kinetic equation for the redistribution of isotopic molecules due to reversible dissociation. Homoexchange of methane, *React. Kinet. Catal. Lett.* 32, No 2 (1986) 307

[57] V.S. Muzykantov, A.A. Shestov, Redistribution kinetics of isotopic molecules due to reversible bimolecular reaction with several atomic channels, *React. Kinet. Catal. Lett.*, 33, No 1 (1987) 197

[58] V.S. Muzykantov, E. Kemnitz, V.V. Lunin, V.A. Sadykov, Analysis of isotope data "without time": non-isothermal exchange of dioxygen with oxides, *Kinetics and Catal.* 46 (2003) 319

[59] F.J. Cheselske, W.E. Wallage, W.K. Hall, The exchange of deuterium Gas with the hydrogen associates with solid catalysts. I. The model tantalum-hydrogen system *J. Phys. Chem.* 63 (1959) 505

[60] W.K. Hall, H.P. Leftin, F.J. Cheselske, D.E. O'Reilly, Studies of the hydrogen held by solids IV. Deuterium exchange and NMR investigations of silica, alumina, and silica-alumina catalysts, *J. Catal.* 2 (1963) 506

[61] V.A. Sadykov, V.V. Kriventsov, E.M. Moroz, Yu.V. Borchert, D.A. Zyuzin, V.P. Kol'ko, T.G. Kuznetsova, V.P. Ivanov, A.I. Boronin, N.V. Mezentseva, E.B. Burgina, J. Ross, Ceria-zirconia nanoparticles doped with La or Gd: effect of the doping cation on the real structure, *Solid State Phenom.* 128 (2007) 81.

[62] V. Sadykov, N. Mezentseva, G. Alikina, A. Lukashevich, V. Muzykantov, R. Bunina, A. Boronin, E. Pazhetnov, E. Paukshtis, V. Kriventsov, A. Smirnova, O. Vasylyev, J. Irvine, O. Bobrenok, V. Voronin, and I. Berger, Doped Nanocrystalline Pt-Promoted Ceria-Zirconia as Anode Catalysts for IT SOFC:Synthesis and Properties, *Mater. Res. Soc. Symp. Proc.* 1023 (2007) JJ02-07.1-6

[63] http://www.ocmol.eu/index.php

List of Attached Publications

1. **Dry Reforming Of Methane Over Fluorite-Like Mixed Oxides Promoted By Pt** N. N. Sazonova, V. A. Sadykov, A. S. Bobin, S. A. Pokrovskaya, E. L. Gubanova, C. Mirodatos *React. Kinet. Catal. Lett. 98 (2009) 35*
2. **Real Structure − Oxygen Mobility Relationship In Nanocrystalline Doped Ceria-Zirconia Fluorite-Like Solid Solutions Promoted By Pt** V. Sadykov, N. Mezentseva, V. Muzykantov, E. Gubanova, N. Sazonova, A. Bobin, V. Voronin, J. Ross, C. Mirodatos *Mater. Res. Soc. Symp. Proc. 1122 (2009) O05-03*
3. **Oxygen Mobility Of Pt-Promoted Doped CeO_2-ZrO_2 Solid Solutions: Characterization And Effect On Catalytic Performance In Syngas Generation By Fuels Oxidation/Reforming** V. Sadykov, V. Muzykantov, A. Bobin, N. Mezentseva, G. Alikina, N. Sazonova, E. Sadovskaya, L. Gubanova, A. Lukashevich, C. Mirodatos *Catalysis Today, 157(2010) 55-60*
4. **Dry Reforming Of Methane Over Pt/PrCeZrO Catalyst: Kinetic And Mechanistic Features By Transient Studies And Their Modeling** V. A. Sadykov, E. L. Gubanova, N. N. Sazonova, S. A. Pokrovskaya, N. A. Chumakova, N. V. Mezentseva, A. S. Bobin, R. V. Gulyaev, A.V. Ishchenko, T. A. Krieger, C. Mirodatos *Catalysis Today, 171 (2011) 140-149*
5. **Partial Oxidation Of Methane On Pt-Supported Lanthanide Doped Ceria-Zirconia Oxides: Effect Of The Surface/Lattice Oxygen Mobility On Catalytic Performance** V. A. Sadykov, N. N. Sazonova, A. S. Bobin, V. S. Muzykantov, E. L. Gubanova, G. M. Alikina, A. I. Lukashevich, V. A. Rogov, E. N. Ermakova, E. M. Sadovskaya, N. V. Mezentseva, E. G. Zevak, S. A. Veniaminov, M. Muhler, C. Mirodatos, Yv. Schuurman, A. C. van Veen *Catalysis Today 169 (2011) 125-137*
6. **Mechanism of CH_4 Dry Reforming on Nanocrystalline Doped Ceria-Zirconia with Supported Pt, Ru, Ni, and Ni–Ru** A. S. Bobin, V. A. Sadykov, V. A. Rogov, N. V. Mezentseva, G. M. Alikina, E. M. Sadovskaya, T. S. Glazneva, N. N. Sazonova, M. Yu Smirnova, S. A. Veniaminov, C. Mirodatos, V. Galvita, G. B. Marin *Topics in Catalysis 56 (2013) 958-968*
7. **Mechanism Of CH_4 Dry Reforming By Pulse Microcalorimetry: Metal Nanoparticles On Perovskite/Fluorite Supports With High Oxygen Mobility** V. Sadykov, V. Rogov, E. Ermakova, D. Arendarsky, N. Mezentseva, G. Alikina, N. Sazonova, A. Bobin, S. Pavlova, Yv. Schuurman, C. Mirodatos *Thermochimica Acta 567 (2013) 27-34*

React Kinet Catal Lett (2009) 98:35–41
DOI 10.1007/s11144-009-0064-7

Dry reforming of methane over fluorite-like mixed oxides promoted by Pt

Natalya N. Sazonova · Vladislav A. Sadykov · Aleksey S. Bobin · Svetlana A. Pokrovskaya · Elena L. Gubanova · Claude Mirodatos

Received: 18 December 2008 / Accepted: 20 July 2009 / Published online: 11 September 2009

Abstract Dry reforming of methane into syngas was studied over complex Pt-promoted fluorite-like oxides (PrCeZrO, GdCeZrO and LaCeZrO) supported on a corundum substrate. Activity and syngas selectivity of these catalysts were found to depend strongly on their composition, pretreatment and reaction conditions. At low temperatures and short contact times, the H_2/CO ratio in the syngas is below 1 due to a fast reverse water–gas shift reaction. The catalyst performance was found to correlate with the bulk oxygen mobility in complex fluorite-like oxides, which prevents the surface coking.

Keywords Methane dry reforming · Syngas · Short contact time · Flow system

Introduction

Catalysts for the dry reforming of methane that possess high stability to coking are of great interest from both the industrial and environmental points of view [1]. Pt supported on ZrO_2 was shown to be very active and stable to coking due to participation of the support in CO_2 dissociation, as well as in delivering oxygen species to oxidize carbon atoms produced by CH_4 decomposition on Pt [2–4]. Hence, the oxygen mobility in the support and the Pt—support interaction appear to

N. N. Sazonova (✉) · V. A. Sadykov · A. S. Bobin · S. A. Pokrovskaya · E. L. Gubanova
Boreskov Institute of Catalysis SB RAS, 630090 Novosibirsk, Russia
e-mail: Sazonova@catalysis.ru

V. A. Sadykov · A. S. Bobin · S. A. Pokrovskaya
Novosibirsk State University, 630090 Novosibirsk, Russia

C. Mirodatos
Institut de Recherches sur la Catalyse, CNRS, 2 Avenue Albert Einstein, Villeurbanne Cédex, France

be important factors that provide the efficient and stable performance of Pt-based catalysts in this reaction. Previously, we investigated the activity and selectivity of Pt-supported PrCeZrO, GdCeZrO and LaCeZrO catalysts in the partial oxidation of CH_4 at millisecond contact times [5, 6]. Their catalytic performance was shown to depend strongly on the Pt—support interaction and surface/bulk oxygen mobility controlled by the chemical composition of oxides, catalysts pretreatment and process parameters. Secondary reactions of steam (SR) and dry (DR) reforming make a considerable contribution to the partial oxidation of methane (POM) mechanism at higher temperatures and longer contact times [5, 6]. Therefore, these catalysts could be attractive as model systems to verify the effect of oxygen mobility in the complex oxide support on the activity and stability of supported Pt in the dry reforming of methane. The practical application of the best compositions could not be excluded as well.

In this work, the activity and selectivity of separate catalytic channels with Pt-supported active components based on PrCeZrO, GdCeZrO or LaCeZrO were studied in the dry reforming of methane at short contact times.

Experimental

In this study of DR, the same structured catalysts as in the POM were used to elucidate the main features of the reaction. The basic characteristics of active components, procedures of their supporting on separate corundum channels and experimental features were described in detail earlier [5–7]. The catalytic activity in DR was measured at atmospheric pressure in the temperature range from 600 to 850 °C, and at contact times in the range from 4.7 to 15.0 ms. The gas feed comprised CH_4 and CO_2 in N_2 with the methane concentration from 7 to 20% ($CH_4/CO_2 = 1$). The feed rate was varied from 5 to 18 L/h. The concentrations of components in the gas flow before and after the reactor were determined with a Test-201 (Bonair, Russia) gas analyzer equipped with IR absorbance, conductometric and polarographic sensors. Before the experiments, the catalysts were kept on stream for 1 h at 750 °C for achieving the steady state in the DR. After that, the catalyst was pretreated in the oxygen flow at 700 °C for 1 h.

Results and discussion

Figs. 1 and 2 present the reagent conversions, $CO + H_2$ sum and H_2/CO ratio as functions of temperature and contact time. The Pr-doped catalyst demonstrates the highest activity in DR, though the conversions (maximum 55% at 780 °C) are about twice as low as those for the partial oxidation of methane [6]. The activity of the Pt/GdCeZrO catalyst is considerably lower, whereas the Pt/LaCeZrO catalyst is almost completely deactivated at 800 °C in the stoichiometric feed with 7% of CH_4. For the catalysts doped with Pr or Gd, the experimental data obtained during the heating of samples to 800 °C coincide with those obtained during the decrease in temperature. For the La-doped sample, CH_4 conversion declines below the sensitivity limit. This

row of high-temperature activity correlates with the lattice oxygen mobility in these systems controlled by their real structure and strength of the Ce–O bond [7].

Note also that the most active Pr-doped sample provided the highest H_2/CO ratio, which approaches the equilibrium value 1 with the increase in temperature (Fig. 1) and contact time (Fig. 2). Since the conversion of CO_2 was always higher than the CH_4 conversion, this deviation of the H_2/CO ratio from the equilibrium at lower temperatures and shorter contact times can be explained by fast consumption of a part of nascent hydrogen for CO_2 reduction yielding CO and H_2O [8]. As was revealed by transient studies of DR of CH_4 on the Pr-doped catalyst (to be presented elsewhere [9]), oxidized Pt centers that strongly interact with the fluorite-like support are more efficient in the CH_4 activation but less active in the reverse water gas shift reaction (RWGSR). Hence, a high lattice mobility of oxygen helps to stabilize these highly active Pt centers and prevents the surface blocking by carbonaceous deposits [2–4].

Since water formed in the RWGSR can be consumed in the steam reforming of CH_4 yielding more hydrogen, which apparently does not occur at low temperatures, the latter process is certainly hampered. This implies that at these temperatures either the surface hydroxyls are rather strongly bound and, hence, not reactive, or

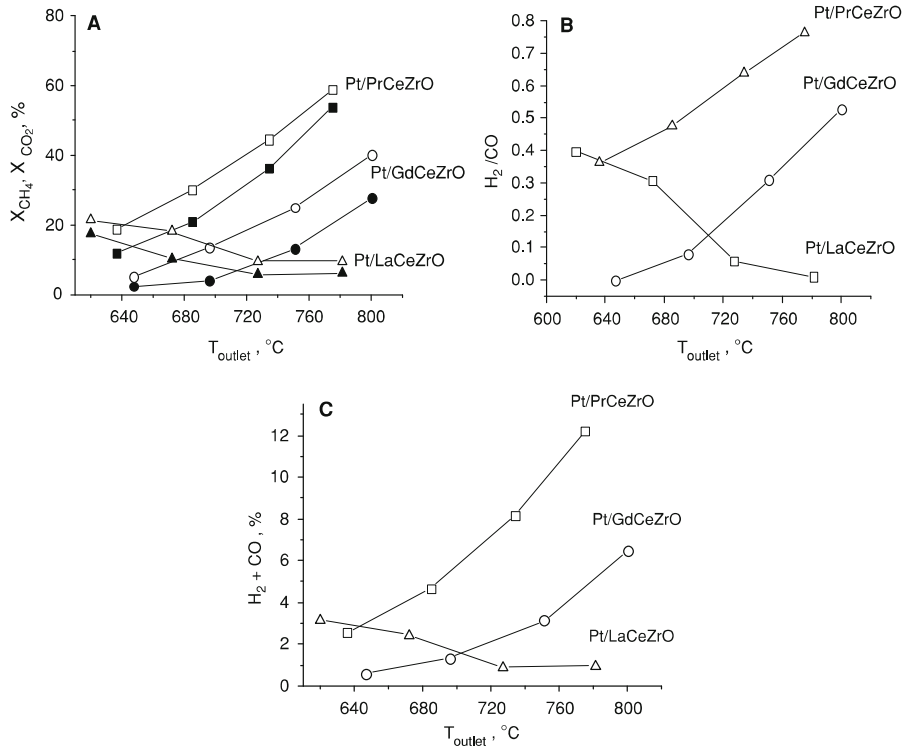

Fig. 1 Temperature dependence of the reagent conversion (**a**, xCH$_4$—*filled symbols*, xCO$_2$—*open symbols*), molar H_2/CO ratio (**b**) and syngas content (**c**) in DR. Feed composition: 7 CH$_4$ % + 7% CO_2 in N_2, contact time 15 ms

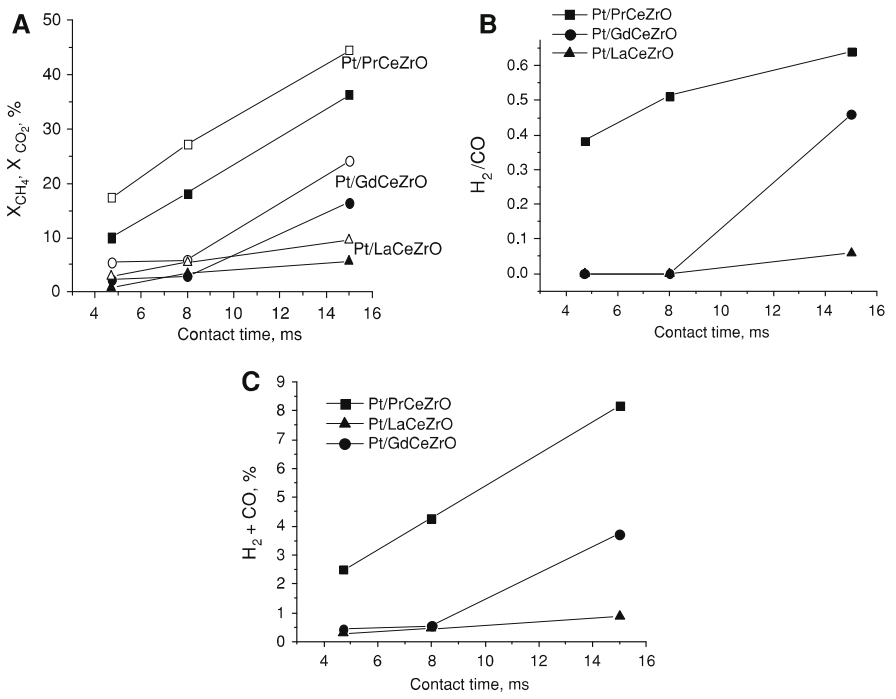

Fig. 2 Effect of the contact time on the reagent conversion (**a**, xCH_4—*filled symbols*, xCO_2—*open symbols*), molar H_2/CO ratio (**b**) and syngas content (**c**). Feed composition: 7% CH_4 + 7% CO_2 in N_2, 750 °C

water readsorption on the surface sites is prevented by surface carbonates and/or carbonaceous species, whose coverage is higher for samples with a lower oxygen mobility in the complex oxide support.

While the catalytic activity of the La-doped catalyst in realistic feeds was practically independent of temperature in POM [6], the methane conversion and syngas formation significantly decline with temperature in dry reforming (Figs. 1, 2) clearly revealing a progressive catalyst deactivation. Moreover, in both POM and DR in realistic feeds, this catalyst demonstrates much lower activity and hydrogen selectivity than earlier estimated values obtained for powdered active component in diluted feeds [7, 10]. All these features can be explained by a stronger deactivation of this catalyst in more reducing feeds [6]. However, the La-doped sample demonstrates the highest performance at 620 °C. At this temperature, the activity order La > Pr > Gd correlates with the surface/near-surface mobility of oxygen in doped ceria-zirconia oxides [7, 10]. Hence, at lower temperatures, when the catalyst surface is more oxidized, the surface oxygen mobility appears to be the main factor controlling performance of Pt-supported catalysts.

A typical dependence of the CH_4 conversion and syngas content on the feed concentration is presented in Fig. 3 for the Gd-containing catalyst. Although the variation of parameters is rather small in general, the minima observed in both CH_4

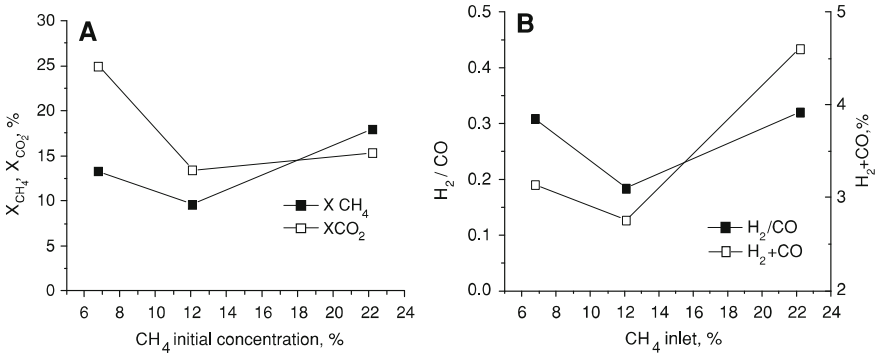

Fig. 3 Effect of the initial concentration of CH_4 in the feed on the reagent conversion (**a**, xCH_4—*filled symbols*, xCO_2—*open symbols*), molar H_2/CO ratio and syngas content (**b**) over the Pt/GdCeZrO catalyst in DR. $CH_4/CO_2 = 1$, contact time 15 ms, temperature 750 °C

conversion and H_2/CO ratio are worth commenting on. A similar minimum in the rate of DR was observed by Kroll et al. [11] for a Ni/SiO_2 catalyst in the close concentration range. They explained this minimum by a Langmuir–Hinshelwood type kinetics including interaction of C and O atoms adsorbed on Ni. However, in the case of Pt supported on a fluorite-like oxide, the sequence of the surface steps is apparently different and includes dissociation of CO_2 on the oxygen vacancy at Pt—support interface [4]. Since at a fixed CH_4/CO_2 ratio, the increase in CH_4 concentration means a respective increase in the concentration of CO_2, namely CO_2 adsorption might be responsible for the observed effect. Indeed, the adsorption of CO_2 on the surface of complex oxides can generate carbonates that block oxygen vacancies and hence hamper the CO_2 dissociation and oxygen diffusion. Besides, in the operation temperature range, chemisorption of CH_4 on the oxide support is negligible, and coverage of Pt by CH_x species for the active Pt-supported sample is small [4]. Consequently, increasing the concentration of CH_4 in the feed only helps to remove surface carbonates by their hydrogenation onto CO with hydrogen produced by the CH_4 dissociation on Pt. Perhaps, at 750 °C and 12% CO_2 in the feed, the coverage of oxide surface sites by carbonates achieves a maximum. Hence, at the further increase in the feed concentration, the increase in the rate of CH_4 activation on Pt sites provides a higher rate of removal of carbonates from the surface. It increases the concentration of oxygen vacancies and the surface oxygen mobility and, as a result, increases the rate of transformation of adsorbed CH_x species into CO and H_2 at the Pt—support interface.

As for the same catalysts in POM, the apparent first-order rate constants of the methane transformation in DR were estimated for all three catalysts using the model of a plug-flow reactor [5, 6]. Comparison of these values revealed that the constants of DR are several times lower than those of POM (Table 1). This implies that at realistic concentrations of the components, dry reforming could not contribute significantly into the process of methane partial oxidation at short contact times at least for the samples doped by Gd or La. Since the effective first-order rate constants of POM, steam and dry reforming were found to be practically identical in the

Table 1 Effective first-order rate constants in DR for Pr, Gd, or La-containing catalysts

T_{outlet}, °C	k (s^{-1}) in DR			k (s^{-1}) in POM		
	Pr	Gd	La	Pr	Gd	La
650	10.5	1.7	9.3	51.0	25.3	35.7
680	14.8	2.4	6.8	56.0	36.8	34.6
700	23.1	4.9	4.5	65.6	48.1	33.4
740	33.4	8.2	3.9	79.0	56.9	32.6
770	49.4	14.5	4.1	105.4	69.6	34.0

Feed composition 7% CH_4 + 7% CO_2 in N_2, contact time: 15 ms

diluted feeds [10], this suggests that in realistic feeds a higher reduction degree of the surface layer in DR favors accumulation of stronger bound carbonates as well as carbonaceous species decreasing the catalysts performance. This is most clearly expressed in this work for the La-doped system. However, in conditions of POM even in realistic feeds providing in general more oxidized state of the surface, which is less prone to the accumulation of carbonates and carbonaceous deposits, a considerable contribution of DR to the methane conversion in the part of the channel where the gas-phase oxygen is absent could not be excluded as well at higher temperatures and longer contact times.

Conclusions

The catalytic performance of Pt-promoted fluorite-like doped ceria-zirconia oxides in the dry reforming of CH_4 at short contact times in realistic feeds correlates with the lattice oxygen mobility required to prevent blocking of surface sites by strongly bound carbonates or carbonaceous species. The reverse water gas shift reaction was found to be rather fast affecting the H_2/CO ratio in the produced syngas. The rate constants of DR over these catalysts are several times lower than are those of POM, which indicates the direct route of methane transformation into syngas in the presence of oxygen.

Acknowledgements This work was carried out in frames of the Associated Russian-French laboratory on catalysis. Support by RFBR-CNRS 05-03-34761 and 09-03-93112 Projects is gratefully acknowledged.

References

1. Bradford MCJ, Vannice MA (1999) Catal Rev Sci Eng 41:1
2. Bitter JH, Seshan K, Lercher JA (1999) J Catal 183:336
3. Nagaoka K, Seshan K, Aika K, Lercher JA (2001) J Catal 197:34
4. O'Connor AM, Schuurman Y, Ross JRH, Mirodatos C (2006) Catal Today 115:191
5. Sazonova NN, Sadykov VA, Bobin AS, Pokrovskaya SA, Gubanova EL, Mirodatos C (2009a) React Kinet Catal Lett. doi:10.1007/s11144-009-0063-8

6. Sazonova NN, Sadykov VA, Bobin AS, Pokrovskaya SA, Gubanova EL, Mirodatos C (2009b) React Kinet Catal Lett. doi:10.1007/s11144-009-0062-9
7. Sadykov VA, Mezentseva NV, Alikina GM, Lukashevich AI, Borchert YuV, Kuznetsova TG, Ivanov VP, Trukhan SN, Paukshtis EA, Muzykantov VS, Kuznetsov VL, Rogov VA, Ross JRH, Kemnitz E, Mirodatos C (2007) Solid State Phenom 128:239
8. Zhang J, Wang H, Dalai AK (2009) Ind Eng Chem Res 48:677
9. Sazonova NN, Sadykov VA, Bobin AS, Pokrovskaya SA, Gubanova EL, Alikina GA, Lukashevich AI, Mirodatos C React Kinet Catal Lett (to be submitted)
10. Sadykov VA, Kuznetsova TG, Alikina GM, Frolova YuV, Lukashevich AI, Muzykantov VS, Rogov VA, Batuev LC, Kriventsov VV, Moroz EM, Zyuzin DA, Paukshtis EA, Burgina EB, Trukhan SN, Ivanov VP, Pinaeva LG, Ivanova YuA, Kostrovskii VG, Neophytides S, Kemnitz E, Sheurel K, Mirodatos C (2006) In: McReynolds DK (ed) New topics in catalysis research, Chap 5. Nova Science Publishers, New York, p 97
11. Kroll VCH, Tjatjopoulos GJ, Mirodatos C (1998) Stud Surf Sci Catal 119:753

Mater. Res. Soc. Symp. Proc. Vol. 1122 © 2009 Materials Research Society 1122-O05-03

Real Structure - Oxygen Mobility Relationship in Nanocrystalline Doped Ceria-Zirconia Fluorite-Like Solid Solutions Promoted by Pt

Vladislav Sadykov[1,2], N. Mezentseva[1], V. Muzykantov[1], D. Efremov[1], E. Gubanova[1], N. Sazonova[1], A. Bobin[1,2], E. Paukshtis[1,2], A. Ishchenko[1,2], V. Voronin[3], J. Ross[4], C. Mirodatos[5], A. van Veen[5].

[1]Boreskov Institute of Catalysis, Novosibirsk, 630090, Russia

[2]Novosibirsk State University, Novosibirsk, 630090, Russia

[3]Institute of Metals Physics UB RAS, Yekaterinburg, 234005, Russia

[4]Centre of Environmental Research, University of Limerick, Limerick, Ireland

[5]Institut de Recherches sur la Catalyse et l'Environnement de Lyon, 69626 Villeurbanne Cedex, France.

ABSTRACT

This work considers effect of type and content of dopant on the real structure, state of surface Pt species and oxygen mobility of nanocrystalline $Ln_x(Ce_{0.5}Zr_{0.5})_{1-x}O_{2-\delta}$ ($Ln=La^{3+}$, Gd^{3+}, $Pr^{3+/4+}$) solid solutions prepared by Pechini route. For the reactions of methane selective oxidation and dry reforming into syngas, catalytic activity correlates rather well with either surface (in diluted feeds) or bulk (in realistic feeds) oxygen mobility as well as Pt dispersion controlled by the type and content of a dopant .

INTRODUCTION

Ceria-zirconia oxide solid solutions with supported precious metals are promising for such applications as automotive catalysis [1], transformation of hydrocarbons or oxygenates into syngas by partial oxidation or autothermal reforming [2,3], anode materials for solid oxide fuel cells [3] etc. The oxygen mobility and state of supported Pt are important factors for their high and stable performance. This work considers effect of type and content of dopant on the real structure, state of surface Pt species and oxygen mobility of nanocrystalline $Ln_x(Ce_{0.5}Zr_{0.5})_{1-x}O_{2-\delta}$ ($Ln=La^{3+}$, Gd^{3+}, $Pr^{3+/4+}$) solid solutions prepared by Pechini route as related to catalysis of methane transformation into syngas.

EXPERIMENT

Dispersed $Ln_x(Ce_{0.5}Zr_{0.5})_{1-x}O_2$ samples with La, Pr, or Gd content in the range of 5–30 at.% were prepared by a polymerized complex precursor route and calcined at 500-700 ^oC for 4 h [4-6]. Pt (1.4 wt.%) was supported from H_2PtCl_6 solution by incipient wetness impregnation followed by drying and calcination at 500 ^oC for 2 h.

Structural features of samples were characterized by X-ray Diffraction (XRD) using an URD-6 diffractometer (Germany) with Cu K_α monochromatic radiation (λ=1.5418 Å). For Ce-Zr-Pr(La)-O series the neutron diffraction studies were performed at room temperature using a D7a neutron diffractometer (IVV-2M reactor, Zarechny, Russia) [5]

The EXAFS spectra were obtained at the EXAFS Station of the Siberian Synchrotron Radiation Center using for data analysis the curve fitting procedure with EXCURV92 code [6].

Transmission Electron Microscopy (TEM) micrographs were obtained with a JEM-2010 instrument (lattice resolution 1.4 Å) and acceleration voltage 200 kV. Local elemental analysis has been carried out using an X-ray dispersion Phoenix spectrometer.

Surface centers were characterized by the Fourier Transform Infra-red Spectroscopy (FTIRS) of adsorbed CO (Shimadzu 8300 spectrometer) [5].

BET specific surface area (S_{sp}) was determined from the Ar thermal desorption data.

Dynamic isotope oxygen exchange was carried out in the temperature-programmed mode in a static installation with MS control of the gas phase as described elsewhere [2, 5]. Activation energy of isotope exchange was estimated following approach suggested by Hall et al [7].

Catalytic activity of samples in the reactions of selective oxidation and dry reforming of CH_4 at short contact times (0.5-25 ms) was studied both in the temperature-programmed and stationary modes at temperatures up to 900 ^oC in a flow installation by using a flow quartz reactor and CH_4+ O_2 (CO_2) in He feeds (CH_4 concentration 1÷ 20%, CH_4/O_2 =2, CH_4/CO_2 =1) following earlier described procedures [2, 5, 8]. In diluted feeds, 0.25-0.5 mm catalysts fractions were tested, while in concentrated feeds, active components were supported on thin (thickness 0.25 mm) walls of separate triangular channel (side 2.5 mm) cut from the corundum honeycomb substrate [2, 8]. The same channels were used in high-vacuum TAP (Temporal Analysis of Products) pulse studies to elucidate atomic -scale effects of oxygen mobility in a complex oxide on primary routes of CH_4 transformation into syngas [8]. In these experiments, a TAP-2 high temperature reactor and a UTI quadruple mass-spectrometer were used.

RESULTS AND DISCUSSION

Structural features

For samples doped by Gd, Pr and La, diffraction patterns correspond to homogeneous fluorite-like solid solution with the lattice parameter increasing with the dopant content [9]. While X-ray reflections in the first approximation can be indexed in the Fm3m space group [9], neutron diffraction patterns for Pr or La-doped samples are better described by the tetragonal ***P4₂/nmc*** space group [10]. Since c/a ratio is rather close to 1 (1.39-1.42), this structure corresponds to t'' -phase with distorted oxygen sublattice [1]. The lattice parameters increase with the doping level reflecting bigger sizes of doping cations. Domain sizes of all studied samples are in the nano-range being comparable and declining with the dopant content (see, i.e. Fig. 1 and 2). This is accompanied by decreasing microstrains density Δd/d as shown in Fig. 2 for Pr-doped system. With a due regard for neutronographic studies by Mamontov et al [11] on the nanoscale heterogeneity of $Ce_{0.5}Zr_{0.5}O_2$ sample comprised of zirconia-enriched domains in ceria-enriched matrix, this trend can be explained by relieving the lattice strains due to replacing small Zr^{4+} cations by large Ln^{3+} cations. However, the isotropic temperature parameter for the oxygen atoms B_O was found to increase with Pr content (Fig. 2). This suggests a complex rearrangement of the oxygen sublattice with doping. Indeed, EXAFS data agree with this suggestion. First of all, in agreement with neutron diffraction data, EXAFS revealed pronounced tetragonal distortion of coordination spheres of all cations in ceria-zirconia samples [9, 10, 12]. Moreover, doping provides a specific rearrangement of coordination polyhedra of different cations. Thus, for Gd-doped series, the increase of Gd content (x) from 0 to 0.3 is accompanied by the increase of Zr-O integral coordination numbers (CN) from 6.7 to 8.0, while distances

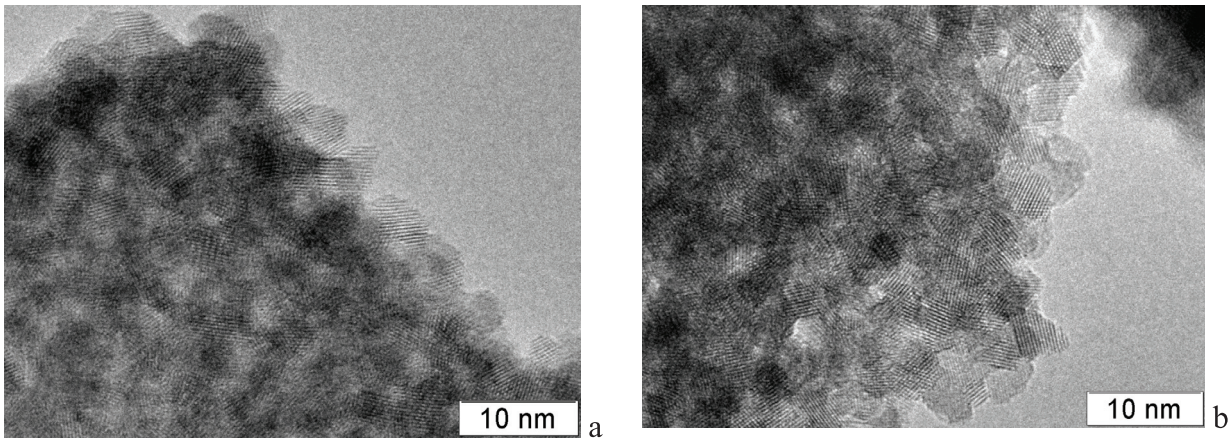

Figure 1. High resolution TEM image of Pt-supported particles of $Ln_{0.3}(Ce_{0.5}Zr_{0.5})_{0.7}O_2$ samples: Ln =Pr(a) and Gd (b)

increase from 2.10-2.26 Å to 2.15-2.32 Å. On contrary, despite the unit cell expansion, Ce-O distances contract with doping (from 2.20 -2.40 Å to 2.18-2.35 Å), while CN decrease from 2.8+4.7 to 2.6+3.0, respectively. A similar trend – decrease of coordination numbers and distances with the doping level was revealed for Gd-O sphere making it more dense and symmetric. Since magnetic susceptibility data revealed clustering of Gd^{3+} cations at a high doping level [12], this suggests that some ordering of Gd distribution in the lattice occurs causing such a local structure rearrangement. This rearrangement removes Ce^{3+}cations (as well as associated "free" anion vacancies) present in ceria-zirconia samples only at a low doping level [12]. Similarly, magnetic susceptibility measurements revealed appearance of Pr^{4+} cations at a high Pr content, their mole fraction reaching up to 30 rel.% at xPr =0.3 [12]. Hence, clustering of doping cations at a high doping level can be a general trend and a driving force for the structure rearrangement.

As follows from the high resolution TEM images of Pt-supported samples (Fig. 1), separate Pt particles are not observed despite rather high (1.4 wt.%) loading. This suggests that supported Pt is mainly present as oxidic species due to strong interaction with support [1] which agrees with the FTIRS data of adsorbed CO (vide infra).

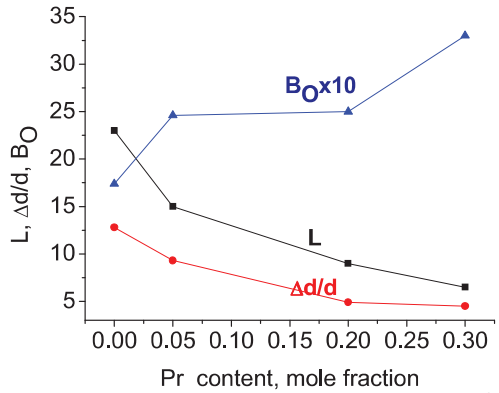

Figure 2. Domain size L (nm), Δd/d 10^3 and B_O for Pr-doped samples

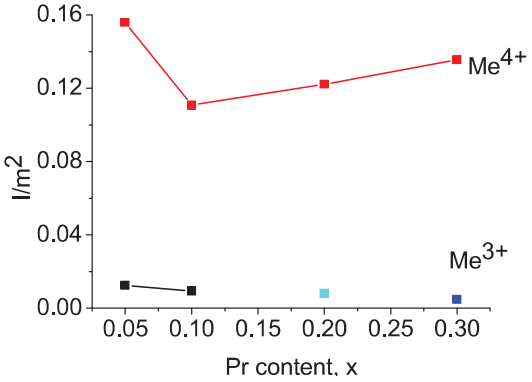

Figure 3. Normalized intensity of Me^{4+} and Me^{3+} carbonyl bands for Pr-doped samples

Surface features

According to XPS and SIMS data [4], the surface is enriched by bigger Pr, Ce and La cations and is depleted by smaller Zr, Gd and cations. This suggests that domain boundaries are as well enriched by bigger cations.

As revealed by FTIRS of adsorbed CO, on the surface of oxides coordinatively unsaturated isolated Ce^{4+}/Zr^{4+} cations (carbonyl bands at 2160-2180 cm^{-1}) and clustered Me^{3+} cations (bands at 2110-2125 cm^{-1}) are present [4]. As a typical example, Fig. 3 shows dependence of the intensity of Me^{4+}-CO and Me^{3+}-CO bands on the Pr content. The decrease of the intensity of Me^{4+}-CO band with Pr content correlates with decreasing the density of microstrains, while subsequent increase can be explained by the increase of the density of domain boundaries (vide supra). Hence, Lewis acid sites -coordinatively unsaturated Me^{4+} cations appear to be located at outlets of extended defects.

For Pt-supported samples, FTIRS of adsorbed CO revealed several Pt species (Pt^{o}, Pt^{+}, Pt^{2+}) [4]. The intensity of high-frequency carbonyl bands corresponding to CO complexes with isolated Pt^{2+} cations (Fig. 4) is strongly affected by the type and content of doping cation. For Pr-doped samples the intensity of Pt^{2+}-CO band correlates with that of Me^{4+}-CO band, thus suggesting that extended defects (domain boundaries) play some role in stabilization of Pt^{2+} species on the surface. The highest intensity of Pt^{2+}-CO band for La-doped samples is explained by the positive role of the largest (and the most basic) La cations in stabilization of Pt cationic species. The decrease of this band intensity at the highest La content can be explained by Pt incorporation into domain boundaries or subsurface layers.

The oxygen mobility and catalytic activity

As follows from Figure 5, the oxygen mobility characterized by a dynamic degree of exchange X_S (amount of oxygen exchanged up to a given temperature) [4] tends to decrease with the dopant content. At 650 ^{o}C, X_S is below a monolayer, so this parameter mainly characterizes the surface/near surface oxygen diffusion [13]. Decrease of the lattice oxygen mobility with Gd or La content certainly correlates with increasing the symmetry and average CN for Zr-O sphere, contraction of Ce-O sphere (hence, strengthening of Ce-O bond) and disappearance of

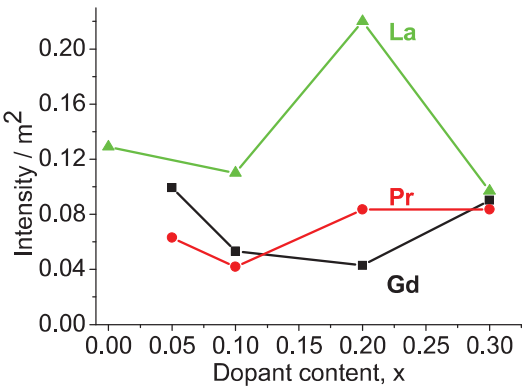

Figure 4. Intensity of Pt^{2+}-CO band vs. dopant content for Pt –supported samples. 16 μmol CO adsorbed at 77K

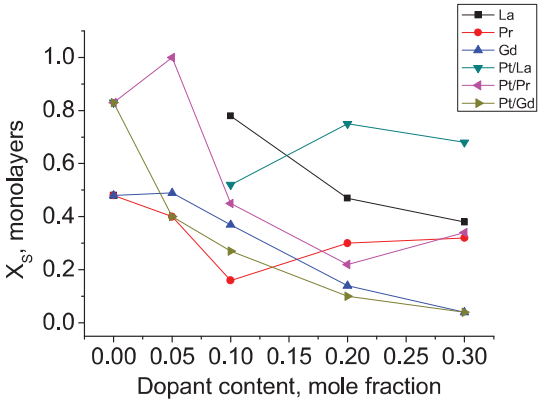

Figure. 5. Dynamic degree of the oxygen heteroexchange at 650 ^{o}C vs. dopant content.

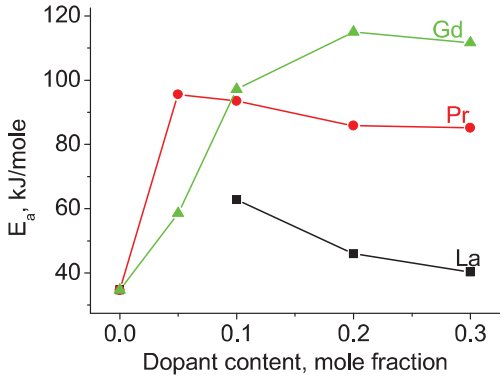

Figure 6. E_a of exchange for $Ln_x(Ce_{0.5}Zr_{0.5})_{1-x}O_2$ samples

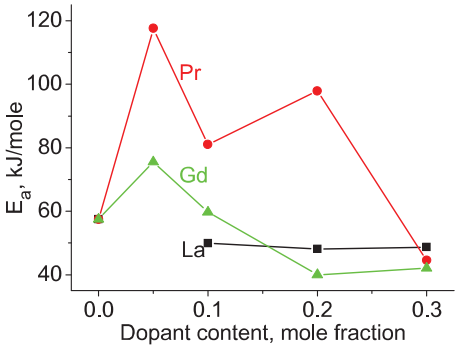

Figure 7. E_a of exchange for $Pt/Ln_x(Ce_{0.5}Zr_{0.5})_{1-x}O_2$ samples

free anion vacancies caused by a complex rearrangement of coordination polyhedra (vide supra). These results agree with known models explaining enhanced oxygen mobility in ceria-zirconia-based solid solutions by the presence of free anion vacancies and/or Frenkel-type defects, distortion of Zr-O sphere and weakening of Ce-O bond [1, 4, 9, 11-13]. Thus, for La-Ce-Zr-O samples, a higher surface/near surface oxygen mobility can be explained by a weaker surface Ce-O bond as revealed by SIMS studies [4, 9]. Some increase of X_S at a high Pr content can be explained by increasing the Pr^{4+} share (vide supra), which favors mixed ionic-electronic conductivity via chains of Pr^{3+}-Pr^{4+} cations, and, hence, oxygen mobility, perhaps, along domain boundaries enriched by Pr cations [4]. In general, E_a of oxygen exchange for samples without Pt (Fig. 6) decreases with increasing the size of doping cation being controlled by the energy barrier for the oxygen migration.

Pt supporting affects surface/near surface oxygen mobility both via incorporation of Pt^{2+} cations into the surface layer/domain boundaries and by facilitating O_2 molecules dissociation [13]. This is reflected in decreasing E_a (Fig. 7) which becomes close for different systems at a high doping level. Detailed analysis of oxygen exchange kinetics by Monte Carlo modeling following earlier described approach [14] revealed that for Pt-supported systems the surface and near-surface constants of oxygen diffusion are indeed comparable, while the highest bulk oxygen mobility is found for Pr-doped system, and the lowest (by 6-9 times)–for La-doped system, which correlates with the higher strength of bulk Ce-O bond for the latter by SIMS [4].

Catalytic activity in methane selective oxidation/dry reforming in diluted feeds was shown to correlate with concentration of Pt^{2+} species (and, hence, its dispersion) as well as the surface oxygen mobility [4], activity of samples series decreasing in the order La>Pr>Gd. This is explained by a high efficiency of CH_4 molecules activation on dispersed oxidized Pt sites yielding H_2 as primary product even in the presence of adsorbed oxygen species. In the TAP experiments (Fig. 8), instantaneous H_2 formation is demonstrated by a sharp H_2 response with a steep profile. The decrease of a time lag between O_2 and CH_4 pulses does not strongly affect H_2 formation since fast bulk oxygen diffusion removes too reactive oxygen species [8].

In concentrated feeds at low temperatures, this order of activity is retained as well (Fig. 9). However, at higher temperatures the highest activity is demonstrated by Pr-doped system, while activity of La-doped system decreases due to coking. The same trend was observed for partial oxidation of methane. Hence, in realistic feeds with a high CH_4 content, a high bulk oxygen mobility is required to prevent coking leading to deactivation

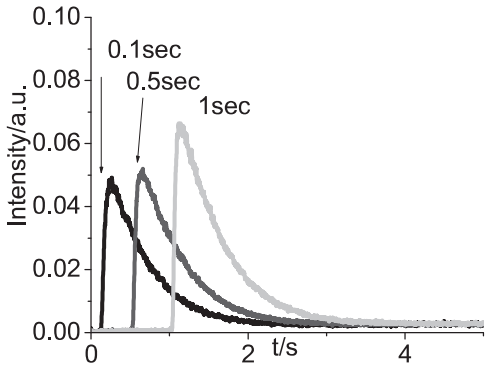

Figure 8. TAP experiment at 700°C on $Pt/Pr_{0.3}(Ce_{0.5}Zr_{0.5})_{0.7}O_2$ sample with time-lag between O_2 and CH_4 pulses 0.1, 0.5 and 1 s

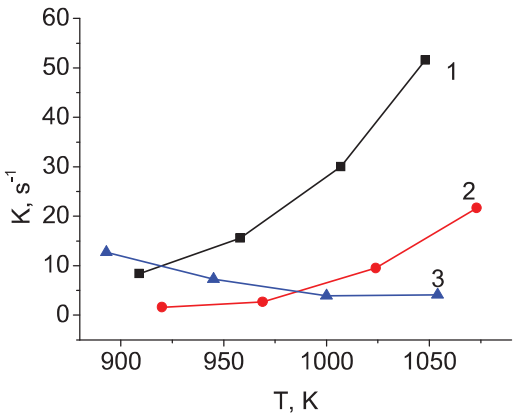

Figure 9. Rate constants of CH_4 dry reforming for channels with active components doped by Pr (1), Gd (2) and La (3). Feed $7\%CH_4+7\%CO_2$

CONCLUSIONS

The real structure of nanocrystalline doped ceria-zirconia samples is characterized by a complex rearrangement of coordination polyhedra with doping. This results in strong variation of the oxygen mobility and state of supported Pt controlling their catalytic properties.

ACKNOWLEDGMENTS

This work is supported by INTAS 05-1000005-7663, RFBR-CNRS 05-03-34761 and ISTC 3234 Projects.

REFERENCES

1. J. Kašpar, P. Fornasiero, in: *Catalysis by Ceria and Related Materials;* (A. Trovarelli, Ed.), (Imperial College Press, London, UK 2002), pp. 217-241.
2. S. Pavlova, N. Sazonova, V. Sadykov, et al *Catal. Today* **105**, 367 (2005).
3. V.A. Sadykov, N. V. Mezentseva et al, *Catal. Today* **131,** 226 (2008).
4. V.A. Sadykov, N.V. Mezentseva et al, *Solid State Phenomena* **128,** 239 (2007).
5. V. A. Sadykov, V.I. Voronin, et al *Mater. Res. Soc. Symp. Proc.* **848,** 231 (2005).]
6. V. A. Sadykov, Yu. V. Frolova et al, *Mater. Res. Soc. Symp. Proc.* **900E,** O10.04 (2006)
7. K.W. Hall, H. Lefftin, F.J. Cheselske, D.E. O'Reilly, *J. Catal.* **2,** 506 (1963).
8. E.N. Gubanova, A. Van Veen, C. Mirodatos, V. A. Sadykov, *Ross. Chem. J.* **52**, 21 (2008).
9. V. Sadykov, V. Kriventsov, E. Moroz et al, *Solid State Phenomena* **128,** 81 **(**2007).
10. V. Sadykov, V. Voronin et al, *Mater. Res. Soc. Symp. Proc.* **1023,** JJ02-07(2007)
11. E. Mamontov, R. Brezny, M. Koranne, T. Egami, *J. Phys. Chem. B.* **107**, 13007 (2003).
12. V. A. Sadykov, N. Mezentseva et al, *Mater. Res. Soc. Symp. Proc.* **988,** QQ06-04 (2007).
13. E. Sadovskaya, C. Mirodatos, V. Sadykov, et al , *J. Phys. Chem.* A **111,** 4498 (2007).
14. D. Efremov, L. Pinaeva, V. Sadykov and C. Mirodatos, *Solid State Ionics* **179**, 847 (2008)

Catalysis Today 157 (2010) 55–60

Contents lists available at ScienceDirect

Catalysis Today

journal homepage: www.elsevier.com/locate/cattod

Oxygen mobility of Pt-promoted doped CeO_2–ZrO_2 solid solutions: Characterization and effect on catalytic performance in syngas generation by fuels oxidation/reforming

V. Sadykov[a,b,*], V. Muzykantov[a], A. Bobin[a,c], N. Mezentseva[a], G. Alikina[a], N. Sazonova[a], E. Sadovskaya[a], L. Gubanova[a], A. Lukashevich[a], C. Mirodatos[c]

[a] Boreskov Institute of Catalysis, Novosibirsk, Russia
[b] Novosibirsk State University, Novosibirsk, Russia
[c] Institut de Recherches sur la catalyse et l'environnement de Lyon, France

ARTICLE INFO

Keywords:
Doped ceria–zirconia
Supported Pt
Oxygen isotope exchange
CH_4
Acetone
Partial oxidation
Dry and autothermal reforming
Syngas

ABSTRACT

For nanocrystalline ceria–zirconia samples doped with rare-earth (Gd, Pr, La) cations prepared via modified Pechini route and promoted by Pt supported by wet impregnation, parameters characterizing their oxygen mobility and reactivity were estimated from results of oxygen isotope exchange experiments in both isothermal and temperature-programmed modes using different procedures. Observed trends in variation of oxygen exchange parameters with the type and content of a dopant were explained with a due regard for the real structure and surface properties of samples earlier characterized in detail. For the reaction of partial oxidation and dry reforming of methane in diluted feeds, catalytic activity correlates both with Pt dispersion and oxygen mobility. For the reactions of acetone autothermal reforming and CH_4 dry reforming in realistic feeds, catalytic activity is mainly determined by the surface/bulk oxygen mobility responsible for coking suppression.

1. Introduction

Ceria–zirconia oxide solid solutions with supported precious metals are promising as catalysts for automotive control, transformation of hydrocarbons or oxygenates into syngas, solid oxide fuel cell anodes etc. [1–4]. The lattice oxygen mobility is an important factor ensuring a high efficiency and stable performance of these systems. The incorporation of rare-earth cations into Ce–Zr–O oxides stabilizes their structure and tunes the oxygen mobility [1,5–7]. Isotope oxygen heteroexchange is one of the most straightforward methods to characterize the oxygen mobility and reactivity [8–18]. However, papers devoted to systematic estimation and analysis of the oxygen exchange parameters for series of Pt-supported doped ceria–zirconia samples are still rare [5,7]. Studies of the real structure and surface properties of ceria–zirconia solid solutions doped by La, Gd or Pr cations carried out last years by authors [7,19–23] provide required basis for such an analysis. This paper is devoted to estimation of parameters characterizing the oxygen mobility in Pt-promoted nanocrystalline ceria–zirconia solid solutions doped by La, Gd, or Pr by using results of isotope exchange experiments in both isothermal and temperature-programmed modes. Factors controlling mobility and reactivity of oxygen were analyzed with a due regard for these samples structure and surface properties. The impact of oxygen mobility on these catalysts performance in partial oxidation of methane (POM), its dry reforming (DR) and autothermal reforming (ATR) of acetone into syngas at short contact times was considered. These three reactions were selected here for comparison because they are known to differ substantially by the coking ability (ATR > DR > POM) [24–27], thus presenting a good possibility for elucidating the relevance of the oxygen mobility for the same series of samples with a due regard for the reaction specificity.

2. Experimental

Dispersed samples of ceria–zirconia based solid solutions $(Ce_{0.5}Zr_{0.5})_{1-x}Ln_xO_{3-\delta}$ (Ln = Pr, La or Gd, $x = 0.05$–0.3) were prepared by polymerized complex precursor route and calcined at 700 °C [2,5]. Pt (1.4 wt.%) was supported from H_2PtCl_6 solution by incipient wetness impregnation followed by drying and calcination at 500 °C for 2 h. Results of detailed characterization of the real structure and surface properties of samples by using combination

* Corresponding author at: Boreskov Institute of Catalysis SB RAS, Prosp. Acad. Lavrentieva, 5, 630090 Novosibirsk, Russia. Tel.: +7 383 3308763; fax: +7 383 3308056.
E-mail addresses: sadykov@catalysis.ru, vasadykov@mail.ru (V. Sadykov).

0920-5861/$ – see front matter © 2010 Elsevier B.V. All rights reserved.
doi:10.1016/j.cattod.2010.03.064

of diffraction (TEM, XRD, neutronography), spectroscopic (EXAFS, SIMS, XPS, FTIRS of adsorbed CO molecules) and magnetic methods are given elsewhere [5,7,19–23]. Specific surface area of samples varies in the range of 50–150 m^2/g increasing with the dopant content and decreasing after Pt supporting [4–7]. All kinetic parameters reported in the paper if required were related per the surface unit of samples.

Oxygen isotope exchange experiments with powdered samples were carried out in a static installation ($V = 680\,cm^3$) with on-line control of the gas phase isotope composition by QMS-200 (Stanford Research Systems, USA) mass-spectrometer in two modes:

1. Isothermal isotope exchange (IIE) at pO_2 1.5–4.5 Torr at 360–650 °C.
2. Temperature-programmed isotope exchange (TPIE) with the temperature ramp 5 K/min from 100 to 750 °C.

The initial ^{18}O content in the gas phase was equal to 96%. Before experiments, samples were pretreated for 2 h under air at 650 °C.

Activation energy of exchange was estimated using IIE data as well as data of TPIE following approach suggested by Cheselske et al. [28].

Catalytic activity of powdered samples (fractions 0.25–0.5 mm) in the reactions of autothermal reforming of acetone (ATR, feed 0.7% C_3H_6O + 0.5% H_2O + 0.5% O_2 in He), partial oxidation (POM, 1% CH_4 + 0.5% O_2 in He) of CH_4 and its dry reforming (DR, 1% CH_4 + 1% CO_2 in He) at short contact times (0.5–25 ms) was studied at temperatures up to 900 °C in a flow installation following earlier described procedures [5–7]. For POM, efficient first-order reaction rate constants were calculated using the integral equation for the plug-flow reactor which was shown to satisfactory describe the experimental data [5] in agreement with results of Wei and Iglesia [29]. Thus, specific rates of methane transformation, related to its inlet content in the feed, were obtained, and their multiplying by the hydrogen selectivity yields the rates of hydrogen generation used for comparison of the samples activity [5]. For the ATR of acetone, due to difficulties in closing the carbon balance, only integral rates of hydrogen generation at 880 °C related to the specific surface area of catalysts were estimated using the steady-state hydrogen concentration in the products and feed rate [20].

To estimate performance in DR in realistic feeds (CH_4 content 7–20%) without impact of heat and mass transfer effects, catalytic activity was tested using thin (~10 μm) catalytic layers supported on the walls of single-channel triangular corundum substrate as described earlier [30,31].

3. Theory

The redistribution of the isotope molecules during heteroexchange $^{18}O_i{}^{16}O_{2-i}$ ($i = 0, 1, 2$) characterized by their molar fractions x_i ($x_0 + x_1 + x_2 = 1$) is described by isotope-kinetic equations [11–14]:

$$\frac{N}{S}\frac{d\alpha}{dt} = -R(\alpha - \alpha_s) \tag{1}$$

$$\frac{N}{S}\frac{dx_1}{dt} = K_1[2\alpha(1-\alpha) - x_1] + K_2[\alpha(1-\alpha_s) + \alpha_s(1-\alpha) - x_1] + K_3[2\alpha_s(1-\alpha_s) - x_1] \tag{2}$$

Here N is the number of O_2 molecules, S is the surface area of oxide, t is the time, $\alpha = 0.5x_1 + x_2$-isotope fraction, $R = 0.5K_2 + K_3$ is the rate of heteroexchange, k_1, k_2 and k_3 are the rates of exchange of the 1st, 2nd and 3rd type (with participation of 0, 1 and 2 surface oxygen atoms, respectively [11–14]), their sum giving the total rate of exchange R.

For a complete description of the isotope redistribution, differential equations reflecting the isotope transfer in the solid phase should be added to this system:

$$\frac{N_s}{S}\frac{\partial\alpha_s}{\partial t} = R(\alpha - \alpha_s) - r_D\frac{N_e}{S}\frac{\partial\alpha_v}{\partial\eta}\bigg|_{\eta=0} \tag{3}$$

$$\frac{\partial\alpha_v}{\partial t} = r_D\frac{\partial^2\alpha_v}{\partial\eta^2} \tag{4}$$

With the initial and boundary conditions:

$$t = 0: \quad \alpha = \alpha^0, \quad \alpha_s = \alpha_v = \alpha_s{}^0; \quad \eta = 0: \quad \alpha_v = \alpha_s$$

where α_v is the fraction of ^{18}O in the oxide bulk, N_s and N_e are the number of oxygen atoms in the surface layer of oxide and the number of exchangeable atoms in the bulk of the oxide, respectively; η is the reduced depth (z) of the oxide layer $\eta = z/h$, where h is the characteristic size of oxide particles; $r_D = D/h^2$ is the effective diffusion coefficient (diffusion relaxation constant), D is the oxygen self-diffusion coefficient.

By transformation of isotope Eqs. (1) and (2), so called isotope-mechanistic equation (5) without time was derived:

$$\ln\left[\frac{v+b}{v^0+b}\right] = -a\ln\left(\frac{s}{s^0}\right), \tag{5}$$

Here $v = z/s^2$, $s = \alpha - \alpha_s$, $z = x_2 - \alpha^2 x_2$, x_2 is the fraction of $^{18}O_2$ molecules, and parameters a and b are determined by the type of mechanism [11]:

$$a = 2\frac{k}{r} = \frac{\kappa_2 + 2\kappa_3 - 1}{0.5\kappa_2 + \kappa_3}$$

$$b = \frac{k_3}{2r - k} = \frac{\kappa_3}{\kappa_2 + 2\kappa_3 - 1}$$

The depth of isotope penetration from the gas phase into the oxide in the course of TPIE can be characterized by the value N_X determined from the relation:

$$2N\alpha^0 + N_X\alpha_S^0 = \alpha(2N + N_X) \tag{6}$$

The value N_X is related to the average depth of isotope incorporation into the solid phase (l_α) by relation $N_X = n_O{}^* S^* l_\alpha$ (here n_O is the number of oxygen atoms in the unit volume of oxide). This quantity termed as "dynamic degree of isotope exchange" [4,5] is expressed in relative units $X_S = N_X/N_S$ and $X_V = N_X/N_V$, corresponding, respectively, to the number of exchanged oxygen monolayers X_s (1 monolayer = 1.4×10^{19} atoms/m^2) and the exchanged fraction of the bulk oxygen, X_v.

Cheselske et al. [28,32] derived equation to estimate apparent activation energy of heteroexchange in experiments with a linear temperature ramp and uniform by reactivity species:

$$E = -\left[RT^2\frac{d\alpha/dT}{\alpha - \gamma}\right]_I \tag{7}$$

Here, $-d\alpha/dT$ is taken at the inflection point where it achieves a maximum value, α is the respective isotope fraction at this point, γ is the equilibrium isotope fraction.

4. Results and discussion

4.1. Oxygen isotope exchange

Temperature-programmed isotope exchange (*TPIE*): For all samples of fluorite-like oxides including those promoted by Pt, linearization of results in coordinates of isotope-mechanistic Eq. (5) revealed domination of the 3rd type of mechanism (a share in the range of 0.7–0.9), without any impact of the 1st type of exchange.

Estimation of the dynamic degree of exchange [5–7] revealed that at temperatures below 600 °C, the oxygen exchange is limited

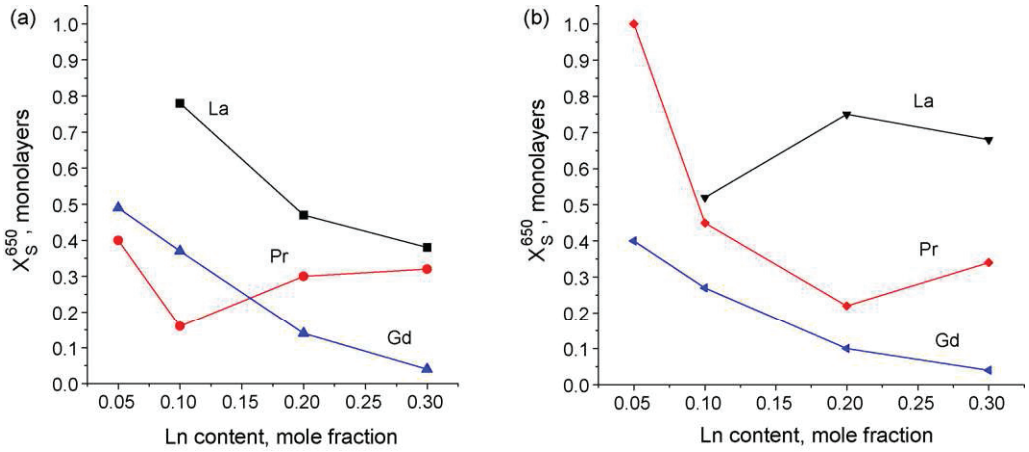

Fig. 1. Dependence of dynamic degree of exchange X_S on the dopant content for samples of $Ln_x(Ce_{0.5}Zr_{0.5})_{1-x}O_{2-y}$ (a) and $Pt/Ln_x(Ce_{0.5}Zr_{0.5})_{1-x}O_{2-y}$ (b). PO_2 2.5 Torr.

to the surface layers (X_S below 1 monolayer) due to much faster surface reaction and diffusion as compared to the bulk diffusion [16–18,33]. At higher temperatures incorporation of isotope into the bulk of oxide particles occurs rather fast, so, for some samples, i.e. for $Pt/Ce_{0.5}Zr_{0.5}O_{2-x}$ sample, X_S achieves 4–5 monolayers at 700–750 °C [5,7]. To characterize mainly the surface/near surface oxygen mobility, 650 °C was selected as the temperature of comparison [4–7]. Indeed, at this temperature for majority of samples considered here X_S is below a monolayer (Fig. 1), thus mainly reflecting the oxygen migration within the surface/near-surface layers. As integral parameter, X_s depends upon all factors controlling dynamics of the surface reaction and diffusion in solid, namely, the sample pretreatment, gas phase oxygen concentration, temperature ramp, etc. For the same sample in strictly fixed experimental conditions, reproducibility of X_s values is ca. 10 rel.%. Comparison of X_S for different samples is the most informative when their specific surface area (particle sizes) and composition do not differ substantially [4–7], as is the case of the present studies.

For the undoped (parent) samples $Ce_{0.5}Zr_{0.5}O_{2-x}$ and $Pt/Ce_{0.5}Zr_{0.5}O_{2-x}$, X_S values at 650 °C and 2.5 Torr O_2 are equal to 0.5 and 1.7, respectively, i.e. being in general higher than for doped samples. This feature was explained by well-known microheterogeneity of the structure of nanocrystalline ceria–zirconia solid solutions consisting of domain enriched by Zr and Ce cations, respectively [34]. This microheterogeneity generates Frenkel-type defects (pairs anion vacancy-oxygen interstitial) revealed in these oxides by detailed neutronographic studies of Mamontov et al. [34]. Such defects decrease the activation barriers for the oxygen diffusion and provide surface sites with a low oxygen bonding strength more active in the oxygen exchange [5,35]. Extended defects present at domain boundaries in $Ce_{0.5}Zr_{0.5}O_{2-x}$ sample and detected also as microstrains by neutron diffraction data analysis [21,23] can also provide paths for facile oxygen migration due to strongly distorted coordination polyhedra in their vicinity. Doping by smaller Pr and Gd cations provides more uniform distribution of Ce and Zr cations [4,6], thus decreasing density of Frenkel-type defects and microstrains and, as the result, decreasing oxygen mobility [5,21]. On the other hand, for largest La cations, X_S increases from 0.5 for undoped sample to 0.8 for moderate (xLa = 0.1) doping level (Fig. 1). In this case, the increase of the lattice parameter accompanied by the decrease of the surface Ce–O bond strength as revealed by SIMS [7,20] appears to be responsible for the increase of X_S for this moderately doped sample.

According to EXAFS data [19–21,23], for samples doped by Gd or La, symmetry and average coordination numbers (CN) for Zr–O and Ce–O spheres increase with the dopant content, while Ce–O sphere contracts, which suggests strengthening of Ce–O bond and disappearance of "free" anion vacancies near Ce cations caused by a complex rearrangement of coordination polyhedra. Usually, for ceria–zirconia solid solutions distortion of Zr–O and Ce–O spheres and lattice expansion leading to appearance of longer (and, hence, weaker) metal–oxygen bonds are considered as the most important factors controlling oxygen mobility [1,6,7,19–21,23]. Hence, clear expressed trend in declining of X_S with the doping level for Gd- or La-containing samples can be explained by such complex rearrangement of coordination spheres and disappearance of "free" oxygen vacancies.

For Pr-doped samples some increase of X_S at a high Pr content can be explained by increasing the Pr^{4+} share which favors mixed ionic-electronic conductivity via chains of Pr^{3+}–Pr^{4+} cations, and, hence, enhanced oxygen mobility, perhaps, along domain boundaries enriched by Pr cations [19–22].

Effect of Pt supporting on X_S (Fig. 1b) depends upon the type and content of doping cation. This suggests specific interaction of Pt with the surface sites/dopants, including, perhaps, even rearrangement of the surface layer caused by leaching of basic-type Ln^{3+} cations during incipient wetness impregnation by acid H_2PtCl_6 solutions and incorporation of Pt^{n+} cations into the surface vacant sites. For undoped sample, high values of X_S (~1.7 at 650 °C [5]) was explained by a high density of microstrains and Frenkel-type defects taking parts in stabilization of ionic Pt forms [5,7,20]. For doped samples, a minor (if any) effect of Pt supporting for Gd-doped samples appears to correlate with mainly subsurface location of small Gd cations, while the strongest effect is observed for samples doped with the biggest La cations segregated in the surface layer [20]. The most positive effect of Pt supporting on X_S, especially at a low dopant content, is observed for Pr-doped samples. This seems to correlate with the highest ability of $Pr^{3+/4+}$ cations to stabilize Pt as 2+/4+ cations [20]. Incorporation of these Pt cations into the subsurface/near surface positions as well as into domain boundaries is expected to generate oxygen vacancies as well as to enhance mixed ionic-electronic conductivity along Pr^{3+}/Pr^{4+} chains thus facilitating oxygen diffusion [20].

Estimation of E_a of heteroexchange by Eq. (7) (vide supra) helps to elucidate the effect of doping cations on the reactivity of surface sites. In typical experiments inflection point is situated at temperatures ~600–700 °C, thus being close to the temperature range of X_S estimation. Hence, estimated in such a way activation energy can be mainly considered as characteristic of the surface reaction steps. For samples without Pt, E_a of isotope exchange is higher for doped samples reflecting variation of the real structure (disappearance of extended defects at domain boundaries, more symmetric

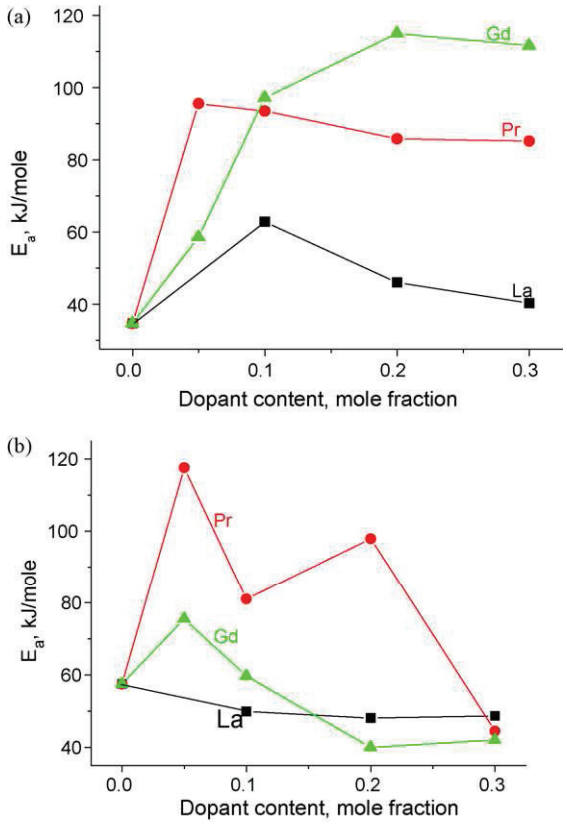

Fig. 2. Effect of dopant content in $Ln_x(Ce_{0.5}Zr_{0.5})_{1-x}O_{2-y}$ (a) and $Pt/Ln_x(Ce_{0.5}Zr_{0.5})_{1-x}O_{2-y}$ (b) samples on E_a estimated by approach of Hall et al.

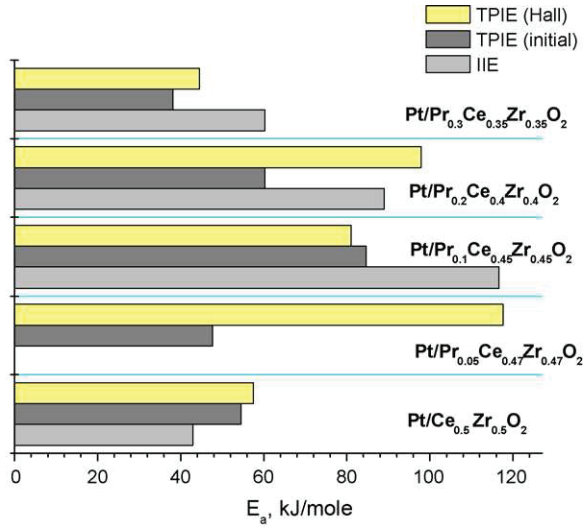

Fig. 3. Comparison of E_a estimated by different procedures for Pt/Pr–Ce–Zr–O samples.

and dense coordination sphere of Ce cations in the surface layer) increasing the Ce–O bond strength and decreasing the density of oxygen vacancies in the surface layer. Decrease of E_a with increasing the size of doping cation Gd < Pr < La (and, hence, increasing the lattice parameter [4,6,7,21]) agrees with this suggestion, since a longer (and, hence, weaker) Ce–O bond strength suggests a lower activation barrier for its rupture as well as a higher density of anion vacancies at chemical equilibrium with the gas phase oxygen.

Pt supporting effect on E_a clearly depends upon the type and content of doping cation (Fig. 2b). Pt supporting on undoped Ce–Zr–O sample increases apparent activation energy (Fig. 2b). Since Pt sites are known to be much more active in oxygen isotope exchange than ceria–zirconia surface centers [16–18,33], this suggests that thus estimated E_a is mainly determined by such steps as oxygen spillover from the Pt to support and/or surface/near surface diffusion. Estimation by fitting SSITKA data for Pt/La–Ce–Zr–O sample revealed that at 650 °C specific rates of exchange on Pt and Pt-support spillover are 1–2 order of magnitude higher than the rates of surface diffusion and exchange on support, the latter being comparable [33]. Hence, the temperature dependence of the exchange rate on Pt-supported samples should be determined mainly by the isotope surface diffusion from the Pt clusters to surrounding oxide regions.

For the largest (and, hence, the most basic) La cation, E_a only decreases with the doping level (Fig. 2b). Since fraction of oxidic Pt forms (oxidic clusters, isolated Pt^{2+} species, including those incorporated into the surface/subsurface layers and domain boundaries) increases with La content [6,7,20], this implies that barriers for the O_2 dissociation and surface/near-surface diffusion are decreased due to such action of Pt oxidic forms. This can be explained by generation of oxygen vacancies due to Pt^{2+} incorporation into the surface layer [6,7,19,21,33,36].

For Gd-doped samples Pt supporting decreases E_a for all doping levels (Fig. 2b). This can be also explained by the same mechanism of oxygen vacancies generation due to Pt^{2+} incorporation into the surface layer. The decrease of activation energy does not increase X_S (Fig. 1). Hence, the concentration factor–the density of "free" oxygen vacancies is more important than the energetic one.

For Pr-doped sample the effect of Pt supporting on E_a is the most complex, increasing it for some compositions and decreasing for others. At the highest doping level E_a is identical for samples with all dopants, agreeing with suggestion about changing the rate-limiting stage determined by the oxygen surface diffusion. A non-uniform distribution of Pt and Pr cations in/on the surface layer and domain boundaries might also affect paths of fast surface diffusion.

Activation energies of exchange were also estimated from the initial low-temperature parts of temperature-programmed exchange curves where the degree of exchange is small. In general, there is a reasonable correlation between the values of activation energy estimated by these two procedures as shown for Pr-doped samples in Fig. 3. The values of E_a estimated from the initial parts of exchange curves tend to be lower than those obtained by the Hall approach. This may be due to both a higher impact of steps occurring on Pt sites [16–18] as well as participation of defect sites with a lower oxygen bonding strength at lower temperatures.

Isothermal isotope exchange: For all samples, dependence of $\alpha(t)$ was close to the exponential one considered as indication on the identical reactivity of exchangeable oxygen forms [11–14]. This allowed to estimate specific rates of exchange R by using a simple integral form of Eq. (1). As follows from Fig. 4, dependence of these rates on the dopant content is similar to that of X_S. This agrees with conclusion that for Pt-supported samples dynamics of the oxygen heteroexchange is controlled by the surface diffusion step.

Activation energies estimated from the temperature dependence of specific rates of heteroexchange obtained in isothermal experiments in general correlate with values derived from results of TPIE experiments (Fig. 3).

To elucidate constants corresponding to the surface process and bulk diffusion, respectively, fitting of IIE data by solving the system of differential rate equations (1)–(4) following earlier verified approach [33] was made. Typical results of fitting are shown in Fig. 5. The rates of heteroexchange estimated from the integral equation and by fitting were found to be quite close. The share of the 3rd type of exchange varies from 0.85 to 0.93, i.e. close to

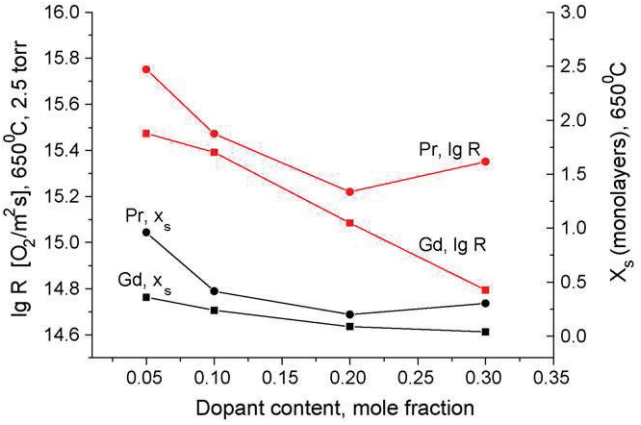

Fig. 4. The rate of oxygen heteroexchange and dynamic degree of exchange for Pr or Gd-doped Pt-supported Ce–Zr–O systems at 650 °C and 2.5 Torr O_2.

that estimated by isotope-mechanistic equation (vide supra). E_a of heteroexchange (~70 kJ/mole) was close to that estimated from IIE data by using an integral equation (~60 kJ/mole).

The values of oxygen self-diffusion coefficients D (10^{-15} to 10^{-16} m^2/s in studied temperature range) found by fitting are by 1–2 order of magnitude higher than the maximum values of D estimated for the near-surface layer for Pt/supported La–Ce–Zr–O sample (~10^{-17} m^2/s) from results of SSITKA experiments [33,36]. As expected, activation energy of bulk diffusion (~150 kJ/mol) is higher than that of the surface processes (vide supra).

4.2. Catalytic activity

Within each series with the same doping cation, catalytic activity in methane selective oxidation (Fig. 6) in diluted feeds correlates with concentration of Pt^{2+} species (and, hence, Pt dispersion) [5,7,20]. This is explained by a high efficiency of CH_4 molecules activation on dispersed oxidized Pt sites yielding H_2 and CO as primary products [5,31]. The difference in activity between the series of samples (Pr > Gd) in POM as well as in DR in diluted feed (Fig. 7) apparently correlates with the surface oxygen mobility characterized by X_S (vide supra). Hence, for the reactions characterized by moderate reducing/coking ability (POM, DR in diluted feed) dispersion of supported Pt seems to be more important factor than the oxygen mobility.

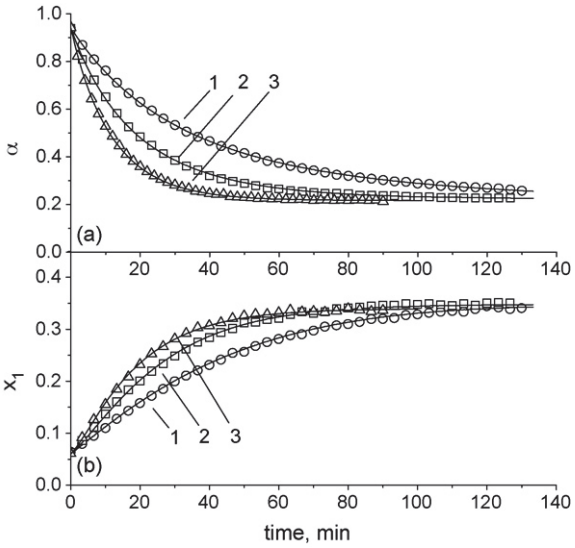

Fig. 5. Results of $\alpha(t)$ (a) $x_1(t)$ (b) fitting in isothermal isotope exchange at (1) 550 °C, (2) 600 °C and (3) 650 °C for Pt/$Pr_{0.3}Ce_{0.35}Zr_{0.35}$ sample.

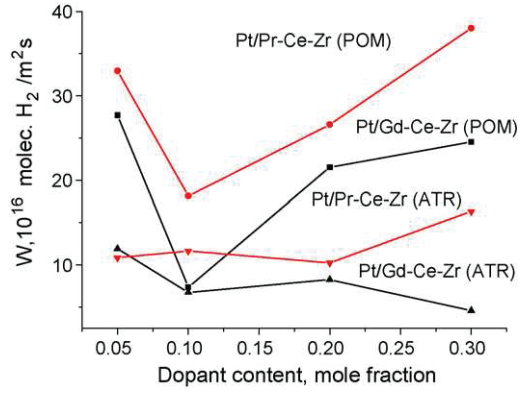

Fig. 6. Specific rates of H_2 formation for POM at 770 °C and acetone ATR at 880 °C.

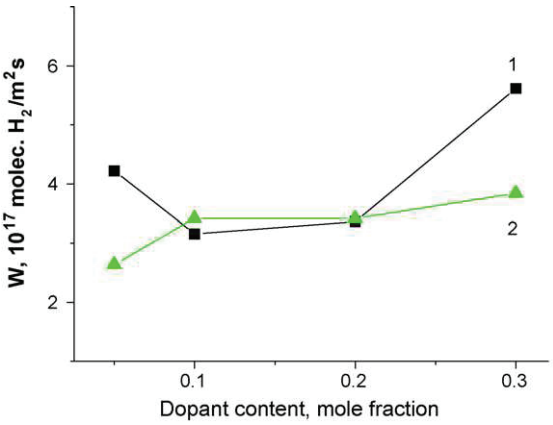

Fig. 7. Specific rates of H_2 formation for methane dry reforming at 770 C. 5 ms contact time, feed 1% CH_4 + 1% CO_2 in He. 1-Pt/$Pr_x(Ce_{0.5}Zr_{0.5})_{1-x}O_{2-y}$ samples and 2-Pt/$Gd_x(Ce_{0.5}Zr_{0.5})_{1-x}O_{2-y}$ samples.

In ATR of acetone characterized by more reducing reaction feed, catalytic performance correlates mainly with the oxygen mobility. This is explained by well-known excessive coking in this reaction counteracted by the oxygen mobility [26].

For the reaction of CH_4 dry reforming in concentrated feeds, correlation of activity with the surface oxygen mobility (X_S) and Pt dispersion (La > Pr > Gd [5]) is observed in the intermediate (up to

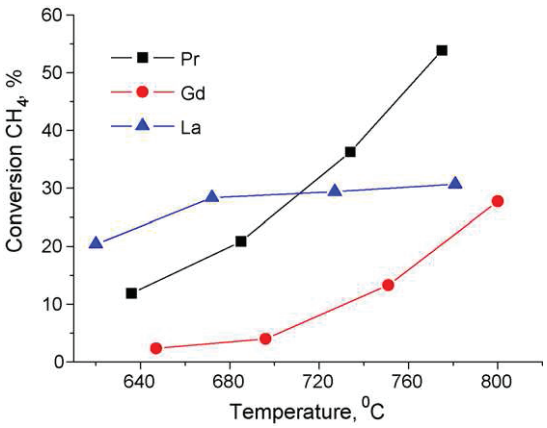

Fig. 8. Temperature dependence of CH_4 conversion in CH_4 DR for 1.4% Pt/$Ln_{0.3}$–Ce–Zr–O catalysts supported on walls of corundum channel. Feed composition 7% CH_4 + 7% CO_2 in He, contact time 15 ms.

650 °C) temperature range (Fig. 8). However, at higher (~800 °C) temperatures the order of activity is changed, and the highest performance is demonstrated by Pr-doped sample. This apparently correlates with the highest bulk oxygen mobility for this sample (vide supra). Since for dry reforming reaction in real feeds the main problem is coking leading to catalysts deactivation [24,25], this result implies that the bulk mobility in complex fluorite-like oxide supports is also an important factor favoring coke precursors gasification by supplying oxygen-containing species to the Pt-support interface.

5. Conclusions

For nanocrystalline Pt-supported ceria–zirconia samples doped with rare-earth (Gd, Pr, La) cations systematic comparison of parameters characterizing their oxygen mobility and reactivity estimated from the results of oxygen isotope exchange experiments in static installation in both isothermal (IE) and temperature-programmed modes (TPIE) using different analysis approaches has been made. Parameters characterizing exchange mechanism (type of exchange) and surface/near-surface oxygen mobility (dynamic degree of exchange X_S, E_a) can be estimated with a reasonable precision from results of high-throughput TPIE using simplified analysis procedures. However, estimation of the specific rates of exchange (especially with a due regard for steps occurring on supported Pt or Pt-support oxygen spillover stage) and bulk oxygen self-diffusion coefficient requires more detailed analysis of isothermal exchange experiments data solving the system of differential rate equations [33] or applying Monte Carlo simulation [36]. For partial oxidation and dry reforming of methane in diluted feeds, catalytic activity correlates both with Pt dispersion and oxygen mobility. Performance in acetone ATR and CH_4 DR in realistic feeds is mainly determined by the oxygen near surface and/or bulk mobility responsible for coking suppression.

Acknowledgements

This work was carried out in frames of Russian-French Associated European laboratory on catalysis. Support by OCMOL FP7 Project and RFBR–CNRS 09-03-93112 Project is gratefully acknowledged.

References

[1] J. Kašpar, P. Fornasiero, In catalysis by ceria and related materials, in: A. Trovarelli (Ed.), Catal. Sci. Ser., vol. 2, Imperial College Press, London, UK, 2002, pp. 217–241.
[2] H. He, H.X. Dai, L.H. Ng, K.W. Wong, C.T. Au, J. Catal. 206 (2002) 1.
[3] M. Mogensen, N.M. Sammes, G.A. Tompsett, Solid State Ionics 129 (2000) 63.
[4] V.A. Sadykov, Yu.V. Frolova, V.S. Muzykantov, V.P. Ivanov, H. Borhart, S. Neophytides, E. Kemnitz, K. Scheurell, Mater. Res. Soc. Symp. Proc. 835 (2005) 199.
[5] V. Sadykov, T.G. Kuznetsova, V.S. Muzykantov, L.G. Pinaeva, E.A. Paukshtis, N.V. Mezentseva, E. Kemnitz, C. Mirodatos, A.C. van Veen, Catal. Today 117 (2006) 475.
[6] V.A. Sadykov, N.V. Mezentseva, G.M. Alikina, A.I. Lukashevich, Yu.V. Borchert, T.G. Kuznetsova, V.P. Ivanov, E.A. Paukshtis, V.S. Muzykantov, V.L. Kuznetsov, V.A. Rogov, J. Ross, E. Kemnitz, C. Mirodatos, Solid State Phenomena 128 (2007) 239.
[7] V.A. Sadykov, T.G. Kuznetsova, G.M. Alikina, Yu.V. Frolova, A.I. Lukashevich, V.S. Muzykantov, V.A. Rogov, L.G. Ivanov, S. Pinaeva, E. Neophytides, K. Kemnitz, C. Scheurel, Mirodatos, in: D.K. McReynolds (Ed.), Book: New Topics in Catalysis Research, Nova Science Publishers, NY, USA, 2007, pp. 97–196 (Chapter 5).
[8] G.K. Boreskov, V.S. Muzykantov, Ann. N.Y. Acad. Sci. 213 (1975) 137.
[9] K. Klier, J. Novakova, P. Jiru, J. Catal. 2 (1963) 479.
[10] V.S. Muzykantov, G. Ewald, G. von Levis, Kinetika i Kataliz 15 (1974) 1512.
[11] V. Muzykantov, E. Kemnitz, V. Sadykov, V. Lunin, Kinetika i Kataliz 44 (2003) 349.
[12] V.S. Muzykantov, React. Kinet. Catal. Lett. 35 (1987) 437.
[13] V.S. Muzykantov, P. Jiru, K. Klier, Coll. Czech. Chem. Commun. 33 (1968) 829.
[14] G.K. Boreskov, Catalytic Activation of Dioxygen, Catalysis—Science and Technology, Springer, Berlin, 1982, v. 3 (Chapter 2).
[15] K. Klier, E. Kucera, J. Phys. Chem. Solids 27 (1966) 1087.
[16] A. Galdikas, C. Descorme, D. Duprez, Solid State Ionics 166 (2004) 147.
[17] A. Galdikas, D. Duprez, C. Descorme, Appl. Surf. Sci. 236 (2004) 342.
[18] D. Duprez, Isotopes in Heterogeneous Catalysis, Imperial College Press, London, 2006, p. 133.
[19] V. Sadykov, N. Mezentseva, G. Alikina, A. Lukashevich, V. Muzykantov, T. Kuznetsova, V. Ivanov, A. Boronin, A. Ishchenko, V. Rogov, J. Ross, E. Kemnitz, Mater. Res. Soc. Symp. Proc. 988 (2007), pp. QQ06–QQ04.
[20] V. Sadykov, V. Kriventsov, E. Moroz, Yu. Borchert, T. Kuznetsova, V. Ivanov, A. Boronin, N. Mezentseva, E. Burgina, J. Ross, Solid State Phenomena 128 (2007) 81.
[21] V. Sadykov, N. Mezentseva, V. Muzykantov, R. Bunina, A. Boronin, V. Voronin, I. Berger, Mater. Res. Soc. Symp. Proc. 1023 (2007) JJ02–07.
[22] T.G. Kuznetsova, V.A. Sadykov, Kinetics Catal. 49 (2008) 840.
[23] V. Sadykov, N. Mezentseva, V. Muzykantov, E. Gubanova, N. Sazonova, A. Bobin, V. Voronin, J. Ross, C. Mirodatos, Mater. Res. Soc. Symp. Proc. 1122 (2009), p. O05-O03.
[24] J.R.H. Ross, Catal. Today 100 (2005) 151.
[25] X.E. Verykios, Int. J. Hydrogen Energy 28 (2003) 1045.
[26] K. Takanabe, K. Aika, K. Seshan, L. Lefferts, Top. Catal. 49 (2008) 68.
[27] V. Sadykov, N. Mezentseva, G. Alikina, R. Bunina, V. Pelipenko, O. Bobrenok, A. Smirnova, J. Ross, O. Smorygo, B. Rietveld, Catal. Today 146 (2009) 132.
[28] F.J. Cheselske, W.E. Wallage, W.K. Hall, J. Phys. Chem. 63 (1959) 505.
[29] J. Wei, E. Iglesia, J. Phys. Chem. B 108 (2004) 4094.
[30] S. Pavlova, N. Sazonova, V. Sadykov, E. Gubanova, Catal. Today 105 (2005) 367.
[31] E.L. Gubanova, A. Van Veen, C. Mirodatos, V.A. Sadykov, N.N. Sazonova, Russ. J. Gen. Chem. 78 (2008) 2191.
[32] W.K. Hall, H.P. Leftin, F.J. Cheselske, D.E. O'Reilly, J. Catal. 2 (1963) 506.
[33] E. Sadovskaya, V. Sadykov, C. Mirodatos, J. Phys. Chem. A: Gen. 111 (2007) 4498.
[34] E. Mamontov, R. Brezny, M. Koranne, T. Egami, J. Phys. Chem. B 107 (2003) 13007.
[35] N. Bulgakov, V. Sadykov, V. Lunin, React. Kinet. Catal. Lett. 76 (2002) 103.
[36] D. Efremov, V. Sadykov, C. Mirodatos, Solid State Ionics 179 (2008) 847.

Catalysis Today 171 (2011) 140–149

Contents lists available at ScienceDirect

Catalysis Today

journal homepage: www.elsevier.com/locate/cattod

Dry reforming of methane over Pt/PrCeZrO catalyst: Kinetic and mechanistic features by transient studies and their modeling

V.A. Sadykov[a,b,*], E.L. Gubanova[a], N.N. Sazonova[a], S.A. Pokrovskaya[a,b], N.A. Chumakova[a,b], N.V. Mezentseva[a], A.S. Bobin[a], R.V. Gulyaev[a], A.V. Ishchenko[a], T.A. Krieger[a], C. Mirodatos[c]

[a] Boreskov Institute of Catalysis SB RAS, 630090 Novosibirsk, Russia
[b] Novosibirsk State University, 630090 Novosibirsk, Russia
[c] Institut de Recherches sur la catalyse et l'environnement de Lyon, Lyon, France

ARTICLE INFO

Article history:
Received 31 October 2010
Received in revised form 29 March 2011
Accepted 1 April 2011
Available online 5 May 2011

Keywords:
Methane dry reforming
Pt
Fluorite-like oxides
Transient studies
Kinetics
Mechanism
Modeling

ABSTRACT

The effect of pretreatment and Pt content on the catalytic properties as well as mechanistic features of DR were investigated for structured catalysts comprised of Pt supported on CeO_2–ZrO_2 oxide doped by Pr. Progressive reduction of cationic Pt species by the reaction feed lowers the activity in CH_4 dry reforming while accelerating the reverse water gas shift reaction catalyzed only by Pt^0, which then decreases progressively the H_2/CO ratio in the effluent. This process is counteracted by the mobility of surface oxygen supplying oxygen atoms to reduced Pt centers thus ensuring their reoxidation and generating in parallel surface oxygen vacancies for the dissociation of CO_2.

A mathematical model and software were developed for numerically studying the transients of the complex catalytic reactions. The processing of experimental data was fulfilled taking into account the importance of cationic forms of Pt, reactivity of carbonate complexes coordinated to these cations and oxygen surface/bulk diffusion. A quantitative evaluation of the density of catalyst's active sites and their coverage by reactive species was accomplished and the rates both of the lattice oxygen diffusion and main stages of the catalytic reaction were estimated.

1. Introduction

Reforming of CH_4 with CO_2 is an attractive reaction due to the production of syngas with a low H_2/CO ratio, suitable for oxo- and Fischer–Tropsch synthesis processes [1,2]. Moreover, methane dry reforming (DR) offers the additional advantage of consuming two greenhouse gases, transforming them into products with high added value. The reaction is also suitable for chemical energy transmission systems [3]. However, the commercial application of dry reforming reaction is limited due to the lack of effective catalysts resistant to carbon formation.

Most group VIII metals, especially Ni based and noble metals have been studied as catalysts for steam reforming, dry reforming, partial oxidation and mixed reforming of methane [4–8]. The deactivation is the main problem to tackle for design of a catalyst suitable for an industrial application. The two most prominent causes for the deactivation in DR are coke deposition and sintering of the active metal phase. Most of the researchers agree that coke formation is the main cause of deactivation. Carbon deposition results from two reactions, methane decomposition ($CH_4 \rightarrow C + 2H_2$) and/or Boudouard reaction ($2CO \rightarrow C + CO_2$). The type and the nature of the formed coke depend on the active metal and in many cases on the support used. In the recent literature reports ceria and zirconia materials have attracted attention as carrier or catalysts for important industrial or environmentally friendly reactions. In addition, the use of ceria-based oxides is known to prevent an accumulation of carbon on the surface of the catalysts thus helping to maintain the activity [9–12]. Literature data demonstrate that CeO_2-based oxides remarkably modify the activity of supported metals [13,14]. $Pt/Ce_xZr_{1-x}O_2$ catalysts with a Ce/Zr ratio of 1, which have the highest redox capacity, were shown to be very active and stable in methane to synthesis gas transformation reactions [15]. However, in high-temperature (especially, hydrothermal) conditions mixed ceria–zirconia oxides are decomposed into phases enriched by ceria and zirconia, respectively, which is accompanied by sintering of both oxide substrate and supported Pt [16]. To increase thermal stability of these catalysts, ceria–zirconia is doped by rare-earth cations, Al, etc. [16,17]. Among lanthanides, Pr as dopant was shown to provide the best activity of Pt-supported ceria–zirconia catalysts in CH_4 dry reforming in concentrated feeds, which was explained by a high surface and lattice oxygen mobility required to suppress coking [18,19].

* Corresponding author at: Boreskov Institute of Catalysis SB RAS, prosp. Akad. Lavrentieva, 5, 630090 Novosibirsk, Russia. Tel.: +7 3833308763; fax: +7 3833308056.
E-mail address: sadykov@catalysis.ru (V.A. Sadykov).

0920-5861/$ – see front matter © 2011 Elsevier B.V. All rights reserved.
doi:10.1016/j.cattod.2011.04.004

Furthermore, it is also important to analyze the mechanistic pathways of the reforming reaction for developing an efficient catalyst. Different steps in the mechanism have been established for the formation of CO and H_2 from CH_4. Bradford and Vannice [20] studied the kinetics of CO_2 dry reforming over supported Pt catalysts suggesting that CH_4 is reversibly activated on Pt producing CH_x species and H_2. They also proposed that CO_2 participates in the reaction via the reverse water-gas shift (RWGS) reaction yielding OH groups which then react with adsorbed CH_x intermediates to form formate-type species (CH_xO). Those intermediates decompose then irreversibly into CO and H_2. In contrast, Wei and Iglesia argued that CH_4 dissociation is the rate-limiting step, and C atoms are the most abundant reaction intermediate on the surface, while other steps are equilibrated [21]. Another reaction scheme for the dry reforming over Pt/Al_2O_3 catalyst was proposed by O'Connor et al. [2]: the CH_4 activation proceeds on free Pt sites, and CO_2 activation is assumed to be the slowest step assisted by hydrogen to form adsorbed CO and OH. The hydroxyl groups of the alumina support are supposed to participate in the reaction mechanism. For Pt/ZrO_2 participation in the reaction mechanism of hydroxocarbonates and formates stabilized on support was suggested [2]. Maestri et al. performed a microkinetic analysis of the dry and steam reforming [22] reporting that CH_4 consumption proceeds via pyrolysis, and oxidation of formed carbon involves superficial OH groups, while CO_2 is activated via interaction with adsorbed H.

The aim of the current investigations was to elucidate the factors controlling performance of Pt-supported $Pr_{0.3}Ce_{0.35}Zr_{0.35}O_{2-x}$ catalysts in CH_4 DR at short contact times. Detailed experimental studies and modeling of the behavior of structured Pt-supported catalysts in this reaction are reported. The steady state and transient operation were studied in a tubular reactor with one-channel catalytic fragment corresponding completely to a real honeycomb monolith catalyst, which allows in turn defining the intrinsic catalytic properties at contact times of 4–5 ms. The application of this kind of structure fragment allows, due to the small amount of applied catalyst, to minimize and control the temperature gradients along the channel [19,23]. The computational analysis of transient experiments on the basis of original software was aimed at determining the rates of main stages of reaction mechanism and lattice oxygen diffusion.

2. Experimental

2.1. Catalysts preparation and characterization

Complex fluorite-like $Pr_{0.3}Ce_{0.35}Zr_{0.35}O_{2-x}$ oxide was prepared by a polymerized complex precursor route (Pechini) followed by drying and calcinations in air at 900 °C for 2 h as described elsewhere [17,24]. Pt (0.5, 1.6 and 4.9 wt.%) was supported from H_2PtCl_6 solution by incipient wetness impregnation followed by drying and calcination at 900 °C. The specific surface area of samples was determined from the Ar thermal desorption data by using the BET method. XRD patterns were obtained with an ARL XTRA diffractometer using Cu Kα monochromatic radiation (λ = 1.5418 Å); the 2θ-scanning region was 20–85°. The TEM micrographs were obtained with a JEM-2010 instrument (lattice resolution 1.4 Å) and acceleration voltage 200 kV. Local elemental analysis was performed with EDX method (a Phoenix Spectrometer) XPS spectra were acquired using an ES-300 spectrometer (Kratos Analytical, UK) equipped with two anodes (AlKα, 1486.6 eV and MgKα, 1253.6 eV) operated at 65 W to prevent reduction of Ce^{4+} in the surface layer. Samples were fixed on a holder by double-side scotch tape. Calibration of XP spectra were made relatively E_B(Ce3d) = 916.7 eV.

To prepare structured catalysts, triangular channels of α-Al_2O_3 monolith (wall thickness 0.2 mm, triangle side 2.33 mm, channel length 10 mm) was washcoated with slurry of oxides with addition of peptizers and surfactants and calcined at 900 °C. Pt (1.6 wt.%) was supported by the wet impregnation followed by drying and calcination under air at 900 °C.

2.2. Steady state and transient experiments

Both steady state and transient experiments were carried out at atmospheric pressure using quartz reactors and flow installation equipped with GC and on-line IR absorbance, electrochemical and polarographic gas sensors for different components as described elsewhere [23,25]. In this reactor, a single channel structural catalytic element was placed [19,23]. The active component was either placed into the triangular corundum channel as 250–500 micron fraction loosely packed within it or supported as thin (~10 microns) layers on its walls. This helps to provide the plug-flow regime of this microreactor operation and minimize the temperature gradients along the channel.

CH_4 concentration in the feed was varied in the range of 3.5–7% with CH_4/CO_2 ratio = 1, the temperature range was 650–800 °C and contact time 4.7–15 ms. Before reaction, the samples were pretreated in O_2 stream at 700 °C. Effect of pretreatment in different streams (O_2, dry He at 900 °C; 1%CO in N_2 or 1%CH_4 in N_2 or pure H_2 at 500 °C for 0.5 h; pure H_2 at 800 °C for 0.5 h) has been studied as well. In the transient experiments after preconditioning a pretreatment flow was purged by He, and then He stream was switched to required reaction mixture. The composition of the mixture was continuously analyzed. Control experiments with a single channel fragment of the corundum showed that, at gas flow rates of about 30 l h^{-1}, the purge time of the system is no longer than 2–4 s.

3. Results and discussion

3.1. Catalysts characterization

For dispersed $Pr_{0.3}Ce_{0.35}Zr_{0.35}O_{2-x}$ oxide, specific surface area is 29 m^2/g. For promoted by Pt samples it varies in the range of 14.6–13.5 m^2/g decreasing with Pt content. This suggests that a part of supported Pt is encapsulated within support particles sintered due to their surface activation by acidic H_2PtCl_6 solution followed by high-temperature calcination [26]. XRD patterns correspond to fluorite-like solid solution [24,27]. In addition, for Pt-promoted samples with Pt loading 1.6 and 4.9 wt.%, reflections at 2θ ~39, 47, 68, 83° corresponding to metal Pt particles with typical sizes ~40–60 nm were observed, their intensity increasing with Pt content. As revealed by analysis of integral intensity of these reflections using Pt/corundum sample as a standard, only a small (<10%) part of Pt is present as metallic particles detected by XRD, which is a typical feature of Pt-supported doped ceria-(ceria–zirconia) oxides [24,26]. This conclusion is supported by TEM data (Figs. 1–3). For as-prepared samples (Fig. 1) only small (typical sizes up to several nanometers) Pt clusters strongly interacting with support and possibly covered by support oxidic fragments are revealed. For samples with the highest Pt content, big Pt particles are very seldom observed at the edges of support platelets. After sample contact with the reaction feed 7% CH_4 + 7% for 5 h at 800 °C, the number of Pt clusters per the support surface unit and their size appear to be somewhat increased, without any pronounced sintering (Fig. 2). Big Pt particles are much more frequently observed after strong reduction by H_2 at 800 °C, though small clusters were observed as well being apparently better crystallized than those on the surface of oxidized samples (Fig. 3).

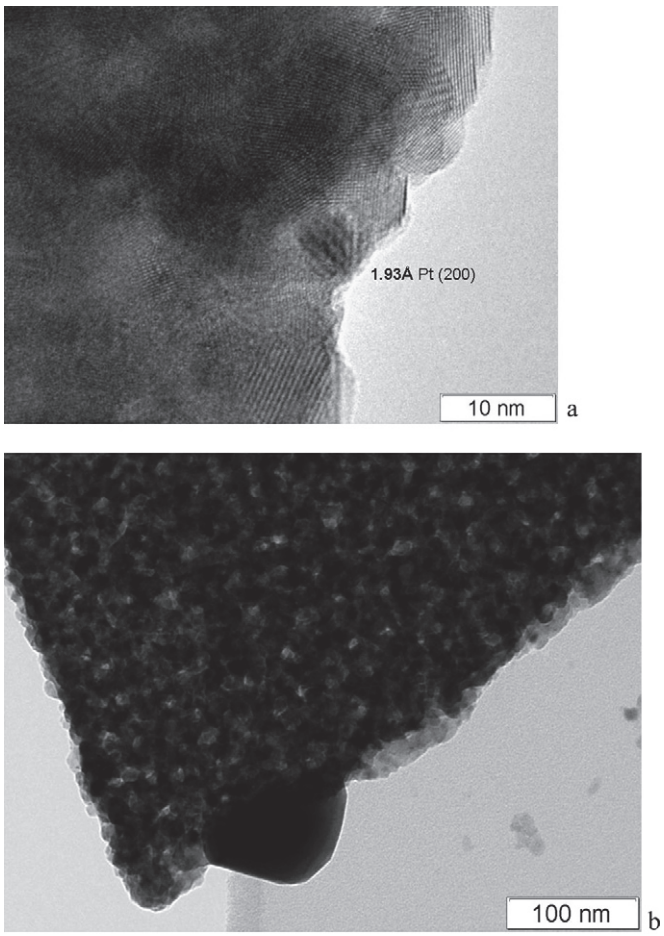

Fig. 1. Typical morphology of Pt particles in oxidized Pt/PrCeZrO samples. (a) Disordered Pt cluster on the surface of 1.6%Pt/PrCeZrO sample, (b) big Pt particle at the edge of support platelet in 4.9%Pt/PrCeZrO sample.

In general, XPS results (Fig. 4) agree with XRD and TEM data. For oxidized samples, three different states of Pt (BE 71-72, 73 and 75 eV) corresponding to species in 0, 2+ and 4+ states [28,29] have been observed (Fig. 4). For sample with the lowest Pt loading, Pt^0 state was not detected. The ratio of surface concentrations of Pt/Pr + Ce + Zr increases from ~0.2% to ~0.45% and ~1% with increasing Pt loading from 0.5 to 1.6 and 4.9 wt.%, respectively. Such a low surface concentration of Pt suggests incorporation of Pt cations into the surface/subsurface layers of fluorite-like oxides and its strong interaction with support (decoration of Pt clusters by support oxidic species) [26]. This agrees with data of infrared spectroscopy of CO test molecules adsorbed on the surface of such samples at liquid N_2 temperature revealing domination of Pt^{2+} and Pt^{+} cationic species [17,24,25]. Pt^{4+} cations even if present on the oxidized surface could not be detected by this method due to reduction by CO even at 77 K. Pretreatment of sample with 1.6% Pt in the reaction feed at high temperature results in reduction of Pt^{2+} to metallic Pt (Fig. 4) while Pt/Pr + Ce + Zr ratio only slightly decreases from ~0. 45% to ~0.4% in agreement with TEM data. High-temperature reduction of this sample by H_2 decreases further Pt/Pr + Ce + Zr ratio to ~0.2%.

3.2. Catalytic activity

3.2.1. Steady-state characteristics

Typical transients observed after contact of oxidized catalyst fraction filling the corundum channel are shown in Fig. 5 for sample with the highest Pt content. For the steady-state regime achieved at times on-stream >3000 s, the effective first-order rate constants were estimated by using the equation for the plug-flow reactor following earlier described approaches [19]. These constants varying in the range of 1–4 m^{-2} s^{-1} are roughly proportional to the surface Pt concentration estimated by XPS (vide supra). At all temperatures, H_2/CO ratio is <1 (Fig. 5), which is the usual feature of CH_4 dry reforming explained by the parallel occurrence of reverse water gas shift (RWGS) reaction consuming hydrogen

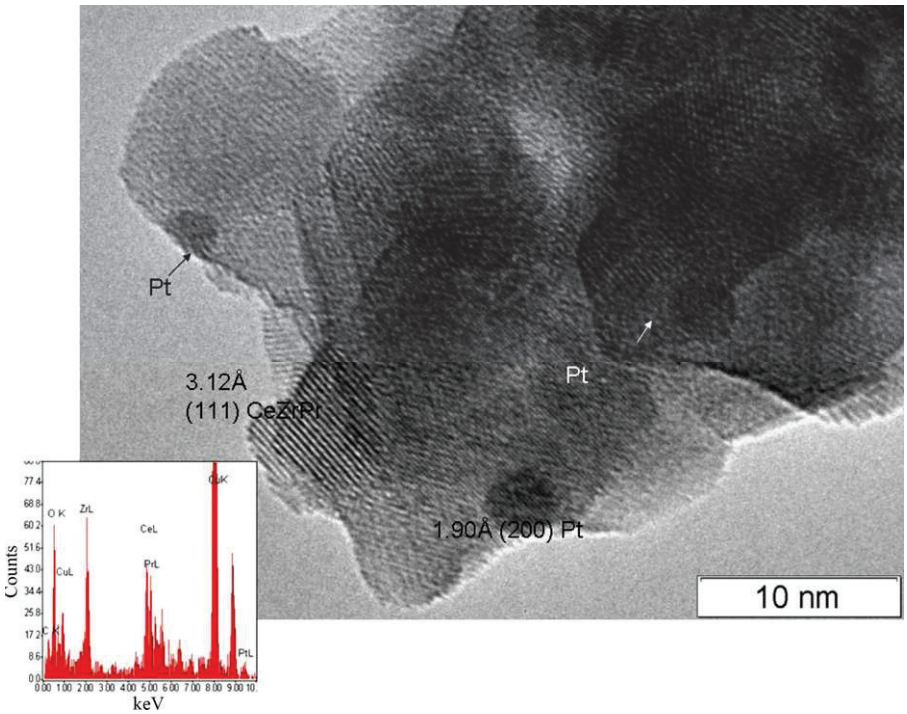

Fig. 2. Typical morphology of Pt clusters on the surface of 1.6%Pt/PrCeZrO sample treated in the reaction at high temperatures and respective EDX spectra.

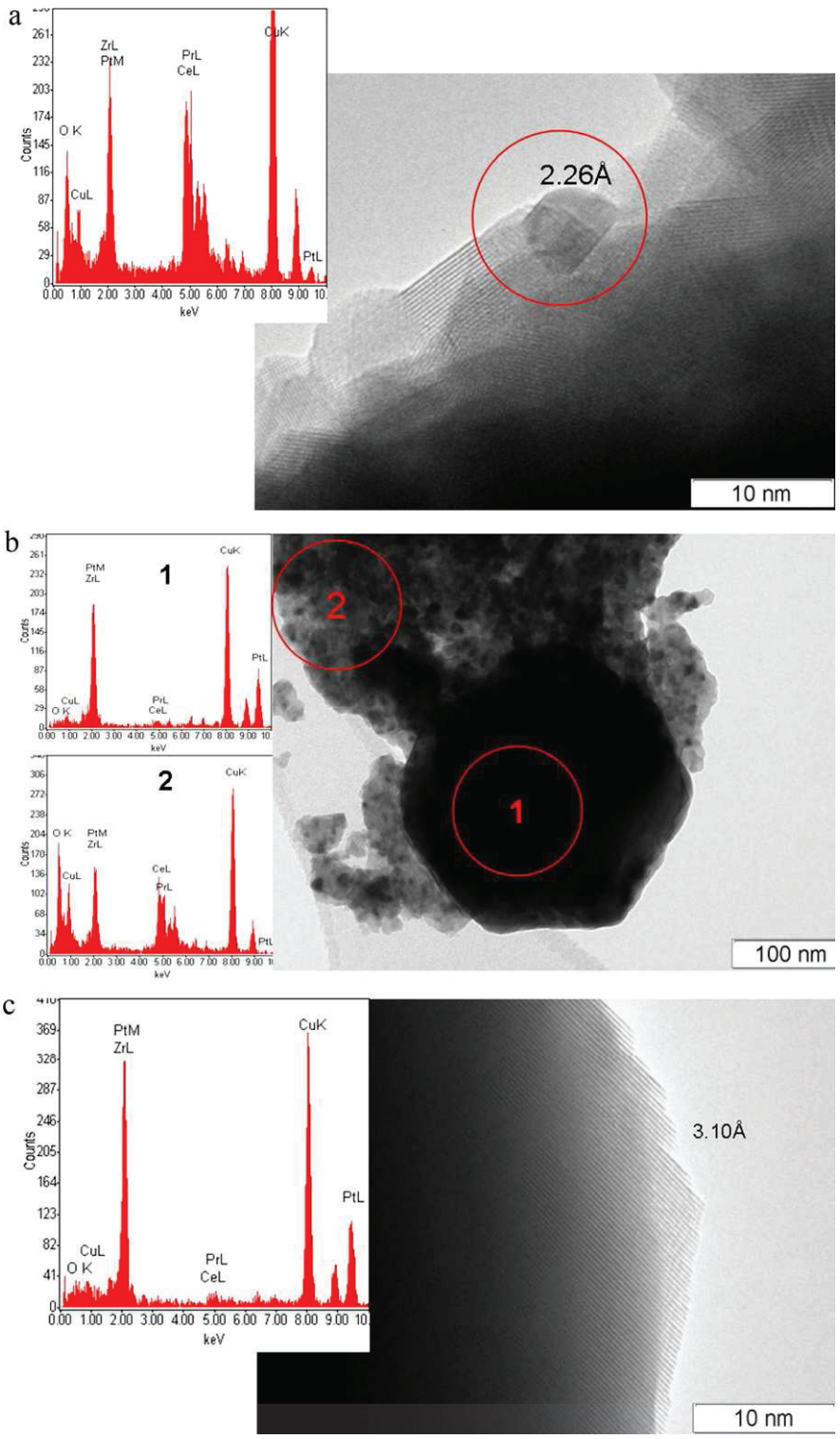

Fig. 3. Typical morphology of Pt particles on the surface of 1.6%Pt/PrCeZrO sample after reduction by H_2 at 800 °C and respective EDX spectra. (a) Small ordered Pt platelet, (b) big Pt particle, (c) high resolution image of the edge of big Pt particle.

and producing H_2O and CO [31]. Comparison of the WGS reaction product ($[H_2]^*[CO_2]$)/($[CO]^*[H_2O]$) with respective equilibrium constant calculated following known approaches [32] (Fig. 6) shows that for sample with a low Pt content this reaction is far from equilibrium. For samples with higher Pt loadings, within uncertainty of analysis, WGSR is rather close to equilibrium, though some deviation due to faster WGSR appears to take place. Hence, at a low Pt loading, RWGS reaction is hampered due to domination of oxidic Pt species not able to activate hydrogen molecules. For samples with higher Pt loadings, some deviation from the WGS reaction equilibrium can be explained either by a slow rate of direct step due to a weak bonding of CO with Pt clusters [31] or conjugation of the reverse WGS reaction with methane dry reforming as suggested by Bradford and Vannice [20]. Since slow transients observed for pretreated in O_2 Pt-supported catalysts (Fig. 5) can be caused by samples reduction in the reaction feed [19,23], special experiments

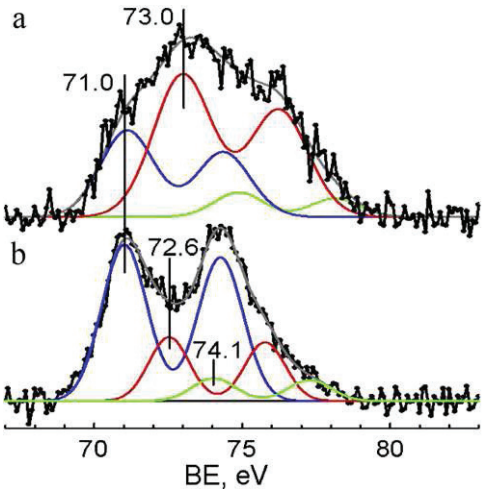

Fig. 4. XPS spectra for 1.6%Pt/PrCeZrO sample after oxidizing pretreatment (a) and after high-temperature treatment in the reaction feed 7% CH_4 + 7% CO_2 in He.

were carried out to clarify the effect of pretreatment on catalysts performance.

3.2.2. *Effect of pretreatment*

Pretreatment in H_2 at 800 °C for 0.5 h leading to complete reduction of fluorite-like oxide strongly deactivates catalysts decreasing CH_4 and CO_2 conversion from ~40–50% to ~10% at 700 °C and 15 ms. According to TEM data (Fig. 3), reduction in H_2 at 800 °C generates big Pt particles located on support, and, as judged by XPS, dispersion of Pt decreases in average as well. EDX spectrum from the edge of such a particle demonstrates that it is essentially free from any trances of Pr, Sm or Zr cations. Hence, deactivation of catalysts due to high-temperature reduction could not be assigned to any effects of strong metal –support interactions such as formation of surface PtCe alloys or ceria overlayers [26]. Rather, it can be explained not only by decreasing Pt surface area but also by ordering the structure of Pt clusters and decreasing their surface coverage by oxidic fragments. While ordering apparently decreases coordinative unsaturation of Pt, and, hence, its reactivity with respect to C–H bond activation in methane molecule [21], decreasing the surface coverage of Pt clusters by oxidic/carbonate species derived from support decreases the Pt-support interface and clearly hampers support-Pt reverse oxygen spillover. All these factors appear to be reflected in the catalyst deactivation caused by severe reduction. On the other hand, such factor as support excessive reduction could not be too important, since in the presence of CO_2 in the reaction feed support can be rapidly reoxidized by carbon dioxide to the steady-state level of stoichiometry. Reduction by H_2 at 500 °C for 0.5 h (removes up to 5 oxygen monolayers [17]) does not change the steady-state activity though transients varied significantly (not shown for brevity). Since features of transients could be affected by the radial and axial mixing occurring even within a narrow channel filled with the catalyst fraction or byproducts (CO_2, H_2O) diffusion within porous catalysts particles with typical sizes up to 0.5 mm, detailed studies of these transients as dependent upon the type of pretreatment have been carried out for thin (~10 microns) layers of 1.6 wt.% Pt/PrCeZrO catalyst supported on walls of separate corundum channel. Selection of this composition as a basic for these studies was determined by compromise between its reasonably good activity and Pt content acceptable for any practical application.

Transient curves of reagents and products responses after switching the stream of He to the reaction feed for this structured catalytic element pretreated in different conditions are presented in Fig. 7. Oxidized catalyst has the highest activity, probably due to a better activation of methane on cationic Pt species stabilized due to interaction with support [20]. For oxidized catalyst, the maximum value of H_2/CO ratio achieved up to 20–30 s of transient after switch from He to CH_4 + CO_2 stream is close to 1. This suggests that CH_4 DR on cationic Pt sites could include interaction of activated CH_x species and (hydroxo)carbonate located in the coordination sphere of the same Pt cation. The lower is the degree of oxidation varied due to pretreatment (pretreatment in He removes up to 0.5 monolayer of oxygen, pretreatment in CO or H_2 removes up to 3 monolayers), the lower is the maximum H_2/CO ratio (Fig. 7e). This shows that the reverse water-gas-shift reaction is indeed favored by the catalyst reduction. Progressive reduction of oxidized catalyst by reaction feed decreases activity in CH_4 reforming with time-on-stream while accelerating reverse water gas shift reaction catalyzed only by Pt^0, thus progressively decreasing H_2/CO ratio in products. Note that pretreatment in He leading to rather mild reduction of catalyst affects fast CO transients even stronger than reduction by CO or CH_4 (Fig. 7). Since high-temperature pretreatment in He not only removes oxygen from support and reduces Pt^{4+} cations to $Pt^{2+/1+}$ state, but also causes a pronounced dehydroxylation of the oxide as well, this suggests that, in agreement with hypothesis of Bradford and Vannice [20], hydroxyls could be involved in the reaction sequence of CH_4 dry reforming reacting with activated CH_x species at least in unsteady-state conditions. Though reduction by CH_4 not only removes the oxygen from fluorite-like oxide but also generates some coke precursors due to methane pyrolysis on Pt^0 sites [17], in studied experimental conditions transients after pretreatment by CO and CH_4 were identical. Hence, the coke precursors even if formed in these mild pretreatment conditions apparently do

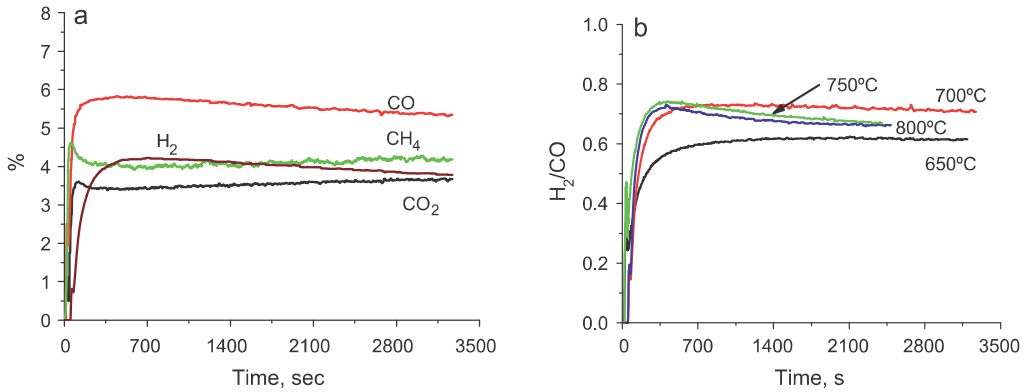

Fig. 5. Typical transients at contact of oxidized 4.9Pt/$Pr_{0.3}Ce_{0.35}Zr_{0.35}O_x$ catalyst with reaction feed at 700 °C (a) and respective variation of H_2/CO ratio in effluent with time-on-stream at different temperatures (b). 7% CH_4, CH_4/CO_2 = 1, contact time 15 ms.

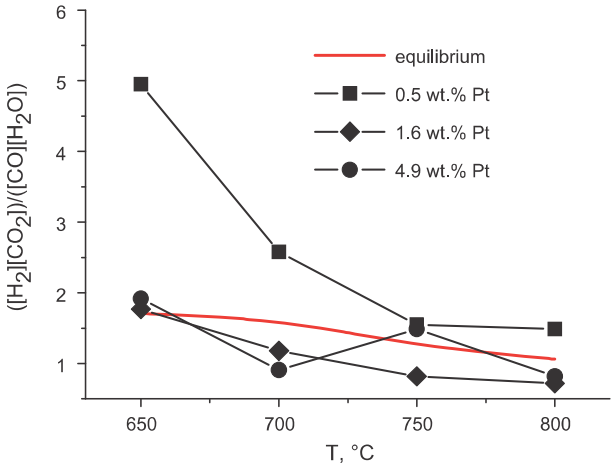

Fig. 6. Temperature dependence of reaction product for WGSR in the course of CH_4 dry reforming on Pt-supported Pr-Ce-Zr-O catalysts (points) and equilibrium constant (line).

not affect the surface steps. Note also that pretreatment by CO or CH_4 not only decreases initial conversions of reagents and concentration of products but also provides a faster deactivation of the catalyst. Hence, transfer of surface or bulk oxygen species from the oxide support to Pt/support interface apparently helps to stabilize highly active Pt cationic species. Hence, these experiments revealed that the most active and selective state of Pt/PrCeZrO catalyst is achieved after oxidizing pretreatment. So, to clarify the mechanistic aspects of CH_4 dry reforming on this catalyst, detailed transient studies have been carried out after oxidizing pretreatment of this sample with a broad variation of contact times and temperatures of experiments.

3.3. *Effect of temperature and contact time on transients*

Fig. 8 presents the transient data obtained at shorter contact times (higher feed rates) when the dead time effect of the system purging is minimized. These results in general agree with those obtained at lower temperatures and longer contact times (Fig. 7). Conversion of reagents, concentration of products and H_2/CO ratio

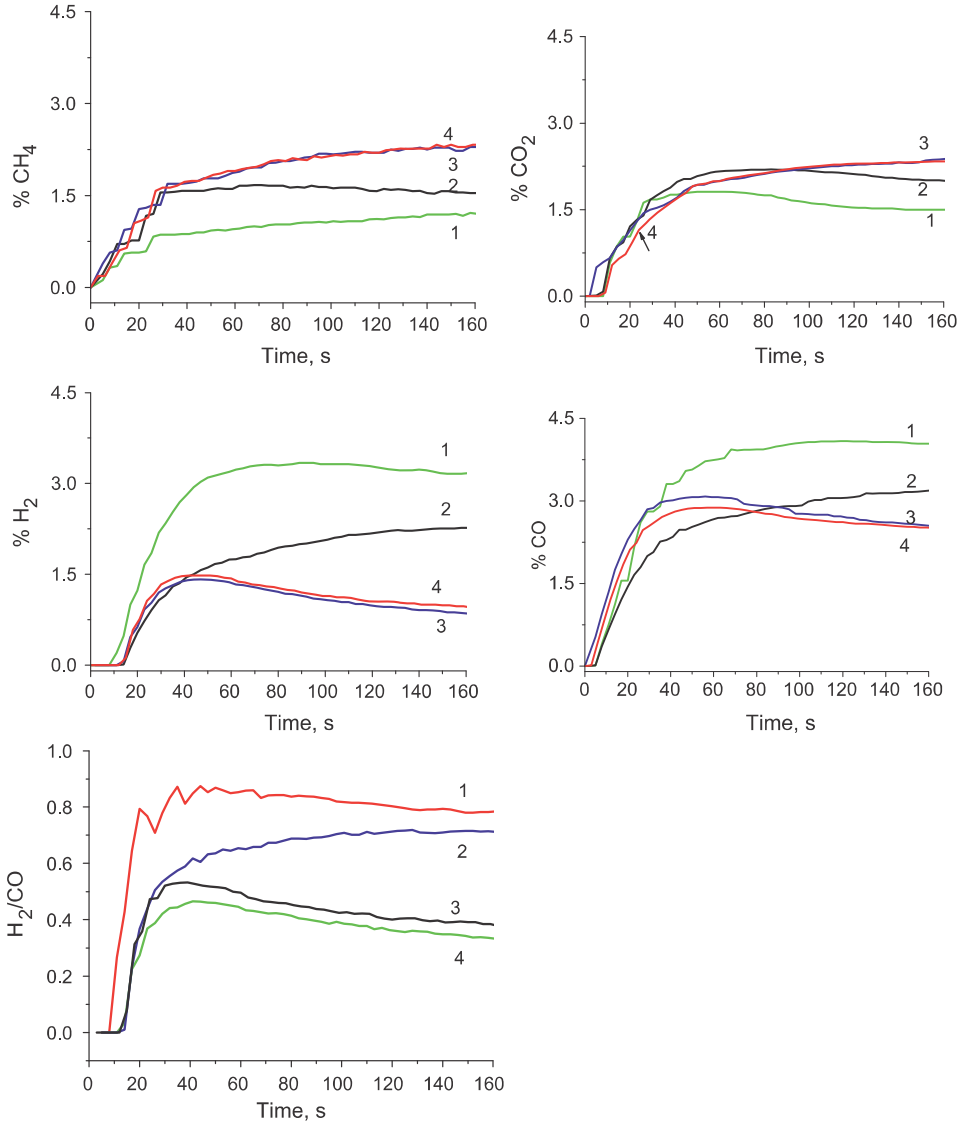

Fig. 7. Effect of pretreatment type (numbered 1–4 on curves) on reaction component transients observed for structured 1.6 wt.% $Pt/Pr_{0.3}Ce_{0.3}Zr_{0.35}O_{2-x}$ catalyst. Feed composition: 3.5% of methane at $CH_4/CO_2 = 1$, contact time 15 ms, $T = 650\,^{\circ}C$. Pretreatment conditions: 1 – pretreatment in O_2, 2 – pretreatment in He, 3 – pretreatment in 1%CO in He, 4 – pretreatment in 1% CH_4 in He; pretreatment time 60 min; temperature of pretreatment 900 °C (1, 2) or 500 °C (3, 4).

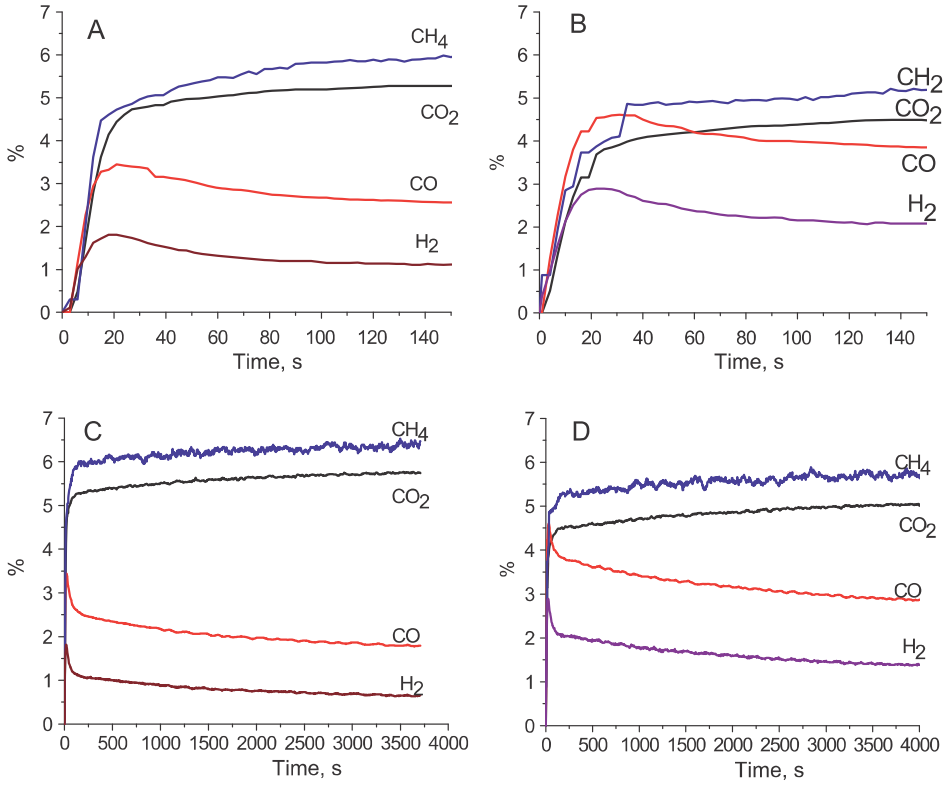

Fig. 8. Fast (A,B) and slow (C,D) parts of for oxidized structured 1.6 wt.% $Pt/Pr_{0.3}Ce_{0.3}Zr_{0.35}O_{2-x}$ catalyst after contact with feed 7% CH_4 + 7% CO_2 in He at 750 °C. Contact time 4.72 ms (A,C) and 8 ms (B,D).

increase with the contact time (Fig. 8). These transients were analyzed in details by applying mathematical modeling.

3.4. Modeling

The mathematical model and software were developed for numerical studying the transients of a complex catalytic reaction in the plug-flow reactor where a fragment with a single channel of the catalytic monolith is placed. The process model describes both the conversion of oxygen-containing species on the catalyst surface by reaction steps and the surface/near surface mobility of oxygen.

3.4.1. Kinetic scheme

The reaction scheme of methane dry reforming has been considered that includes the syngas formation by interaction of methane and CO_2 as well as the water-gas shift reaction. The rates of Boudouard reaction and CH_4 decomposition are assumed to be negligible, so coke formation in the time range considered here is not taken into account.

The analysis of experimental data given above shows that reaction steps on the catalyst surface could occur on the Pt centers as well as on the available active sites of CeO_2–ZrO_2 mixed oxide schematically presented in Fig. 9.

The kinetic scheme consisting of 6 catalytic stages has been considered. The catalytic stages have been selected on the basis of the analysis of experiments presented above as well as the literature data [2]. The scheme reflects the methane transformation on the active cationic Pt-centers, stabilization of Pt centers by the lattice oxygen, the interaction of carbon dioxide with oxidized Pt centers and surface oxygen vacancies of the catalyst layer, and the step providing RWGS reaction pathway:

$$\begin{aligned}
&1)\ CO_2 + [PtO] \leftrightarrow [PtCO_3]\\
&2)\ CH_4 + [PtCO_3] \rightarrow 2CO + 2H_2 + [PtO]\\
&3)\ CH_4 + [PtO] \rightarrow CO + 2H_2 + [Pt]\\
&4)\ [Pt] + [O_s] \leftrightarrow [PtO] + [V_s]\\
&5)\ CO_2 + [V_s] \rightarrow CO + [O_s]\\
&6)\ H_2 + [PtO] \rightarrow H_2O + [Pt]
\end{aligned} \qquad (1)$$

Here [PtO] and [Pt] denote the oxidized and vacant Pt-centers, $[PtCO_3]$ is the carbonate complex, $[O_s]$ and $[V_s]$ are the oxidized and vacant sites inside the lattice layer.

The following stoichiometric pathways correspond to this set of catalytic stages:

$$\begin{aligned}
&\text{I. } CH_4 + CO_2 \leftrightarrow 2CO + H_2\\
&\text{II. } CO_2 + H_2 \leftrightarrow CO + H_2O
\end{aligned} \qquad (2)$$

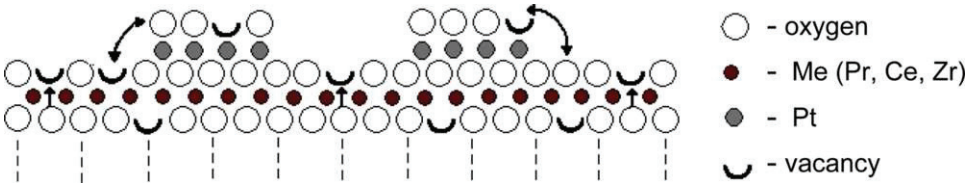

Fig. 9. Scheme of the near-surface layer of Pt/PrCeZrO catalyst.

According to the mass action law the rates of catalytic steps look as follows:

$$\begin{aligned} r_1 &= k_1 C_{CO_2}\theta_1, \qquad r_{-1} = k_{-1}\,\theta_2 \\ r_2 &= k_2 C_{CH_4}\theta_2 \\ r_3 &= k_3 C_{CH_4}\theta_1 \\ r_4 &= k_4(1-\theta_1-\theta_2)\theta_3, \qquad r_{-4} = k_{-4}\theta_1(1-\theta_3) \\ r_5 &= k_5 C_{CO_2}(1-\theta_3) \\ r_6 &= k_6 C_{H_2}\theta_1 \end{aligned} \tag{3}$$

where r_i is the rate of the ith catalytic stage (i = 1,2,. . ., 6); C_{CH_4}, C_{CO_2}, and C_{H_2} are the concentrations of H_4, CO_2 and H_2 in the gas mixture correspondingly; θ_1, θ_2, and θ_3 are the relative surface concentrations of oxidized Pt-centers [PtO], carbonate complexes [$PtCO_3$], and oxidized lattice layer sites [O_s] respectively; k_i is the rate constant of the ith catalytic stage (i = 1,2,. . ., 6).

It is assumed that the total number of active Pt-centers is equal to

$$[ZO] + [ZCO_3] + [Z] = \alpha N_\theta, \tag{4}$$

and the number of active lattice layer sites available for spillover is equal to

$$[ZO^*] + [Z^*] = \beta N_\theta \tag{5}$$

where N_θ is the total number of active centers on the catalyst surface, α is the relative surface concentration of Pt-centers, β is the ratio of the number of active lattice layer sites under the surface to the total number of active surface centers.

Since Pt^{4+} cations are easily transformed into Pt^{2+} even after catalyst purging by He at high temperatures after pretreatment in O_2, and reoxidation of Pt^{2+} cations to Pt^{4+} state by oxygen atoms migrating from support is apparently impossible under reaction conditions, Pt^{4+} cationic species revealed by XPS were not considered separately in suggested reaction scheme.

3.4.2. Mathematical model and numerical algorithm

The preliminary estimates of the intraparticle pore-diffusion resistance inside the catalyst fragment, the rates of axial diffusion and mass transfer between the catalyst channel wall and reacting gas mixture flow [33] showed that these processes do not influence significantly the rates of catalytic transformations. Therefore, the mathematical description includes the following equations:

- the first-order partial differential equations of the mass balance of the reagents and products in the gas phase (CO_2, CH_4, CO, and H_2) which reflect both the convective term due to the gas flow along the catalyst fragment length and the term related to the chemical transformations of the reactive mixture components on the catalyst surface at every cross-section of the channel,
- the second order parabolic type equation at each axial position describing the unsteady oxygen transport from the near surface layers of the catalyst lattice towards the active Pt-centers on the catalyst surface where the catalytic reaction proceeds (the diffusion mechanism is assumed),
- two ordinary differential equations describing the time behavior of the concentrations of oxidized Pt centers and carbonate complexes on the catalyst surface at each axial cross-section point; the dynamics depends on the local rates of catalytic transformations at the surface and of oxygen diffusion through the catalyst lattice.

Thus, the developed mathematical model is the initial-boundary value problem for a system of differential equations of different type.

The algorithm proposed bases on the second order finite-difference approximation with respect to two spatial coordinates (the length of the catalyst fragment, the distance between a point inside the catalyst lattice and the catalyst surface) and time. At each time step, the method of alternating directions is used to construct the numerical solution of the discrete approximation equations.

3.4.3. Modeling results

Using the software developed, a number of computational transient runs have been performed with the process parameters corresponded to the experimental response curves after reaction mixture feed on the catalyst pretreated in O_2 stream: gas feed rate u = 10.6 and 18 l h^{-1}, temperature T = 750 °C, inlet concentrations both of CH_4 and CO_2 are 7%, contact time τ = 4.7 and 8 ms.

It has been assumed that

(a) The total number of active centers on the catalyst surface is equal to maximal monolayer coverage $N_\theta = 1.28 \times 10^{15}$ at O/cm^2.
(b) Before reaction mixture feeding, at time t = 0, all active centers are oxidized, i.e., $\theta_1 = \theta_2 = 1$.

At first, the verification of the hypothesis about the kinetic scheme given above was carried out. For this purpose, the computational runs of transient regimes have been performed on the base of mathematical model with the simple redox kinetic scheme that includes only three steps: 3–5 of the kinetic scheme (1), the rates of the formation and conversion of carbonate intermediates and the step of RWGS reaction are assumed to be equal to zero. Modeling has revealed that this scheme does not describe the transients since in this case concentrations of CH_4 and CO_2 change contrariwise, while in the experiment they vary in parallel (Fig. 8). Hence, a route should exist providing an efficient CO_2 transformation on the oxidized surface.

Thus, modeling has been continued with overall kinetic scheme (1). The constants of catalytic stage rates and the parameters defining the rate of oxygen supply from the lattice to the surface have been varied during the computational runs:

- rate constants of catalytic steps k_1, k_{-1}, k_2, k_3, k_4, k_{-4}, k_5, and k_6;
- the coefficient D of bulk diffusion of oxygen;
- the depth H of the subsurface layer of the catalyst lattice available for oxygen mobility;
- the fraction α of the surface covered by Pt-centers;
- the fraction β of the surface with active lattice layer sites.

The initial approximation for all parameters of the model for processing has been estimated from the steady state experimental data and the data of XPS, FTIRS of adsorbed CO and oxygen isotope exchange [17,25,27,30]. Results of computations revealed that in studied conditions, the time of relaxation determined by achievement of catalyst steady state coverage by reactive species involved in catalytic cycle could not exceed few seconds, which agrees with analytic simple estimations following approach suggested by Temkin [34].

Analyzing the transient curves up to 300 s, it has been demonstrated convincingly that

- the character and shape of response curves is mainly defined by the rates of carbonates formation and consumption, the rates of "spillover," and the subsequent interaction of CO_2 with vacant centers of the catalyst oxide;
- the transient time period is determined by parameters characterizing the catalyst structure and the lattice oxygen mobility, such as the catalyst specific surface S_b, the quantity of active centers on the catalyst surface N_θ, the fractions of the surface Pt centers

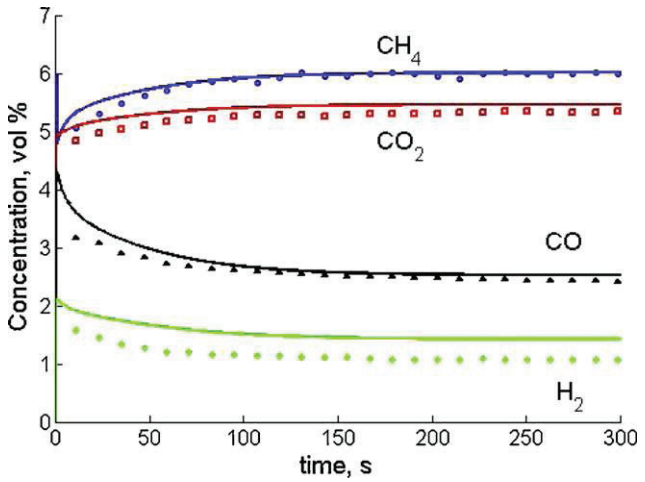

Fig. 10. Comparison of the experimental (points) and computed (lines) time dependences of concentrations in transient experiments 750 °C, gas feed rate 18 l h^{-1}, feed 7%CH_4 + 7%CO_2 in He, contact time 4.7 ms.

α and the lattice layer sites β, the rate and characteristic length of the oxygen bulk diffusion.

Data processing has allowed to evaluate the kinetic parameters and characteristics of the catalyst structure. Some examples of comparing modeling and experimental results are given in Fig. 10 for the following values of parameters: $\tau = 4.7$ s, $k_1 = 200\ s^{-1}$, $k_{-1} = 0.6\ s^{-1}$, $k_2 = 600\ s^{-1}$, $k_3 = 60\ s^{-1}$, $k_4 = 300\ s^{-1}$, $k_{-4} = 5\ s^{-1}$, $k_5 = 55\ s^{-1}$, $k_6 = 1100\ s^{-1}$, $\alpha = 0.04$, $\beta = 0.2$, $S_b = 20 \times 10^4\ cm^{-1}$, $D = 2.5 \times 10^{-13}\ cm^2/s$, $H = 5 \times 10^{-6}$ cm.

Fig. 10 demonstrates that the suggested kinetic scheme reflects the main peculiarities of the catalyst behavior rather well. The experimental values of gas concentrations and the modeling data are in a good agreement. Note that the key characteristics of the catalyst (the number of oxide surface active sites, Pt surface concentration, characteristic oxygen diffusion length) determined on the base of computational results agree with the values independently estimated by XPS, FTIRS of adsorbed CO methods, and oxygen isotope exchange data [17,18,25,27,30].

Fig. 11 shows the calculated values of relative surface concentrations of Pt centers occupied by oxygen and carbonates. After feeding the reaction mixture with CH_4 and CO_2 to the system the number of oxidized Pt sites decreases quickly because of high rates of CH_4

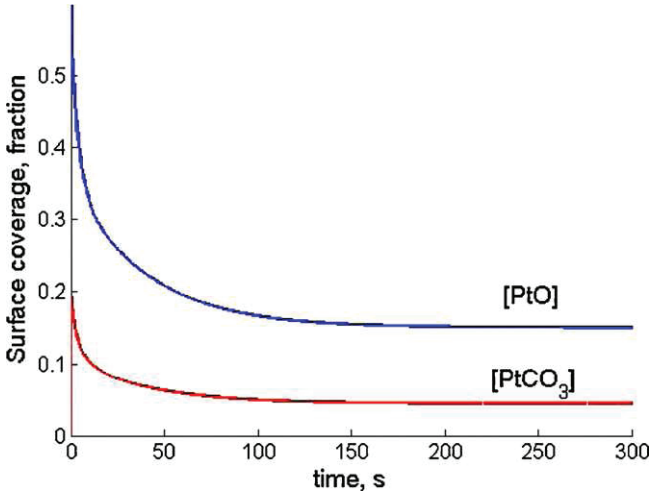

Fig. 11. Time dependence of the surface coverage fraction with intermediates [PtO] and [$PtCO_3$]. The operation conditions correspond to ones in Fig. 10.

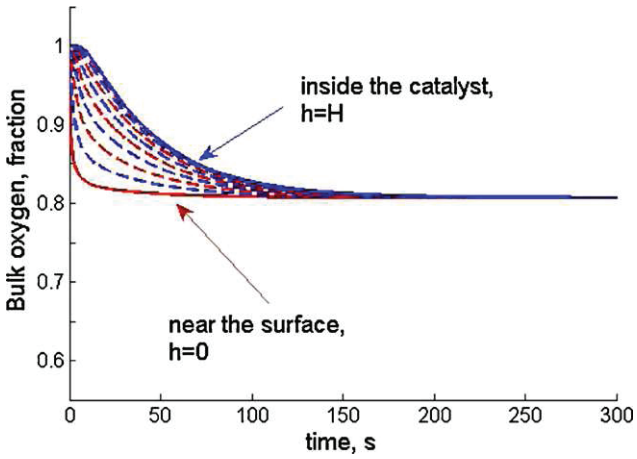

Fig. 12. Time dependence of the bulk oxygen fraction. The operation conditions correspond to ones in Fig. 10.

and CO_2 adsorption, so the surface coverage by carbonates has a sharp peak during a few seconds. Then, slow decline of these concentrations towards the steady values occurs due to stabilization of Pt centers by the oxygen of near-surface layers (Fig. 11). Similarly, concentration of bulk oxygen varies as well reaching the steady-state level within ~300 s (Fig. 12). Hence, it could be concluded that the transients caused by the catalyst reduction by reaction feed occur within ~300 s, stoichiometry of the bulk of oxide particles being affected. Longer (up to 3000 s) transients observed in our experimental conditions (Fig. 8) can be caused only by slower processes such as Pt aggregation (in general, decreasing Pt-support interface/interaction and ordering Pt clusters) and coke deposition. Since temperature-programmed oxidation by oxygen after reaction of this sample as well as TEM studies revealed no carbon deposition, Pt aggregation appears to be the main cause of slow transients. In fact, even syngas generation via route comprised of combination of steps (1) and (2) depends upon the metal-support interaction, since PtO in the absence of gas-phase oxygen can be regenerated only by oxygen migrating from the support (step 4), direct reoxidation of Pt sites by CO_2 being impossible. Apart from pure kinetic aspect, it is possible that carbonates can be stabilized only by Pt cations having as neighbors reducible cations of support such as Ce or Pr cations. Such Pt cations can be either incorporated into the surface position of support or situated at perimeter of Pt clusters. Decoration of the surface of Pt clusters by Pr or Ce oxidic species could also stabilize such carbonates coordinated to Pt cations as well.

Routes of dry reforming and RWGS corresponding to steps (3)–(6) involve also PtO sites which at present could not be reliably differentiated from those stabilizing carbonates due to lack of experimental data. So they are including in the balance of active Pt sites $[ZO] + [ZCO_3] + [Z] = \alpha N_\theta$, in Eq. (4).

Analysis of rates of CH_4 consumption by different mechanisms revealed that contribution of mechanism 1 (via carbonates) is considerably higher for the oxidized catalyst at the first seconds of contact with the reaction mixture, the ratio of step 2 and 3 rates being ~3. The decrease of the surface oxidation level results in lowering the fraction of Pt centers occupied by carbonates, and, as the result, the ratio of step rates 2 and 3 decreases to 1.6.

4. Conclusion

The combination of the steady state and transient experiments for CH_4 DR on structured Pt/PrCeZrO catalyst at millisecond contact times along with their modeling allowed to elucidate main factors responsible for the catalyst activity and performance stability. Both Pt-support interaction and lattice oxygen mobility in

the complex oxide support are responsible for the efficient performance of catalyst pretreated in O_2. Kinetic parameters of the reaction steps occurring on these catalysts were determined by processing the kinetic transients with a due regard for the oxygen species diffusion, participation of carbonate complexes stabilized in the coordination sphere of Pt cationic forms in CH_4 oxidative transformation and occurrence of reverse water gas shift reaction catalyzed by metallic Pt. Long (>3000 s) transients can be explained only by slow Pt aggregation and ordering of Pt clusters caused by complex oxide support reduction thus decreasing metal-support interaction.

Acknowledgements

This work was carried out in frames of Associated Russian–French Laboratory on Catalysis. Support by FP7 Project OCMOL, Interdisciplinary Integration Project no.107 of Siberian Branch of the Russian Academy of Sciences, RFBR–CNRS 09-03-93112 Project and Russian Federal Innovation Agency via the program "Scientific and Educational cadres" is gratefully acknowledged. The Embassy of France in Moscow is gratefully acknowledged for the joint PhD studentship grant of A. Bobin.

References

[1] F. Pompeo, N.N. Nichio, M.M.V.M. Souza, D.V. Cesar, O.A. Ferretti, M. Schmal, Appl. Catal. A 316 (2007) 175.
[2] A.M. O'Connor, Y. Schuurman, J.R.H. Ross, C. Mirodatos, Catal. Today 115 (2006) 191.
[3] J.T. Richardson, S.A. Paripatyadar, Appl. Catal. 61 (1990) 293.
[4] E. Ruckenstein, Y. Hang Hu, Appl. Catal. A 133 (1995) 149.
[5] J.R. Rostrup-Nielsen, L.J. Christiansen, Appl. Catal. A 126 (1995) 381.
[6] T. Osaki, T. Mori, J. Catal. 204 (2001) 89.
[7] S. Wang, G.Q. Lu, Appl. Catal. B 19 (1998) 267.
[8] J.M. Wei, B.Q. Xu, J.L. Li, Z.X. Cheng, Q.M. Zhu, Appl. Catal. A 196 (2000) L167.
[9] F.B. Norohna, E.C. Fendley, R.R. Soares, W.E. Alvarez, D.E. Resasco, Chem. Eng. J. 82 (2001) 21.
[10] Y. Denkwitz, A. Karpenko, V. Pizak, R. Leppelt, B. Schumacher, R.J. Behm, J. Catal. 246 (2007) 74.
[11] A. Pintar, J. Batista, S. Hocever, J. Colloid Interface Sci. 307 (2007) 145.
[12] L.F. Liotta, G. Di Carlo, G. Pantaleo, G. Deganello, Appl. Catal. B: Environ. 70 (2007) 314.
[13] J. Kašpar, P. Fornasiero, M. Graziani, Catal. Today 50 (1999) 285.
[14] S. Damyanova, B. Pawelec, K. Arishtirova, M.V. Martinez Huerta, J.L.G. Fierro, Appl. Catal. B: Environ. 89 (2009) 149.
[15] F.B. Passos, E.R. Oliveira, L.V. Mattos, F.B. Noronha, Catal. Today 101 (2005) 23.
[16] J. Kašpar, P. Fornasiero, in: A. Trovarelli (Ed.), Catalysis by Ceria and Related Materials, Imperial College Press, 2002, pp. 217–241.
[17] V.A. Sadykov, N.V. Mezentseva, G.M. Alikina, A.I. Lukashevich, Yu.V. Borchert, T.G. Kuznetsova, V.P. Ivanov, S.N. Trukhan, E.A. Paukshtis, V.S. Muzykantov, V.L. Kuznetsov, V.A. Rogov, J. Ross, E. Kemnitz, C. Mirodatos, Solid State Phenom. 128 (2007) 239.
[18] V. Sadykov, V. Muzykantov, A. Bobin, N. Mezentseva, G. Alikina, N. Sazonova, E. Sadovskaya, L. Gubanova, A. Lukashevich, C. Mirodatos, Catal. Today 157 (2010) 55.
[19] N.N. Sazonova, V.A. Sadykov, A.S. Bobin, S.A. Pokrovskaya, E.L. Gubanova, C. Mirodatos, React. Kinet. Catal. Lett. 98 (2009) 35.
[20] M.C.J. Bradford, M.A. Vannice, Appl. Catal. A: Gen. 142 (1996) 97.
[21] J. Wei, E. Iglesia, J. Catal. 224 (2004) 370.
[22] M. Maestri, D.G. Vlachos, A. Beretta, G. Groppi, E. Tronconi, J. Catal. 259 (2008) 211.
[23] E.L. Gubanova, A. Van Veen, C. Mirodatos, V.A. Sadykov, N.N. Sazonova, Russ. J. Gen. Chem. 78 (2008) 2191.
[24] V.A. Sadykov, T.G. Kuznetsova, G.M. Alikina, Yu.V. Frolova, A.I. Lukashevich, V.S. Muzykantov, V.A. Rogov, L.Ch. Batuev, V.V. Kriventsov, D.I. Kochubei, E.M. Moroz, D.A. Zyuzin, E.A. Paukshtis, E.B. Burgina, S.N. Trukhan, V.P. Ivanov, L.G. Pinaeva, Yu.A. Ivanova, V.G. Kostrovskii, S. Neophytides, E. Kemnitz, K. Scheurel, C. Mirodatos, in: D.K. McReynolds (Ed.), New Topics in Catalysis Research, Nova Science Publishers, NY, USA, 2007, pp. 97–196, Chapter 5.
[25] V. Sadykov, T. Kuznetsova, Yu. Frolova-Borchert, G. Alikina, A. Lukashevich, V. Rogov, V. Muzykantov, L. Pinaeva, E. Sadovskaya, Yu. Ivanova, E. Paukshtis, N. Mezentseva, L. Batuev, V. Parmon, S. Neophytides, E. Kemnitz, K. Scheurell, C. Mirodatos, A. van Veen, Catal. Today 117 (2006) 475.
[26] S. Bernal, J.J. Calvino, J.M. Gatica, C.L. Cartes, J.M. Pintado, in: A. Trovarelli (Ed.), Catalysis by Ceria and Related Materials, Imperial College Press, 2002, pp. 85–168.
[27] V. Sadykov, N. Mezentseva, V. Muzykantov, D. Efremov, E. Gubanova, N. Sazonova, A. Bobin, E. Paukshtis, A. Ishchenko, V. Voronin, J. Ross, C. Mirodatos, A. van Veen, Mater. Res. Soc. Symp. Proc. 1122 (2009) 1–6, 1122-O05-03.
[28] W. Yang, Y. Ma, J. Tang, X. Yang, Colloids Interface A: Phys Eng. Aspects 302 (2007) 628.
[29] Z. Yi, W. Wei, S. Lee, G. Jianhna, Catal. Commun. 8 (2007) 906.
[30] V. Sadykov, N. Mezentseva, G. Alikina, A. Lukashevich, V. Muzykantov, T. Kuznetsova, L. Batuev, M. Fedotov, E. Moroz, D. Zyuzin, V. Kolko, V. Kriventsov, V. Ivanov, A. Boronin, E. Pazhetnov, V. Zaikovskii, A. Ishchenko, V. Rogov, J. Ross, E. Kemnitz, Mater. Res. Soc. Symp. Proc. 988 (2007) 1–6, QQ06-04.
[31] N. Laosiripojana, S. Assabumrungrat, Appl. Catal. B: Environ. 60 (2005) 107.
[32] D. Wolf, M. Barré-Chassonnery, M. Höhenberger, A. van Veen, M. Baerns, Catal. Today 40 (1998) 147.
[33] N.N. Sazonova, S.N. Pavlova, S.A. Pokrovskaya, N.A. Chumakova, V.A. Sadykov, Chem. Eng. J. 154 (2009) 17.
[34] M.I. Temkin, Kinet. Catal. 17 (1976) 1095.

Catalysis Today 169 (2011) 125–137

Contents lists available at ScienceDirect

Catalysis Today

journal homepage: www.elsevier.com/locate/cattod

Partial oxidation of methane on Pt-supported lanthanide doped ceria–zirconia oxides: Effect of the surface/lattice oxygen mobility on catalytic performance

Vladislav A. Sadykov[a,b,*], Nathalia N. Sazonova[a], Aleksei S. Bobin[a,d], Vitalii S. Muzykantov[a], Elena L. Gubanova[a,c], Galina M. Alikina[a], Anton I. Lukashevich[a], Vladimir A. Rogov[a], Eugenia N. Ermakova[b], Ekaterina M. Sadovskaya[a], Nathalia V. Mezentseva[a], Ekaterina G. Zevak[b], Sergei A. Veniaminov[a], Martin Muhler[c], Claude Mirodatos[d], Yves Schuurman[d], Andre C. van Veen[c,d]

[a] Boreskov Institute of Catalysis SB RAS, Pr. Lavrentieva 5, Novosibirsk 630090, Russia
[b] Novosibirsk State University, Pirogova, 2, Novosibirsk 630090, Russia
[c] Lehrstuhl für Technische Chemie, Ruhr-Universität Bochum, Universitätsstraße 150, 44780 Bochum, Germany
[d] Institut de Recherches sur la catalyse et l'environnement de Lyon (IRCELYON), UMR 5256 (CNRS/Université Claude Bernard Lyon1), Université de Lyon – Université Claude Bernard Lyon1, 2 Avenue Albert Einstein, Villeurbanne Cedex 69626, France

ARTICLE INFO

Article history:
Received 19 July 2010
Received in revised form 25 October 2010
Accepted 27 October 2010
Available online 21 December 2010

Keywords:
Selective oxidation of CH_4
Syngas
Pt
Fluorite-like oxides
Oxygen mobility and reactivity
Oxygen isotope exchange
Transient studies
Mechanism

ABSTRACT

Partial oxidation of methane into syngas at short contact times (5–15 ms) was studied in both steady-state and transient modes at temperatures up to 850 °C in realistic feeds (CH_4 content up to 20%, $CH_4/O_2 = 2$) with a minimum impact of mass and heat transfer for structured catalysts carrying $Pt/Ln_{0.3}Ce_{0.35}Zr_{0.35}O_{2-y}$ (Ln = La, Pr, Gd) as thin layers on walls of corundum channel substrates. Oxygen mobility and reactivity of the active phase were characterized by oxygen isotope heteroexchange, temperature-programmed O_2 desorption and CH_4 reduction, isothermal pulse reduction by methane with wide variation of CH_4 concentrations and TAP pulse studies. Experimental data point towards a selective oxidation of methane into syngas via a direct route with oxygen-assisted methane activation. This mechanistic feature is related to the strong Pt-support interaction stabilizing highly dispersed oxidic Pt species less active in CH_4 and syngas combustion than metallic Pt clusters. Support activates O_2 molecules and supplies active oxygen species to Pt sites. A high rate of oxygen diffusion on the surface and in the bulk of the support and Pt-support oxygen spillover stabilizes Pt in a well dispersed partially oxidized state while preventing coking at high concentrations of CH_4 in the feed.

1. Introduction

Detailed studies on the mechanism of catalytic oxidations over oxide catalysts by Prof. Haber combined successfully the point of view of organic and solid state chemists (see, i.e. [1]). He stressed the importance of a reliable estimation of parameters related to the activation and transfer of oxygen on the surface and in the bulk of oxides and their interrelation with the real/defect structure of catalysts changing under the effect of the reaction media. On the other hand, activation and routes of transformation of organic molecules into deep or partial oxidation products strongly depend upon the state of the oxide catalysts surface controlling mobility and reactivity of oxygen species.

Catalytic partial oxidation of methane (CPOM) into syngas at short contact times using monolithic catalysts is now considered as promising alternative to the traditional steam reforming [2]. CPOM presents an interesting (though difficult to study) example of the above mentioned strong interrelation between the catalysts performance characteristics (activity and selectivity of CH_4 transformation into syngas) and surface oxygen mobility and reactivity. Recent research suggests that catalysts comprised of platinum supported on complex fluorite-like oxides Ce–Zr–Ln–O (Ln = Pr, Gd or La) favor the so called direct route of methane oxidation into syngas [3,4]. The direct pathway postulates the formation of H_2 and CO as primary products further oxidized into CO_2 and H_2O depending on process conditions (contact time, O/C ratios, etc.). The main evidence supporting the occurrence of the direct route is the observation of syngas at extremely short contact times in the presence of unreacted oxygen [3]. The question if the reaction mechanism depends on such factors as the mobility/reactivity of the surface/lattice oxygen is still a matter

* Corresponding author at: Boreskov Institute of Catalysis SB RAS, Pr. Lavrentieva 5, Novosibirsk 630090, Russia. Tel.: +7 383 3308763.
E-mail addresses: sadykov@catalysis.ru, vasadykov@mail.ru (V.A. Sadykov).

0920-5861/$ – see front matter © 2010 Elsevier B.V. All rights reserved.
doi:10.1016/j.cattod.2010.10.098

of debates [4]. At least, for Rh supported on α-alumina, which is an example of the oxide with very low (if any) oxygen mobility and reactivity, detailed CPOM studies at realistic feed composition by the group of Forzatti proved that syngas is formed via the indirect combustion-steam reforming route [5]. The latter is due to a faster oxidation of CO and H_2 than that of CH_4 on Rh in the inlet part of reactor where the gas phase oxygen is present. When however small Pt clusters are supported on an oxide with a high lattice oxygen mobility and moderate bonding strength, CH_4 is activated on Pt producing CH_x species while oxygen molecules are activated on the oxide sites. Interaction of CH_x fragments with oxygen species supplied to the Pt-support interface by the surface diffusion (reverse spillover) provides an efficient bifunctional route for the CH_4 transformation into syngas [6,7].

Some arguments in favor of the bifunctional scheme of methane partial oxidation can be obtained by comparing the specific rate of CPOM for catalysts with a comparable Pt dispersion but broadly varying surface/bulk oxygen mobility. This mobility can be estimated by dynamic methods either for the standard oxidized state of samples (oxygen isotope exchange, temperature-programmed oxygen desorption) or for their partially reduced state (H_2 or CH_4 TPR). However, for strengthening the bi-functional scheme, an estimation of the transfer rate of the oxygen-containing species between the Pt particles and the support in the course of catalytic reaction would be of crucial importance. This can be achieved using kinetic transients, where relaxation curves fitting allows to estimate the rate constants of corresponding steps [7–9].

However, papers devoted to the systematic estimation and analysis of the oxygen exchange parameters for a series of Pt-supported doped ceria–zirconia samples are still scarce [10,11].

One of the reasons for the limited knowledge on the active component structure – dispersion of supported Pt-oxygen mobility on and in the support – catalyst activity interrelationship is that short-contact-time and high-temperature reaction mechanisms are difficult to study. The method of studying the dynamics of product formation upon pulse feeding of the reagents at low pressure (Temporal Analysis of Products, TAP) seems to provide one of the most promising approaches for elucidation of mechanism [4,6]. This method allows assessing the effect of the oxidation level of a catalyst on its activity in the direct methane oxidation, which is a challenging problem in the case of fast reactions at atmospheric pressure. The TAP technique makes it possible to fix a certain oxidation level of a catalyst and then to test the reactivity of the latter by its exposure to small methane pulses which scarcely affect the surface. Since the quantities of reactants in a pulse are very small, the TAP technique allows evaluating the effect of the oxidation level of the surface without complicating thermal effects. Certainly, to verify the significance of mechanistic features of CPOM derived from TAP experiments for real-pressure processes, that data should be compared to steady-state characteristics of the catalyst activity and kinetic transients at ambient pressure [4]. To minimize the heat and mass transfer effects, supporting thin layers of active components either on the ceramic tube (annular reactor of Forzatti et al. [5]) or on walls of triangular channels cut from the corundum honeycomb substrates [12,13] was shown to be quite efficient approach for studies of POM reaction kinetic and mechanistic features in real feeds. Pulse studies at real concentrations of reagents, though strongly changing the surface oxygen coverage, could also be useful for estimating the rate of oxygen redistribution between the surface and subsurface layers [14,15], especially when combined with estimation of the heats of oxygen adsorption/methane oxidation or decomposition in a flow calorimeter [16,17].

This paper summarizes results of research aimed at elucidating effect of the surface/lattice oxygen mobility and reactivity for Pt-supported $Ln_{0.3}Ce_{0.35}Zr_{0.35}O_{2-y}$ (Ln = La, Pr, Gd) catalysts on their performance in POM at short contact times applying a complex of sophisticated kinetic methods. These catalysts containing 30 at.% of doping cation in ceria–zirconia solid solution were selected here due to close values of Pt dispersion combined with broadly varying surface oxygen mobility, which correlates with catalytic activity in POM in diluted feeds changing in the order La > Pr > Gd [11–13,18–24]. In this work the main attention is paid to elucidation and critical analysis of kinetic (especially, transient) features which might support or reject bifunctional scheme of POM mechanism with a due regard for the Pt-support interaction, oxygen transfer between Pt and surface sites/bulk of complex oxide supports and effect of realistic reaction feeds on the state of catalyst and its activity/syngas selectivity.

2. Experimental

2.1. Catalysts preparation

2.1.1. Powder catalysts

Samples were prepared according to the method yielding dispersed $Ln_x(Ce_{0.5}Zr_{0.5})_{1-x}O_2$ materials with Ln = La, Pr, or Gd content in the range of 5–30 at.% via a polymerized complex precursor route and successive calcinations at 500–900 °C for 4 h [4–6]. Pt (1.4 wt.%) was deposited from H_2PtCl_6 solutions by incipient wetness impregnation followed by drying and calcination at 700 °C for 2 h. Detailed characteristics of their structural and surface properties are given elsewhere [11,18–24].

2.1.2. Catalytic channels

A piece of a hollow thin-walled triangular prismatic corundum substrate (wall thickness 0.2 mm, inner triangle side 2.33 mm, length 10 mm) used in this work was cut from an α-Al_2O_3 honeycomb monolith annealed at 1300 °C (specific surface area 3 m^2/g). A layer of a $Ln_{0.3}Ce_{0.35}Zr_{0.35}O_{2-y}$ complex oxide was supported on this substrate by washcoating with the suspension made by ultrasonically dispersing the oxide powder in isopropanol with the addition of polyvinyl butyral. Several consecutive impregnations (typically 4) were required to attain the active component content of 7–10 wt.% (the porous layer thickness ca. 10 μm). After each impregnation, the samples were dried and calcined at 900 °C in air. Pt (1.4 wt.%) was supported by the incipient wetness impregnation with an H_2PtC_6 solution followed by drying and calcination at 900 °C in air.

2.2. Catalyst testing

CPOM tests were carried out in a plug-flow quartz reactor with the inner diameter of 6 mm. The space between the reactor walls and the catalyst channel was sealed up with α-Al_2O_3 fibers to provide the gas flow only through the channel. The catalyst was pretreated for 1 h in the flow of either O_2 at 700 °C (oxidizing pretreatment) or 30% H_2 in He at 900 °C (reducing pretreatment). The experiments were carried out at atmospheric pressure. The reaction mixture (7–20 vol.% CH_4, CH_4:O_2 = 2, N_2 balance) was fed in a flow rate range of 5.6–18.0 L/h corresponding to contact times of 4.7–15.0 ms as estimated from the flow rate and the volume of channel walls. The inlet and outlet temperatures of the catalyst channel were monitored during testing. Blank experiments with both the empty reactor and the reactor loaded with bare corundum substrate carrying no active component verified that homogeneous reactions did not occur under the studied conditions. The reagents and reaction products were analyzed with a quantitative analyzing gas chromatograph (Tsvet-500) as well as with calibrated on-line IR absorbance, electrochemical and polarographic gas sensors for

different components. In all the experiments, the carbon balance was close to 100 ± 5%.

Relaxation experiments at atmospheric pressure were performed in the same device in small quartz reactors. After preconditioning oxygen was flushed out with helium (control by the zero point of the oxygen sensor) and then helium was displaced with a required reaction mixture. The composition of the mixture was continuously analyzed by in-line gas sensors [4]. Control experiments with a single-channel fragment of the corundum carrier showed that, at gas flow rates of about 30 L/h, the purge time of the system during the concentration step up is no longer than 2–4 s.

2.3. Oxygen isotope heteroexchange

For powdered samples, experiments were carried out in the flow reactor using a SSITKA mode following earlier described procedures [10]. After achieving dynamic oxygen adsorption–desorption equilibrium at 500–700 °C, a flow of 1% $^{16}O_2$ in N_2 was switched for that of 1% $^{18}O_2$ in N_2, and concentrations of $^{16}O_2$, $^{16}O^{18}O$ and $^{18}O_2$ were monitored by the mass-spectrometer UGA 200 (Stanford Research Systems, USA).

For corundum channels with supported thin layer of Pr-doped active components, oxygen isotope exchange experiments were carried out in a closed reactor using a static installation (V = 680 cm^3) with on-line control of the gas phase isotope composition by QMS-200 (Stanford Research Systems, USA) mass-spectrometer both in the isothermal and the temperature-programmed mode (TPIE) (temperature ramp 5 K/min) in the temperature range 100–750 °C at $p(O_2)$ 1.5–4.5 Torr. The initial ^{18}O content in the gas phase was equal to 96%. Before experiments, samples were pretreated for 2 h under air at 650 °C for achieving a saturation of the solid phase with ^{16}O.

Parameters characterizing the rate of exchange, its mechanism and surface/bulk oxygen mobility were estimated from the data obtained in static or flow kinetic installations by using isotope-kinetic equations and analysis procedures described earlier in details [10,11,25,26].

2.4. Pulse studies

2.4.1. TAP experiments

The capability of the fully oxidized catalyst to react with methane was evaluated using the TAP system (TAP-1 reactor upgraded with a Stanford Research Systems, SRS RGA300 quadrupole mass spectrometer). The reactor was loaded with 20 mg of the powdered sample, evacuated and fed with a constant flow of 10% O_2 in Ne for reaching almost atmospheric pressure with closed high pressure assembly. Full oxidation of the catalyst and removal of hydrocarbon residuals was achieved by heating at 800 °C for 30 min in the flowing O_2/Ne mixture and successive cooling to 250 °C where the reactor was evacuated. Pulse experiments were conducted by stepwise increasing of the sample temperature and admission of a 25% CH_4 in Ar mixture with a pulse size of 2×10^{15} molecules per pulse. Pulse responses were recorded at characteristic masses of amu 2 (H_2), 15 (CH_4), 18 (H_2O), 28 (CO), 40 (Ar) and 44 (CO_2). Preliminary experiments revealed that the oxidized state of the catalyst could be preserved until a temperature of 525 °C before the thermal desorption of oxygen leads to a significant change of the catalyst. For quantitative analysis, the mass spectrometer was calibrated by reference experiments using the same experimental procedure over an inert quartz bed.

The TAP experiments were simulated with a one dimensional pseudo homogeneous model accounting for 3 zones (inert/active/inert) and temperature gradients in the inert sections. Calculations were performed by simultaneously solving the partial differential equations, denoting for the time (t) and space (z) dependency of concentration (c) and coverage (θ), with a FORTRAN program based on the method of lines. Assuming a non-reversible molecular Langmuir adsorption, the processes in the active zone are described by the partial differential equations for the gas phase oxygen (Eq. (1)) and adsorbed (Eq. (2)) species, respectively:

$$\frac{\partial c}{\partial t} = D_{\text{eff}} \cdot \frac{\partial^2 c}{\partial z^2} - \rho_S \cdot k_0 \cdot \exp\left(-\frac{E_a}{R \cdot T}\right) \cdot c \cdot (1-\theta) \quad (1)$$

$$\frac{\partial \theta}{\partial t} = k_0 \cdot \exp\left(-\frac{E_a}{R \cdot T}\right) \cdot c \cdot (1-\theta) \quad (2)$$

The kinetic parameters, site density ρ_s, frequency factor k_0 and activation energy E_a, were determined by their variation until the best possible fit between model prediction and experimental result had been achieved.

2.4.2. Ambient pressure pulse experiments

Pulse experiments were carried out using a Setaram Sensys DSC TG calorimeter and a pulse kinetic installation. The reagents and products concentrations were determined by a gas chromatograph "Chromos GH-1000". Sample 1.4% Pt/$Pr_{0.3}Ce_{0.35}Zr_{0.35}O_2$ (93 mg) was pretreated in the flow of 5% O_2 in He at 700 °C for 0.5 h and then in He for 0.5 h at the same temperature with subsequent cooling down in the He flow (flow rate 40 mL/min) to the temperature of experiments. Sample was reduced by pulses of 2% CO/He or 7% CH_4 in He (pulse volume 1–5 mL, time interval between pulses 15 min) removing several monolayers of oxygen.

2.5. Oxygen mobility/reactivity by temperature-programmed experiments

Experiments for temperature-programmed oxygen desorption in the flow of He (TPD O_2) and reduction of samples by CH_4 (1% CH_4 in He feed) were carried out in a flow installations equipped with quartz reactors, GC and PEM-2M gas analyzers under the temperature ramp of 5 °/min up to 880 °C with the isothermal plateau at 880 °C for 70 min [21,22].

3. Results and discussion

3.1. Steady-state catalytic activity in POM

Fig. 1 presents main characteristics of catalytic activity of corundum channels with supported active components. In all experiments, oxygen was completely consumed within the channel. For studied catalysts, CH_4 conversions at different contact times were satisfactorily fitted by the apparent first-order rate equation for the plug-flow reactor [13]. This implies that in studied experimental conditions variation of the gas-phase oxygen concentration profile with the superficial velocity has a weak impact on the rate constant of CH_4 transformation. Hence, in the first approximation, complete conversion of oxygen within channels does not obscure the difference between the intrinsic characteristics of catalytic activity of various active components supported on walls of corundum channels. This conclusion is also supported by the values of CH_4 conversion at short contact times being much lower than the equilibrium values (>90% at T > 700 °C) [12] as well as by a low (<30 °C) temperature gradient along the channel even for feed containing 20% CH_4. Reasonably high (~50 kJ/mol) activation energy of CH_4 consumption for Pr-containing catalysts possessing the highest activity at enhanced temperatures agrees with conclusion about negligible effect of heat and mass transfer on the catalyst performance in studied experimental conditions [12,13].

As follows from Fig. 1, at the lowest temperature range studied here the most active and selective is sample doped by La. This

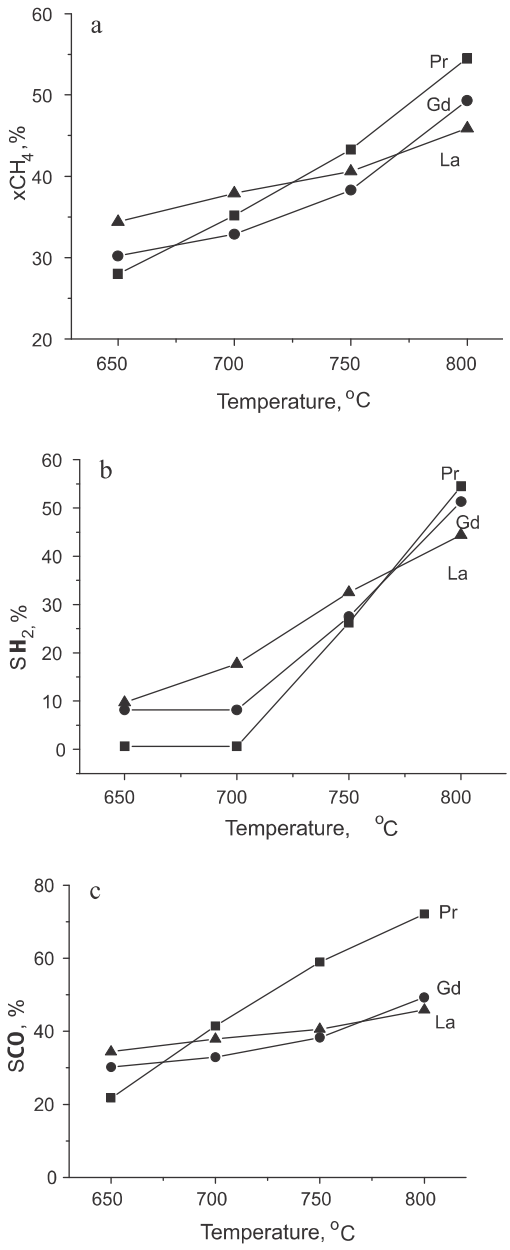

Fig. 1. Temperature dependence of CH_4 conversion (a), SH_2 (b) and SCO (c) for channels with Pt-supported supported ceria–zirconia oxides doped by Pr, Gd or La. Contact time 4.72 ms, feed 7% CH_4 + 3.5% O_2 in He.

agrees with results of experiments with diluted feeds carried out for powdered samples of Pt-supported doped ceria–zirconia solid solutions, where POM activity was shown to correlate with Pt dispersion and the surface oxygen mobility [24]. For La-doped sample, analysis of results of SSITKA experiments allowed to explain a high surface oxygen mobility by defects generated due to incorporation of Pt cations into the surface layer [10].

At highest temperatures, the most active and selective sample contains Pr as doping cation (Fig. 1). Analysis of oxygen isotope heteroexchange data for Pr-doped sample in a closed reactor revealed that indeed for this sample the oxygen bulk diffusion coefficient greatly exceeds that for La-doped sample [11]. Hence, at high temperatures, catalytic activity of Pt-supported doped ceria–zirconia catalysts appears to correlate with the lattice oxygen mobility. To verify this conclusion, the oxygen mobility in Pr-doped catalysts was studied in more details.

3.2. Oxygen isotope exchange

3.2.1. SSITKA

Fig. 2 presents data on the isotope fractions $\alpha_g(t)$ and $f_{34}(t)$ vs. time on stream as measured in SSITKA experiments over both $Pr_{0.3}Ce_{0.35}Zr_{0.35}O_2$ (Fig. 2a) and $Pt/Pr_{0.3}Ce_{0.35}Zr_{0.35}O_2$ (Fig. 2b) samples at 600 °C. Similar results were obtained at 500 and 700 °C.

The quantity of exchangeable oxygen in both samples as estimated from the difference in concentrations of labeled oxygen atoms at the reactor inlet and outlet ($N_O = (2C_{O_2}U/\alpha_g^{input}) \int_0^{t_{end}} (\alpha_g^{input} - \alpha_g)dt$) remains practically unchanged as the temperature rises and lies around 7×10^{21} at/g. This value is close to the stoichiometric content of oxygen in sample. Hence, in the course of isotope exchange, practically all ^{16}O in the sample was replaced by ^{18}O. As follows from this figure, Pt supporting increases the rate of oxygen exchange.

Numerical analysis of the dynamics of isotope transients carried out in frames of model [10] revealed that:

- The distribution of oxygen isotopes observed in these experiments corresponds to the mechanism of exchange with participation of two surface oxygen atoms denoted as K_3 [11,25] (cf. fitting by K_2 and K_3 mechanisms shown in Fig. 2).
- At temperatures below 600 °C, for both samples the rate of the lattice oxygen exchange is limited by the rate of the surface exchange. Rather fast oxygen diffusion provides a uniform distribution of labeled oxygen atoms in the bulk of oxide particles. Starting from 700 °C, the isotope exchange of oxygen in the bulk of oxide is controlled by the diffusion, which is the most clearly manifested for Pt-supported sample.

By fitting experimental curves, parameters of exchange model [10] were estimated (Table 1). Modeling results demonstrated that, similar to the majority of oxides, the mechanism of exchange involves interaction of O_2 molecule with two surface oxygen atoms, thus including the stage of O_2 dissociation [11,24,25]. The increase of the rate of exchange for Pt-supported sample is apparently caused by a fast O_2 dissociation on Pt followed by spillover of oxygen atoms to the oxide surface. Assuming that activity of oxide centers in the oxygen exchange is not changed due to Pt supporting ($R_{\text{oxide Pt/CeZrPrO}} = R_{\text{oxide CeZrPrO}} = K_{3\ \text{CeZrPrO}}$), the rate of exchange on Pt sites can be estimated:

$$R_{Pt} = \frac{(K_3 - R_{oxide})SL}{N_{Pt}}$$

Here N_{Pt} is the number of surface Pt atoms estimated to be ~10% of the total number of Pt atoms in sample [10,20–24]. Estimated values of R_{Pt} (Table 1) exceed those for oxide centers by two orders of magnitude despite good description of transients by the model of exchange on the uniform surface. This means that due to fast spillover and surface diffusion, labeled oxygen atoms are uniformly distributed on the surface of $Pt/CeZrPrO_x$. Apparently, to provide this result, the rate of spillover R_{sp} should substantially exceed the rate of exchange on Pt R_{Pt}. According to our estimation $R_{SPILL} \geq 2.5R_{Pt}$ (Table 1)

3.2.1.1. The mechanism of bulk oxygen diffusion. By taking the average particle radius $r = 3V/S = 6 \times 10^{-8}$ m (V – volume, S – specific surface area) as characteristic diffusion length, the bulk diffusion coefficient D is estimated to be $\approx 10^{-16}$ m^2/s. This value exceeds by several orders of magnitude known values for diffusion coefficients for ceria–zirconia oxides [26]. Such a phenomenon can be explained by specific structural features of studied nanocrystalline sample, namely, developed domain boundaries providing fast oxygen transfer from the surface of particle to the surface of domains

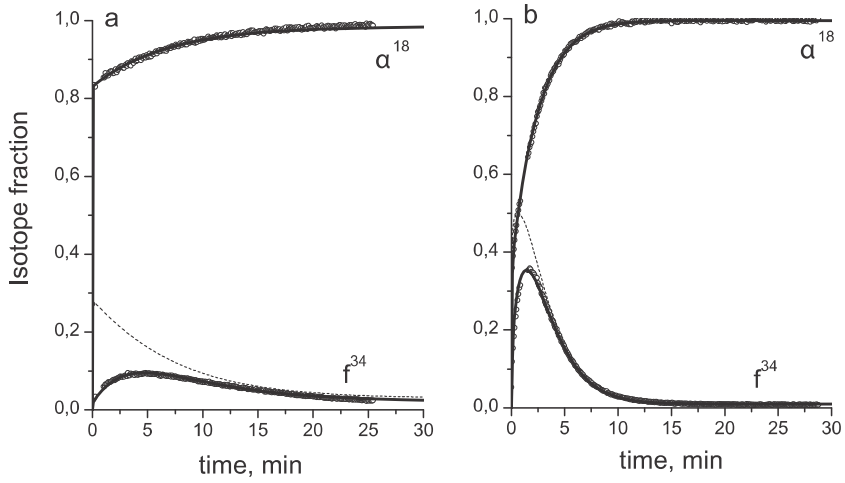

Fig. 2. Atomic fraction of ^{18}O in the gas phase (α) and fraction of $^{16}O^{18}O$ molecules (x_1) versus time of exchange for $Pr_{0.3}Ce_{0.35}Zr_{0.35}O_2$ (a) and 1.4% $Pt/Pr_{0.3}Ce_{0.35}Zr_{0.35}O_2$ samples (b). 600 °C, feed rate 300 mL/min, weight 0.05 g. Points – experiment, lines – fitting (dashed line by K_2 mechanism, solid line by K_3 mechanism).

[10,18–22]. Hence, dynamics of the isotope transfer into the bulk of oxide is controlled by the combination of two processes:

(a) by the surface diffusion of oxygen atoms along domains boundaries;
(b) by diffusion of oxygen atoms within the bulk of domains, their size determining diffusion length in this case.

According to structural data [20–24], the typical thickness of platelet-like domains in these samples is ca. 20 nm, so characteristic length $h \approx 10 \times 10^{-9}$ m. This allows to estimate the coefficients of oxygen diffusion in oxide domains D_{oxide} and along domain boundaries D_{mobile} from the effective coefficient of oxygen diffusion D_{eff} (Table 1):

$$D_{oxide} = D_{eff} \times h^2$$

$$D_{oxide} \geq D_{eff} \times r^2 \left(\frac{N_O}{N_{Omobil}}\right)$$

where N_{Omobil} is the number of oxygen atoms located within domain boundaries estimated to be ~5% of the total number of oxygen atoms in sample N_O. Estimated values of D_{oxide} and D_{mobile} for Pt/PrCeZrO sample are given in Table 1 along with parameters of oxygen exchange for Pt/LaCeZrO sample possessing the highest oxygen mobility for all series of La-doped samples [10]. While the constants of surface steps are close for both samples, the diffusion characteristics differ strongly. The rate of diffusion for La-doped sample was found to sharply decline with the particle depth due to specific structure and composition of the surface layers affected both by La and Ce surface segregation and Pt cations incorporation [20–24]. For Pr-doped sample, this phenomenon was not observed. Coefficients of oxygen diffusion within domains and along domain boundaries for this sample are higher than those for La-doped sample for 1 and 2 orders of magnitude, respectively.

Hence, results of SSITKA experiments confirm that Pr-doped sample indeed possesses much higher bulk oxygen mobility than La-doped sample, which agrees with its higher catalytic activity in the high-temperature range.

Since these results were obtained for powdered samples, oxygen isotope exchange in closed reactor has been carried out to verify that supporting active component on walls of corundum channel has not affected oxygen mobility.

3.2.2. *Oxygen isotope exchange for corundum channel with supported Pt/PrCeZrO$_x$ active component*

Fig. 3 shows typical results of oxygen isotope heteroexchange in closed reactor in the temperature-programmed (dynamic) mode. The depth of isotope penetration from the gas phase into the oxide in the course of TPIE can be characterized by the value N_X determined from the relation $2N\alpha^0 + N_X\alpha_S^0 = \alpha(2N + N_X)$. Here N is the number of O_2 molecules, N_X – number of oxygen atoms in solid, α^0 and α_S^0 – initial isotope fraction in the gas phase and solid, respectively.

Table 1
Parameters of oxygen exchange from SSITKA experiments.

T (°C)	Surface				Volume		
	K_3 (s^{-1})				D_{eff} (s^{-1})	D_{oxide} ($m^2\ s^{-1}$) × 10^{18}	D_{mobile} ($m^2\ s^{-1}$) × 10^{16}
	$Pr_{0.3}Ce_{0.35}Zr_{0.35}O_2$						
600	0.17				>0.02	>2	>14
700	0.25				>0.02	>2	>14
	1.4% $Pt/Pr_{0.3}Ce_{0.35}Zr_{0.35}O_2$						
	K_3 (s^{-1})	R_{oxide} (s^{-1})	R_{Pt} (s^{-1})	R_{sp} (s^{-1})			
400	0.02				>0.001	>0.1	>0.1
500	0.22				>0.01	>1	>8
600	0.5	0.17	11	≥30	>0.025	>2.5	>20
700	1	0.25	25	≥60	0.04	4	>33
	1.4% $Pt/La_{0.2}Ce_{0.4}Zr_{0.4}O_2$						
650	0.6	0.3	10	≥100	Bulk 0.004	0.4	0.45
					Sub. surf 0.04		0.7

Values of R_{Pt} and R_{sp} as calculated per Pt atom.

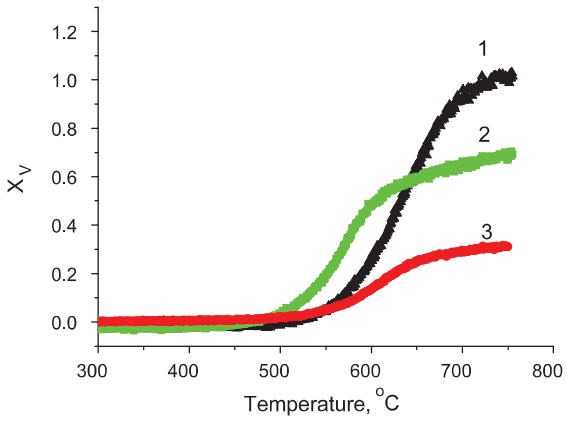

Fig. 3. Temperature dependence of the dynamic degree of exchange X_V for layers of $Pr_{0.3}Ce_{0.35}Zr_{0.35}O_x$ (1), $Pt/Pr_{0.3}Ce_{0.35}Zr_{0.35}O_x$ (2 and 3) supported on the walls of corundum channels. (1 and 2) Fresh samples, and (3) after testing in POM. PO_2 1.7–1.8 Torr.

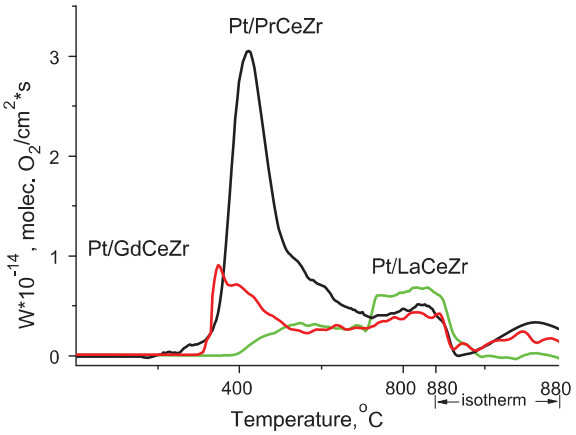

Fig. 4. O_2 TPD spectra for Pt/Ln–Ce–Zr–O samples calcined at 900 °C. Pretreatment in O_2 at 700 °C for 1 h.

The value $\mathbf{N_X}$ is related to the average depth of isotope incorporation into the solid phase ($\mathbf{l_\alpha}$) by relation $\mathbf{N_X = n_O \times S \times l_\alpha}$ (here $\mathbf{n_O}$ is the number of oxygen atoms in the unit volume of oxide). This quantity termed as "dynamic extent of isotope exchange" [18,24] is expressed here in relative units $X_V = (N_X/N_V)$, corresponding to the exchanged fraction of the bulk oxygen.

In agreement with SSITKA data for powdered samples, for Pr-doped ceria–zirconia oxide supported as a thin layer on corundum channel walls, all lattice oxygen is rather fast equilibrated with the gas-phase O_2. Pt supporting accelerates oxygen exchange at lower temperatures which is explained by a higher rate of exchange on Pt sites (vide supra). However, a slower increase of X_V at higher temperatures for Pt-promoted sample is not expected and could be explained by some variation of complex oxide properties caused by impregnation with acid H_2PtCl_6 solution, perhaps, caused by some leaching of aluminum cations from the corundum substrate. Even stronger and clearly negative effect is caused by catalyst testing in POM at high temperatures: both surface reaction and bulk oxygen diffusion are hampered. This is apparently caused by reduction of cationic forms of Pt incorporated into the surface layer of oxide followed by Pt aggregation. Subsequent reoxidation before oxygen exchange experiments apparently does not provide complete Pt redispersion.

Similar features as related to Pt supporting and reaction feed effect were observed in the isothermal exchange experiments (Table 2).

Hence, oxygen isotope heteroexchange experiments with catalytic channel demonstrated pronounced and irreversible reaction media effect on the oxygen mobility in Pt-supported catalysts. This effect might be much more pronounced for La-doped sample, which, along with a low bulk oxygen mobility, could explain its lowest activity at high temperatures.

3.3. Temperature-programmed O_2 desorption

Typical O_2 TPD spectra for samples pretreated in oxygen at 500 °C are shown in Fig. 4. The total amount of oxygen desorbed in TPD run varies from 14% monolayer (Pr) to 5–6% monolayer (Gd, La), thus corresponding only to a very small part of the total oxygen content in samples. Oxygen desorption from doped ceria–zirconia oxides without supported Pt starts in the same temperature range [22], hence, easily desorbed surface oxygen forms are bound not only with Pt cations but also with some surface defects on the surface of oxide particles as well. Moreover, oxygen desorption is accompanied by the oxygen diffusion along domain boundaries to the surface. With a due regard for the ^{18}O SSITKA data (vide supra), nearly all oxygen desorbed in TPD run can originate from domain boundaries. Indeed, a higher rate of oxygen desorption at ~400 °C from Pt/PrCeZr sample as compared with that for Pt/LaCeZr (Fig. 4) correlates with a higher coefficient of oxygen diffusion along domain boundaries for the former catalyst (Table 1).

3.4. Temperature-programmed reduction by CH_4

In these experiments, all reducible Me^{4+} cations (Ce^{4+}, Pr^{4+}) are reduced to Me^{3+} state after keeping under contact with CH_4 stream at 880 °C [22], which corresponds to removal ~10 monolayers of oxygen. Hence, reduction process is clearly associated with rapid oxygen diffusion from the bulk of oxide support particles to their surface where it is consumed by interaction with CH_x species generated by dissociation of CH_4 molecules on Pt sites. Such a dissociation continues at high temperatures even after nearly complete reduction of samples when CO_x evolution is practically not observed (Fig. 5).

The parallel evolution of CO, CO_2 and H_2 at ~400 °C (Fig. 5) for all oxidized samples demonstrates ability of these systems selectively transform CH_4 into syngas. The intensity of these low-temperature peaks clearly correlates with the surface/near-surface

Table 2
Oxygen isothermal exchange in a closed reactor for channels.

Sample	T (°C)	lg R, O_2 c^{-2} M^{-2}	E_a of heteroexchange (kJ/mol)	X_V^∞
$PrCeZrO_x$	650	17.0	110	0.54
	550	16.3		0.52
	500	15.8		0.56
$Pt/PrCeZrO_x$	650	17.2	90	0.42
	550	16.6		0.39
$Pt/PrCeZrO_x$ discharged from POM reactor	650	17.0	130	0.20
	600	16.6		0.22
	550	16.1		0.21

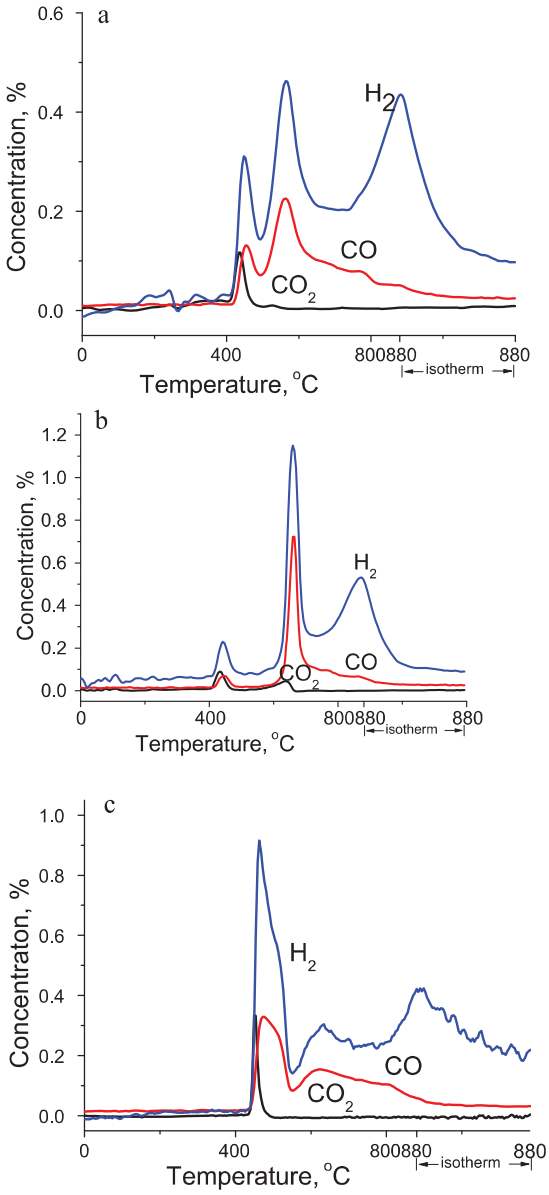

Fig. 5. CH_4 TPR spectra for Pt-supported ceria–zirconia oxides doped by Pr (a), Gd (b) or La (c).

oxygen mobility characterized by X_S (La > Pr > Gd) [11,18,24] and activity in both diluted feed [11] and concentrated feed (Fig. 1) at ~700 °C.

For Pr-doped sample the second peak of syngas evolution apparently controlled by the lattice oxygen diffusion and reactivity of strongly bound surface oxygen forms is situated at the lowest temperature (~550 °C) among studied samples. This apparently correlates with the highest catalytic activity of Pt/PrCeZrO in the high-temperature region in concentrated feeds (Fig. 1).

3.5. TAP

Quantitative exploitation of the recorded pulse responses indicated that for Pt/PrCeZrO sample a methane uptake occurs at temperatures higher than 360 °C, which agrees well with results of CH_4 TPR (Fig. 5). It is important to note that there is no pulse broadening at lower temperatures, which would be expected when methane could adsorb. Hence, it can be concluded that methane reacts as soon as it adsorbs. Furthermore, the oxidized state of the catalyst is crucial to activate methane as highlighted by the fact that catalyst pretreated at 800 °C in vacuum or reduced by hydrogen does not significantly activate methane in the temperature range between 360 and 525 °C. Most likely the methane activation over the fully oxidized catalyst proceeds according to an oxygen-assisted mechanism.

The result of the parameter estimation according to the simple model of irreversible molecular Langmuir adsorption for Pt/PrCeZrO sample can be summarized as follows:

site density $\rho_s = 3.4$ mol/m^3_{cat};
frequency factor $k = 68.6\ s^{-1}$ at 923 K;
activation energy $E_a = 65.9$ kJ mol^{-1}.

The activation energy of POM for this sample in real feeds (ca. 50 kJ/mol [13]) is rather close for that of CH_4 irreversible adsorption. This suggests that the stage of activated CH_4 adsorption is rate-limiting.

It should be noted that the match of the simulated and the experimental responses decreases at temperatures higher than 686 K. In parallel, first responses for CO_2 were recorded above this temperature. Obviously, a model accounting for the conversion of adsorbed methane could lead to a more suitable description of the methane responses. On the other hand, CO_2 responses were broad and had a low peak intensity thus requiring additional experimental efforts in order to reach a signal quality sufficient for further parameter estimation.

The performance of the fully oxidized Pt/PrCeZrO_x catalyst at 670 °C was established by pulse experiments supplying a 25% CH_4 in Ar mixture. However, at this temperature oxygen desorbs from the catalyst (see Fig. 4) and is only partially resupplied from the bulk of PrCeZrO_x particles. Hence, the availability of the most reactive oxygen species on the surface decreases with time. This decline in the oxygen surface concentration is clearly reflected by the increasing intensity of CH_4 pulse responses with time, i.e. a lowering of the CH_4 conversions reflected in the responses from the back to the foreground. Obviously, the CH_4 activation is oxygen assisted given the higher conversions are achieved at a higher degree of oxidation. Focusing on the responses for the products CO_2 and CO, with the latter being obtained from the responses at amu 28 and subtraction of the contribution of CO_2 on this amu, it comes clear that CO is a primary product with very sharp responses, while CO_2 as secondary product shows much broader pulse responses. Furthermore, CO_2 has a maximum yield at a high degree of oxidation, while the maximum yield of CO is only achieved after some oxygen was removed from the catalyst surface by desorption. These findings are indeed perfectly in line with the above mentioned assignment of CO being the primary product of the CH_4 partial oxidation and CO_2 being then formed from CO by over-oxidation.

3.6. Pulse reduction experiments at realistic CH_4 concentrations

In general, variation of CH_4 conversion and CO/CO_2 selectivity with the pulse number (degree of sample reduction) observed in these experiments (Fig. 7) reasonably agrees with that for TAP data (Fig. 6). The CO formation even for the first pulse of CH_4 supplied to the oxidized sample surface supports hypothesis about a primary route of syngas formation via a CH_4 pyrolysis-partial oxidation route. Rather high degrees of CH_4 conversion after removal from the sample ~ monolayer of oxygen clearly demonstrate a high rate of oxygen diffusion from the bulk of oxide particle to the surface. The average heat of oxygen adsorption on partially reduced surface (~600 kJ/mol O_2, Fig. 8) is close to values corresponding to bonding strength of bridging (M_2O) oxygen forms located at Ce cations [27]. Its weak variation with the reduction degree can be explained by dynamic equilibrium between on-top (terminal) M–O oxygen

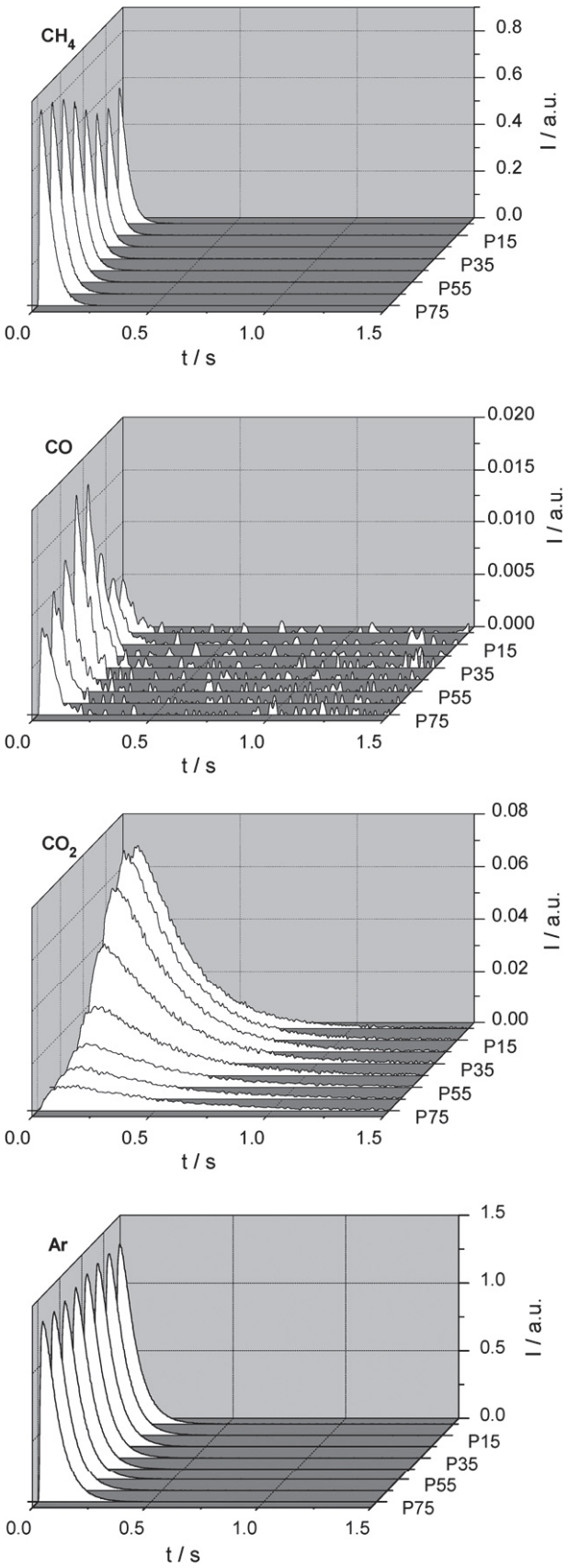

Fig. 6. Three-dimensional representations (intensity–time–pulse number) of the pulse responses for CH_4, CO_2, CO and Ar (reference gas) at 670 °C after oxidizing pretreatment.

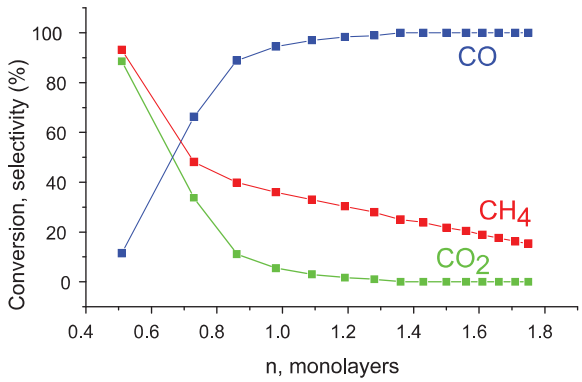

Fig. 7. Dependence of CH_4 conversion, CO and CO_2 selectivity on the degree of Pt/PrCeZrO sample reduction (n) by pulses of 7% CH_4 in He at 600 °C.

forms (average heats of adsorption for ceria–zirconia solid solutions ~300–500 kJ/mol O_2 [27]) supplied to the surface by diffusion from the bulk of particles and bridging M_2O oxygen forms as considered within the frames of so called partially flexible model of the surface [28]. The main point of this model is that reduction of oxide sample via removal of bridging oxygen forms could increase the density of surface sites for stabilization of less strongly bound terminal oxygen forms via rearrangement of the real/defect structure. For ceria–zirconia solid solutions this possibility appears due to formation of fragments with pyrochlore-type structure in the course of reduction where coordination of Zr cations changes from 8-fold to octahedral one. A partial reoxidation of the surface layer by oxygen migrating from the bulk of oxide particle could thus generate oxygen interstitials in the subsurface layer with associated surface site for oxygen stabilization in the moderately bound on-top form [27].

The enthalpy of CH_4 interaction with the catalyst (Fig. 9, endothermic process) increases with the reduction degree corresponding to the enthalpy of its transformation into deep and partial oxidation products with a due regard for syngas selectivity and variation of the average oxygen bonding strength. Some decline of the heat of reduction at reduction degree exceeding 1.5 monolayer can be explained by increasing contribution of CH_4 pyrolysis in agreement with results of CH_4 TPR data (Fig. 5). Nearly linear (i.e., rather weak) dependence of CH_4 conversion on the reduction degree agrees with this weak variation of the heat of CH_4 transformation. Hence, the rate of CH_4 transformation in studied range of sample reduction degree is mainly determined by the surface coverage with reactive terminal oxygen forms replenished between pulses via diffusion from the bulk of oxide particles to the surface.

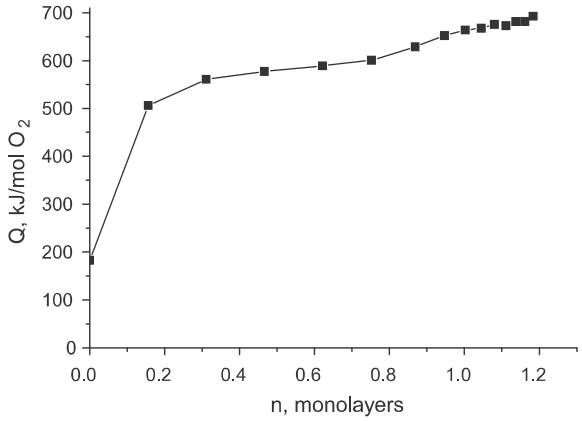

Fig. 8. Enthalpy of oxygen adsorption (Q) versus reduction degree (n) estimated from the heats of 1.4% $Pt/Pr_{0.3}Ce_{0.35}Zr_{0.35}O_2$ sample reduction by CO pulses at 600 °C.

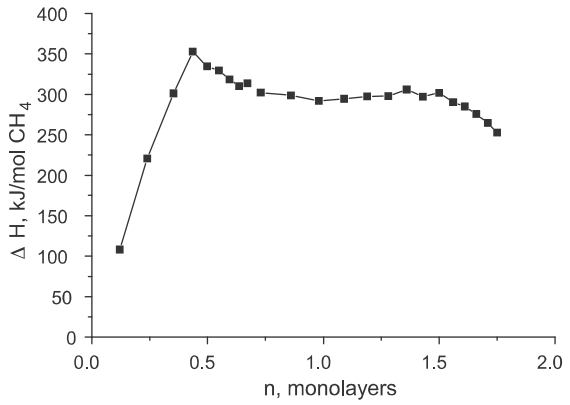

Fig. 9. Enthalpy of CH_4 interaction with 1.4% $Pt/Pr_{0.3}Ce_{0.35}Zr_{0.35}O_2$ sample as a function of reduction degree (n) at 600 °C.

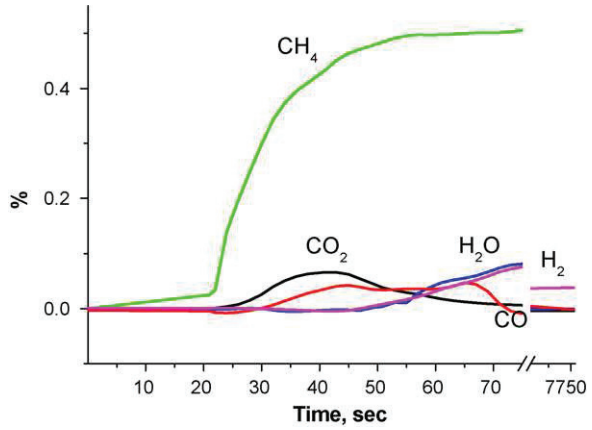

Fig. 11. Transients in the course of $Pt/Pr_{0.3}CeZrO_x$ channel reduction by 0.5% CH_4 in He at 700 °C after pretreatment in He. Contact time 5 ms.

Since the rate of the surface diffusion (reverse oxygen spillover from the support to Pt) is high, this provides some coverage of Pt by adsorbed oxygen thus helping in the activation of CH_4 molecules.

3.7. Kinetic transients for separate structured catalytic elements (channels)

3.7.1. Interaction with CH_4

Kinetic analysis of results of catalysts reduction by pulses of CH_4 at realistic concentrations in the flow reactors is known to be complicated by inevitable time lag between pulses required for the products analysis, indefinite regime of gas flow through the layer of a powdered catalyst (radial and back flow mixing, etc.), impact of the mass and heat transfer, etc. [14–17]. These problems were mainly avoided while using a continuous flow through the reactor equipped with a separate structural catalytic element – corundum channel with the active component supported on its walls [12,17,29,30]. Hence, a series of experiments for elucidating the effect of mild reducing pretreatment on kinetic features of CH_4 interaction under real-pressure conditions with the Pt/PrCeZrO catalyst supported on the corundum channel walls have been carried out. The main aim of these experiments was to verify conclusion of TAP studies about importance of oxidation state of Pt and oxygen transfer from support to Pt sites for the primary transformation of CH_4 into syngas.

Figs. 10 and 11 present results of transient studies when the stream of He was switched at 700 °C for that containing 0.5% CH_4 in He. For the catalyst pretreated in O_2, results apparently support conclusion of high-vacuum TAP studies. CO appears at the reactor outlet simultaneously with CH_4 corresponding to behavior of the primary product, while CO_2 curve is delayed as should be for the secondary product. Hydrogen is delayed even more suggesting its fast oxidation by reactive oxygen species. Primary route of CH_4 activation on oxidized Pt sites producing CO and hydroxyls (or water) could not be excluded as well.

Catalyst pretreatment in He removing rather small amount of oxygen located at the surface sites and within domain boundaries (vide supra) strongly deactivates it which also agrees with results of TAP studies. CH_4 is more strongly adsorbed on the surface of mildly reduced catalyst, and its subsequent transformation is accompanied by appearance of first CO_2 then CO and hydrogen when the surface is more reduced. Hence, presence of the mobile surface/near surface oxygen and oxidized Pt species not only helps to activate methane but also affects the mode of its primary transformation into products of partial or deep oxidation.

3.7.2. Interaction with $CH_4 + O_2$ stream

Addition of 0.5% O_2 to the feed 1% CH_4 in He strongly affects transients (Figs. 12 and 13). Apparently gas-phase or weakly bound oxygen species provide fast combustion of the products of CH_4 activation on oxidized Pt sites, so CO_2 and H_2O appear first. Subsequent appearance of hydrogen and later CO accompanied by the increase of CH_4 consumption is associated with the sample reduction along with carbonization and hydroxylation of the surface layer. Hence, at low CH_4 concentrations in the feed, gas-phase oxygen increases the rate of oxidation of activated CH_x species, apparently via increase

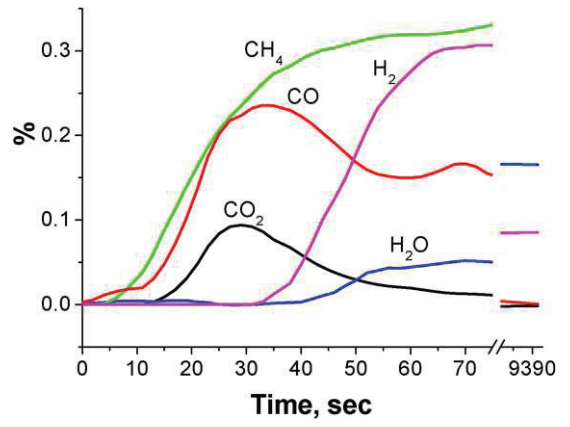

Fig. 10. Transients in the course of $Pt/Pr_{0.3}CeZrO_x$ channel reduction by 0.5% CH_4 in He at 700 °C after pretreatment in O_2. Contact time 5 ms.

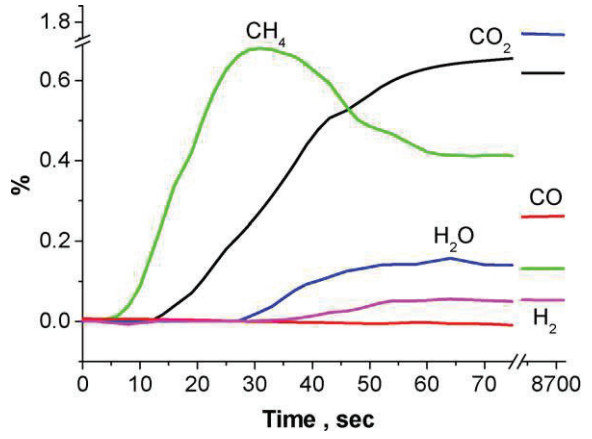

Fig. 12. Transients in the course of $Pt/Pr_{0.3}CeZrO_x$ channel contact with the feed 1% CH_4 + 0.5% O_2 at 700 °C after pretreatment in O_2. Contact time 5 ms.

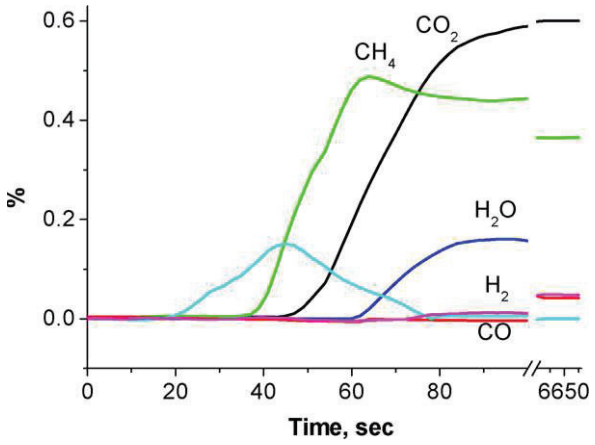

Fig. 13. Transients in the course of $Pt/Pr_{0.3}CeZrO_x$ channel contact with the feed 1% CH_4 + 0.5% O_2 at 700 °C after pretreatment in He. Contact time 5 ms.

of the rate of reverse oxygen spill-over from the oxide sites to Pt. Similar results were obtained in TAP experiments when decreasing the time lag between the oxygen and methane pulses resulted in a lower syngas selectivity [4].

Pretreatment in He strongly deactivates sample with respect to interaction with diluted $CH_4 + O_2$ feed (Fig. 13), which agrees with results presented in Section 3.7.1. Hence, the main factor is apparently a low reactivity of more reduced and/or more aggregated supported Pt species. It is noteworthy that even prolonged contact of sample pretreated in He with diluted reaction feed does not allow to achieve syngas yield equal to that for sample pretreated in O_2. This suggests that Pt aggregation caused by the high-temperature pretreatment in He is accompanied by catalyst deactivation, either due to decrease of Pt-support interface or by rearrangement of the structure of oxide surface or that of domain boundaries hampering oxygen diffusion.

For the same active component, transients in realistic concentrated $CH_4 + O_2$ feed (Fig. 14) revealed substantial difference with those observed for diluted feed (Fig. 12). In concentrated feed simultaneous appearance of CH_4 and products of its partial and deep oxidation clearly suggests realization of the primary route of CH_4 transformation into syngas followed by subsequent oxidation of CO and H_2 in the inlet part of the channel where the gas phase oxygen is present. A slow decline of exit CO_2 concentration with time accompanied by the increase of syngas yield (Fig. 14) is apparently caused by the partial reduction of catalyst by reaction feed similar to the case of oxygen-pretreated catalyst in diluted feed (Fig. 12). Hence, the key difference with diluted feed is that for the oxidized surface syngas selectivity in concentrated feed is much higher. In general case, it can be explained by interplay of several factors including pure kinetic ones (different kinetic orders of CH_4 and oxygen adsorption), mass transfer limitations for O_2 consumption [3] and variation of the catalytic properties of supported Pt, surface sites of complex oxide and Pt-support interaction as dependent upon the feed composition due to fast accumulation of some intermediates (CH_xO species), hydroxyls and carbonates. At least suggestion about different kinetic orders of CH_4 and O_2 adsorption (1 and 0, respectively) agrees well with a weak adsorption of CH_4 by TAP data (vide supra) as well as the POM order in CH_4 ~1 in realistic feeds demonstrated in experiments with channel-supported catalysts [12,13].

At longer contact times (Fig. 15) for the same feed composition transient characteristics are rather similar with the exception of some delay in CO appearance. By analogy with results for diluted feed (Fig. 12), this feature can be explained by faster oxidation of CO as compared with hydrogen in the inlet part of the channel. Since

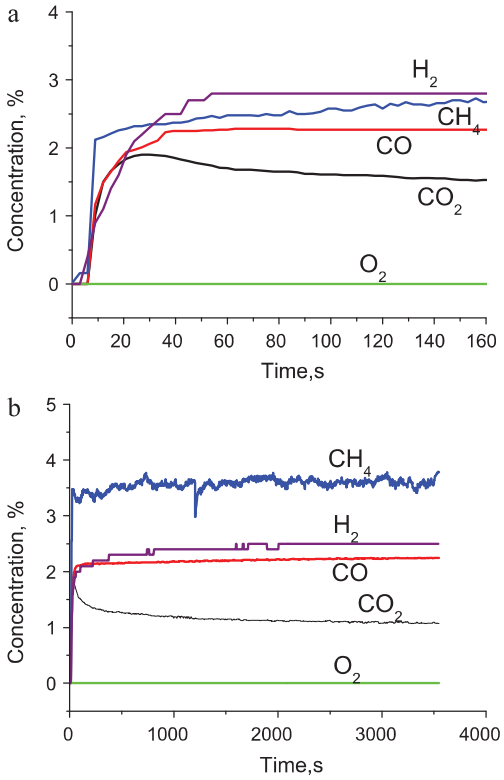

Fig. 14. Typical kinetic transients for channel with $Pt/PrCeZrO_x$ active component after oxidizing pretreatment. (a) Initial period and (b) slow transients. 750 °C, contact time 3.54 ms, feed 7% CH_4 + 3.5% O_2 in He.

at longer contact times oxygen is expected to be consumed within a narrower inlet part of the channel, subsequent CH_4 steam and dry reforming reactions as well as water gas shift reaction can also affect both dynamics of CO evolution as well as its steady-state concentration. However, sample pretreatment in hydrogen (Fig. 15c) revealed that reduced surface is much less reactive with respect to CH_4 than the oxidized one, so steam and dry reforming reaction occurring under the initial moments of reaction feed contact with oxidized catalyst surface are certainly to be much slower than the partial oxidation providing only a moderate increment to the methane conversion in the steady-state conditions at high temperatures [12,13]. This conclusion agrees with direct estimations of the rate constants of CH_4 steam and dry reforming on these catalysts which were shown to be several times lower than those of POM in feeds with realistic CH_4 content [29,30].

Dynamics of transients for reduced sample (Fig. 15c) clearly demonstrates that the gas phase or physically adsorbed oxygen species do not play any noticeably role in deep or partial oxidation of methane – all products appear after delay required for sample oxidation. Moreover, Pt aggregation caused by sample pretreatment with hydrogen (and, hence, weakened Pt-support interaction) only deteriorates syngas selectivity.

For Gd-doped catalyst kinetic transients in real feeds are rather similar to those for Pr-doped one (Fig. 16). During initial period (Fig. 16a) CO and CO_2 appear simultaneously with methane which agrees with primary route of methane transformation into syngas. The most pronounced difference with Pr-doped sample consists in a slow decline of syngas concentration with time-on-stream. At lower temperatures (650 °C), for Pt/GdCeZr catalyst decline of exit concentration of CO and H_2 with time-on-stream from the maximum to a steady-state level was much stronger (by three times) than for Pt/PrCeZr sample (<25 rel.%) [4]. For La-doped sample a similar slow decline of CO and H_2 concentrations with time-on-

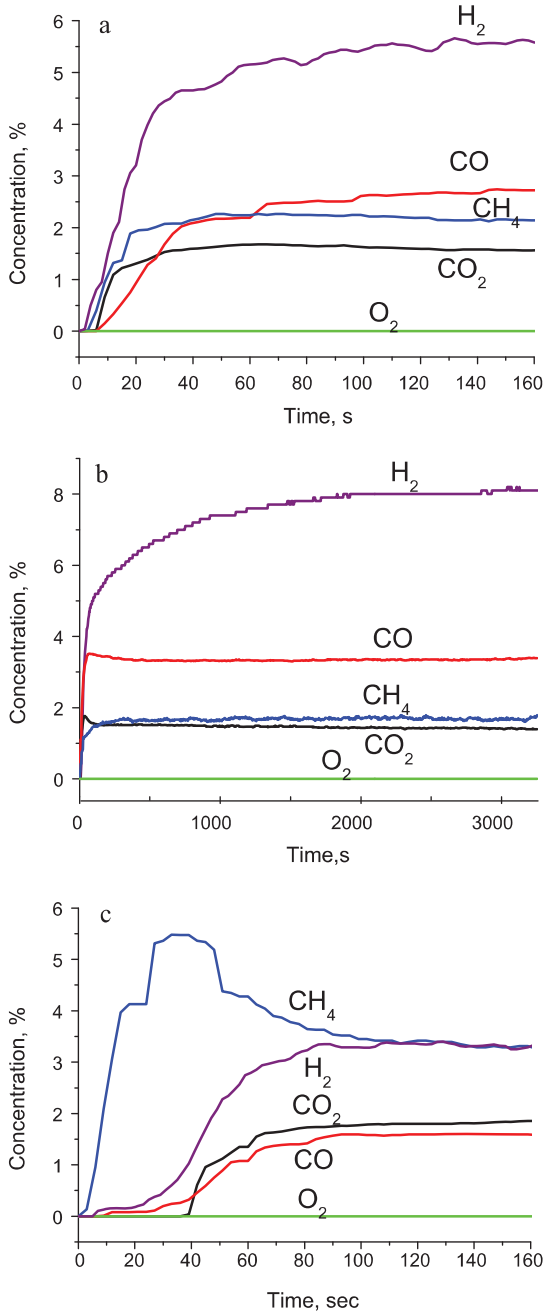

Fig. 15. Typical kinetic transients for channel with $Pt/PrCeZrO_x$ active component after oxidizing (a and b) or reducing (c) pretreatment. (a and c) Initial period and (b) slow transients. 750 °C, contact time 15 ms, feed 7% CH_4 + 3.5% O_2 in He.

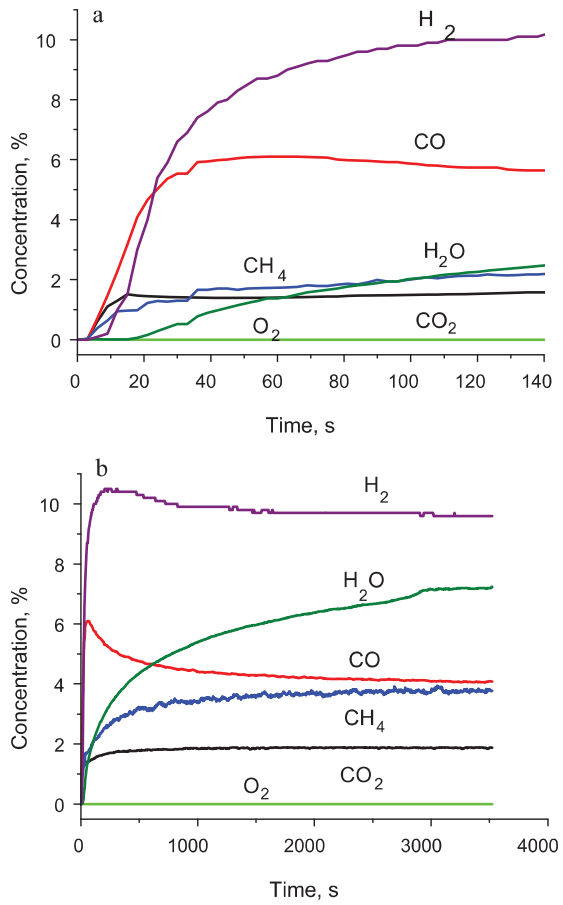

Fig. 16. Typical kinetic transients for channel with $Pt/GdCeZrO_x$ active component after oxidizing pretreatment. (a) Initial period and (b) slow transients. 750 °C, contact time 15 ms, feed 10% CH_4 + 5% O_2 in He.

stream was observed (Fig. 17), being also much stronger at 650 °C. Since the most clear difference between Pr- and Gd- or La-doped samples consists in the much higher bulk oxygen mobility for the former sample, this result supports conclusion about importance of lattice oxygen mobility to provide a high and stable performance of Pt-supported doped ceria–zirconia oxides in POM.

3.8. Basic steps of reaction mechanism

While detailed analysis of kinetic transients for POM in concentrated feeds on channels is still in progress (to be presented elsewhere), basic features of these transients are qualitatively similar to those studied earlier for powdered Pt/CeZrO and Pt/LaCeZrO catalysts in more diluted feed (4.6% CH_4 + 2.2% O_2 in He) [7,22,24].

Moreover, constants obtained by such an analysis combined with published data on the elementary steps of POM mechanism were successfully applied for description of steady-state and transient regimes of POM on monolithic catalysts with this type of active component [31]. Hence, it seems to be reasonable and useful to present here constants of some lump steps of the microkinetic POM scheme estimated for studied types of catalysts [7,32,33] (Table 3) as a basis for more detailed discussion of the effect of the oxygen mobility and metal-support interaction on the activity and stability in POM.

The most important point here is that the rate constant of step 5 (selective oxidation of CH_4 into syngas by PtO) is comparable with

Table 3
Basic microkinetic steps of the mechanism of CH_4 partial oxidation on $Pt/LnCeZrO_x$ catalysts [7,31].

No.	Step	K at 650 °C (s^{-1})
1	$O_2 + 2Pt \leftrightarrow 2PtO$	10^4
2	$H_2O + z \leftrightarrow H_2 + zO$	1.5
3	$zO + Pt \leftrightarrow PtO + Z$ spillover	>50
4	$O_{bulk} + z \leftrightarrow zO + V_O$ (bulk) diffusion	>10 along domain boundaries
5	$CH_4 + PtO \rightarrow CO + 2H_2 + Pt$	10^4
6	$CH_4 + 4PtO \rightarrow CO_2 + 2H_2O + 4Pt$	10^2
7	$CO + PtO \rightarrow CO_2 + Pt$	3.5×10^2
8	$H_2 + PtO \rightarrow H_2O + Pt$	$<1 \times 10^2$
9	$Pt + CO + H_2O \leftrightarrow CO_2 + H_2 + Pt$	$>10^4$ WGS reaction by associated mechanism

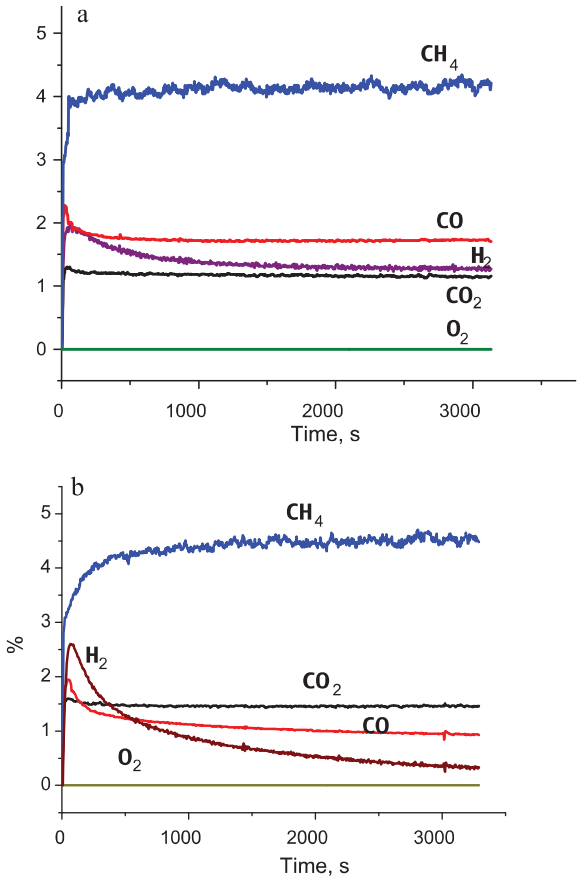

Fig. 17. Typical kinetic transients for channel with Pt/LaCeZrO$_x$ active component after oxidizing pretreatment. (a) 750 °C and (b) 650 °C. Contact time 4.72 ms, feed 7% CH_4 + 3.5% O_2 in He.

that for the oxygen adsorption (step 1) and exceeds much those for CH_4 combustion (step 6) and CO and H_2 oxidation (steps 7 and 8). This feature clearly explains syngas generation on these types of Pt-supported catalysts even in the presence of gas-phase oxygen. For Rh and Pt catalysts, either bulk or supported on irreducible oxides (alumina, MgO, etc.) [5,34] the situation is reversed, and indirect route of syngas formation is realized due to much faster combustion and CO/H_2 oxidation in the presence of gas-phase oxygen. Hence, strong Pt-support interaction, which results in domination of cationic forms of Pt for studied systems [18–22], provides radical variation of the chemical reactivity of supported Pt enhancing its reactivity in methane transformation along selective route of syngas generation while suppressing its combustion activity. This would be rather expected since combustion requires at least several available surface oxygen atoms adsorbed on a cluster comprised of several Pt atoms. Moreover, sticking coefficients and reactivity of CO and H_2 are well-known to be much lower for the oxygen covered Pt surface [35].

From the point of view of this scheme, a high rate of surface/bulk oxygen diffusion helps to stabilize Pt in the oxidized state thus preventing its aggregation leading to increase of combustion activity. In turn, a high Pt dispersion provides developed Pt-support interface required for the efficient reverse oxygen spill-over from support to Pt. Though rate constants of the surface diffusion and spill-over are smaller that those of oxygen adsorption and consumption (stages 5–8), nevertheless, when the latter rates are comparable, and, hence, their difference is small, stages of surface/bulk diffusion could noticeably affect the oxygen coverage of Pt sites, and, hence, activity and syngas selectivity. In the part of the channel where oxygen is absent, fast water gas shift reaction (Table 3) apparently occurs even at short contact affecting products distribution.

Another point is that for partially reduced support containing Ce and Pr cations, adsorption and dissociation of O_2 on the oxide vacancies as well as their reoxidation by water (stage 2) provide required replenishment of surface species to provide continuous oxygen flux to Pt-support interface. Certainly, the role of support is more complex including stabilization of some intermediates such as formates [36], or spectators such as carbonates affecting the surface oxygen mobility/reactivity, especially at lower temperatures, which requires further studies.

Certainly, conclusion of this work about important role played by highly dispersed Pt oxidic species stabilized due to Pt-support interaction requires further detailed studies aimed at their detection and characterization under real operation conditions applying *in situ* spectroscopic techniques with a due regard for the oxygen concentration gradient along the catalytic bed/channel length and its variation with the temperature and feed rate. Raman spectroscopy [22,37] and XANES/EXAFS [38–40] were shown to be among the methods the most sensitive to the oxidation state of Pt group metals and compatible with design of catalytic microreactors. Thus, X-ray absorption spectroscopy revealed that even for Rh (Rh + Pt)/Al_2O_3 catalysts with a rather moderate metal-support interaction, after ignition of CH_4 partial oxidation into syngas the Rh and Pt are mainly in the oxidized state in the narrow entrance zone of the catalytic bed and in the metallic state towards the end of the bed [38–40]. Some modification of the Pt-supported structured catalyst design (i.e., supporting catalytic layer on the wall of a quartz capillary for Raman studies, etc.) would be required as well for such future studies to provide required spatial resolution.

4. Conclusions

The combination of information on structural properties revealed by detailed characterization and kinetic information obtained at relevant conditions by various transient techniques allowed to rationalize the unique reactivity of Pt deposited on optimized supports with OSC. The selective oxidation of methane into syngas at short contact times on Pt-supported lanthanide doped ceria–zirconia catalysts was shown to proceed through direct route with oxygen-assisted methane activation on Pt. This is contrary to conventional catalysts having Pt deposited on support materials without significant oxygen mobility. Hence, catalysts with OSC supports and high oxygen surface mobility present relevant feature to allow conducting the CPOM reaction according to a bifunctional mechanism. The specific catalytic performance seems provided by strong Pt-support interaction stabilizing highly dispersed oxidic Pt species less active in CH_4 and syngas combustion than bulk Pt. It seems reasonable assuming that a limited coverage of electrophilic oxygen on the Pt surface and the dominant course of the reaction at the interface between Pt and the support interface manifests macroscopically in the primary formation of synthesis gas. Additionally, a high rate of surface/bulk oxygen diffusion and Pt-support oxygen spillover stabilizes these species while preventing coking.

Acknowledgements

This work was carried out in frames of Russian-French Associated European laboratory on catalysis. Support by OCMOL FP7 Project, RFBR–CNRS 09-03-93112 Project and Russian Federal Innovation Agency via the program “Scientific and Educational cadres” is gratefully acknowledged. The DFG collaborative research center SFB558 is kindly acknowledged for supporting the research stay of E. Gubanova. The Embassy of France in Moscow is

gratefully acknowledged for the joint PhD studentship grant of A. Bobin.

References

[1] J. Haber, Stud. Surf. Sci. Catal. 110 (1997) 1.
[2] D.A. Hickman, L.D. Schmidt, Science 259 (1993) 343.
[3] E.L. Gubanova, Y. Schuurman, V.A. Sadykov, C. Mirodatos, A.C. van Veen, Chem. Eng. J. 154 (2009) 174.
[4] E.L. Gubanova, A. van Veen, C. Mirodatos, V.A. Sadykov, N.N. Sazonova, Russ. J. Gen. Chem. 78 (2008) 2191.
[5] A. Donazzi, A. Beretta, G. Groppi, P. Forzatti, J. Catal. 255 (2008) 241.
[6] E.L. Gubanova, V.A. Sadykov, A.C. van Veen, C. Mirodatos, React. Kinet. Catal. Lett. 97 (2009) 349.
[7] C. Mirodatos, Y. Schuurman, A.C. van Veen, V.A. Sadykov, L.G. Pinaeva, E.M. Sadovskaya, Stud. Surf. Sci. Catal. 167 (2007) 287.
[8] E. Odier, Y. Schuurman, K. Barral, C. Mirodatos, Stud. Surf. Sci. Catal. 147 (2004) 79.
[9] M. Fathi, F. Monnet, Y. Schuurman, A. Holmen, C. Mirodatos, J. Catal. 190 (2000) 439.
[10] E.M. Sadovskaya, Y.A. Ivanova, L.G. Pinaeva, G. Grasso, T.G. Kuznetsova, A. van Veen, V.A. Sadykov, C. Mirodatos, J. Phys. Chem. A 111 (2007) 4498.
[11] V. Sadykov, V. Muzykantov, A. Bobin, N. Mezentseva, G. Alikina, N. Sazonova, E. Sadovskaya, L. Gubanova, A. Lukashevich, C. Mirodatos, Catal. Today 157 (2010) 55–60, doi:10.1016/j.cattod.2010.03.064.
[12] N.N. Sazonova, V.A. Sadykov, A.S. Bobin, S.A. Pokrovskaya, E.L. Gubanova, C. Mirodatos, React. Kinet. Catal. Lett. 98 (2009) 19.
[13] N.N. Sazonova, V.A. Sadykov, A.S. Bobin, S.A. Pokrovskaya, E.L. Gubanova, C. Mirodatos, React. Kinet. Catal. Lett. 98 (2009) 27.
[14] V.A. Sadykov, T.G. Kuznetsova, S.A. Veniaminov, D.I. Kochubey, B.N. Novgorodov, E.B. Burgina, E.M. Moroz, E.A. Paukshtis, V.P. Ivanov, S.N. Trukhan, S.A. Beloshapkin, Yu.V. Potapova, V.V. Lunin, E. Kemnitz, A. Aboukais, React. Kinet. Catal. Lett. 76 (2002) 83.
[15] C. Batiot-Dupeyrat, G. Valderrama, A. Meneses, F. Martinez, J. Barrault, J.M. Tatibouet, Appl. Catal. A: Gen. 248 (2003) 143.
[16] Yu. Bychkov, Yu. Tulenin, O. Krylov, V. Korchak, Kinet. I Katal. 43 (2002) 775.
[17] Yu. Bychkov, Yu. Tulenin, O. Krylov, V. Korchak, Kinet. I Katal. 44 (2003) 384.
[18] V.A. Sadykov, N.V. Mezentseva, G.M. Alikina, A.I. Lukashevich, Yu.V. Borchert, T.G. Kuznetsova, V.P. Ivanov, E.A. Paukshtis, V.S. Muzykantov, V.L. Kuznetsov, V.A. Rogov, J. Ross, E. Kemnitz, C. Mirodatos, Solid State Phenom. 128 (2007) 239.
[19] V. Sadykov, E. Kriventsov, E. Moroz, Yu. Borchert, T. Kuznetsova, V. Ivanov, A. Boronin, N. Mezentseva, E. Burgina, J. Ross, Solid State Phenom. 128 (2007) 81.
[20] V. Sadykov, N. Mezentseva, V. Muzykantov, R. Bunina, A. Boronin, V. Voronin, I. Berger, Mater. Res. Soc. Symp. Proc. 1023 (2007), JJ02-07.1-6.
[21] V. Sadykov, N. Mezentseva, V. Muzykantov, E. Gubanova, N. Sazonova, A. Bobin, V. Voronin, J. Ross, C. Mirodatos, Mater. Res. Soc. Symp. Proc. 1122 (2009), O05-03.
[22] V.A. Sadykov, T.G. Kuznetsova, G.M. Alikina, Yu.V. Frolova, A.I. Lukashevich, V.S. Muzykantov, V.A. Rogov, L.G. Ivanov, S. Pinaeva, E. Neophytides, K. Kemnitz, C. Scheurel, Mirodatos, in: D.K. McReynolds (Ed.), New Topics in Catalysis Research, Nova Science Publishers, New York, 2007, pp. 97–196 (Chapter 5).
[23] T.G. Kuznetsova, V.A. Sadykov, S.A. Veniaminov, G.M. Alikina, E.M. Moroz, V.A. Rogov, O.N. Martyanov, V.F. Yudanov, I.S. Abornev, S. Neophytides, Catal. Today 91–92 (2004) 161.
[24] V. Sadykov, T.G. Kuznetsova, V.S. Muzykantov, L.G. Pinaeva, E.A. Paukshtis, N.V. Mezentseva, E. Kemnitz, C. Mirodatos, A.C. van Veen, Catal. Today 117 (2006) 475.
[25] V.S. Muzykantov, E. Kemnitz, V.A. Sadykov, V.V. Lunin, Kinet. Catal. 46 (2003) 319, doi:10.1023/A:1024486716938.
[26] F. Dong, A. Suda, T. Tanabe, Y. Nagai, H. Sobukawa, H. Shinjoh, M. Sugiura, C. Descorme, D. Duprez, Catal. Today 827 (2004) 93.
[27] N.N. Bulgakov, V.A. Sadykov, V.V. Lunin, E. Kemnitz, React. Kinet. Catal. Lett. (2002) 111.
[28] V.A. Sadykov, S.F. Tikhov, N.N. Bulgakov, A.P. Gerasev, Catal. Today 144 (2009) 324, doi:10.1016/j.cattod.2008.12.018.
[29] S.N Pavlova, N.N. Sazonova, V.A. Sadykov, G.M. Alikina, A.I. Lukashevich, E. Gubanova, R.V. Bunina, Stud. Surf. Sci. Catal. 167 (2007) 343.
[30] N.N. Sazonova, V.A. Sadykov, A.S. Bobin, S.A. Pokrovskaya, E.L. Gubanova, C. Mirodatos, React. Kinet. Catal. Lett. 98 (2009) 35.
[31] V. Vernikovskaya, L.N. Bobrova, L.G. Pinaeva, V.A. Sadykov, I.A. Zolotarskii, V.A. Sobyanin, I. Buyakou, V. Kalinin, S. Zhdanok, Chem. Eng. J. 134 (2007) 180.
[32] Yu. Ivanova, E. Sadovskaya, G. Pinaeva, V. Sadykov, C. Mirodatos, Chem. Sustain. Develop. 7 (2009) 371.
[33] D. Efremov, L. Pinaeva, V. Sadykov, C. Mirodatos, Solid State Ionics 179 (2008) 847.
[34] A.B. Mhadeshwar, D.G. Vlachos, Ind. Eng. Chem. Res. 46 (2007) 5310.
[35] G. Ertl, Adv. Catal. 37 (1990) 213.
[36] J. Zhu, J.G. van Ommen, L. Lefferts, J. Catal. 225 (2004) 388.
[37] Y. Liu, F.-Y. Huang, J.-M. Li, W.-Zh. Weng, Ch.-R. Luo, M.-L. Wang, W.-Sh. Xia, Ch.-J. Huang, H.-L. Wan, J. Catal. 256 (2008) 192.
[38] W.J. Stark, J.-D. Grunwaldt, M. Maciejewski, S.E. Pratsinis, A. Baiker, Chem. Mater. 17 (2005) 3352.
[39] J.-D. Grunwaldt, A. Baiker, Catal. Lett. 99 (2005) 5.
[40] S. Hannemann, J.-D. Grunwaldt, N. van Vegten, A. Baiker, P. Boye, Ch.G. Schroer, Catal. Today 126 (2007) 54.

Top Catal (2013) 56:958–968
DOI 10.1007/s11244-013-0060-z

ORIGINAL PAPER

Mechanism of CH_4 Dry Reforming on Nanocrystalline Doped Ceria-Zirconia with Supported Pt, Ru, Ni, and Ni–Ru

A. S. Bobin · V. A. Sadykov · V. A. Rogov · N. V. Mezentseva · G. M. Alikina · E. M. Sadovskaya · T. S. Glazneva · N. N. Sazonova · M. Yu Smirnova · S. A. Veniaminov · C. Mirodatos · V. Galvita · G. B. Marin

Published online: 10 May 2013

Abstract Specificity of CH_4 dry reforming mechanism for Me-supported doped ceria-zirconia catalysts with high oxygen mobility was elucidated using a combination of transient kinetic methods (TAP, SSITKA) with pulse microcalorimetry and in situ FTIRS. Steady-state reaction of CH_4 dry reforming is described by a simple redox scheme with independent stages of CH_4 and CO_2 activation. This is provided by easy CO_2 dissociation on reduced sites of oxide supports followed by a fast oxygen transfer along the surface/domain boundaries to metal sites where CH_4 molecules are transformed to CO and H_2. The rate-limiting stage is irreversible transformation of CH_4 on metal sites, while CO_2 transformation proceeds much faster being reversible for steady-state surface. The oxygen forms responsible for CH_4 selective transformation into syngas correspond to strongly bound bridging oxygen species with heats of desorption ≈600–650 kJ/mol O_2, most probably bound with pairs of Pr and/or Ce cations able to change their oxidation state. Ni + Ru clusters could be involved in CO_2 activation via facilitating C–O bond breaking in the transition state, thus increasing the rate constant of the surface reoxidation by CO_2. Strongly bound carbonates are spectators.

Keywords Methane · Dry reforming · Me-supported doped ceria-zirconia · Oxygen bonding strength and reactivity · Mechanism · Transient kinetic studies

1 Introduction

Catalysts comprising doped ceria-zirconia oxides with supported precious metals and/or Ni demonstrate a high activity and coking stability in carbon dioxide reforming of methane, which is explained by a high lattice oxygen mobility of these oxides and strong metal—support interaction [1–12]. However, factors controlling main features of reaction mechanism on these catalysts, first of all, activation of reagents, remain unspecified though they are known to be important for providing stable performance in CH_4 dry reforming [12–15]. Thus, Bradford and Vannice [14] proposed that CO_2 participates in the CH_4 DR reaction via the reverse water–gas shift (RWGS) reaction yielding OH groups, which then react with adsorbed CH_x intermediates to form formate-type species (CH_xO). For Pt/Al_2O_3 catalyst, O'Connor et al. [15] suggested that CH_4 activation proceeds on free Pt sites, and CO_2 activation is assumed to be the slowest step assisted by hydrogen to form adsorbed CO and OH. For Pt/ZrO_2, participation in the reaction mechanism of hydroxocarbonates and formates stabilized on support was suggested [15]. On the other hand, Bychkov et al. [16, 17] demonstrated by using microcalorimetric measurements that for Pt/Al_2O_3 CO_2 is activated via direct interaction with the surface carbon atoms, which is the

A. S. Bobin · V. A. Sadykov (✉) · V. A. Rogov · N. V. Mezentseva · G. M. Alikina · E. M. Sadovskaya · T. S. Glazneva · N. N. Sazonova · M. Y. Smirnova · S. A. Veniaminov
Boreskov Institute of Catalysis SB RAS, Prospect Akademika Lavrentieva, 5, 630090 Novosibirsk, Russia
e-mail: sadykov@catalysis.ru

V. A. Sadykov · V. A. Rogov · N. V. Mezentseva
Novosibirsk State University, Novosibirsk, Russia

C. Mirodatos
Institut de Recherches sur la Catalyse et l'Environnement de Lyon, Lyon, France

V. Galvita · G. B. Marin
University of Gent, Ghent, Belgium

slowest step of DR. For Ni/SiO_2 catalyst, transient studies of Schuurman and Mirodatos revealed that CO_2 is activated by direct dissociation on Ni atoms, while the rate-limiting step is interaction between C and O species adsorbed on Ni [18]. For Ni/lanthana catalyst, a "bi-functional" mechanism was proposed by Slagtern et al. [19] to account for the observed kinetic behavior: methane is activated on the Ni particles, and carbon dioxide interacts with La_2O_3 to form carbonates which scavenge carbon from nickel at the Ni–La_2O_3 interface. Hence, as dependent upon the support, even for the same metal, different routes of reagents activation and rate-determining stages seem to control catalysts performance. However, it should be mentioned that according to Wei and Iglesia [20], for all traditional supports without noticeable oxygen mobility and reactivity and supported metals, only CH_4 activation by C–H bond rupture is of any kinetic significance, all other stages proceeding much faster. It could not be excluded that features of CH_4 dry reforming mechanism depend not only on support and supported metal, but on operation conditions (concentration of reagents and temperature) and oxygen mobility in support as well. This requires to carry out transient kinetic experiments in realistic conditions to be sure that mechanistic features thus clarified have any significance for the real catalysis of CH_4 DR. Similarly, the oxygen mobility in complex oxide supports is to be characterized not only in the standard oxidized state, but also after achieving the steady state in realistic feeds as well when relatively weakly bound and, hence, mobile oxygen species are to be absent [21–24]. In this respect, oxygen isotope heteroexchange between catalyst and $C^{18}O_2$ is very useful to characterize the oxygen mobility in the catalysts reduced by reaction feed.

This work presents results on elucidating specificity of the mechanism of CH_4 dry reforming for ceria-zirconia-based catalysts with supported Pt, Ru, Ni, and Ni + Ru using transient kinetic methods (including pulse and SSITKA studies) combined with pulse microcalorimetry and in situ FTIRS in realistic feeds at temperatures up to 750 °C.

2 Experimental

2.1 Catalysts Preparation and Characterization

Complex fluorite-like Ln_x $(Ce_{0.5}Zr_{0.5})_{1-x}O_2$ (Ln = Pr, Sm, Pr + Sm; x = 0.3) oxides were prepared by polymerized complex precursor (Pechini) route followed by drying and calcinations in air at 900 °C for 2 h as described elsewhere [8, 21, 22]. Nanocomposite 80 %$Sm_{0.3}Ce_{0.35}Zr_{0.35}O_2$ + 10 % $Y_{0.08}Zr_{0.92}O_2$ (YSZ) +10 %NiO was prepared by one-pot Pechini route [23–25]. Pt (~1 wt%), Ru (~1 wt%), Ni (5–7 wt%), $LaNiO_3$ (7 wt%) and their combinations were supported from solutions of respective salts (H_2PtCl_6, $RuCl_3$, Ni, and La nitrates) or their mixtures by incipient wetness impregnation followed by drying and calcination at 800 °C.

The specific surface area of samples was determined from the Ar thermal desorption data by using BET method. XRD patterns were obtained with an ARL XTRA diffractometer using Cu Kα monochromatic radiation (λ = 1.5418 Å); the 2θ scanning region was 20–85°. The TEM micrographs were obtained with a JEM-2010 instrument (lattice resolution 1.4 Å, acceleration voltage 200 kV). Local elemental analysis was performed with EDX method (a Phoenix Spectrometer) [8, 21–25].

2.2 Kinetic and Mechanistic Studies

Oxygen isotope heteroexchange experiments were carried out in a flow reactor (SSITKA mode) following earlier described procedures [26]. After achieving dynamic oxygen adsorption–desorption equilibrium at 500–700 °C, a flow of 1 % $^{16}O_2$ in He was switched for that of 1 % $^{18}O_2$ in He, and concentrations of $^{16}O_2$, $^{16}O^{18}O$, and $^{18}O_2$ were monitored by a mass-spectrometer UGA 200 (Stanford Research Systems, USA). In a similar mode oxygen isotope heteroexchange was carried out using a flow of 1 % $C^{18}O_2$ in He (^{18}O fraction 75 %) for samples after different pretreatments (either in O_2 or after achieving the steady state in CH_4 DR).

Both steady state and transient experiments in CH_4 dry reforming were carried out at atmospheric pressure using quartz reactors and flow installation equipped with GC and on-line IR absorbance, electrochemical and polarographic gas sensors for different components as described elsewhere [10, 21–25]. To compare specific catalytic activities of samples, effective first-order rate constants satisfactorily describing methane conversion data in plug-flow reactors [5, 10, 23] were calculated. Transient kinetic experiments were carried out by switching the stream of reaction mixture to that containing CO_2, CH_4, $^{13}CH_4 + CO_2$ or $CH_4 + {}^{13}CO_2$ in He following earlier described approaches [18]. Analysis of ^{13}C SSITKA experiments was carried out by solving the system of differential equations for the plug-flow reactor [27].

The Temporal Analysis of Products reactor set-up used in this work (TAP-1) was described by Gleaves et al. [28]. TAP experiments were performed in quartz microreactor placed in vacuum (10^{-4}–10^{-5} Pa). The weight of the catalyst sample was 20 mg. A narrow pulse of gas molecules (~10^{14} molecules) was injected into the reactor by means of two high speed pulse valves. The products and unreacted reactants were monitored at the exit of the reactor by a UTI 100C quadrupole mass spectrometer at fixed atomic mass units (AMU): 40 for Ar, 44 for CO_2, 16 for CH_4, 2 for H_2,

28 for CO, 18 for H_2O, and 32 for O_2. The catalysts were pretreated by injecting a number of high intensity hydrogen pulses ($\sim 10^{14}$ molecules/pulse) until the outlet hydrogen responses were stable. In single-pulse experiment, a small amount of molecules ($\sim 10^{13}$ molecules/pulse) was admitted to the reactor using one pulse valve. In pump-probe experiment, the reactants were subsequently injected from the two pulse valves with a variable time interval between two pulses. The species created during the first pulse (pump pulse) were probed with a suitable reactant during the second pulse (probe pulse). In each experiment, 25 responses of each AMU were collected and averaged. All reaction mixtures were prepared with Ar as one of the components, so that the admitted amount of components can be determined from the Ar response. A temperature range of 773–1,023 K was covered.

Pulse microcalorimetric studies were carried out using a Setaram Sensys DSC TG calorimeter and a pulse kinetic installation. The reagents and products concentrations were determined by a gas chromatograph Chromos GH-1000. Samples were pretreated in the flow of 5 % O_2 in He at 700 °C for 0.5 h and then in He for 0.5 h at the same temperature with subsequent cooling down in the He flow (flow rate 40 mL/min) to the temperature of experiments. Steady state of catalysts in CH_4 dry reforming was usually achieved by flowing reaction feed 7 % CH_4 + 7 % CO_2 in He at 700 °C for 2 h. Pulses of different compositions (7 % CH_4 in He, 7 % CH_4 + 7 % CO_2 in He, 7 % CO_2 in He, 5 % O_2 in He) with volume 1–5 mL and time interval between pulses 15 min were fed in different sequences onto the stream of He flowing through the reactor (vide infra). Due to rather small weights of catalysts ($\sim 30 + 60$ mg quartz fraction) and rather big reactor volume (≈ 5 cm^3), these pulse experiments were carried out in the batch-flow mode.

For in situ FTIRS studies of the reactivity of surface carbonates, thin pellets (2.8–3.6 cm^2 in area and 60–90 mg in weight) were prepared from the catalysts powders without a binder and evacuated at 500 °C for 1 h in IR cell earlier described in details [29]. Further, the temperature in IR cell was adjusted to experimental temperature (600, 650 °C). IR spectra were registered using a FTIR-8300 Shimadzu spectrometer in the region of 400–6,000 cm^{-1} with 4 cm^{-1} resolution and accumulation of 100 scans. CO_2 was injected into IR cell (50 torr) from a separate vessel connected with the cell through a valve, and the spectra were registered until the stationary state of the surface was obtained. After that, carbon dioxide was removed from the gas phase by freezing CO_2 vessel with liquid nitrogen, and IR spectrum was registered. Then, CH_4 was injected (50 torr), and the IR spectra were registered until the stationary state of the surface was obtained.

3 Results and Discussion

3.1 Phase Composition and Microstructure

Specific surface area of studied catalysts varies in the range of 15–30 m^2/g (Table 1). Detailed characteristics of catalysts phase composition, microstructure and oxygen mobility/reactivity are given in previous publications [5, 6, 8–12, 20–26, 30]. Doped ceria-zirconia fluorite-like oxides are single-phase samples. In as-prepared samples, metals (Pt, Ru, Ru + Ni) supported on fluorite-like oxides or nanocomposites are mainly in the form of oxidic species strongly interacting with oxide particles and partially incorporated into their surface layers. For nanocomposites prepared via one-pot Pechini route, NiO particles decorated by fluorite-like oxidic fragments are present as well [23–25]. In reduced steady state of CH_4 DR catalysts, metal or metal alloy nanoparticles/clusters (including Ni (Ru, Pt) alloy clusters segregated from supported LaNi(Pt, Ru)O_3) are epitaxially bound with supports and partially decorated by support oxidic species [23–25].

3.2 Catalytic Activity

At 700 °C and contact time 15 ms, the first-order specific rate constants (s^{-1} m^{-2}) for studied samples (Table 1) varied in the row Pt/PrSmCeZr < Pt/PrCeZr ~ LaNi/PrSmCeZr = LaNiPt/PrSmCeZr < Ru/PrSmCeZr < Ru + Ni/PrSmCeZr/YSZ < Ru + Ni/PrSmCeZr. For the same type

Table 1 Chemical composition, abbreviation, specific surface area and specific catalytic activity of Me-supported fluorite-like catalysts

Chemical composition	Abbreviation	S_{BET} (m^2/g)	K (s^{-1} m^{-2}) at 700 °C
8 %$LaNiO_3$/$Pr_{0.15}Sm_{0.15}Ce_{0.35}Zr_{0.35}O_2$	LaNi/PrSmCeZr	21	1.7
8 %$LaNiO_3$ +1 %Pt/$Pr_{0.15}Sm_{0.15}Ce_{0.35}Zr_{0.35}O_2$	LaNiPt/PrSmCeZr	21	1.7
1.4 %Pt/$Pr_{0.15}Sm_{0.15}Ce_{0.35}Zr_{0.35}O_2$	Pt/PrSmCeZr	30	0.7
1.4 %Pt/$Pr_{0.3}Ce_{0.35}Zr_{0.35}O_2$	Pt/PrCeZr	16	1.5
1 %Ru + 10 %NiO/$Pr_{0.15}Sm_{0.15}Ce_{0.35}Zr_{0.35}O_2$/YSZ	Ru + Ni/PrSmCeZr/YSZ	30	4
1.4 %Ru/$Pr_{0.15}Sm_{0.15}Ce_{0.35}Zr_{0.35}O_2$	Ru/PrSmCeZr	20	2.4
1.4 %Ru + 6.6 %Ni/$Pr_{0.15}Sm_{0.15}Ce_{0.35}Zr_{0.35}O_2$	Ru + Ni/PrSmCeZr	18	7.5

of supported active component, specific catalytic activity correlates with the oxygen mobility in complex oxide support [4, 10, 21, 31, 32]. For the same support, specific activity is apparently higher for Ru + Ni-supported active component due to formation of mixed Ni–Ru alloy nanoparticles [23–25]. Addition of Pt does not improve performance of supported $LaNiO_3$, perhaps, due to excessive decoration of alloy nanoparticles by La hydroxocarbonates.

3.3 Isotope Transients

Figure 1 demonstrates typical transients in the case of switches of the feed with normal isotope composition to that containing labeled CH_4. As follows from these results, the transients are fast, so the steady-state surface coverage by carbon-containing species is quite low, not exceeding 10 % of monolayer. In the case of labelled CH_4, redistribution of ^{13}C among all C-containing components of feed is observed. Kinetic parameters characterizing the rate of exchange and specific rates of CH_4 and CO_2 consumption are shown in Table 2. The rate constants of CO_2 transformation estimated by SSITKA data analysis exceed those of CH_4 consumption by an order of magnitude. These results explain a high coking stability of studied catalysts.

Figure 2 shows variation of the ^{13}C isotope fraction in CO and CO_2 after switching the stream of $^{12}CH_4 + {}^{12}CO_2 + He$ to that of $^{12}CH_4 + {}^{13}CO_2 + He + 1$ %Ar for Ru + Ni/PrSmCeZr catalyst at 650 °C. Fractions of ^{13}C in CO and CO_2 in the exit stream increase without any delay relative to Ar concentration, and at each moment the total number of ^{13}C atoms in CO and CO_2 is equal to that in the inlet $^{13}CO_2$, so there is no carbon isotope accumulation on the catalyst surface. Hence, this experiment also demonstrates that concentration of C-containing intermediates (carbonates, etc.) on the steady-state surface is negligible.

According to the reaction stoichiometry

$$CH_4 + CO_2 = 2CO + 2H_2$$

and provided the absence of carbon exchange between carbon-containing molecules, the fraction of ^{13}C in CO should be equal to a half sum of ^{13}C fractions in CO_2 and CH_4:

$$\alpha_{CO} = \frac{\alpha_{CO_2} + \alpha_{CH_4}}{2} \quad (1)$$

In our case, ^{13}C fractions in reagents were equal to $\alpha_{CO_2} = 0.7$, $\alpha_{CH_4} = 0$. In this case, estimated ^{13}C fraction in CO should be equal to 0.35, while experimental value is 0.4. At the same time, ^{13}C fraction of CO_2 in the exit stream is much lower than that in the inlet feed being equal to 0.46. This means that in the course of reaction the exchange of carbon atoms between CO and CO_2 proceeds, while there is no transfer of ^{13}C into CH_4 (Fig. 2). This proves that stages of catalyst interaction with CH_4 and CO_2 are independent, the first one being irreversible, and the second one—reversible. The simplest mechanism conforming to this conclusion can be presented as follows:

(1) $[ZO] + CH_4 \rightarrow [Z] + CO + 2H_2$,
(2) $[Z] + CO_2 \leftrightarrow [ZO] + CO$

Here, methane irreversibly interacts with oxidized centers of catalyst with CO and H_2 formation, which is followed by reoxidation of reduced centers by carbon dioxide. Though a more detailed description should take into account the occurrence of reverse water gas shift reaction, which decreases H_2/CO ratio in products, for studied catalysts its effect is not so strong (CH_4 and CO_2 conversions

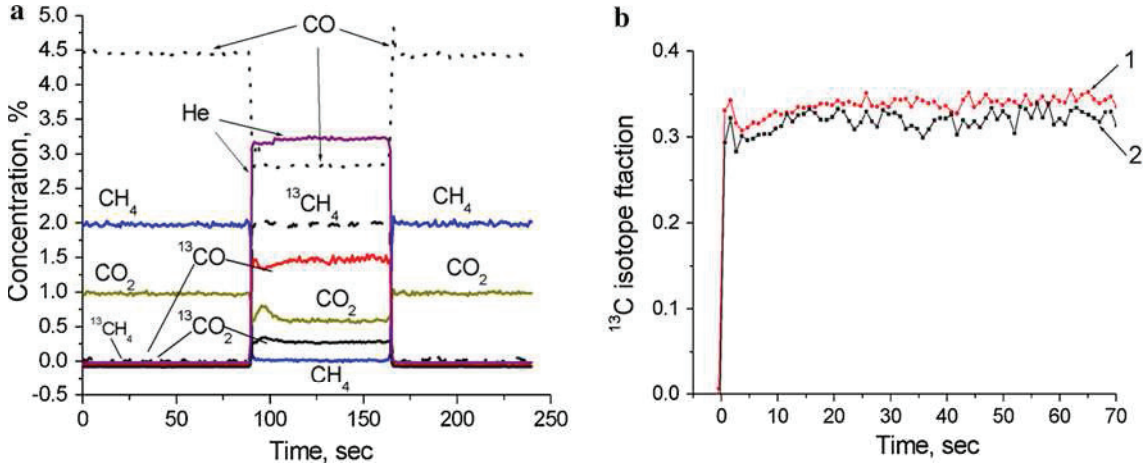

Fig. 1 **a** Isotope transients after switches $CH_4 + CO_2 + He \rightarrow {}^{13}CH_4 + CO_2 + He \rightarrow CH_4 + CO_2 + He$ for Pt/PrCeZr sample at 830 °C, 15 ms contact time and inlet concentration of CH_4 and CO_2 4 %; **b** Time dependence of ^{13}C isotope fraction in CO (1) and CO_2 (2) after switching $CH_4 + CO_2 + He \rightarrow {}^{13}CH_4 + CO_2 + He$ for Pt/PrCeZr sample at 830 °C, 15 ms contact time and inlet concentration of CH_4 and CO_2 4 %

Table 2 Estimation of the rates of basic stages of CH_4 dry reforming by SSITKA

T (°C)	α_{CO_2}	α_{CO}	w_2/w_1	w_1 (mcmol/g · min)	w_2 (mcmol/g · min)	w_{-2} (mcmol/g · min)
Pt/PrCeZr						
735	0.12	0.14	42	0.6	25	24
785	0.21	0.23	34	1.0	34	33
830	0.32	0.34	30	1.6	48	46
Ru + Ni/PrSmCeZr						
550	0.52	0.46	7.7	4.2	32	28
600	0.49	0.42	6.0	6.2	36	30
650	0.46	0.39	5.5	7.6	42	34
Ru + Ni/PrSmCeZr/YSZ						
550	0.49	0.46	11.5	1.5	17	15
600	0.44	0.42	24	2.0	47	45
650	0.40	0.39	43	2.5	106	103

1) $[ZO] + CH_4 \rightarrow [Z] + CO + 2H_2$,

2) $[Z] + CO_2 \leftrightarrow [ZO] + CO$

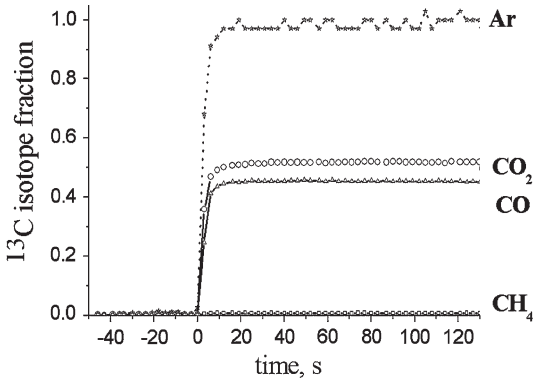

Fig. 2 Time dependence of ^{13}C isotope fraction in CO, CO_2, and CH_4 after switch $CH_4 + CO_2 \rightarrow CH_4 + {}^{13}CO_2 + He + Ar$ for the Ru + Ni/PrSmCeZr sample at 650 °C and 15 ms contact time. Feed composition: 3.8 % CH_4 + 3.8 % CO_2 (+1 % Ar) in He

differ by less than 10 rel. %), so it will not affect a conclusion about the nature of rate-limiting stage. Though different active sites are to be considered for steps 1 and 2 occurring on metal and oxide sites, respectively, in the case of very fast redistribution of oxygen species between these sites due to surface diffusion (vide infra), in the first approximation this simplified scheme would allow one at least to estimate a relation between the specific rates of CH_4 and CO_2 activation.

3.4 Rate-Limiting Stage

The total rate of CO formation in frames of this scheme is equal to:

$$w_{\Sigma CO} = w_1 + w_2 - w_{-2}. \quad (2)$$

The rate of ^{13}CO formation is equal to:

$$w_{^{13}CO} = w_1 \times \alpha_{CH_4} + w_2 \times \alpha_{CO_2} - w_{-2} \times \alpha_{CO} \quad (3)$$

Then the fraction of ^{13}C in CO will be determined by the relation:

$$\alpha_{CO} = \frac{w_1 \times \alpha_{CH_4} + w_2 \times \alpha_{CO_2} - w_{-2} \times \alpha_{CO}}{w_1 + w_2 - w_{-2}} \quad (4)$$

Taking into account that in steady-state conditions of catalytic reaction

$$w_{-2} = w_2 - w_1 \quad (5)$$

and $\alpha_{CH_4} = 0$, Eq. 4 can be rewritten as:

$$\alpha_{CO} = \frac{w_2 \times \alpha_{CO_2} - (w_2 - w_1) \times \alpha_{CO}}{2w_1} \quad (6)$$

which can be simply transformed into:

$$\frac{w_2}{w_1} = \frac{\alpha_{CO}}{\alpha_{CO_2} - \alpha_{CO}} \quad (7)$$

Thus calculated w_2/w_1 ratios are given in Table 2. As follows from this Table, the rate of the catalyst reoxidation by CO_2 greatly exceeds that of its reduction by methane. Hence, in steady-state conditions, the rate of methane dry reforming is limited by the stage of methane interaction with catalyst. Note that both w_1 (rate of CH_4 transformation) and w_2 (rate of catalyst reoxidation by CO_2) at a lower (550 °C) temperature are apparently higher for catalysts containing Ru + Ni as compared with those for Pt/PrCeZr at a higher (735 °C) temperature. Since specific activity of Pt/PrSmCeZr catalyst is even lower than that of Pt/PrCeZr catalyst (Table 1), this difference could not be explained by the effect of support composition. Hence, in agreement with Shuurman and Mirodatos data on direct dissociation of CO_2 on metallic Ni sites [18], this result suggests that Ru + Ni alloy nanoparticles are not only involved in CH_4 activation, but help to activate carbon dioxide as well.

3.5 Tap

Typical results of TAP studies are shown in Figs. 3, 4, 5, 6, 7 for the case of Ni + Ru-supported catalysts. In oxidized state, these catalysts possess rather low activity providing only complete oxidation (combustion) of methane, which is a well-known feature of Ni/Ru containing catalysts [23–25] (not shown for brevity). For catalysts reduced by hydrogen, successive pulses of CO_2 and CH_4 are efficiently transformed into CO and CO + H_2, respectively (Fig. 3). As follows from this figure, amounts of CO produced in the pulse of CO_2 and subsequent pulse of CH_4 are very close, which agrees with the conclusion about independent activation of reagents based on SSITKA results. Variation of time delays between CO_2 and CH_4 pulses only slightly affects the amount of CO produced in CH_4 pulse (Fig. 4). Since SSITKA results suggest participation of Ni + Ru alloy particles in activation of CO_2 molecules (vide supra), redistribution of reactive oxygen species between adsorption sites located on metal and oxide surface could occur. For the Ni + Ru/PrSmCeZr/YSZ nanocomposite with a bigger amount of Ni and larger sizes of Ni particles [23–25], a decline of the amount of CO produced in CH_4 pulse with delay time is more pronounced (Fig. 4b), which suggests also some incorporation of oxygen atoms into the bulk of Ni particles. Since the number of molecules in each pulse is very small (<0.1 % of monolayer), it is clear that the spatial distribution of oxygen atoms on the surface of catalysts after one pulse of CO_2 can be strongly non-uniform, thus favoring the occurrence of oxygen diffusion processes. Indeed, pump-probe experiments with oxygen-labelled $C^{18}O_2$ confirmed rapid oxygen redistribution between different centres of catalysts with high oxygen mobility (Fig. 5). Here, pulse of $C^{18}O_2$ produces only $C^{16}O$, which can be possible only in the case of fast

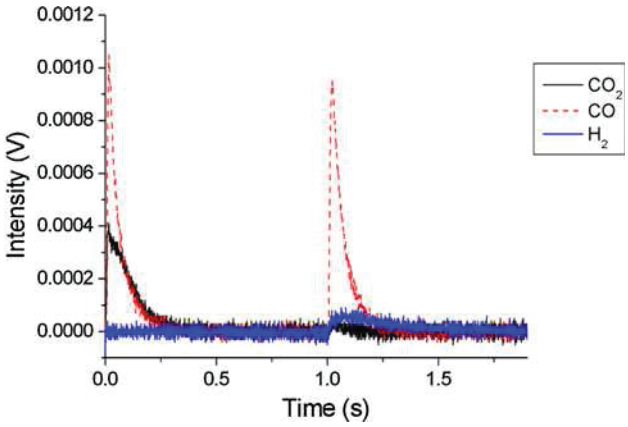

Fig. 3 CO_2, CO, CH_4, and H_2 responses corresponding to CO_2 and CH_4 pump-probe experiment over reduced Ru + Ni/PrSmCeZr at 754 °C. Injection times were 0 s for CO_2 and 1.0 s for CH_4

equilibration between ^{18}O surface oxygen atoms produced by $C^{18}O_2$ dissociation, ^{16}O surface/subsurface oxygen atoms of the catalyst and even ^{18}O atoms of formed CO molecules. Since subsequent pulse of CH_4 apparently activated on metal sites produces only $C^{16}O$, this suggests that CO_2 dissociates on the oxide support sites and not on the metal sites. Hence, the surface oxygen diffusion is really very fast to supply oxygen atoms with equilibrium isotope composition to the metal/support interface during a 0.6 s time lag between CO_2 and CH_4 pulses.

A comparison of CO responses for mixed CH_4 + CO_2 pulse and separate pulses of components (Fig. 6) shows that the amount of CO produced in the mixed pulse corresponds to the sum of CO produced in separate pulses. This demonstrates that activation and transformation of CO_2 and CH_4 indeed proceed independently.

Results of $^{13}CO_2$ and $^{12}CH_4$ pump-probe experiments confirm this conclusion (Fig. 7). Indeed, pulse of $^{13}CO_2$

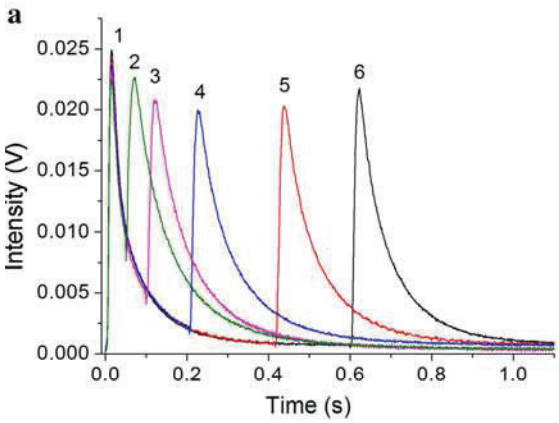

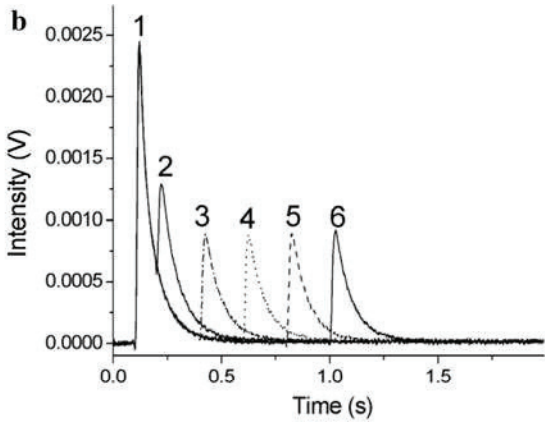

Fig. 4 **a** CO responses corresponding to CO_2 and CH_4 pump-probe experiments with various time delays between CO_2 (1) and CH_4 (2–6) pulses over reduced Ru + Ni/PrSmCeZr at 754 °C; **b** CO responses corresponding to CO_2 and CH_4 pump-probe experiments with various time delays between CO_2 (1) and CH_4 (2–6) pulses over reduced Ru + Ni/PrSmCeZr/YSZ at 700 °C

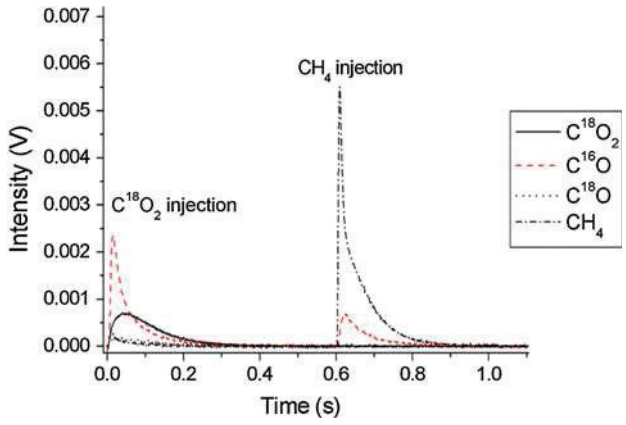

Fig. 5 $C^{18}O_2$, $C^{18}O$, $C^{16}O$, and CH_4 responses corresponding to $C^{18}O_2$ and CH_4 pump-probe experiment over reduced Ru + Ni/PrSmCeZr at 750 °C. Injection times were 0 s for $C^{18}O_2$ and 0.6 s for CH_4

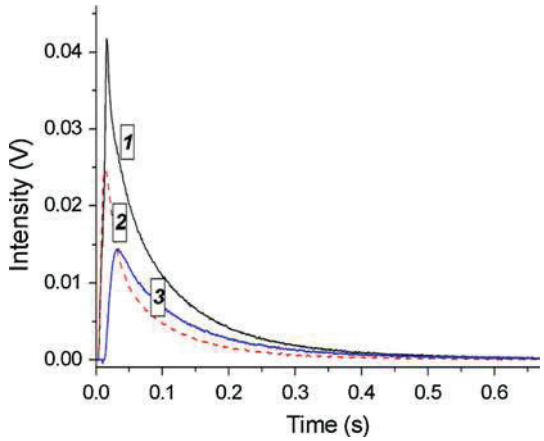

Fig. 6 CO responses obtained over reduced Ru + Ni/PrSmCeZr catalyst at 754 °C in: *1* CO_2 and CH_4 pump-probe experiment (time delay between CO_2 and CH_4 pulses was 0.01 s); *2* CO_2 single-pulse experiment; *3* CH_4 single-pulse experiment

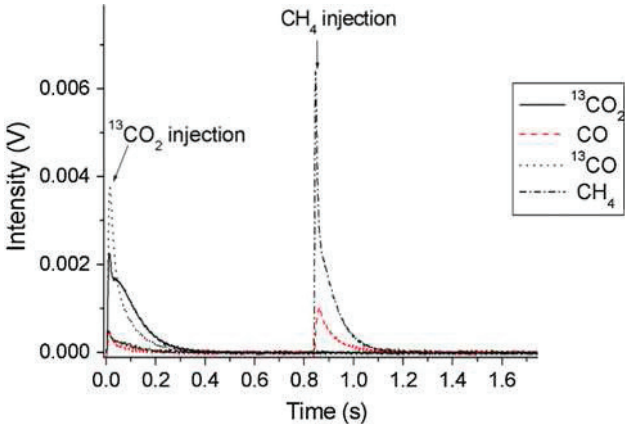

Fig. 7 $^{13}CO_2$, ^{12}CO, ^{13}CO, and CH_4 responses corresponding to $^{13}CO_2$ and $^{12}CH_4$ pump-probe experiment over reduced Ru + Ni/PrSmCeZr at 750 °C. Injection times were 0 s for $^{13}CO_2$ and 0.8 s for CH_4

produces only ^{13}CO, while subsequent pulse of $^{12}CH_4$ gives only ^{12}CO. This clearly excludes any exchange of carbon atoms between reagents, and hence the existence of any common intermediate.

3.6 Heat Effects and Dynamics of Steady-State Catalysts Reduction by CH_4 Pulses and Reoxidation by CO_2 and O_2 Pulses

For all catalysts in the steady state (ss), the heat effects generated by reduction with CH_4 pulses were very close to each other, varying rather weakly with reduction degree up to 0.3–0.5 monolayer. As a typical example, Fig. 8a shows this dependence for Ru + Ni/PrSmCeZr sample. As products of CH_4 transformation, only CO and H_2 are observed (Fig. 9), degree of CH_4 conversion in the 1st pulse being equal to that in the reaction feed pulse, decreasing only slightly with the catalyst reduction degree. This result clearly agrees with conclusion on the independent activation of CH_4 and CO_2 based on the results of SSITKA and TAP studies (vide supra). Since the amount of oxygen removed by each pulse is in the range of 5–10 % of monolayer, exceeding the amount of oxygen adsorbed on the metal sites, it is clear that only fast oxygen migration from the surface/subsurface sites to metal clusters could provide a high rate of CH_4 conversion in this series of pulses. The strength of reactive oxygen species bonding with the ss surface estimated from respective heat effects with a due regard for stoichiometry of CH_4 transformation at this stage of reduction (Fig. 9b) corresponds to bridging M_2O form (heat of O_2 desorption $\approx$650 kJ/mol [33]) (Table 3). Note that for all studied samples heats of oxygen desorption estimated from experiments with CH_4 pulses are also close to each other. This proves that oxygen is removed from the oxide support and not from the supported active component. At a deeper reduction degree, reaction heats decline (Fig. 8) due to onset of CH_4 pyrolysis with carbon deposition on the catalyst surface, as follows from the carbon imbalance (Fig. 9b). As the result, the heat effect approaches the level corresponding to the enthalpy of CH_4 dissociation into C (graphite) and H_2 ($\sim$75 kJ/mol).

Reoxidation (up to 20–50 % of monolayer oxygen coverage) of ss surface by CO_2 pulses proceeds with nearly constant heats of reaction (from −60 to −40 kJ/mol CO_2) (Fig. 8b), also weakly depending upon the type of supported active component. CO_2 consumption in each pulse is accompanied by formation of the equivalent amount of CO with small (if any at all) retention of CO_2 as surface carbonates. With a due regard for the standard enthalpy of reaction $CO_2 = CO + 1/2O_2$ (283 kJ/mol), these heat values correspond to replenishing the bridging surface oxygen forms with the desorption heat $\approx$600–650 kJ/mol O_2

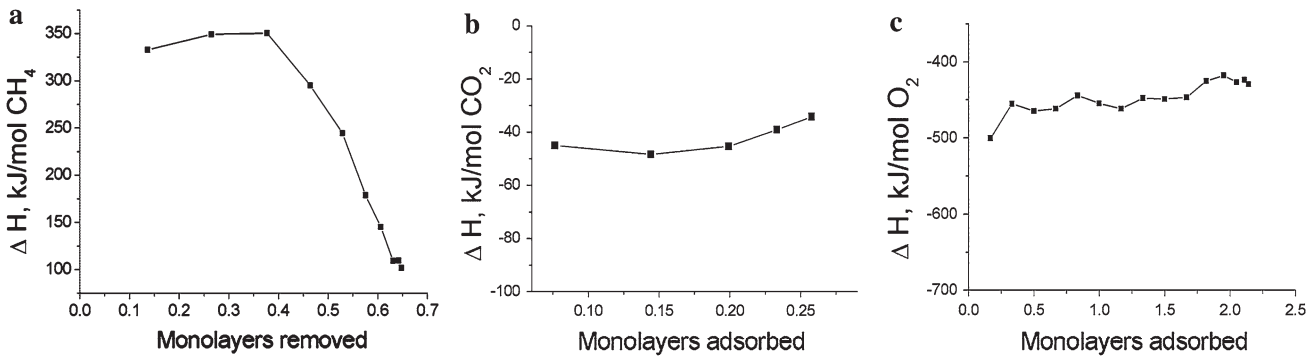

Fig. 8 Variation of heat effects measured in pulses of 7 %CH_4 in He (**a**), 7 %CO_2 in He (**b**) and 5 %O_2 in He (**c**) supplied to steady-state Ru + Ni/PrSmCeZr catalyst at 700 °C

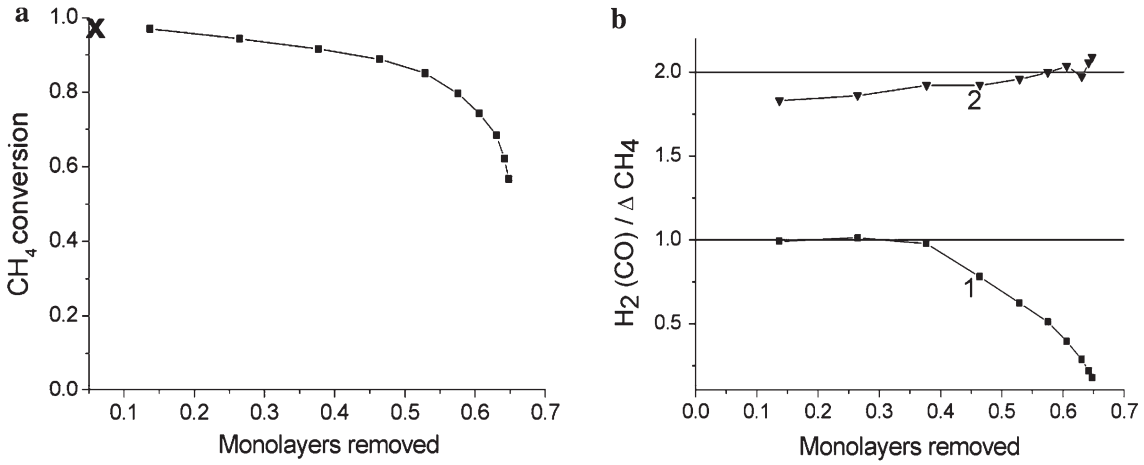

Fig. 9 Variation of CH_4 conversion (**a**, *x* on the ordinate axes marks CH_4 conversion in the mixed CH_4 + CO_2 pulse) and products selectivity (**b**, *1* CO/ΔCH_4; *2* $H_2/\Delta CH_4$) in the course of steady-state Ru + Ni/PrSmCeZr catalyst reduction by pulses of 7 % CH_4 in He at 700 °C

Table 3 Characteristics of bonding strength of reactive bridging oxygen forms for catalysts in the steady state by reduction of CH_4 or CO pulses and reoxidation by CO_2 or O_2 pulses at 700 °C

Catalyst composition	Heat of oxygen desorption (kJ/mol O_2)			
	CO_2*	CH_4*	CO*	O_2*
Pt/PrCeZr	640	650	640	640
LaNi/PrSmCeZr	660	630	650	560
Ru + Ni/PrSmCeZr	630	670	635	550
Ru + Ni/PrSmCeZr/YSZ	640	740	645	550

* Estimated by using pulses of respective component

(Table 3). The same values were obtained by using results of experiments on reduction of steady-state catalysts by CO pulses (not shown for brevity) (Table 3).

These reactive bridging oxygen species are apparently bound with pairs of $Ce^{4+}(Pr^{4+})$ cations in different coordination environment able to easily change their charge state due to reduction/reoxidation [31]. Hence, in agreement with CH_4 pulse studies (vide supra), the reactive oxygen forms responsible for CH_4 transformation into syngas are efficiently produced by CO_2 dissociation on the surface vacancies of fluorite-like support. The degree of CO_2 conversion in the first pulse supplied to the steady-state surface is equal to that in the pulse of reaction feed (Fig. 10). In agreement with SSITKA and TAP studies (vide supra), these results demonstrate that, contrary to catalysts on irreducible oxide supports [15–19], for metal-supported fluorite-like oxides CO_2 activation proceeds independently of CH_4. Note that CO_2 conversion rapidly declines with the pulse number as catalyst is reoxidized (Fig. 10). In agreement with calorimetric data demonstrating the constant heat of the surface reoxidation by CO_2 (Fig. 8b), such kinetics reasonably fitted by the first-order equation for the batch-flow reactor corresponds to filling the surface sites uniform by the adsorption energy. The rate constants of CO_2 consumption are very close for Pt or $LaNiO_3$-supported samples ($\sim 10^2$ s^{-1}), while being an order of magnitude higher for Ni + Ru-supported sample ($\sim 10^3$ s^{-1}). In agreement with SSITKA results (vide supra), this suggests that Ni–Ru alloy nanoparticles

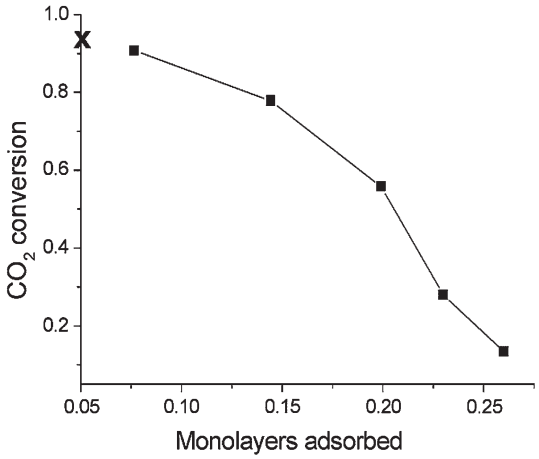

Fig. 10 Variation of CO_2 conversion in the course of steady-state Ru + Ni/PrSmCeZr catalyst oxidation by pulses of 7 % CO_2 in He at 700 °C; *x* on the ordinate axes marks CO_2 conversion in the mixed $CH_4 + CO_2$ pulse

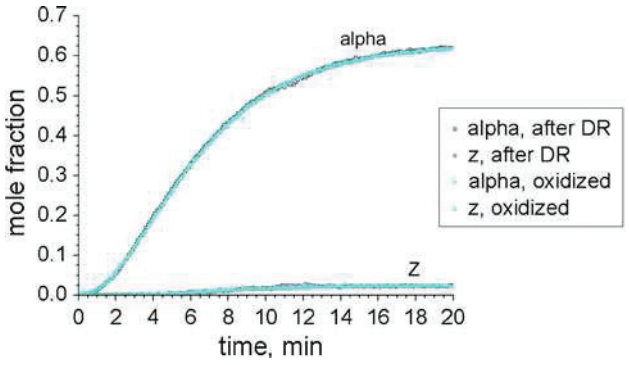

Fig. 11 Effect of pretreatment on isotope transients in the course of $C^{18}O_2$ exchange with the LaNiPt/PrSmCeZr sample at 700 °C; $\alpha = 0.5\ X_1 + X_2$, where α—fraction of ^{18}O in the gas phase, X_2 = fraction of $C^{18}O_2$, X_1 = fraction of $C^{16}O^{18}O$; $z = X_2 - \alpha^2$—deviation from the binomial distribution for $C^{18}O_2$ molecules with fraction X_2

participate in CO_2 activation, perhaps, via facilitation of C–O bond rupture in CO_2 molecules adsorbed at the metal-support interface. For Pt-supported sample, CO_2 is activated only on the sites of support—oxygen vacancies in the coordination sphere of Ce/Pr cations. For the steady-state of all studied catalysts, no evidence for CO_2 interaction with adsorbed CH_x species or CH_4 activation by carbonates was found. This is explained by the fast rate of CO_2 dissociation on support sites and a high surface oxygen mobility providing fast oxygen transfer from support sites to metal sites where CH_4 molecules are activated.

Initial heats of reoxidation of the steady-state catalysts by pulses of O_2 (Fig. 8c; Table 3) are rather close to those estimated from experiments with CH_4 and CO_2 pulses, though being somewhat smaller in magnitude (oxygen bonding strength). The heats of oxygen adsorption decline with samples reoxidation, reflecting apparent non-uniformity of the oxygen bonding strength on the surface due to existence of several types of adsorption sites including also Ni and Ru atoms. Since several monolayers of oxygen are adsorbed before the oxygen conversion in a pulse declines from 100 % in the 1st pulse to 5–10 % in the 15–20th pulse (Fig. 8c), a fast diffusion of oxygen atoms from the surface into the bulk of oxide particles is apparent.

3.7 Oxygen Diffusion Characteristics in the Steady State by $^{18}CO_2$ SSITKA

Since pulse microcatalytic studies revealed that reoxidation by CO_2 is limited only to the fraction of the surface sites, SSITKA of $^{18}CO_2$ allows one to estimate the effect of the catalyst reduction by the reaction feed on the oxygen mobility in fluorite-like oxide support. As follows from Fig. 11, for the LaNiPt/PrSmCeZr catalyst, isotope transients are practically identical for the case of pretreatment in oxygen and after achieving the steady-state in the reaction feed. Similar to the case of oxygen heteroexchange with $^{18}O_2$ [26, 31], all oxygen atoms contained in the catalyst were equilibrated with the oxygen in the gas phase. Estimation of the oxygen diffusion coefficients in the bulk of oxide domains (D_{bulk}) and along domain boundaries ($D_{interfaces}$) following procedures described in detail previously [26, 31] (Table 4) revealed that they were somewhat decreased as compared with values found for completely oxidized states, but remained at a high level. According to analysis of the dynamics of CH_4 dry reforming on Pt/PrCeZr [30], the values of oxygen diffusion coefficients along interfaces (surface and domain boundaries) $\sim 10^{-12}$ to 10^{-13} cm^2/s are sufficient to

Table 4 Coefficients of oxygen diffusion in the Pt/PrCeZr and LaNiPt/PrSmCeZr catalysts by $^{18}O_2$ and $C^{18}O_2$ SSITKA

Sample	D_{eff} (s^{-1})*	D_{bulk} (10^{-18} m^2/s)**	$D_{interfaces}$ (10^{-16} m^2/s)***
Pt/PrCeZr			
$^{18}O_2$ [31]	0.04	4	>33
$C^{18}O_2$	0.003	–	>2
LaNiPt/PrSmCeZr			
$^{18}O_2$ [31]	>0.03	3	>25
$C^{18}O_2$	0.008	–	>5

* D_{eff} effective average oxygen diffusion coefficient for catalyst estimated by solving the system of differential equation describing SSITKA data [26, 31]

** D_{bulk} oxygen diffusion coefficient within oxide domains estimated by using D_{eff} and domain size [26, 31]

*** $D_{interfaces}$ oxygen diffusion coefficient along domain boundaries estimated with regard for the relative amount of oxygen located within domain boundaries [26, 31]

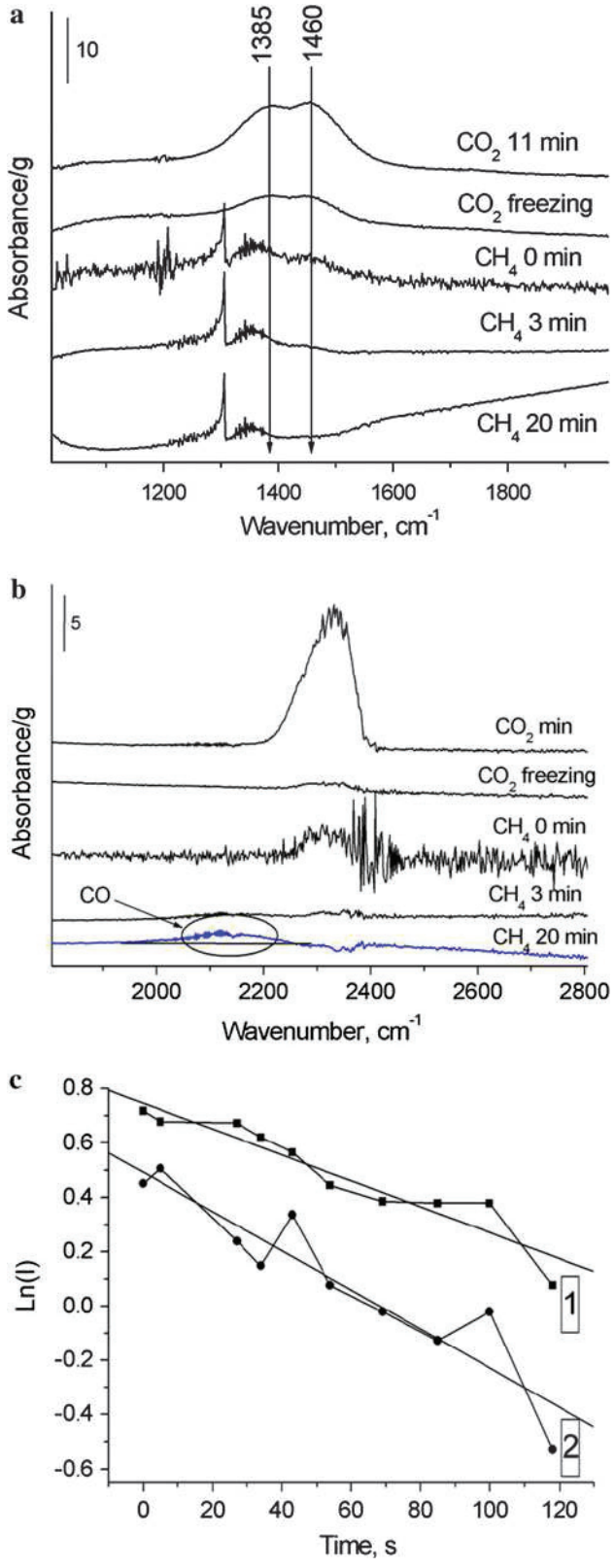

◀ **Fig. 12** FTIR spectra of LaNi/PrSmCeZrO$_2$ sample in the range of surface carbonates (**a**) and CO and CO$_2$ gas phase molecules (**b**) vibrations under contact with CO$_2$ followed by admission of CH$_4$ at 600 °C; variation of the intensity of carbonate bands with time under contact with CH$_4$ in coordinates of the first-order rate equation (**c**): *1* 1,385 cm^{-1}, *2* 1,460 cm^{-1}

Table 5 Rate constants of interaction of surface carbonates with gas-phase CH$_4$

Sample	Temperature (°C)	Constant (s^{-1})
Ru/PrSmCeZr	600	0.003
LaNi/PrSmCeZr	600	0.007
LaNi/PrSmCeZr	650	0.009

3.8 Reactivity of Surface Carbonates

To elucidate whether reductive transformation of CO$_2$ in reaction conditions could proceed via carbonates as intermediates, the reactivity of surface carbonates was studied for catalysts with La-containing active components. Figure 12 and Table 5 present typical results for the LaNi/SmPrCeZr catalyst, for which carbonates bound with La cations are expected to be more abundant than for other catalysts. As follows from Fig. 12, at operation temperatures of CH$_4$ dry reforming bridging carbonates (bands at 1,385 and 1,460 cm^{-1}) [19] are formed on the surface of reduced catalyst under contact with CO$_2$. Though their intensity strongly declines after removing gas-phase CO$_2$, they are still retained on the surface. Moreover, they apparently react with CH$_4$, since respective bands disappear (Fig. 12a) and gas-phase CO is formed (Fig. 12b) when CH$_4$ was admitted into the cell.

Linearization of the intensity variation in coordinates of the first-order equation revealed their identical slopes for both bands, which confirms their assignment to the same bridging carbonate (Fig. 12c). The values of respective first-order rate constants ($\sim 10^{-2}$ s^{-1}) (Table 5) are much smaller than the rate constants of the rate-determining stage of CH$_4$ dissociation ($\sim$1 to 10 s^{-1}), not speaking about the rate constants of CO$_2$ dissociation (>10^2 s^{-1}) estimated from CO$_2$ pulse reoxidation experiments (vide supra). Hence, in agreement with transient experiments, strongly bound carbonates can be only spectators.

4 Conclusions

For catalysts comprising metals (Pt, Ru, Ni + Ru) supported on nanocrystalline complex fluorite-like doped ceria-zirconia oxides, the mechanism of CH$_4$ dry reforming under steady-state conditions in realistic feeds includes provide effective supply of oxygen species to the metal/oxide interface required for maintaining high catalytic activity.

independent stages of CH_4 and CO_2 activation on metal and support sites, respectively. Conjugation between these stages is provided by high oxygen mobility along the surface and domain boundaries of fluorite-like oxides. The oxygen forms responsible for CH_4 selective transformation into syngas are strongly bound bridging oxygen species with heats of desorption $\approx$600–650 kJ/mol O_2, most probably bound with pairs of Pr and/or Ce cations able to change their oxidation state. This conclusion is supported by moderate (20–40 % of monolayer) surface coverage by these forms in steady-state conditions as revealed by CO_2 pulse reoxidation studies. While supported metals do not stabilize these oxygen forms, Ni + Ru clusters could be involved in the transition state of CO_2 activation, thus increasing the rate constant of the surface reoxidation by CO_2. Strongly bound carbonates are only spectators.

References

1. Roh HS, Potdar HS, Jun KW, Kim JW, Oh YS (2004) Appl Catal A 276:231–239
2. Roh HS, Potdar HS, Jun KW, Ji M, Liu ZW (2002) Catal Lett 84:95–101
3. Horvath A, Stefler G, Geszti O, Kienneman A, Pietraszek A, Guczi L (2011) Catal Today 169:102–111
4. Roh HS, Potdar HS, Jun KW (2004) Catal Today 93–95:39–45
5. Pavlova SN, Sazonova NN, Sadykov VA, Alikina GM, Lukashevich AI, Gubanova EL, Bunina RV (2007) Stud Surf Sci Catal 167:343–348
6. Kambolis A, Matralis H, Trovarelli A, Papadopoulou Ch (2010) Appl Catal A 377:16–26
7. Damyanova S, Pawelec D, Arishtirova K, Martinez Huerta MV, Fierro JLG (2009) Appl Catal B 89:149–159
8. Mezentseva NV, Sazonova NN, Sadykov VA, Patent RU 2453366 C1, 29.11.2010
9. Stagg-Williams SM, Noronha FB, Fendley G, Resasco DE (2000) J Catal 194:240–249
10. Sazonova NN, Sadykov VA, Bobin AS, Gubanova EL, Pokrovskaya SA, Mirodatos C (2009) React Kinet Catal Lett 98:35–41
11. Kim DK, Stöwe K, Müller F, Maier WF (2007) J Catal 247:101–111
12. Guo J, Lou H, Mo L, Zheng X (2010) J Mol Catal A 316:1–7
13. García-Diéguez M, Pieta IS, Herrera MC, Larrubia MA, Malpartida I, Alemany LJ (2010) Catal Today 149:380–387
14. Bradford CJ, Vannice MA (1996) Appl Catal A 142:97–122
15. O'Connor AM, Schuurman Y, Ross JRH, Mirodatos C (2006) Catal Today 115:191–198
16. Bychkov V, Tyulenin Yu, Krylov O, Korchak V (2002) Kinet Catal 43:775–782
17. Bychkov V, Tyulenin Yu, Krylov O, Korchak V (2003) Kinet Catal 44:384–390
18. Schuurman Y, Mirodatos C (1997) Appl Catal A 151:305–331
19. Slagtern A, Schuurman Y, Leclercq C, Verykios X, Mirodatos C (1997) J Catal 172:118–126
20. Wei J, Iglesia E (2004) J Catal 224:370–383
21. Sadykov VA, Mezentseva NV, Alikina GM, Lukashevich AI, Borchert YUV, Kuznetsova TG, Ivanov VP, Trukhan SN, Paukshtis EA, Muzykantov VS, Kuznetsov VL, Rogov VA, Ross J, Kemnitz E, Mirodatos C (2007) Solid State Phenom 128:239–248
22. Sadykov VA, Kuznetsova TG, Alikina GM, Frolova YUV, Lukashevich AI, Muzykantov VS, Rogov VA, Batuev LCh, Kriventsov VV, Kochubei DI, Moroz EM, Zyuzin DA, Paukshtis EA, Burgina EB, Trukhan SN, Ivanov VP, Pinaeva LG, Ivanova YuA, Kostrovskii VG, Neophytides S, Kemnitz E, Scheurel K, Mirodatos C (2007) Ceria-based fluorite-like oxide solid solutions promoted by precious metals as catalysts of methane transformation into syngas, chap 5. In: McReynolds DK (ed) New topics in catalysis research. Nova Science Publishers, New York, pp 97–196
23. Sadykov V, Mezentseva N, Alikina G, Bunina R, Pelipenko V, Lukashevich A, Tikhov S, Usoltsev V, Vostrikov Z, Bobrenok O, Smirnova A, Ross J, Smorygo O, Rietveld B (2009) Catal Today 146:132–140
24. Sadykov V, Sobyanin V, Mezentseva N, Alikina G, Vostrikov Z, Fedorova Y, Pelipenko V, Usoltsev V, Tikhov S, Salanov A, Bobrova L, Beloshapkin S, Ross JRH, Smorygo O, Ulyanitskii V, Rudnev V (2010) Fuel 89:1230–1240
25. Sadykov V, Mezentseva N, Alikina G, Bunina R, Pelipenko V, Lukashevich A, Vostrikov Z, Rogov V, Krieger T, Ishchenko A, Zaikovsky V, Bobrova L, Ross J, Smorygo O, Smirnova A, Rietveld B, van Berkel F (2011) Nanocomposite materials, theory and applications. INTECH, Vienna
26. Sadovskaya E, Ivanova Y, Pinaeva L, Grasso G, Kuznetsova T, van Veen A, Sadykov V, Mirodatos C (2007) J Phys Chem A 111:4498–4505
27. Sadovskaya E, Suknev A, Pinaeva L, Goncharov V, Bal'zhinimaev B, Chupin C, Perez-Ramirez J, Mirodatos C (2004) J Catal 225:179–186
28. Gleaves JT, Yablonsky G, Zheng X, Fushimi R, Mills PL (2010) J Mol Catal A 315:108–134
29. Beloshapkin S, Paukshtis E, Sadykov V (2000) J Mol Catal A 158:355–359
30. Sadykov V, Gubanova E, Sazonova N, Pokrovskaya S, Chumakova N, Mezentseva N, Bobin A, Gulyaev R, Ishchenko A, Krieger T, Mirodatos C (2011) Catal Today 171:140–149
31. Sadykov V, Sazonova N, Bobin A, Muzykantov V, Gubanova E, Alikina G, Lukashevich A, Rogov V, Ermakova E, Sadovskaya E, Mezentseva N, Zevak E, Veniaminov S, Muhler M, Mirodatos C, Schuurman Y, van Veen A (2011) Catal Today 169:125–137
32. Sadykov V, Kuznetsova T, Frolova-Borchert Y, Alikina G, Lukashevich A, Rogov V, Muzykantov V, Pinaeva L, Sadovskaya E, Ivanova Y, Paukshtis E, Mezentseva N, Batuev L, Parmon V, Neophytides S, Kemnitz E, Scheurell K, Mirodatos C, van Veen A (2006) Catal Today 117:475–483
33. Bulgakov N, Sadykov V, Lunin V, Kemnitz E (2002) React Kinet Catal Lett 76:111–116

Thermochimica Acta 567 (2013) 27–34

Contents lists available at SciVerse ScienceDirect

Thermochimica Acta

journal homepage: www.elsevier.com/locate/tca

Mechanism of CH_4 dry reforming by pulse microcalorimetry: Metal nanoparticles on perovskite/fluorite supports with high oxygen mobility

Vladislav Sadykov[a,b,*], Vladimir Rogov[a,b], Eugenia Ermakova[b], Dmitry Arendarsky[a], Natalia Mezentseva[a,b], Galina Alikina[a], Natalia Sazonova[a], Aleksei Bobin[a], Svetlana Pavlova[a], Yves Schuurman[c], Claude Mirodatos[c]

[a] Boreskov Institute of Catalysis, Novosibirsk, Russia
[b] Novosibirsk State University, Novosibirsk, Russia
[c] Institut de Recherches sur la catalyse et l'environnement de Lyon, France

ARTICLE INFO

Article history:
Received 15 October 2012
Received in revised form 28 January 2013
Accepted 30 January 2013
Available online 16 February 2013

Keywords:
CH_4 dry reforming
Metal clusters
Perovskite and fluorite oxide supports
Redox mechanism
Pulse microcalorimetry
Bonding strength and reactivity of oxygen species

ABSTRACT

The mechanism of CH_4 dry reforming on Pt, Ru, Ni, Ni + Ru-supported perovskite ($PrFeO_x$, $LaPrMnCrO_x$) or fluorite ($LnCeZrO_x$) oxides was studied using a Setaram Sensys DSC TG calorimeter and a pulse kinetic installation. For catalysts in the steady-state, CH_4 and CO_2 transformation in separate pulses proceeds with the rate and products selectivity equal to that in mixed $CO_2 + CH_4$ pulses. Heat effects of separate stages correspond to CH_4 oxidation into syngas by strongly bound bridging oxygen forms of support (heat of adsorption up to 650 kJ mol^{-1} O_2 for fluorites and ~500 kJ mol^{-1} O_2 for perovskites) and their replenishment by CO_2 dissociation, respectively. These features demonstrate a step-wise red-ox (Mars-van-Crevelen) mechanism of CH_4 dry reforming. Fast oxygen transfer from the sites of oxide support to the metal/oxide interface provides required conjugation of stages.

1. Introduction

Catalysts comprised of metal clusters (Pt, Ru, Ni, Ni + Ru) supported on the surface of fluorite-like (Ln–Ce–Zr–O)/perovskite-like ($LnFeO_x$, $LaPrMnCrO_x$) oxides with a high surface/lattice oxygen mobility and reactivity demonstrate a high activity and coking stability in dry [1–9] and steam [10–12] reforming of methane. It is explained by the bifunctional scheme of reaction mechanism including CH_4 activation of metal sites, CO_2 (H_2O) – on oxide sites followed by fast transfer of oxygen species to the metal-support interface where they interact with activated CH_x species producing syngas [13]. However, up to now, direct evidence of such mechanism is still lacking, and question remains what is the nature of the rate-determining stage and whether for these systems activation of both reagents is really independent or conjugated. Indeed, for traditional catalysts such as alumina-supported Pt, Ni and Co, pulse microcalorimetric studies of Bychkov et al. [14,15] reliably demonstrated that CO_2 is activated via direct interaction with the carbon atoms on the Me surface, which is the slowest step of DR. For Ni/SiO_2 catalyst, transient studies of Schuurman and Mirodatos revealed that CO_2 is activated by direct dissociation on Ni atoms, while the rate-limiting step is interaction between C and O adsorbed on Ni [16]. For Ni/lanthana catalyst, Slagtern et al. [17] proposed that methane is activated on the Ni particles, and carbon dioxide interacts with La_2O_3 to form carbonates which scavenge carbon from nickel at the Ni–La_2O_3 interface. Hence, as dependent upon the support, even for the same metal, different routes of CO_2 activation could operate. Estimation of reagents conversion in mixed and separate pulses fed to the steady-state catalyst is the usual approach to elucidate the reaction mechanism of catalytic red-ox reactions [14–19]. However, it has not yet been applied to studies of CH_4 dry reforming on metal-supported catalysts with a high mobility and reactivity of oxygen in complex oxide supports.

In this work, pulse microcalorimetric studies have been carried out to clarify basic features of CH_4 DR reaction mechanism for catalysts with a high oxygen mobility and reactivity following approaches used in work of Bychkov et al. [14,15]. To elucidate effect of the oxide support and supported active component on the nature of basic stages, the catalysts composition was broadly varied. For comparison, some experiments were carried out for traditional supported Ni/alumina catalyst.

* Corresponding author at: Boreskov Institute of Catalysis, Prospect Akad. Lavrentieva, 5, Novosibirsk 630090, Russia. Tel.: +7 383 330 8763; fax: +7 383 330 8056.
E-mail addresses: sadykovy@academ.org, sadykov@catalysis.ru (V. Sadykov).

0040-6031/$ – see front matter © 2013 Elsevier B.V. All rights reserved.
http://dx.doi.org/10.1016/j.tca.2013.01.034

Table 1
Specific surface area and catalytic activity of samples.

Catalyst composition (wt.%)	Abbreviation	$S_{sp.}$ [a], $m^2\ g^{-1}$	k, [b] $s^{-1}\ m^{-2}$
1.4%Pt/$Pr_{0.3}Ce_{0.35}Zr_{0.35}O_2$	Pt/PrCeZr	29	1.5
6%$LaNiO_3$/$Sm_{0.15}Pr_{0.15}Ce_{0.35}Zr_{0.35}O_2$	LaNi/PrSmCeZr	28	1.7
1.4%Ru/$Sm_{0.15}Pr_{0.15}Ce_{0.35}Zr_{0.35}O_{22}$	Ru/SmPrCeZr	20	2.4
1%Ru/80%$Sm_{0.3}Ce_{0.35}Zr_{0.35}O_2$ +10%NiO + 10%YSZ	RuNi/SmCeZr/YSZ	24	4
(0.57%Ru + 6.6%NiO)/$Sm_{0.15}Pr_{0.15}Ce_{0.35}Zr_{0.35}O_2$	RuNi/SmPrCeZr	21	7.5
$PrFe_{0.6}Ru_{0.1}Ni_{0.3}O_3$	PrFeNiRu	4	5
1.4%Ru/80% $La_{0.8}Pr_{0.2}Mn_{0.2}Cr_{0.8}O_3$ + 10%NiO + 10% YSZ	RuNi/LaPrMnCr/YSZ	6	8

[a] Specific surface area by BET.
[b] Specific first-order rate constant estimated at 700 °C and contact time 15 ms related to the total specific surface unit [4,8,9].

2. Experimental

2.1. Catalysts preparation

Complex fluorite-like $Ln_x(Ce_{0.5}Zr_{0.5})_{1-x}O_2$ (Ln = Pr, Sm, Pr + Sm; $x = 0.3$) and perovskite-like $PrFe_{0.6}Ru_{0.1}Ni_{0.3}O_3$ oxides were prepared by polymerized complex precursor [20] route followed by drying and calcination in air at 900 °C for 2 h as described elsewhere [8–12]. Nanocomposites 80%$La_{0.8}Pr_{0.2}Mn_{0.2}Cr_{0.8}O_3$ + 10%$Zr_{0.92}Y_{0.08}O_{2-\delta}$ (YSZ) + 10%NiO and 80%$Sm_{0.3}Ce_{0.35}Zr_{0.35}O_2$ + 10%YSZ + 10%NiO were prepared by one-pot Pechini route [10–12]. Pt (1 wt.%), Ru (0.6–1.0 wt.%), Ni (7 wt.%), $LaNiO_3$ (7 wt.%) and their combinations were supported on fluorites or nanocomposites from solutions of respective salts (H_2PtCl_6, $RuCl_3$, Ni and La nitrates) by incipient wetness impregnation followed by drying and calcination at 800 °C. Commercial sample of γ-Al_2O_3 ($S_{BET} = 150\ m^2\ g^{-1}$) manufactured by OJSC "Catalyzator" (Novosibirsk) was used for preparation of Ni (7 wt.%)-supported sample by incipient wetness impregnation.

2.2. Catalysts characterization

The specific surface area of samples was determined from the Ar thermal desorption data by using BET method. Structural and microstructural characteristics of samples elucidated by X-ray diffraction and transmission electron microscopy with elemental analysis are given elsewhere [4,5,8–12].

2.3. Kinetic and calorimetric set-ups

Performance of catalysts in CH_4 dry reforming was estimated at atmospheric pressure for feed comprised of 10% CH_4 + 10% CO_2 in He using quartz reactors and flow installation equipped with GC and on-line IR absorbance, electrochemical and polarographic gas sensors for different components as described elsewhere [4,5,8–12]. To compare specific catalytic activities of samples, effective first-order rate constants satisfactorily describing methane conversion data in plug-flow reactors [4,5] were calculated.

Pulse experiments were carried out using a Setaram Sensys DSC TG calorimeter and a pulse kinetic installation. The reagents and products concentrations were determined by a gas chromatograph "Chromos GH-1000". The sample (30–90 mg) was loaded into a tubular quartz reactor with a diameter of 6 mm, which was located in a measuring channel of the calorimetric unit. In the comparison channel an empty reactor was placed. Samples were pretreated in the flow of 5% O_2 in He at 700 °C for 0.5 h and then in He (flow rate 40 mL min^{-1}) for 0.5 h at the same temperature. Steady-state of catalysts in CH_4 dry reforming was usually achieved by flowing reaction feed 7% CH_4 + 7% CO_2 in He at 700 °C for 2 h. Pulses of different compositions (7% CH_4 in He, 7% CH_4 + 7% CO_2 in He, 7% CO_2 in He, 5% O_2 in He) with volume 1–5 mL and time interval between pulses 15 min were fed in different sequences onto the stream of He flowing through the reactor. Due to rather small weights of catalysts and rather big (~5 mL) reactor volume (equal to or exceeding the pulse volume), the gas flow through the reactor in pulse titration experiments can be decribed by the batch-flow model, which suggests the absence of gas phase concentration gradient within the reactor due to intermixing. The amount of oxygen removed from a catalyst by CH_4 pulse or inserted by CO_2/O_2 pulse was expressed either as a fraction of the total amount of oxygen in oxidized sample or a number of the oxygen monolayers (1 monolayer is equal to 10^{19} atoms m^{-2}).

3. Results and discussion

3.1. Phase composition and microstructure

Specific surface area of studied catalysts varies in the range of 10–50 $m^2\ g^{-1}$ (Table 1). Detailed characteristics of catalysts phase composition, microstructure and oxygen mobility/reactivity are given in previous publications [5,8–12,21–25]. Doped ceria-zirconia fluorite-like oxides and complex perovskite-like precursor are single-phase samples. In as-prepared samples, metals (Pt, Ru, Ru + Ni) supported on fluorite-like oxides or nanocomposites are mainly in the form of oxidic species partially incorporated into the surface layers of supports [12,20–22]. Supported $LaNiO_3$ is present as thin perovskite layers on the surface of doped ceria-zirconia particles [12]. XRD pattern of oxidized Ni/γ-Al_2O_3 catalyst does not contain any reflections of NiO phase, which is explained by incorporation of Ni cations into the surface layers of alumina forming the surface spinel phase [5]. In the steady-state of CH_4 DR, metal or metal alloy nanoparticles/clusters (including Ni-(Ru, Fe) alloy clusters with typical sizes <5 nm) are segregated from reduced oxides-supported $LaNiO_3$ or mixed Pr ferrite-nickelate perovskites. These nanoparticles are epitaxially bounded with supports (disordered $PrFeO_x$ + PrO_x nanocomposite in the case of $PrFe_{0.6}Ru_{0.1}Ni_{0.3}O_3$ precursor [8,9]), and their surface is decorated by support oxidic species [4,8–10].

3.2. Catalytic activity

At 700 °C and contact time of 15 ms, for studied catalysts the first-order specific rate constants (Table 1) vary within an order of magnitude. As follows from Table 1, specific catalytic activity of Ru supported on fluorite-like complex oxides is higher than that of supported Pt. Since, according to Wei and Iglesia [26], specific catalytic activity related per the surface atom (turn-over frequency, TOF) of Ru supported on alumina is much lower than that of Pt, this suggests that namely strong interaction of Ru with doped ceria-zirconia provides its high steady-state specific activity in CH_4 dry reforming. Specific activity of LaNi/PrSmCeZr sample is comparable with that of supported Pt and Ru, though TOF for Ni supported on alumina is substantially lower than that of Ru or Pt [26]. It can be explained by a high dispersion of Ni (small sizes of Ni clusters) segregated from $LaNiO_3$ in reducing reaction conditions and stabilized by lanthana patches on the surface of doped ceria-zirconia

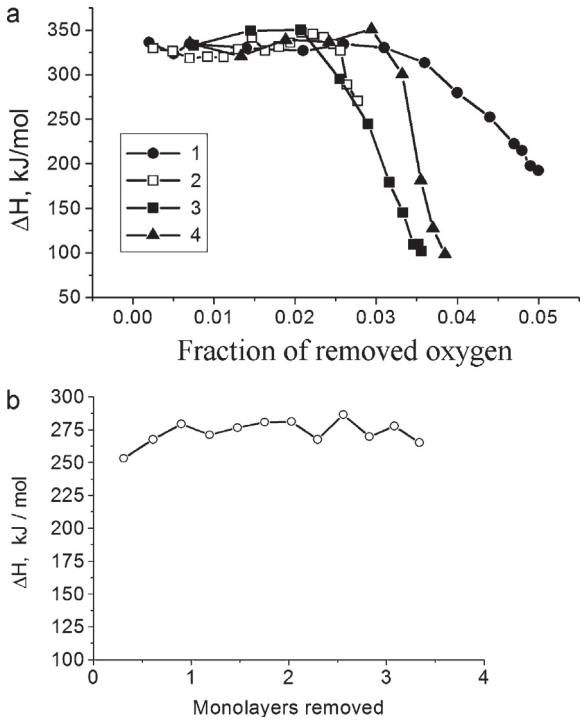

Fig. 1. Dependence of heat effects of steady-state catalysts reduction by CH_4 pulses at 700 °C on the amount of removed oxygen. (a) 1, Pt/PrCeZr; 2, LaNi/SmPrCeZr; 3, NiRu/SmPrCeZr; and 4, RuNi/SmCeZr/YSZ and (b) PrFeRuNi.

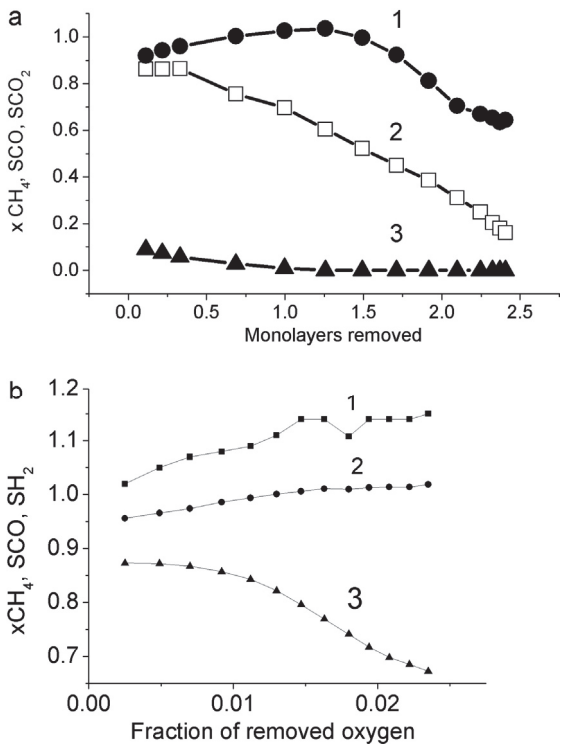

Fig. 2. Variation of CH_4 conversion and products selectivity in the course of steady-state catalysts reduction (a, Pt/PrCeZr and b, LaNi/SmPrCeZr) by pulses of 7% CH_4 in He at 700 °C. (a) 1, SCO; 2, xCH_4; and 3, SCO_2 and (b) 1, SH_2; 2, SCO; and 3, xCH_4.

[5,12]. Combination of Ni and Ru provides non-additive increase of specific activity due to formation of mixed disordered Ni-Ru alloy nanoparticles [4,9]. Indeed, disordering of metal nanoparticles due to the size effect [26] or alloys formation/strong metal support interaction [1–4] helps to facilitate C—H bond ruptute in CH_4 molecule known to be the rate-determining stage of reforming reaction [4,13–15,26]. For the same type of supported active component, specific catalytic activity correlates with the oxygen mobility in complex oxide support [4,8]. Stability of these catalysts to coking in dry [9] as well as steam [10–12] reforming of real natural gas was demonstrated.

3.3. Heat effects and dynamics of steady-state catalysts reduction by CH_4 pulses

For all catalysts based on fluorite-like oxide supports, in the steady-state (ss) of CH_4 dry reforming, the heat effects measured in the course of their reduction with CH_4 pulses are very close to each other in the initial part of the reduction curve (Fig. 1a). They only weakly depend on the reduction degree up to ~2% of the overall oxygen content in samples (up to ~1 oxygen monolayer in average). This means that at this stage of reduction, heat effects are controlled by CH_4 interaction with oxygen species rapidly migrating to the metal/support interface from the surface sites of fluorite-like oxides. For catalysts based on perovskite-like oxide supports, the reaction heat in CH_4 pulses is less endothermal (Fig. 1b), and a larger amount of oxygen (up to 4 monolayers) can be removed at this initial stage of the steady-state catalyst reduction. This suggests a lower bonding strength and a higher mobility of reactive oxygen forms rapidly migrating not only from the surface sites of perovskites but from their subsurface layers as well.

As follows from Fig. 2, in the initial stage of the steady-state catalysts reduction, CH_4 is transformed into H_2 and CO. An admixture of CO_2 is present as well due to interaction of CO with the surface hydroxyls (water gas shift reaction) [13]. Selectivity of H_2 formation ($S\,H_2$) by the reaction $CH_4 + O_s = CO + 2H_2$ is close to 1. A somewhat higher $S\,H_2$ can be explained by the water gas shift reaction (Fig. 2b). Thus determined selectivity of CH_4 transformation into products allowed to estimate the bonding strength of reactive oxygen species of oxide supports usually expressed as enthalpy of O_2 adsorption process generating these species $O_2 + 2^* = 2\,O^*$, where (*) is an adsorption site. These values (~ $-650\,kJ\,mol^{-1}$ O_2 for fluorite-like oxides and ~ -500–$550\,kJ\,mol^{-1}$ for perovskite-like oxides) correspond to strongly bound bridging M_2O form of surface oxygen species [27,28]. A lower bonding strength of reactive oxygen species for perovskite-like oxides is clearly explained by a lower Me—O bond strength for transition metals (Fe, Mn, Cr) as compared with Zr, Ce and Pr [27,28]. The amount of oxygen removed by each pulse is in the range of 5–10% of monolayer exceeding the amount of oxygen which could be retained on the metal sites of catalysts in the steady-state [22]. Hence, only fast oxygen migration from the surface/subsurface sites of the oxide support to metal clusters could provide a high rate of CH_4 consumption in these series of pulses. Rather moderate variation of CH_4 conversion in this initial range of reduction (Fig. 2) agrees with this conclusion.

At a deeper reduction degree, when the oxygen storage capacity of subsurface layers is depleted, the reaction heat declines approaching values corresponding to the enthalpy of CH_4 dissociation into C (graphite) and H_2 (~$75\,kJ\,mol^{-1}$) (Fig. 1). For $LaNiO_3$ or Ni + Ru-supported fluorites pyrolysis starts earlier than for Pt-supported catalyst (Fig. 1) due to a higher concentration of supported metal as well as a higher ability of Ni for the carbon nucleation [15]. This onset of CH_4 cracking with carbon deposition on the surface is also reflected in the decrease of CO selectivity (Fig. 2a) and increase of H_2 selectivity (Fig. 2b). For Pt-supported sample fast decrease of CH_4 conversion with the pulse number is explained by formation of graphitic carbon blocking metal sites [15].

When $CH_4 + CO_2$ pulses are supplied after a long series of CH_4 pulses (and, hence, to partially coked catalyst), the surface carbon

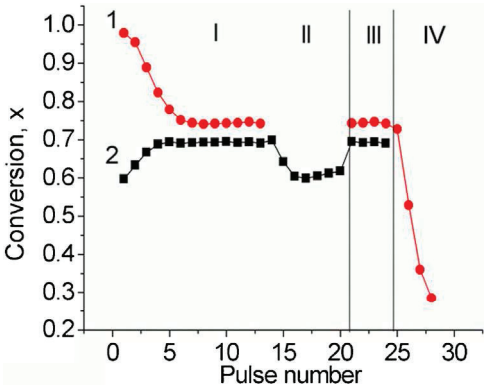

Fig. 3. Conversion of CO_2 (1) and CH_4 (2) in pulses of 7%CH_4 + 7%CO_2 in He (series I and III), 7%CH_4 in He (series II) and 7%CO_2 in He (series IV) on RuNi/LaPrMnCr/YSZ catalyst at 700 °C. Pretreatment in O_2 at 700 °C followed by the flow of reaction feed and pulses of CH_4.

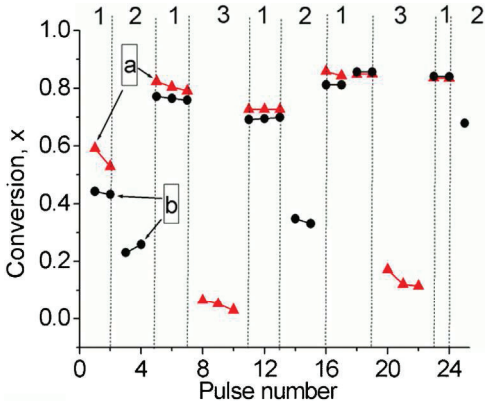

Fig. 4. Conversion of CO_2 (a) and CH_4 (b) in mixed (series 1) and separate (CH_4 – series 2, CO_2 – series 3) pulses supplied on the Ni/alumina catalyst at 700 °C after reduction by CH_4 pulses at the same temperature.

is oxidized by CO_2. It is reflected in CO_2 conversion exceeding that of CH_4 (Fig. 3), decreased heat effect in first pulses (~200 kJ mol^{-1} CH_4) and increased (up to ~2.5) ratio of produced CO molecules to converted CH_4 molecules (CO/ΔCH_4 ratio). Somewhat higher CO_2 conversion as compared with that of CH_4 remains even in the steady-state (Fig. 3) due to occurrence of the reverse water gas shift reaction $CO_2 + H_2 = CO + H_2O$ [4,8,9]. At the same time, the ratio of produced H_2 molecules to converted CH_4 molecules ($H_2/\Delta CH_4$) is slightly increased (up to 2.2) only in the first pulse of reaction feed supplied onto the coked catalyst. This means that the surface coke contains only a small amount of hydrogen atoms which agrees with the results for Ni catalysts on other supports [15–17]. When pulses of methane are supplied to the catalysts after series of reaction feed pulses, CH_4 conversion is identical in the mixed $CH_4 + CO_2$ pulse and in the first CH_4 pulse, which is shown as a typical example for Ni + Ru/LaPrMnCr/YSZ catalyst (Fig. 3). This demonstrates that activation and transformation of CH_4 on catalysts with a high mobility and reactivity of oxygen species of oxide supports does not depend on the presence of another reagent —CO_2. Apparently, CH_4 molecules dissociate on metal sites yielding H_2 and surface C atoms or CH_x fragments, which are rapidly transfomed into CO (or $CO + H_2$) by reaction with oxygen species at the metal/oxide support interface. Since the rate, energetics and selectivity of CH_4 transformation into products in separate CH_4 pulse are identical to those in mixed pulse, this suggests that CH_4 dissociation on metal sites is the rate-determining stage, and all other stages proceed faster as agrees with Wei and Inlesia conclusions [24].

This conclusion agrees with a weak effect of the nature of supported active component on the heat effects in CH_4 pulses before methane cracking starts (Fig. 1a). Indeed, if the rates of oxygen species transfer from support to the metal sites and their interaction with activated CH_x fragments are much higher than the rate of CH_4 dissociation, the heat effect will depend only on the energetics of initial and final states of reagents (i.e. bonding strength of reactive oxygen species of the oxide support) and products. On the other hand, the nature of supported active component determines the rate -limiting stage of methane molecule activation [26]. Hence, specific rate of catalytic reaction characterized by the specific rate constant (Table 1) reflects dependence of the rate of methane activation on the nature of active component. More detailed analysis requires estimation of the accessible surface area of supported metal by CO or H_2 chemisorption which is outside the scope of this paper and will be given elsewhere. Specificity of support-perovskite or fluorite oxide nature strongly affects both the surface/lattice oxygen bonding strength and mobility: a lower bonding strength of oxygen in perovskites provides a higher oxygen mobility, thus supressing coking even in the case of dry reforming of real natural gas containing admixtures of C_2–C_4 alkanes [9].

3.4. Heat effects and dynamics of steady-state catalysts oxidation by CO_2 pulses

For the steady-state of catalysts based on both perovskite-like and fluorite-like supports, CO_2 conversion was found to be identical in the mixed $CH_4 + CO_2$ pulse and in the first pulse of CO_2 supplied after mixed pulse (see i.e. Fig. 3 for RuNi/LaPrMnCr/YSZ catalyst). Consumption of CO_2 molecules is accompanied by formation of stoichiometric amount of CO molecules with small (if any) retention of CO_2 as surface carbonates (not shown for brevity). Hence, under the action of $CH_4 + CO_2$ pulses, all carbon is rapidly removed by reverse Boudouard reaction $CO_2 + C = 2\,CO$ from the surface of this catalyst partially coked by CH_4 pulses (vide supra 3.3). This suggests that for this type of catalysts with a high oxygen mobility and reactivity, in reaction conditions direct Boudouard reaction $2\,CO = CO_2 + C$ is suppressed due to easy oxidation of carbon atoms by oxygen species produced by CO_2 dissociation. Therefore, for catalysts with a high oxygen mobility, CO_2 is also activated independently of CH_4 as required by the step-wise (Mars-van Crevelen) reaction mechanism. On contrary, for Ni/Al_2O_3 as a typical example of catalyst based on non-reducible support, conversion of CH_4 and CO_2 in separate pulses is much lower than in mixed pulses (Fig. 4). This is explained by activation of CO_2 in dry reforming reaction with participation of adsorbed C(H_x) species [29] or metal carbides [14–16].

For all steady-state catalysts with a high oxygen mobility, reoxidation by CO_2 pulses is mildly exothermal process as is shown in Fig. 5 for the case of catalysts on fluorite-like supports. The thermal effect weakly depends upon the type of supported active component and number of CO_2 pulses (Fig. 5). This again confirms that for steady-state catalysts on fluorite-like and perovskite-like supports studied here, the surface carbon is absent, and CO_2 is consumed by dissociation into CO and oxygen species filling oxide supports vacancies. By using the standard enthalpy of reaction $CO_2 = CO + 1/2O_2$ (283 kJ mol^{-1}), enthalpies of O_2 adsorption yielding these oxygen species were estimated (Table 2). As judged by their values (~ −600 kJ mol^{-1} O_2 perfectly agreeing with estimation by CH_4 pulse studies, vide supra), these oxygen species are strongly bound bridging M_2O forms of oxide support. Hence, reactive oxygen forms responsible for CH_4 transformation into syngas are efficiently regenerated by CO_2 dissociation on the surface vacancies of fluorite or perovskite supports. Somewhat lower heats of adsorption were again obtained for perovskite oxide supports.

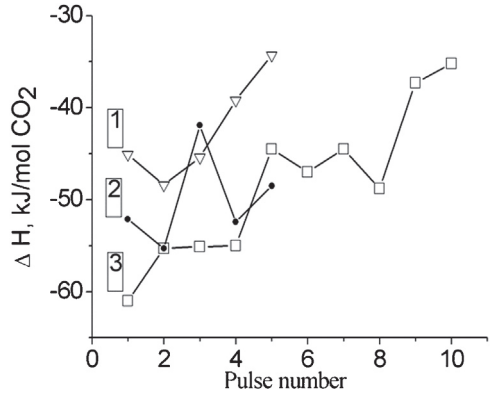

Fig. 5. Variation of heats measured in pulses of 7% CO_2 in He supplied at 700 °C on steady-state catalysts. 1, Ru/NiSmPrCeZr, 2, RuNi/SmCeZr/YSZ, and 3, LaNi/SmPrCeZr.

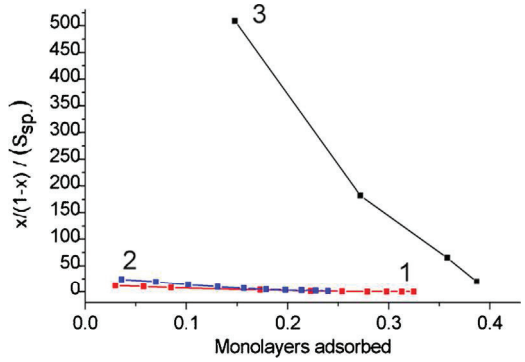

Fig. 6. Fitting kinetics of steady-state catalysts reoxidation by CO_2 by the first-order rate equation. 1, Pt/PrCeZr; 2, LaNi/SmPrCeZr; and 3, RuNi/SmPrCeZr.

In all cases, CO_2 conversion was found to rapidly decline with the pulse number as catalysts are reoxidized (Fig. 3). In agreement with calorimetric data, such kinetics reasonably fitted by the first-order equation for the batch-flow reactor corresponds to filling the surface sites of support with the same adsorption energy. The rate constants of CO_2 consumption proportional to the slope of dependencies in Fig. 6 is the highest for Ni + Ru-supported sample. This suggests that Ni–Ru alloy nanoparticles participate in CO_2 activation, probably via facilitation of C—O bond rupture in CO_2 molecules adsorbed at the metal-support interface. Since dissociation of CO_2 molecules on Pt is not possible [14], for Pt-supported sample CO_2 can be activated only on the support sites–oxygen vacancies in the coordination sphere of Ce/Pr cations. Somewhat higher rate constant of CO_2 consumption for $LaNiO_3$-supported sample implies that Ni atoms at Ni-support interface can accelerate CO_2 dissociation as well. Hence, these experiments demonstrate that the rate of CO_2 dissociation depends on the nature of supported active component even though the final state of thus produced oxygen species located at support sites is the same.

Table 2
Bonding strength of O_s forms regenerated by CO_2.

Catalyst	$-\Delta H$ of oxygen adsorption (kJ mol^{-1} O_2)
Pt/PrCeZr	630
LaNi/PrSmCeZr	660
RuNi/SmPrCeZr	630
RuNi/SmCeZr/YSZ	640
PrFeNiRu	600
RuNi/LaPrMnCr/YSZ	590

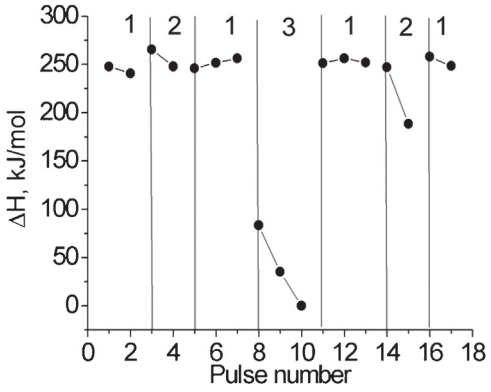

Fig. 7. Heat effects on Ni/alumina in consecutive pulses of reaction feed (1), CH_4 (2) and CO_2 (3) at 700 °C.

For Ni/Al_2O_3 catalyst in the steady-state, the heat effects measured in CO_2 pulses are endothermic (Fig. 7) being determined by rather fast interaction of CO_2 with C atoms adsorbed on Ni particles (heat effect ~100 kJ mol^{-1}) followed by a slower process of CO_2 dissociation into CO_{gas} and adsorbed Ni—O species [14,15]. Some variation of heat effects as well as reagents conversion degrees for different sequence of pulses for Ni/Al_2O_3 catalyst (Figs. 4–7) could be due to migration of carbon atoms from Ni particles to support affecting reactivity of both coke and metal sites [14,15].

For catalysts on supports with a high oxygen mobility, complete reversibility of conversions and heat effects (Fig. 8) was observed for consecutive pulses of reaction mixture alternating with pulses of CH_4 or CO_2. Apparently, such a reversibility is provided by fast oxygen migration between the surface sites of oxide supports and metal nanoparticles as well as by absence of the surface coke deposits.

3.5. Heat effects and dynamics of steady-state catalysts oxidation by O_2 pulses

For all steady-state catalysts based on supports with a high lattice oxygen mobility, CO_2 pulses provide reoxidation of only the surface sites increasing oxygen coverage not more than by ~0.5 monolayer. Hence, bridging surface oxygen species regenerated by CO_2 pulses do not migrate into the subsurface layers/bulk of oxide support particles. On contrary, by CH_4 pulses a higher (up to several monolayers) amount of oxygen can be removed from the steady-state catalysts by CH_4 pulses (vide supra). A similar feature was earlier observed for supported MnO/alumina oxide catalysts and explained by formation of surface carbonates blocking sites for

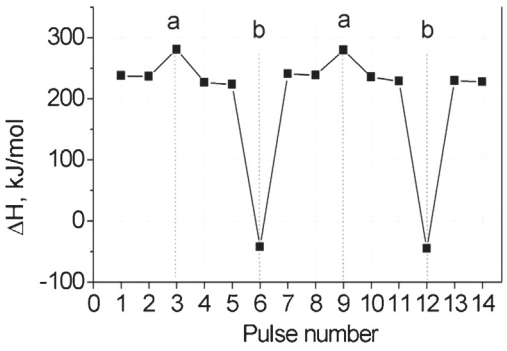

Fig. 8. Heat effects measured in two consecutive pulses of reaction feed $CH_4 + CO_2$ separated by one pulse of CH_4 (a) or CO_2 (b) supplied onto Pt/PrCeZr catalyst at 700 °C.

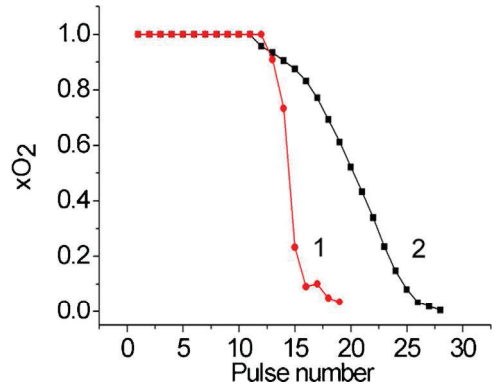

Fig. 9. Dependence of degree of O_2 consumption in pulses of 5% O_2 in He supplied at 700 °C to Pt/PrCeZr (1) and RuNi/LaPrMnCr/YSZ (2) catalysts after achieving the steady state of CH_4 dry reforming.

CO_2 activation [30]. Since reversible CO_2 adsorption can also affect the oxygen mobility, the catalysts in the steady-state of CH_4 dry reforming were also oxidized by pulses of O_2 in He to check the effect of oxidant nature on the energetics and reactivity of reduced surface sites.

For all catalysts, kinetics of oxygen consumption was found to be identical and quite different from that of samples reoxidation by CO_2: oxygen is completely consumed in first 10–20 pulses followed by rather fast decline of conversion to zero in subsequent pulses (Fig. 9). Neither CO nor CO_2 evolution was observed under oxygen pulses, so coke was absent on the surface of catalysts in the steady state. The amount of oxygen consumed in each pulse is around 20% of the monolayer, so a part of oxygen is apparently transferred into the bulk of particles in the time interval between pulses (15 min). For catalysts based on perovskite-like oxides, such a diffusion is apparently faster, which is reflected in less steep decline of O_2 conversion with the pulse number (Fig. 9) as well as in a bigger amount of oxygen absorbed by catalysts in the process of reoxidation: up to 2 monolayers for fluorites, up to 4 monolayers for RuNi/$PrFeO_x$ and up to 18 monolayers for RuNi/LaPrMnCr/YSZ. Hence, oxygen pulses indeed provide faster and deeper reoxidation of catalysts in the steady state as compared with CO_2 pulses, which certainly correlates with much higher exothermicity of oxygen adsorption. In general, the initial heat of oxygen adsorption on the steady-state surface of catalysts (Fig. 10) is close to that estimated from experiments with CO_2 pulses, being only slightly smaller (cf. Table 2). However, in contrary to experiments with CO_2 pulses, the heat of O_2 adsorption clearly varies with the amount of adsorbed oxygen though remaining in the range corresponding to oxygen adsorption in the bridging M_2O form (heat of desorption >350 kJ mol^{-1}). This means that on the surface of catalysts in the steady state, along with sites able to provide dissociation of CO_2 molecule (apparently mainly pairs of Pr and Ce cations), coexist sites with a smaller heat of oxygen adsorption including also transition metal cations/atoms. It is possible that they are in part blocked by carbonates or CO_2 molecules in near-equilibrium conditions of CO_2 pulse adsorption, which prevents their participation in CO_2 dissociation or oxygen diffusion in agreement with results of Krylov et al. [30]. However, in dynamic conditions of CH_4 dry reforming or reduction by CH_4 pulses, these coordinatively unsaturated centers could provide paths for fast surface oxygen diffusion to the metal/support interface. Indeed, due to rather small difference of oxygen bonding strength between centers able to dissociate CO_2 and O_2 molecules (~100 kJ mol^{-1}), the energetic barriers for oxygen atoms jumps between neighboring bridging sites differing by structure and/or chemical nature are expected to be rather low. In conditions of the steady-state catalysts oxidation

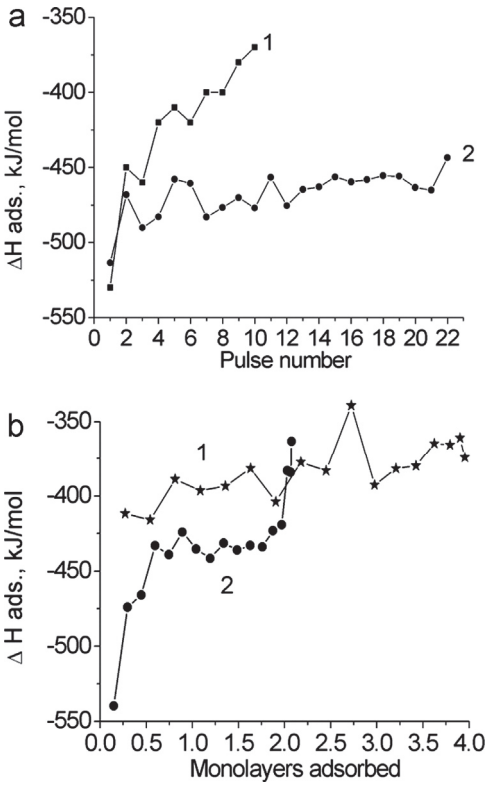

Fig. 10. Variation of heat effect in pulses of O_2 in He at 700 °C versus pulse number (a) or amount of adsorbed oxygen (b). (a) 1, Pt/PrCeZr and 2, RuNi/LaPrMnCr/YSZ and (b) 1, PrFeNiRu and 2, RuNi/SmCeZr/YSZ.

by CO_2 pulses producing CO as product, coverage of centers with a lower bonding strength by oxygen is expected to be quite low since such oxygen forms are easily removed by reaction with CO as checked in special experiments (not shown for brevity). Hence, another factor determining a limited degree of the steady-state catalysts surface reoxidation by CO_2 pulses is reversibility of this reaction.

In general, our results of studies of the mechanism of CH_4 dry reforming on catalysts with a high oxygen mobility in oxide supports and high dispersion of supported active components – metal or metal alloy nanoparticles agree with bi-functional pathway of methane dry reforming [13] realized due to fast diffusion of surface oxygen species of oxide support to developed metal-support interface. Decreasing supported metals dispersion will decrease the metal-support interface and, hence, effect of oxygen mobility in support. As the result, mechanistic features for catalysts with a low dispersion of supported metals/poor metal-support interaction will be similar to those on non-reducible supports (silica, alumina, lanthana, etc. [13–17,29–31]. Indeed, for Pt/PrCeZr catalyst, pretreatment in hydrogen increasing the sizes of Pt particles resulted in the decrease of catalytic activity in CH_4 dry reformimg up to an order of magnitude [4]. In this work, such a difference of the mechanism of CH_4 dry reforming for the same active component – Ni on reducible (perovskite, fluorite) and irreducible (alumina) support was reliably demonstrated as well. Even for Ni supported on irreducible oxides (γ-Al_2O_3, $MgAl_2O_4$), a fast deactivation due to coke accumulation was observed for Ni/γ-Al_2O_3 with big Ni particles, while performance of Ni nanopartiles stabilized by strong interaction with $MgAl_2O_4$ spinel support was stable due to developed Ni-support interface at which efficient interaction of CH_x species with CO_2 occurs [31].

4. Conclusions

For catalysts comprised of metal (Pt, Ni, Ni + Ru) clusters supported on nanocrystalline complex fluorite-like and perovskite-like oxides with a high oxygen mobility, after achieving the steady state in methane dry reforming at temperatures ~700 °C and realistic (7%) concentrations of CH_4 and CO_2 in the feed, transformation of CH_4 and CO_2 in their separate pulses proceeds with the rate and products selectivity equal to that in mixed $CO_2 + CH_4$ pulses. Heat effects measured in pulses of reagents correspond to methane oxidation into $CO + 2H_2$ by strongly bound bridging oxygen species of support (rate-limiting stage) and reoxidation of these reduced oxide sites by CO_2 yielding CO. These features prove the step-wise bifunctional mechanism of CH_4 dry reforming with independent stages of CH_4 and CO_2 transformation on metal and oxide sites, respectively. Conjugation between these stages is provided by fast diffusion of oxygen species from the oxide support sites to the developed metal-support interface. The bonding strength of these oxygen forms with the steady-state surface of catalysts (characterized by the heat of desorption into the gas phase and calculated from the heats measured in pulses of CH_4, CO_2 or O_2) does not depend upon the nature of supported active component. It is lower for perovskite like oxide supports (ΔH desorption ~500 kJ mol^{-1} O_2) as compared with that for doped ceria-zirconia oxides (up to 650 kJ mol^{-1} O_2). This difference is explained by a lower Me—O bonding strength for transition metal cations (Mn, Cr, Fe) versus that for rare–earth cations (Ce, Zr, Pr). Kinetics of the steady-state surface reoxidation by CO_2 is satisfactorily described by the model of uniform by energetics and reactivity surface sites of supports. Ni and Ni + Ru clusters could be involved in the transition state of CO_2 activation thus increasing the rate constant of the surface reoxidation by CO_2.

Acknowledgements

Support by OCMOL FP7 Project, RFBR–CNRS 09-03-93112 Project and Russian Federal Innovation Agency via the program "Scientific and Educational cadres" is gratefully acknowledged. The Embassy of France in Moscow is gratefully acknowledged for the joint PhD studentship grant of A. Bobin.

References

[1] B. Koubaissy, A. Pietraszek, A.C. Roger, A. Kiennemann, CO_2 reforming of methane over Ce–Zr–Ni–Me mixed catalysts, Catal. Today 157 (2010) 436–439.
[2] A. Kambolis, H. Matralis, A. Trovarelli, Ch Papadopoulou, Ni/CeO_2–ZrO_2 catalysts for the dry reforming of methane, Appl. Catal. A 377 (2010) 16–26.
[3] S. Damyanova, B. Pawelec, K. Arishtirova, M.V.M. Huerta, J.L.G. Fierro, The effect of CeO_2 on the surface and catalytic properties of Pt/CeO_2–ZrO_2 catalysts for methane dry reforming, Appl. Catal. B 89 (2009) 149–159.
[4] V.A. Sadykov, E.L. Gubanova, N.N. Sazonova, S.A. Pokrovskaya, N.A. Chumakova, N.V. Mezentseva, A.S. Bobin, R.V. Gulyaev, A.V. Ishchenko, T.A. Krieger, C. Mirodatos, Dry reforming of methane over Pt/PrCeZrO catalyst: kinetic and mechanistic features by transient studies and their modeling, Catal. Today 171 (2011) 140–149.
[5] S.N. Pavlova, N.N. Sazonova, V.A. Sadykov, G.M. Alikina, A.I. Lukashevich, E.L. Gubanova, R.V. Bunina, Study of synthesis gas production over structured catalysts based on LaNi(Pt)O_x- and Pt(LaPt)–CeO_2–ZrO_2, Stud. Surf. Sci. Catal. 167 (2007) 343–348.
[6] G. Valderrama, M.R. Goldwasser, C.U. Navarro, J.M. Tatibouet, J. Barrault, C. Batiot-Dupeyrat, F. Martinez, Dry reforming of methane over Ni perovskite type oxides, Catal. Today 107–108 (2005) 785–791.
[7] G.S. Gallego, J.G. Marin, C. Batiot-Dupeyrat, J. Barrault, F. Mondragon, Influence of Pr and Ce in dry methane reforming catalysts produced from $La_{1-x}A_xNiO_{3-\delta}$ perovskites, Appl. Catal. A 369 (2009) 97–103.
[8] L. Kapokova, S. Pavlova, R. Bunina, G. Alikina, T. Krieger, A. Ishchenko, V. Rogov, V. Sadykov, Dry reforming of methane over $LnFe_{0.7}Ni_{0.3}O_{3-\delta}$ perovskites: influence of Ln nature, Catal. Today 164 (2011) 227–233.
[9] S. Pavlova, L. Kapokova, R. Bunina, G. Alikina, N. Sazonova, T. Krieger, A. Ishchenko, V. Rogov, R. Gulyaev, V. Sadykov, C. Mirodatos, Syngas production by CO_2 reforming of methane using LnFeNi(Ru)O_3 perovskites as precursors of robust catalysts, Catal. Sci. Technol. 2 (2012) 2099–2108.
[10] V. Sadykov, N. Mezentseva, G. Alikina, R. Bunina, V. Pelipenko, A. Lukashevich, S. Tikhov, V. Usoltsev, Z. Vostrikov, O. Bobrenok, A. Smirnova, J. Ross, O. Smorygo, B. Rietveld, Nanocomposite catalysts for internal steam reforming of methane and biofuels in solid oxide fuel cells: design and performance, Catal. Today 146 (2009) 132–140.
[11] V. Sadykov, V. Sobyanin, N. Mezentseva, G. Alikina, Z. Vostrikov, Yu. Fedorova, V. Pelipenko, V. Usoltsev, S. Tikhov, A. Salanov, L. Bobrova, S. Beloshapkin, J.R.H. Ross, O. Smorygo, V. Ulyanitskii, V. Rudnev, Transformation of CH_4 and liquid fuels into syngas on monolithic catalysts, Fuel 89 (2010) 1230–1240.
[12] V. Sadykov, N. Mezentseva, G. Alikina, R. Bunina, V. Pelipenko, A. Lukashevich, Z. Vostrikov, V. Rogov, T. Krieger, A. Ishchenko, V. Zaikovsky, L. Bobrova, J. Ross, O. Smorygo, A. Smirnova, B. Rietveld, F. van Berkel, Nanocomposite catalysts for steam reforming of methane and biofuels: design and performance, in: Nanocomposite Materials, Theory and Applications, INTECH, Austria, Vienna, 2011, pp. 909–946.
[13] J.H. Bitter, K. Seshan, J.A. Lercher, Mono and bifunctional pathways of CO_2/CH_4 reforming over Pt and Rh based catalysts, J. Catal. 176 (1998) 93–101.
[14] V. Bychkov, Yu Tyulenin, O. Krylov, V. Korchak, Methane reforming with carbon dioxide on the Co/α-Al_2O_3 catalyst: the formation, state, and transformations of surface carbon, Kinet. Catal. 43 (2002) 724–730.
[15] V. Bychkov, Yu. Tyulenin, O. Krylov, V. Korchak, The mechanism of methane reforming with carbon dioxide: comparison of supported Pt and Ni (Co) catalysts, Kinet. Catal. 44 (2003) 353–359.
[16] Y. Schuurman, C. Mirodatos, Uses of transient kinetics for methane activation studies, Appl. Catal. A: Gen. 151 (1997) 305–331.
[17] A. Slagtern, Y. Schuurman, C. Leclercq, X. Verykios, C. Mirodatos, Specific features concerning the mechanism of methane reforming by carbon dioxide over Ni/La_2O_3 catalyst, J. Catal. 172 (1997) 118–126.
[18] S.N. Pavlova, V.A. Sadykov, N.N. Bulgakov, M.N. Bredikhin, The influence of support on the low-temperature activity of Pd in the reaction of CO oxidation: 3. Kinetics and mechanism of the reaction, J. Catal. 161 (1996) 517–523.
[19] V.A. Sadykov, S.F. Tikhov, N.N. Bulgakov, A.P. Gerasev, Catalytic oxidation of CO on CuO_x revisited: impact of the surface state on the apparent kinetic parameters, Catal. Today 144 (2009) 324–333.
[20] M.P. Pechini (1967). Method of preparing lead and alkaline earth titanates and niobates and coating method using the same to form a capacitor. U.S. Patent 3 330 697.
[21] V.A. Sadykov, N.V. Mezentseva, G.M. Alikina, A.I. Lukashevich, Yu.V. Borchert, T.G. Kuznetsova, V.P. Ivanov, S.N. Trukhan, E.A. Paukshtis, V.S. Muzykantov, V.L. Kuznetsov, V.A. Rogov, J. Ross, E. Kemnitz, C. Mirodatos, Pt-supported nanocrystalline ceria-zirconia doped with La, Pr or Gd: factors controlling syngas generation in partial oxidation/autothermal reforming of methane or oxygenates, Solid State Phenom. 128 (2007) 239–248.
[22] V.A. Sadykov, T.G. Kuznetsova, G.M. Alikina, Yu.V. Frolova, A.I. Lukashevich, V.S. Muzykantov, V.A. Rogov, L.Ch. Batuev, V.V. Kriventsov, D.I. Kochubei, E.M. Moroz, D.A. Zyuzin, E.A. Paukshtis, E.B. Burgina, S.N. Trukhan, V.P. Ivanov, L.G. Pinaeva, Yu.A. Ivanova, V.G. Kostrovskii, S. Neophytides, E. Kemnitz, K. Scheurel, C. Mirodatos, Ceria-based fluorite-like oxide solid solutions promoted by precious metals as catalysts of methane transformation into syngas, in: New Topics in Catalysis Research, Nova Science Publishers, Inc., New York, 2007, pp. 97–196.
[23] V. Sadykov, T. Kuznetsova, Yu. Frolova-Borchert, G. Alikina, A. Lukashevich, V. Rogov, V. Muzykantov, L. Pinaeva, E. Sadovskaya, Yu Ivanova, E. Paukshtis, N. Mezentseva, L. Batuev, V. Parmon, S. Neophytides, E. Kemnitz, K. Scheurell, C. Mirodatos, A. van Veen, Fuel-rich methane combustion: role of the Pt dispersion and oxygen mobility in a fluorite-like complex oxide support, Catal. Today 117 (2006) 475–483.
[24] E.M. Sadovskaya, Y.A. Ivanova, L.G. Pinaeva, G. Grasso, T.G. Kuznetsova, A. van Veen, V.A. Sadykov, C. Mirodatos, Kinetics of oxygen exchange over CeO_2–ZrO_2 fluorite-based catalysts, J. Phys. Chem. A 111 (2007) 4498–4505.
[25] V.A. Sadykov, N.N. Sazonova, A.S. Bobin, V.S. Muzykantov, E.L. Gubanova, G.M. Alikina, A.I. Lukashevich, V.A. Rogov, E.N. Ermakova, E.M. Sadovskaya, N.V. Mezentseva, E.G. Zevak, S.A. Veniaminov, M. Muhler, C. Mirodatos, Y. Schuurman, A.C. van Veen, Partial oxidation of methane on Pt-supported lanthanide doped ceria-zirconia oxides: effect of the surface/lattice oxygen mobility on catalytic performance, Catal. Today 169 (2011) 125–137.
[26] J. Wei, E. Iglesia, Mechanism and site requirements for activation and chemical conversion of methane on supported Pt clusters and turnover rate comparisons among noble metals, J. Phys. Chem. B 108 (2004) 4094–4103.
[27] N.N. Bulgakov, V.A. Sadykov, V.V. Lunin, E. Kemnitz, Lattice defects and oxygen absorption/migration in ceria/ceria-zirconia solid solutions: analysis by semiempirical interacting bonds method, React. Kinet. Catal. Lett. 76 (2002) 111–116.
[28] V.A. Sadykov, S.N. Pavlova, T.S. Kharlamova, V.S. Muzykantov, N.F. Uvarov, Yu.S. Okhlupin, A.V. Ishchenko, A.S. Bobin, N.V. Mezentseva, G.M. Alikina, A.I. Lukashevich, T.A. Krieger, T.V. Larina, N.N. Bulgakov, V.M. Tapilin, V.D. Belyaev, E.M. Sadovskaya, A.I. Boronin, V.A. Sobyanin, O.F. Bobrenok, A.L. Smirnova, O.L. Smorygo, J.A. Kilner, Perovskites and their nanocomposites with fluorite-like oxides as materials for solid oxide fuel cells cathodes and oxygen-conducting membranes: mobility and reactivity of the surface/bulk oxygen as a key

factor of their performance, in: Perovskites: Structure, Properties and Uses, Nova Science Publishers, Inc., New York, 2010, pp. 67–178.
[29] A.M. Becerra, M.E. Iriarte, A.E. Castro-Luna, Catalytic activity of nickel on alumina catalyst in the CO_2 reforming of methane, React. Kinet. Catal. Lett. 79 (2003) 119–125.
[30] O.V. Krylov, A.K. Mamedov, S.R. Mirzabekova, Interaction of carbon dioxide with methane on oxide catalysts, Catal. Today 42 (1998) 211–215.
[31] J. Guo, H. Lou, L. Mo, X. Zheng, The reactivity of surface active carbonaceous species with CO_2 and its role on hydrocarbon conversion reactions, J. Mol. Catal. A: Chem. 316 (2010) 1–7.